



Pergamon

Progress in Oceanography 51 (2001) 1–123

**Progress in  
Oceanography**

www.elsevier.com/locate/pocean

# The monsoon circulation of the Indian Ocean

Friedrich A. Schott <sup>a,\*</sup>, Julian P. McCreary Jr. <sup>b</sup>

<sup>a</sup> *Institut für Meereskunde an der Universität Kiel, Kiel, Germany*

<sup>b</sup> *International Pacific Research Center, University of Hawaii, Honolulu, Hawaii, USA*

---

## Abstract

In this paper, we review observations, theory and model results on the monsoon circulation of the Indian Ocean. We begin with a general overview, discussing wind-stress forcing fields and their anomalies, climatological distributions of stratification, mixed-layer depths, altimetric sea-level distributions, and seasonal circulation patterns (Section 2). The three main monsoon circulation sections deal with the equatorial regime (Section 3), the Somali Current and western Arabian Sea (Section 4), and the Bay of Bengal, seasonally reversing monsoon currents south of India and Sri Lanka, and the eastern and central Arabian Sea (Section 5). For the equatorial regime, we discuss equatorial jets and undercurrents, their interactions with the eastern and western boundaries, and intraseasonal and vertically propagating signals. In the Somali Current section, we describe the ocean's responses to the summer and winter monsoon winds, and outline the modelling efforts that have been carried out to understand them. In the Bay of Bengal section, we present observational and modeling evidence showing the importance of remote forcing from the east, which to a large extent originates along the equator. In the following three sections, we review the southern-hemisphere subtropical regime and its associated boundary currents (Section 6), the Indonesian Throughflow (Section 7), the Red Sea and Persian Gulf circulations (Section 8), and discuss aspects of their interactions with other Indian-Ocean circulations. Next, we describe the Indian Ocean's deep and shallow meridional overturning cells (Section 9). Model results show large seasonal variability of the meridional overturning streamfunction and heat flux, and we discuss possible physical mechanisms behind this variability. While the monsoon-driven variability of the deep cell is mostly a sloshing motion affecting heat storage, interesting water-mass transformations and monsoonal reversals occur in the shallow cross-equatorial cell. In the mean, the shallow cell connects the subduction areas in the southern subtropics and parts of the Indonesian Throughflow waters with the upwelling areas of the northern hemisphere via the cross-equatorial Somali Current. Its near-surface branch includes a shallow equatorial roll that is seasonally reversing. We close by looking at coupled ocean-climate anomalies, in particular the large events that were observed in the tropical and subtropical Indian Ocean in 1993/94 and 1997/98. These events have been interpreted as an independent Indian-Ocean climate mode by some investigators and as an ENSO-forced anomaly by others. © 2001 Elsevier Science Ltd. All rights reserved.

---

## Contents

1. Introduction . . . . .	4
---------------------------	---

---

\* Corresponding author.

*E-mail address:* fschott@ifm.uni-kiel.de (F.A. Schott).

2.	Overview	5
2.1.	Winds	5
2.1.1.	Climatologies	5
2.1.2.	Annual cycle and means	6
2.1.3.	Intraseasonal to interannual variability	8
2.2.	Water masses	9
2.3.	Circulations	12
3.	Equatorial regime	21
3.1.	Wyrтки Jets	21
3.1.1.	Observations	21
3.1.2.	Models	25
3.1.3.	Enhanced semiannual response	27
3.1.4.	Weak fall WJs	28
3.2.	Undercurrents	28
3.2.1.	Observations	29
3.2.2.	Models	29
3.3.	Vertically propagating waves and deep equatorial jets	31
3.3.1.	Observations	31
3.3.2.	Models	32
3.4.	Intraseasonal oscillations	33
3.4.1.	Observations	33
3.4.2.	Models	34
4.	Somali Current and northern Arabian Sea	37
4.1.	Somali Current, summer monsoon	38
4.1.1.	Observations	38
4.1.2.	Models	43
4.2.	Somali Current, winter monsoon	48
4.2.1.	Observations	48
4.2.2.	Models	49
4.3.	Somali Undercurrents	50
4.3.1.	Observations	50
4.3.2.	Models	51
4.4.	Deep mixed layer during the SW monsoon	53
4.5.	Northern Arabian Sea	55
4.5.1.	Observations	55
4.5.2.	Models	56
5.	Bay of Bengal, monsoon currents, central and eastern Arabian Sea	57
5.1.	Observations	57
5.1.1.	Bay of Bengal and EICC	57
5.1.2.	WICC	60
5.1.3.	Laccadive High and Low	61
5.1.4.	Eastern and central Arabian Sea	61
5.1.5.	Monsoon currents	63
5.2.	Models	65
5.2.1.	EICC	65
5.2.2.	EICC undercurrent	67
5.2.3.	Sri Lanka Dome	67
5.2.4.	WICC	68
5.2.5.	Laccadive High and Low	68

5.2.6.	Eastern and central Arabian Sea . . . . .	69
5.2.7.	Southwest Monsoon Current . . . . .	69
5.2.8.	Northeast Monsoon Current . . . . .	70
6.	Southern hemisphere . . . . .	70
6.1.	Low-latitude eastern-boundary circulation . . . . .	70
6.1.1.	Near-equatorial boundary circulation . . . . .	70
6.1.2.	Northwest Australian shelf and Arafura Sea . . . . .	71
6.2.	Leeuwin Current . . . . .	72
6.2.1.	Observations . . . . .	72
6.2.2.	Models . . . . .	75
6.3.	Subtropical circulation and western-boundary currents . . . . .	76
6.3.1.	Observations . . . . .	76
6.3.2.	Models . . . . .	80
7.	Indonesian Throughflow . . . . .	81
7.1.	Annual-mean circulation . . . . .	82
7.1.1.	Observations . . . . .	82
7.1.2.	Models . . . . .	83
7.2.	Seasonal cycle . . . . .	86
7.3.	Interannual variability . . . . .	87
8.	Red Sea and Persian Gulf . . . . .	88
8.1.	Red Sea . . . . .	88
8.1.1.	Circulation and exchange through Bab el Mandeb . . . . .	88
8.1.2.	Spreading in the Indian Ocean . . . . .	91
8.2.	Persian Gulf . . . . .	92
9.	Meridional overturning cells . . . . .	92
9.1.	Deep circulations . . . . .	93
9.1.1.	Observations . . . . .	93
9.1.2.	Deep upwelling and mixing . . . . .	95
9.1.3.	Models . . . . .	95
9.2.	Shallow cells . . . . .	98
9.2.1.	Observations . . . . .	98
9.2.2.	Models . . . . .	99
9.3.	Heat transports . . . . .	101
9.3.1.	Mean meridional transport . . . . .	101
9.3.2.	Seasonal variability . . . . .	102
10.	Climate modes . . . . .	104
10.1.	Indian Ocean Equatorial mode . . . . .	105
10.2.	The 1993–94 anomaly . . . . .	106
10.3.	The 1997–98 anomaly . . . . .	106
10.4.	Sequential development of the equatorial mode . . . . .	108
10.5.	A subtropical mode? . . . . .	108
11.	Summary and conclusions . . . . .	110
	Acknowledgements . . . . .	113
	Appendix A. List of acronyms . . . . .	113

## 1. Introduction

During the past 40 years, an intensive coordinated study of the Indian Ocean has taken place every decade or so. The first coordinated investigation was carried out during the International Indian Ocean Expedition (IIOE) in 1964–66. It consisted of a basin-wide survey that subsequently resulted in a comprehensive hydrographic atlas (Wyrtki, 1971) and of a number of regional studies, including the first survey of the monsoon circulation of the Somali Current (Swallow & Bruce, 1966). The next intensive study was the Indian Ocean Experiment (INDEX) during the first GARP Global Experiment (FGGE), which investigated the summer-monsoon response of the Somali Current (e.g., Swallow, Molinari, Bruce, Brown, & Evans, 1983). In the following decade, only a few individual or bilateral studies were carried out. These studies included the high-resolution 32°S section of Toole and Warren (1993), boundary-current studies of the South Equatorial Current inflow regime to the Somali Current (e.g., Swallow, Fieux, & Schott, 1988; Swallow, Schott, & Fieux, 1991; Schott, Fieux, Kindle, Swallow, & Zantopp, 1988), an investigation of the seasonal cycle of the near-equatorial Somali current and its complex set of undercurrents (Schott, Swallow, & Fieux, 1990), and regional studies of the Indian coastal currents (Shetye et al., 1990; Shetye et al., 1991a) and the west Australian boundary circulations (e.g., Smith, Huyer, Godfrey, & Church, 1991). At the same time, considerable additional data were obtained by Expendable Bathythermograph (XBT) surveys from volunteer observing ships, GEOSAT satellite altimetry (e.g., Perigaud & Delecluse, 1992), and surface drifter studies (Molinari, Olson, & Reverdin, 1990).

In parallel to the developing observational data base, a number of theoretical and modelling studies were also carried out, in an effort to explain the observed features. Much of this work was targeted at understanding the Somali Current response to the onset of the monsoon. Beginning with Lighthill's (1969) seminal work noting the possible influence of equatorial-wave reflection, a number of studies have explored the role of various wind-forcing patterns, coastal inclination or inertial overshoot of cross-equatorial inflow from the south (e.g., Anderson & Moore, 1979; Cox, 1979, 1981; McCreary & Kundu, 1985, 1988). McCreary, Kundu, and Molinari (1993; MKM, for printing errors see the erratum after page 248 of *Progress in Oceanography*, 1994, Vol.33, number 3) provided a comprehensive analysis of the entire monsoon cycle using a  $2\frac{1}{2}$ -layer model. They forced the model with annual wind-stress and heat-flux climatologies, compared their solution to the existing observational data base, and reviewed prior modelling work. Among other things, MKM first pointed out the importance of remote-forcing effects from the Bay of Bengal on Arabian-Sea circulations, effects that have since been confirmed in more recent studies as discussed below.

In the context of the World Ocean Circulation Experiment (WOCE), a fresh increase in research activities began in the early 1990s, which culminated in a coordinated ship survey of the entire Indian Ocean during 1995–96. This effort yielded high-quality data sets of the distributions of hydrographic properties and various tracers, also current profiles measured by both a shipboard Acoustic Doppler Current Profiler (ADCP) and an ADCP lowered with the CTD rosette (LADCP). In addition, deep float and surface drifter deployments, moored arrays, repeat XBT sections, and especially high-precision TOPEX/Poseidon (T/P) altimetry, which has been operational since 1993, have provided new insights into physical variability and its relations to the forcing fields. In the northern Arabian Sea, a large observational program within the context of the Joint Global Ocean Flux Study (JGOFS) was carried out during 1994–96, including intensive studies on the monsoon response and mixed-layer deepening (e.g., Weller, Baumgartner, Josey, Fischer, & Kindle, 1998; Lee, Jones, Brink, & Fischer, 2000) as well as the regional circulation and upwelling off Oman (e.g., Flagg & Kim, 1998; Shi, Morrison, Böhm, & Manghnani, 2000).

Recent studies based on analyses of historical data, new observations, and modeling have focussed on the interannual variability in the monsoon circulation, noting the existence of prominent ocean-atmosphere

events in the Indian Ocean region. One such event occurred in 1993/94, which led to anomalously weak eastward surface currents along the equator in spring 1994 (Reppin, Schott, Fischer, & Quadfasel, 1999; Vinayachandran, Saji, & Yamagata, 1999b). These caused anomalously cool surface waters, lowered sea level in the eastern ocean, and increased throughflow from the Pacific (Potemra, Lukas, & Mitchum, 1997). An even stronger event occurred in 1997/98, which was marked by easterlies along the equator and the formation of a cold wedge in the east, similar to the equatorial upwelling regimes of the other oceans, suggesting a possible mode of ocean-atmosphere interaction local to the Indian Ocean (Webster, Moore, Loschnigg, & Leben, 1999; Saji, Goswami, Vinayachandran, & Yamagata, 1999; Murtugudde, McCreary, & Busalacchi, 2000).

In this paper, we review the current state of knowledge on the monsoon circulation, both with regard to recent observations and to the hypotheses put forward for their interpretation. Many of the new observations, particularly regarding upper-layer monsoon-related phenomena, have now been published or are in various stages of the publication process. We will summarize, and try to reconcile, classical concepts and interpretations with the newly-available observations. Our focus is on the monsoon circulation north of about 10°S. This is the region of strong monsoonal wind forcing variability, while to the south the Southeast Tradewind regime is present year-round, although with a significant annual cycle superimposed.

The monsoon circulation is predominately wind-driven, although in some locations it is modified by heat and fresh-water fluxes. For this reason, the wind-forced response makes up the core of this review, and effects of thermohaline forcings are only addressed in passing, in relation to regional phenomena.

The paper is organized as follows. To provide background information for subsequent sections, we begin with a general overview of the region's wind forcing, prominent water masses, and seasonal circulation patterns (Section 2). Then, we discuss phenomena in various regions in detail, namely the equatorial region, the Somali Current and Arabian Sea, the Bay of Bengal and the Monsoon Current, the southern hemisphere and Indonesian Throughflow, and the Red Sea and Persian Gulf outflows (Sections 3, 4, 5, 6, 7 and 8). Finally we review the role of monsoon variability in meridional overturning circulations (Section 9), and report recent evidence for modes of interannual-to-interdecadal climate variability in the Indian Ocean (Section 10).

## 2. Overview

Here, we first give an overview of climatological wind stresses, discussing their seasonal cycle and interannual variability (Section 2.1). Then we review the water masses (Section 2.2) and large-scale circulation patterns (Section 2.3) of the tropical-subtropical regime to set the scene for subsequent sections, which deal with the regional processes and phenomena in more detail.

### 2.1. Winds

Indian-Ocean wind climatologies are available from different sources, and different forcing fields have been used for the model runs discussed below. For example, Anderson and Carrington (1993) have shown that there are significant differences in the annual cycles of model solutions forced by different wind products (see Section 3.2.2). Here, we compare some of the climatologies, specifically for the equatorial region where solutions appear to be particularly sensitive.

#### 2.1.1. Climatologies

Initially, model simulations were typically driven by the mean seasonal climatology of Hellerman and Rosenstein (1983; HR), in which monthly-mean stresses were calculated by bulk formulae from ship-wind observations on a 2°×2° grid. Pseudostresses devised by Florida State University (FSU) (e.g., Luther &

O'Brien, 1985; Legler, Navon, & O'Brien, 1989) then became available for studies of interannual variability. These are monthly-mean interpolations of ship observations, to which users apply a drag coefficient of their choice. In the Comprehensive Ocean Atmosphere Data Set (COADS; Slutz et al., 1985) individual monthly means of wind stresses and heat fluxes, also determined from ship observations using bulk formulae, have been compiled from 1880 until the present.

In recent years, winds, stresses and air-sea fluxes have become available from atmospheric forecast-models at diurnal or even higher resolution, such as from the European Center for Medium-range Weather Forecast (ECMWF), the UK Meteorological Office (UKMO), the US National Centers for Environmental Prediction (NCEP), and the Fleet Numerical Meteorology and Oceanography Center (FNMOC). In the following, we use the NCEP wind stresses to discuss overall patterns of variability, comparing them with other products in particular areas of interest, but seasonal means from the other products look similar. A new method of measuring winds that has become available during the past decade is satellite scatterometry from the ERS-1 and ERS-2 satellites (e.g., Halpern et al., 1998), and we will show intercomparisons between interannual variability of these winds and NCEP.

### 2.1.2. Annual cycle and means

The monsoon cycle of the wind-stress fields is shown in Fig. 1, for January, April, July and October from the NCEP seasonal-mean climatology. South of 10°S, the Southeast Trades persist throughout the year. They have their seasonal maximum and most northerly extent during southern winter. In the northern hemisphere during winter, the monsoon winds are directed away from the Asian continent, causing northeasterly wind stresses over the Arabian Sea and Bay of Bengal (Fig. 1a), whereas during the summer monsoon, stresses are southwesterly over both basins (Fig. 1c). In contrast to the winter situation, there is now a continuation of the southern-hemisphere trade winds into the Arabian Sea in the form of a narrow atmospheric jet, the Findlater (1971) Jet.

The curl fields change in correspondence to the seasonal wind stress reversals (Fig. 2) with large reversals between the seasons in the northern hemisphere. During the summer monsoon, anticyclonic curl resides over most of the Arabian Sea and equatorial Indian Ocean north of about 15°S. Its maximum lies over the central Arabian Sea, to the right of the Findlater Jet axis. It reverses to become cyclonic during the winter monsoon, whereas over the western Bay of Bengal, the curl is cyclonic in summer, and anticyclonic in winter.

A unique wind forcing pattern occurs over the Indian Ocean, which is unlike the pattern in other equatorial oceans. It involves the occurrence of semi-annual eastward winds over the equator, during April to June and October to November (Fig. 1b,d). These winds generate an annual-mean equatorial zonal wind stress that is eastward and so mean surface temperatures along the equator are warm, in marked contrast to the situation in the other tropical oceans. Fig. 3 compares monthly-mean zonal wind stresses over the central equatorial Indian Ocean from different climatologies. While the much-used Hellerman and Rosenstein (HR, 1983) stresses and those from ECMWF model output (1990–98 average) remain eastward during northern summer, the NCEP and FNMOC stresses become weakly westward during this time, with NSCAT somewhere in the middle. Such differences of the forcing fields cause, for example, differences in the model results in the intensity of eastward surface jets between spring and fall (Section 3.1), and determine whether or not an eastward equatorial undercurrent appears during northern summer (Section 3.2).

During April to May, weak alongshore winds occur off Somalia (Fig. 1). The subsequent onset of the monsoon over the Arabian Sea has been found to occur in several different ways (Fieux & Stommel, 1977). The onset can be an abrupt change from the weak pre-monsoonal winds into the fully developed Southwest Monsoon in early to mid-June. Alternatively the onset may be gradual, extending over several weeks, or there may be multiple onsets during which the monsoon dies down again for interim phases after the first onset. The Southwest Monsoon becomes most strongly developed in late July but then may undergo phases

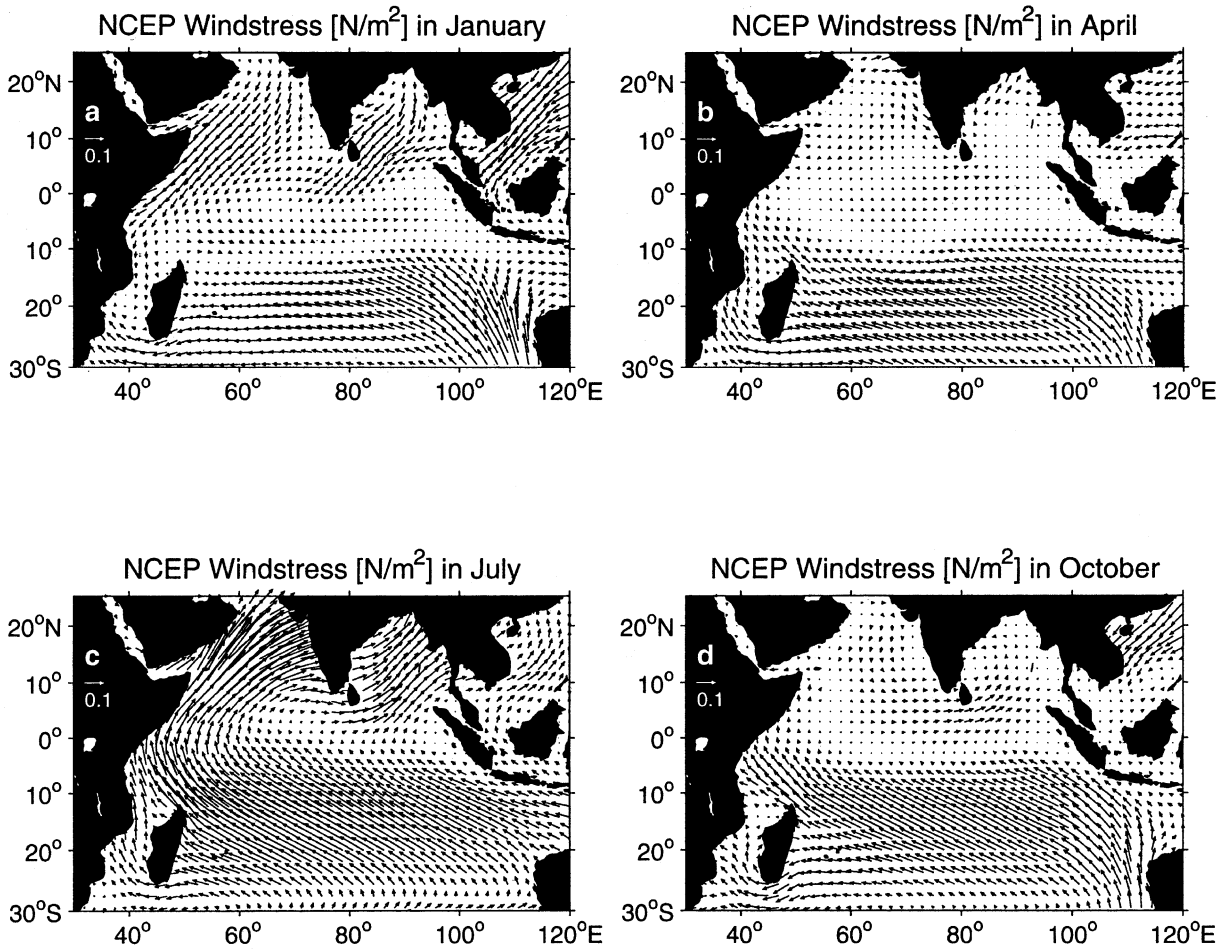


Fig. 1. Monsoon wind stress fields from the NCEP climatology for a) January; b) April; c) July; d) November.

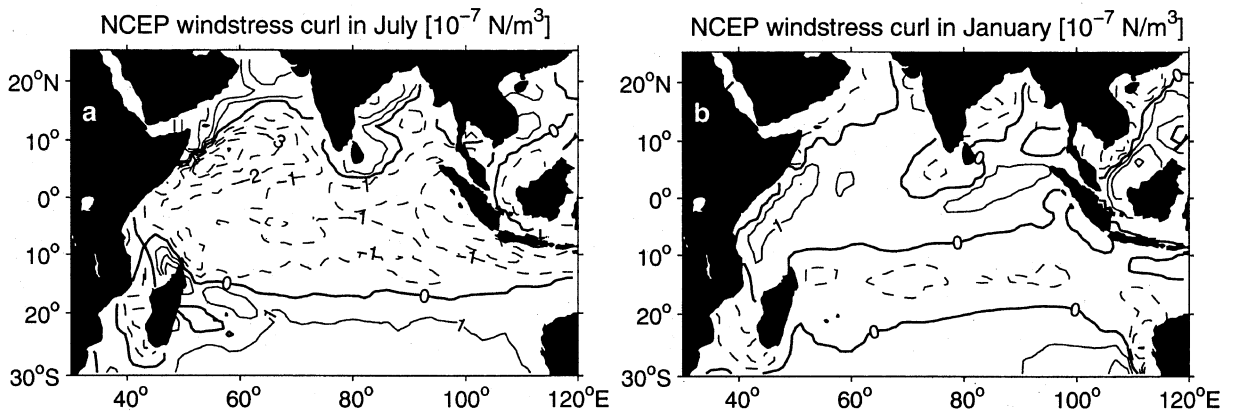


Fig. 2. Mean seasonal wind-stress curl for the Indian Ocean, based on the NCEP wind stress climatology for a) July; b) January.

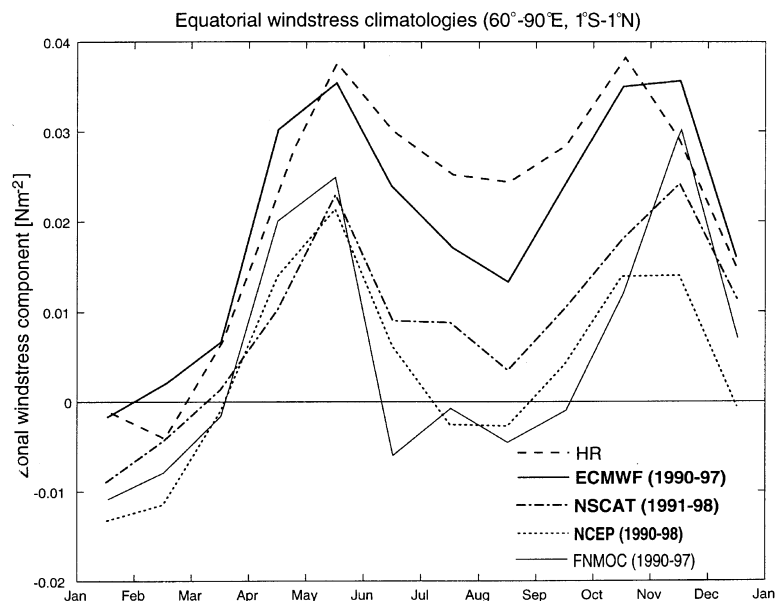


Fig. 3. Mean seasonal cycle of zonal wind stress component, averaged from 60–90°E, 1°S–1°N band for 1990–97 from ECMWF, FNMOC (Courtesy J. Kindle), from NCEP for 1990–98 and ERS-1/2 for 1991–98 (Courtesy R. Schoenefeldt) and from the multidecadal Hellerman/Rosenstein (HR,1983) climatology.

of breaks, which may be associated with the 40–60 day Madden and Julian (1972) oscillations or other large-scale intraseasonal signals.

The summer monsoon winds overwhelm the other seasons in the northern hemisphere in the annual mean, and the mean stresses in the Arabian Sea are therefore anticyclonic (Fig. 4a). The mean curl is anticyclonic over the Indian Ocean north of about 15°S, with the exception of small areas around Madagascar and India. (Fig. 4b).

### 2.1.3. Intraseasonal to interannual variability

Several earlier studies (e.g., Barnett, 1983; Reverdin, Cadet, & Gutzler, 1986) demonstrated that there is considerable variability in interannual wind-stress in the equatorial zone. In addition, during the past decades a considerable research effort has been aimed at discovering leading indices of Indian Ocean SST and other parameters that might serve as predictors for precipitation anomalies over India, so far mostly unsuccessfully.

Recently, several strong wind stress events and flux anomalies have been documented while at the same time in situ observations have been collected, which we will review in a later section (Section 10). Mean seasonal cycles and anomalies for the NCEP and ERS scatterometer winds are shown in Fig. 5a for the central Indian Ocean, averaged from 1°S–1°N and 60–90°E. Two periods of particularly large westward anomalies are obvious, during the second half of 1994 and 1997. The latter event coincided with the 1997/98 ‘monster’ El Niño, whereas the 1994 event coincided with a weak El Niño. Overall, it is interesting to note that the zonal equatorial stress anomalies, which are responsible for driving the anomalous equatorial surface currents and undercurrents, have a magnitude similar to that of the mean annual cycle. Hence, a comparison of seasonal climatologies from different time periods could differ significantly if such large anomalies were, for example, part of one climatology but not of the other one. In contrast, the meridional equatorial anomalies are much smaller than the seasonal cycle (Fig. 5b).

Fig. 6 illustrates the mean seasonal wind stress cycles and anomalies for the northwest Arabian Sea, for

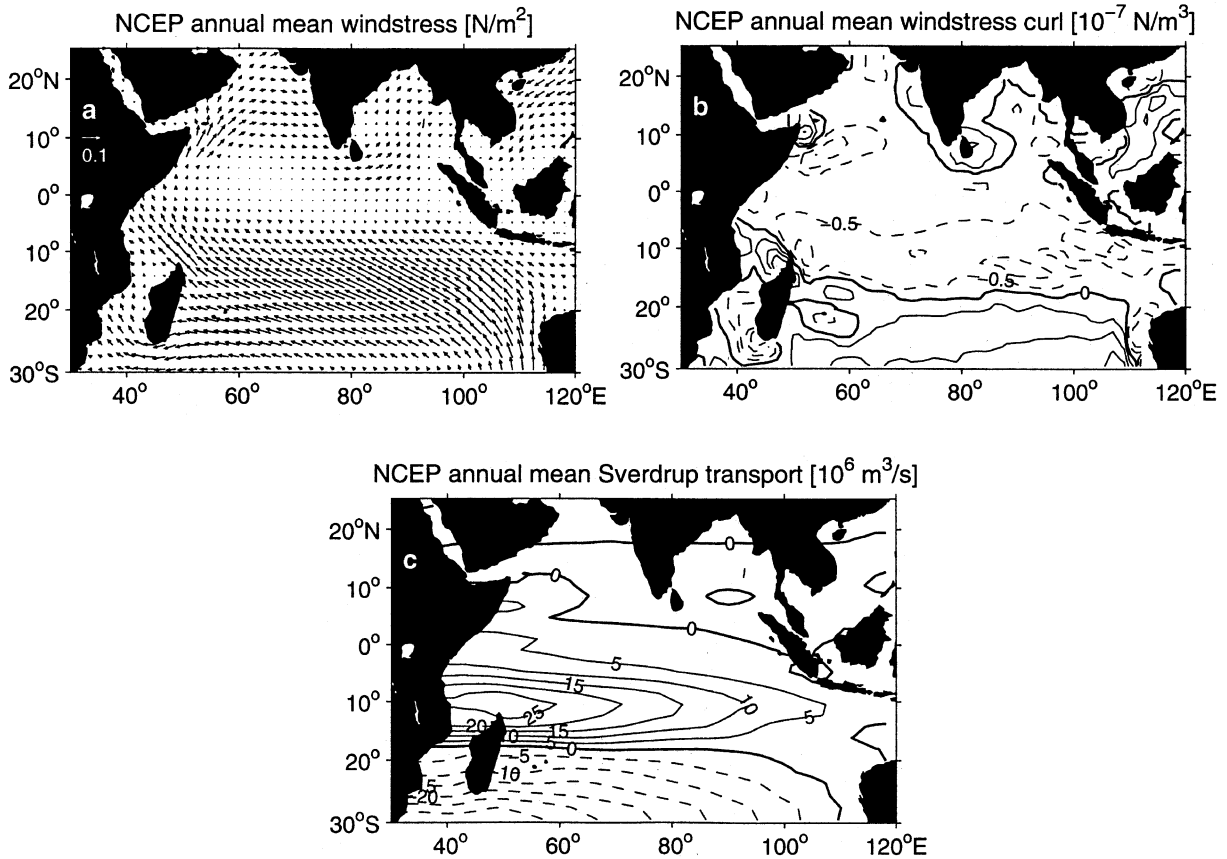


Fig. 4. Annual mean fields of a) wind stress; b) wind stress curl; c) Sverdrup transport function (in  $Sv=10^6 \text{ m}^3 \text{ s}^{-1}$ ), from NCEP climatology.

the wind stress component toward the northeast, determined by averaging both stress products from 8–15°N, 54–60°E, i.e., in the region of the Findlater Jet. In this case, the anomalies are typically less than about 10% of the mean cycle and the larger anomalies all occur during the summer monsoon.

Overall, the comparison shows that, whereas the big events are similarly represented by the different forcing fields, significant differences exist between the various wind stress products that will affect model simulations of the seasonal, intraseasonal and interannual variability. For example, studies of regional heat budgets suffer from inaccurate representation of advective terms as a result of these forcing errors. In conclusion, more intercomparison and calibration studies, using moored buoys in critical regions (e.g., Weller et al., 1998), are needed to sort out these discrepancies.

## 2.2. Water masses

Fig. 7 presents a composite temperature/salinity (T/S) diagram that illustrates properties of water masses in specific regions that we will address later (see also Wyrtki, 1971; Tomczak & Godfrey, 1994 for a discussion of Indian Ocean water masses and core layers). Three basic kinds of water masses can be distinguished: those that are generated within the open Indian Ocean by subduction, those that are mixing

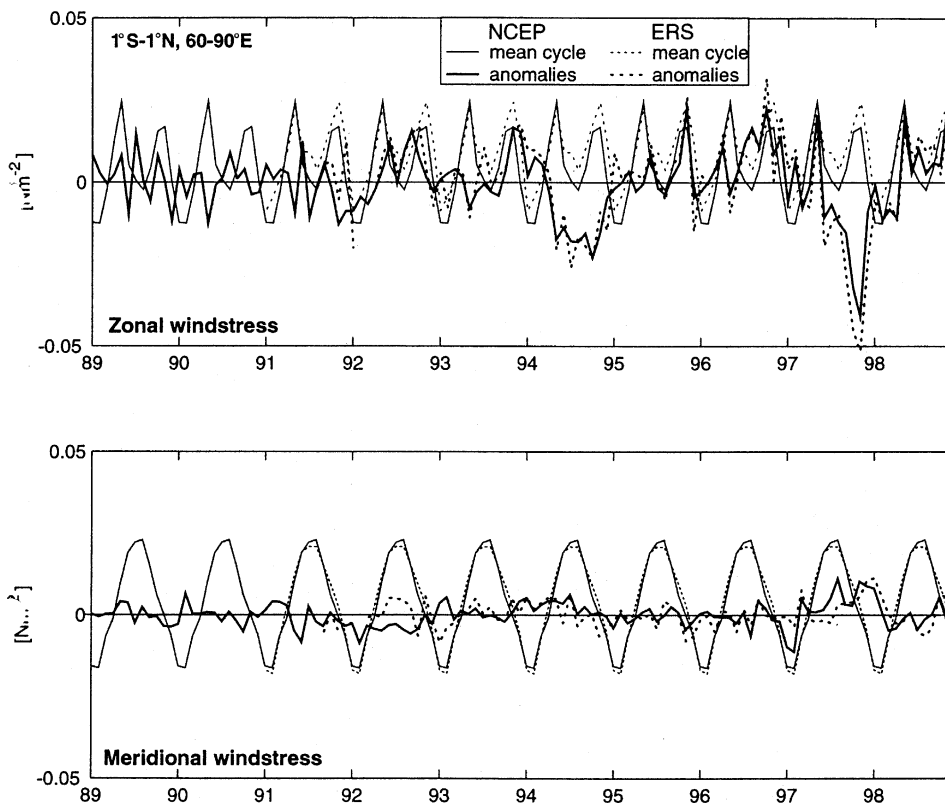


Fig. 5. Mean seasonal cycle and anomalies 1989–98 for the NCEP and ERS wind stresses for the central equatorial Indian Ocean, averaged from 60–90°E, 1°S–1°N for a) zonal and b) meridional components. Note the big zonal anomalies in 1993/94 and 1997/98, while meridional anomalies are small compared to seasonal cycle.

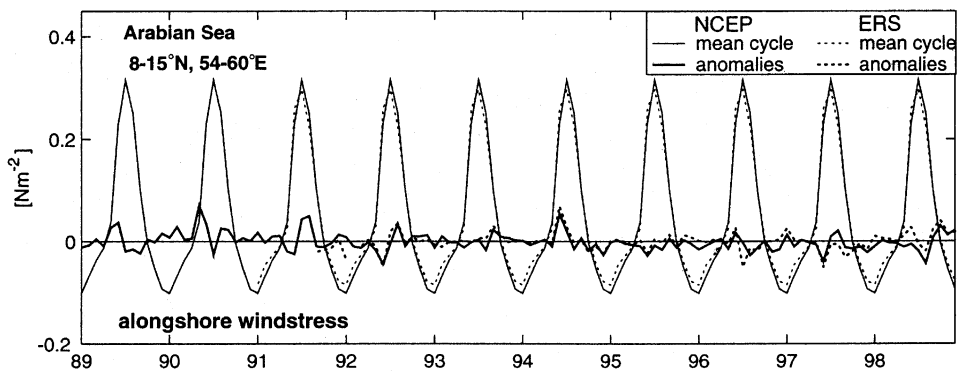


Fig. 6. Mean seasonal cycle and anomalies for the NCEP and ERS wind stresses over the northwestern Arabian Sea (shown is component towards NE, in the direction of the Findlater Jet; compare Fig. 1c), determined for a box average of the wind stresses in the region 8–15°N, 54–60°E.

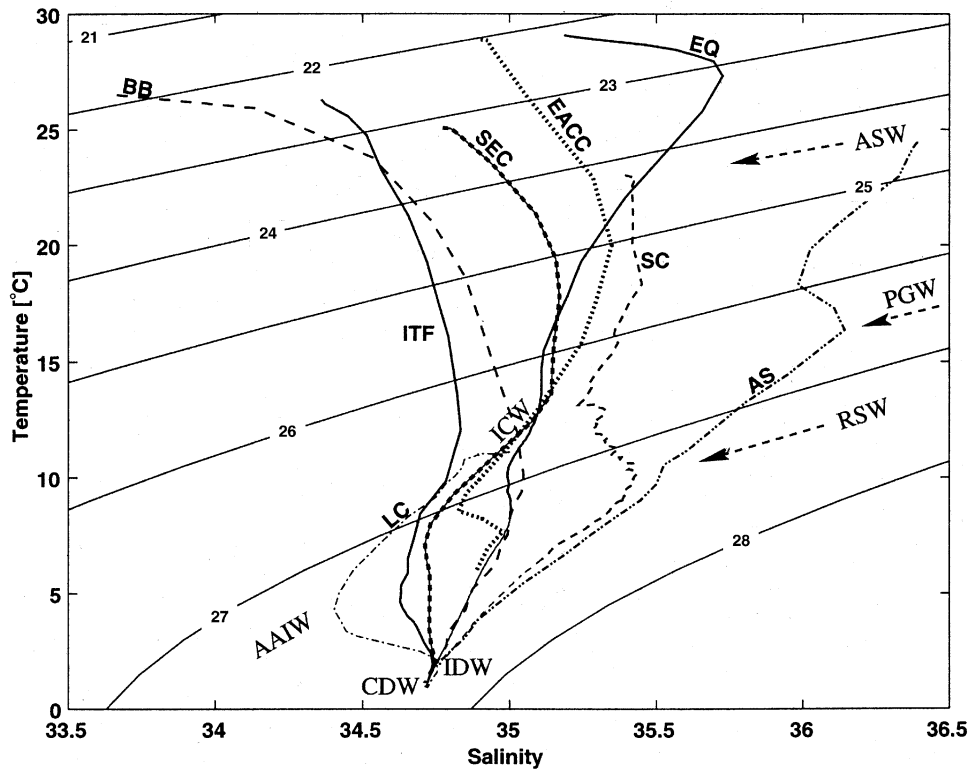


Fig. 7. Temperature-Salinity diagram of Indian Ocean water masses taken from Levitus and Boyer (1994a,b) climatology for the Bay of Bengal (BB), northern Arabian Sea (AS), equatorial region of western basin (EQ), South Equatorial Current (SEC), western exit of Indonesian Throughflow (ITF), and Leeuwin Current (LC). The Somali Current (SC) curve is from August 1993 measurements in northern upwelling wedge. Core water masses indicated are Circumpolar Deep Water (CDW), Indian Deep Water (IDW), Antarctic Intermediate Water (AAIW), Indian Central Water (ICW), Red Sea Water (RSW), Persian Gulf Water (PGW), and Arabian Sea Water (ASW). Profiles are for respective winter seasons in each hemisphere.

products of other water masses, and those that enter from outside. We briefly summarize their characteristics, beginning with those in the near-surface layers.

Two shallow water masses are formed by subduction and enter the upper thermocline. Arabian Sea Water (ASW, Fig. 7) is formed in the northern Arabian Sea during the northeast monsoon and spreads as a salinity maximum just underneath the surface-mixed layer (Morrison, 1997; Schott & Fischer, 2000). Another shallow salinity maximum-water forms in the subtropical gyre of the southern hemisphere, where evaporation exceeds precipitation. This is Subtropical Subsurface Water (SSW), which has a core density of  $\sigma_\theta=25.8 \text{ kg/m}^3$ . When it joins the SEC, it has a core depth of 200–250 m, it spreads with the westward flow toward the western boundary, and shallows to about 100 m (Swallow et al., 1988). In the northern Bay of Bengal (curve BB, Fig. 7), waters of very low salinities are generated through the combined effects of large river discharge and excess precipitation. These low salinity waters can spread around India/Sri Lanka and be identified in the eastern Arabian Sea (Stramma, Fischer, & Schott, 1996). Another northern salty near-surface water mass, which is clearly distinct from ASW, is Persian Gulf Water (PGW). It spreads at a core depth of  $\sigma_\theta=26.6 \text{ kg/m}^3$ , corresponding to a depth of about 250–300 m. The influence of PGW does not extend very far beyond the northern Arabian Sea.

Indian Central Water (ICW) is formed in the subtropics of the southern hemisphere, marked by a near-

linear T/S relation above about 7°C and a T/S maximum associated with SSW below 7°C. The SSW, spreads westward with the South Equatorial Current (see the linear slope of curve SEC) and then northward across the equator with the Somali Current, where it finally participates in supplying the upwelling water off Somalia and Arabia. In the Northern Hemisphere, it is referred to as North Indian Central Water, an aged type of ICW. The lower thermocline is ventilated by subtropical mode waters inserted in regions where warm meridional currents flow into colder environments, such as the Agulhas Current and its recirculation in the west, the Leeuwin Current in the east, and subantarctic mode waters just north of the subpolar frontal zone.

The water masses entering through the Indonesian passages originate mostly from the thermocline in the North Pacific (see Section 7.1). Initially they are marked by a salinity maximum, but become transformed by strong vertical mixing as they flow over the various sills of the Indonesian passages (Ffield & Gordon, 1992), and so assume new characteristics, showing a relative salinity minimum in the Indian Ocean environment (curve ITF, Fig. 7). They are referred to either as Banda Sea Water or as Australian Mediterranean Water (AAMW) in the Indian Ocean.

The equatorial regime has its own specific thermocline water-mass, Indian Equatorial Water (IEW), which is marked by small vertical salinity differences. It is a mixing product of Indonesian Throughflow water coming from the east and Indian Ocean waters from the north and south (You & Tomczak, 1993).

At intermediate depths, Antarctic Intermediate Water (AAIW, curve LC) with a core density of  $\sigma_\theta = 27.1\text{--}27.3 \text{ kg/m}^3$  enters the basin in the southeastern region (Fine, 1993). It is generated by subduction in the subpolar frontal zone, and marked by low salinities because of the precipitation excess over evaporation in that area and by an oxygen maximum. At that same density, warm and saline Red Sea Water (RSW) spreads from the north, out of the Gulf of Aden, as indicated by the Arabian Sea (AS) and Somali Current (SC) curves in Fig. 7. Its preferred spreading route into the Indian Ocean is through the passage between Socotra and the African continent and then further south into the Mozambique Channel (Beal, Ffield, & Gordon, 2000a). Its distribution in the northwest Indian Ocean is very inhomogeneous as a result of the intense eddy activity in the Somali Current and northern Arabian Sea (Quadfasel & Schott, 1982).

At greatest depths, Lower Circumpolar Deep Water (CDW) enters the Madagascar and West Australian basins (Toole & Warren, 1993), but direct entry into the central Indian Basin is obstructed by the deep ridges (Fig. 20). Indian Deep Water (IDW) is a water mass specific to the northern Indian Ocean; it flows in the density range just above CDW, and presumably is generated by deep upwelling out of the CDW. It is oxygen-poor and has high salinity as a result of its mixing with older intermediate waters above; it is also high in silica derived from the discharges of the northern rivers. In the southwest, it has the characteristics of diluted North Atlantic Deep Water, i.e., increased oxygen and salinity (e.g., Mantyla & Reid, 1995).

### 2.3. *Circulations*

For later reference, Figs. 8 and 9 schematically illustrate the prominent surface currents during both monsoon seasons, as observed from ship-drift climatologies (Cutler & Swallow, 1984) and from drifters (Molinari et al., 1990; Shenoi, Saji, & Almeida, 1999). Transport values, observed at some key sections by moored current meter arrays, are also indicated in the schematic maps and will be referred to later. For comparison and later reference, Figs. 10 and 11 show the upper-layer currents and layer thickness derived from MKM's main-run solution, Fig. 12 presents the Sverdrup transport functions resulting from the mean and seasonal curl fields (Fig. 4c), and Figs. 13 and 14 show the surface-layer currents of the high-resolution Parallel Ocean Program Model (POP) described by Maltrud, Semtner, and Malone (1998) and Gordon and McClean (1999). January and July maps are from 10 year averages of POM which was forced by 3 daily winds.

To show the climatological cycle of the stratification, Fig. 15 shows the seasonal development of temperature both at the surface and at 100 m (Rao & Sivakumar, 2000), Figs. 16 and 17 show the seasonal

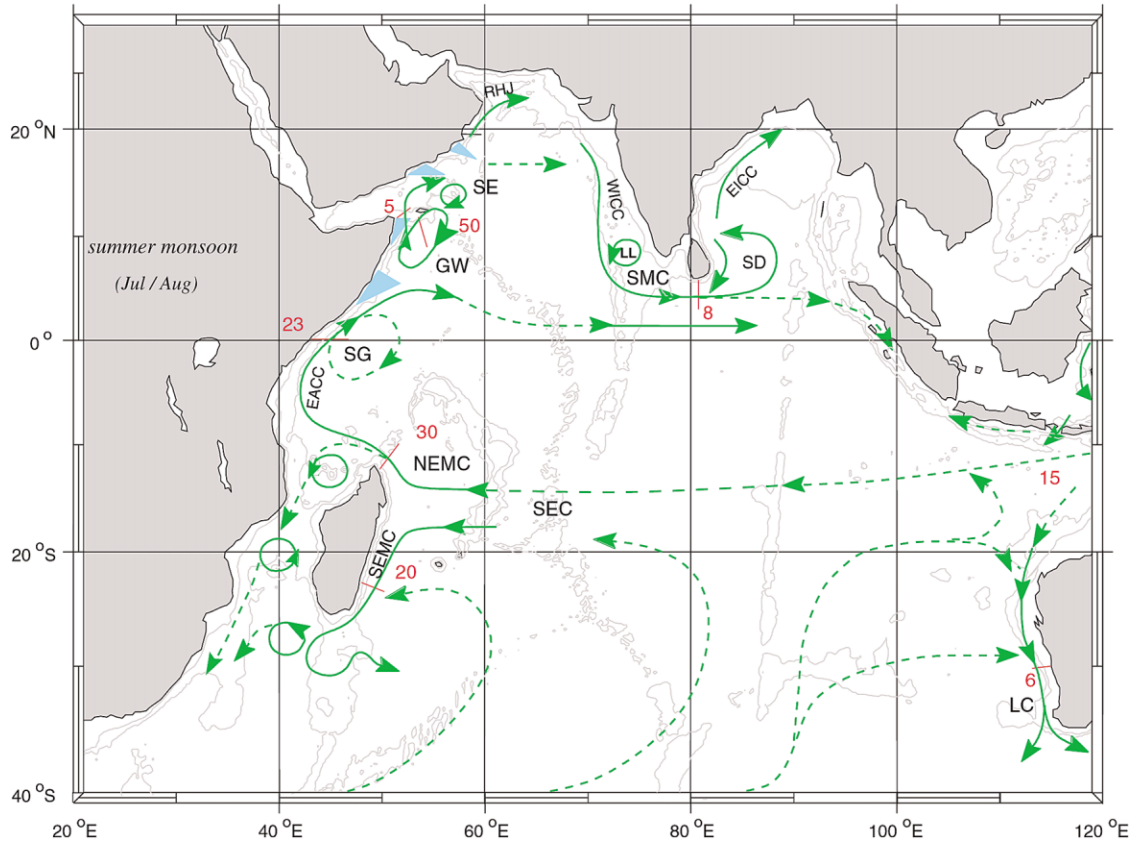


Fig. 8. A schematic representation of identified current branches during the Southwest Monsoon, including some choke point transport numbers ( $Sv=10^6\text{m}^3\text{s}^{-1}$ ). Current branches indicated (see also Fig. 9) are the South Equatorial Current (SEC), South Equatorial Countercurrent (SECC), Northeast and Southeast Madagascar Current (NEMC and SEMC), East African Coast Current (EACC), Somali Current (SC), Southern Gyre (SG) and Great Whirl (GW) and associated upwelling wedges, Socotra Eddy (SE), Ras al Hadd Jet (RHJ) and upwelling wedges off Oman, West Indian Coast Current (WICC), Laccadive High and Low (LH and LL), East Indian Coast Current (EICC), Southwest and Northeast Monsoon Current (SMC and NMC), South Java Current (JC) and Leeuwin Current (LC). See text for details.

development of the surface-mixed layer thickness (Rao, Molinari, & Festa, 1989), and Fig. 18 the steric height field relative to 400 dbar for both monsoon seasons (Peter & Mizuno, 2000). Seasonal sea-level height variability is shown in Fig. 19, and the topography and major basin configuration of the Indian Ocean in Fig. 20. In the following we briefly review the major circulation features that are discussed in greater detail in subsequent sections.

*Southern Hemisphere:* Similar to the situation in the other oceans, there is a broad zonal inflow by the South Equatorial Current (SEC), driven by the Southeast Trades (Fig. 1) which supplies the western boundary currents east of Madagascar within the latitude range  $12\text{--}25^\circ\text{S}$  (Fig. 8). At about  $17^\circ\text{S}$ , the SEC splits into northward- and southward-flowing branches. The northern branch, known as the Northeast Madagascar Current, flows past the northern tip of Madagascar at Cape Amber and feeds into the East African Coast Current (EACC). This circulation is also displayed in Figs. 10 and 11. The large-scale southern hemispheric circulation basically follows Sverdrup dynamics, as a comparison with the transport function of Fig. 4c indicates. The POP vector maps (Figs. 13 and 14) show that the path of the SEC is more irregular, because of the effects of the underlying topography (Fig. 20) and Rossby-waves. Available



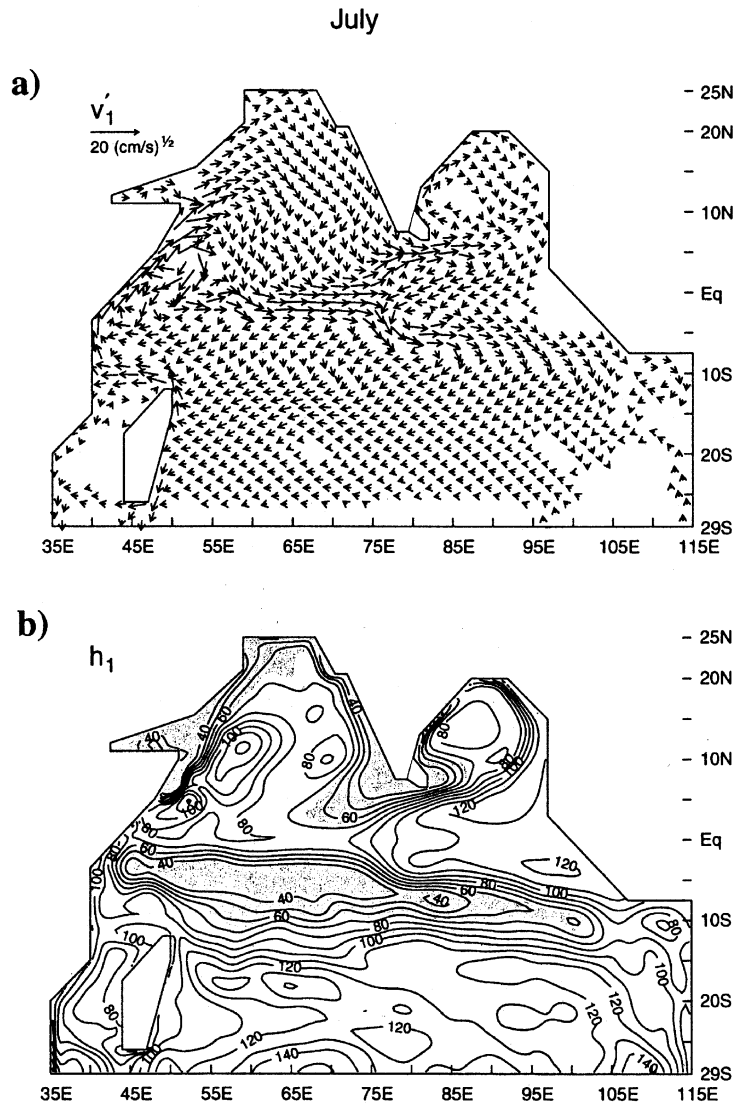


Fig. 10. Plots of a) upper-layer current vectors and b) upper-layer thickness during July from the MKM solution.

Bay of Bengal. It is supplied by inflow from the south, partially by flow out of the SMC around a cyclonic dome to the east of Sri Lanka (Fig. 19c).

During the summer monsoon, the Ekman flow is directed southward on both sides of the equator (e.g., Levitus, 1988), suggesting that there is a southward flow of surface water across the equator in the interior of the ocean. Observational evidence for the concept of southward Ekman transport was given by Chereskin, Wilson, Bryden, Field, and Morrison (1997), who evaluated surface-layer ADCP currents across the 8°N line in the Arabian Sea and contrasted these with geostrophy; they obtained good agreement between measured Ekman transports and those derived from wind stress.

Undercurrents have been observed under the Somali Current and WICC during different times of the year. These are not shown in the schematic maps, but will be addressed in the following sections.

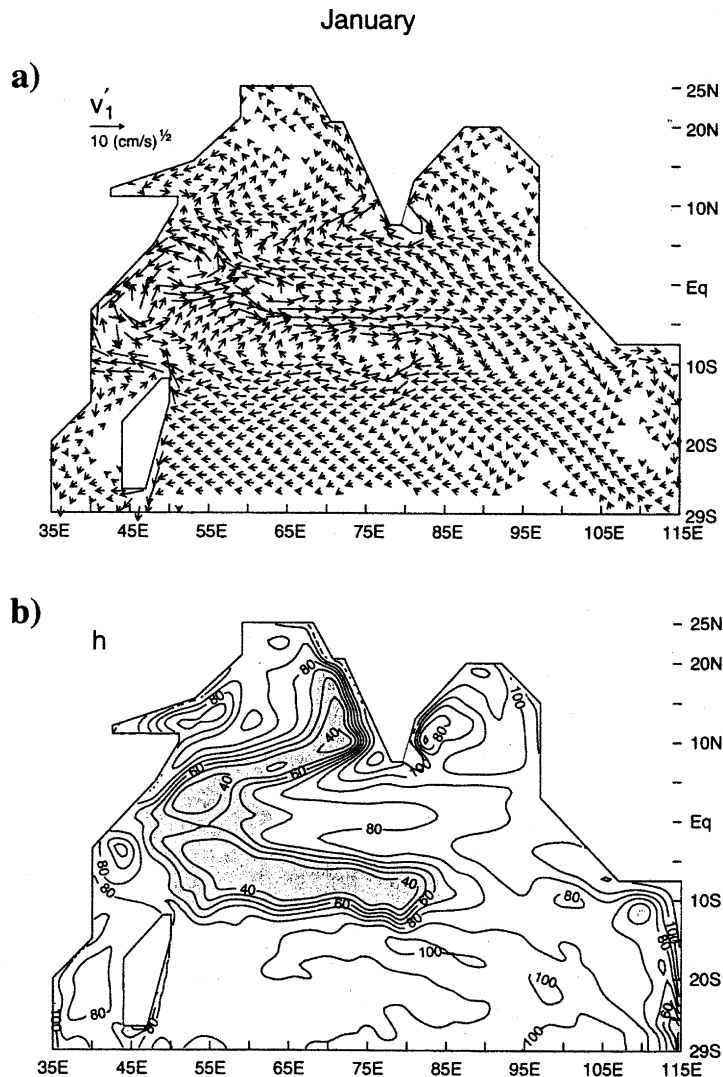


Fig. 11. Same as Fig. 10 but for January.

*Winter monsoon:* During the winter monsoon, the EACC meets the then southward-flowing, near-surface Somali Current in a confluence zone at 2–4°S, and the two flows then supply the eastward-flowing South Equatorial Countercurrent (SECC, Fig. 9). This pattern is also seen in the MKM model (Fig. 11a) and in the Sverdrup transport map (Fig. 12b). At the eastern end of the SECC, a boundary Current, the South Java Current (JC, Fig. 9) flows southeastward at this time. The Somali Current has a northward undercurrent beneath the cross-equatorial southward flow at this time of year, as discussed later. There is inflow from the east into the Somali Current from across the Arabian Sea, which seems to occur in several branches. A low-latitude supply originates from the westward-flowing Northeast Monsoon Current (NMC) south of Sri Lanka, which also supplies the WICC after circulating around the Laccadive High (Bruce, Johnson, & Kindle, 1994). This High is expressed as a seasonal anomaly of more than 12 cm in the altimetry signal of Fig. 19, stretching westward along about 5°N. This feature was also pointed out by MKM (Fig. 11b).

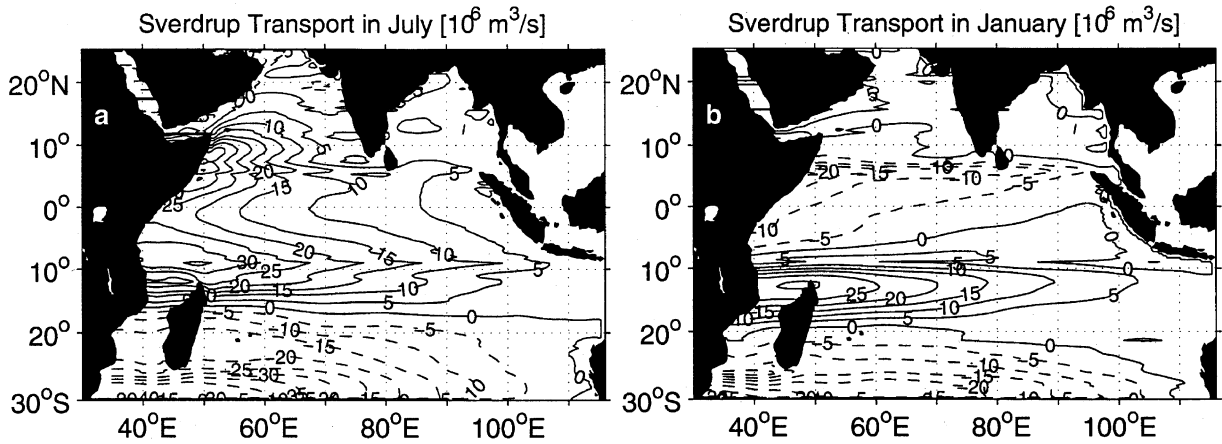


Fig. 12. Equivalent Sverdrup transport functions (in  $Sv=10^6 m^3 s^{-1}$ ), for a) July, b) January, (based on quasi-stationary response to seasonal wind stress curl, Fig. 2) for the NCEP climatology.

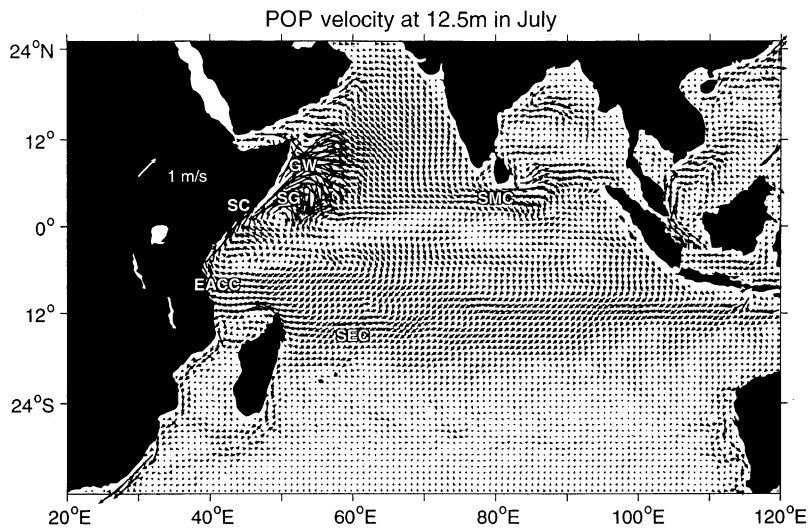


Fig. 13. Surface-current vectors of the high-resolution POP simulation, for July, averaged for 1985–94. (Courtesy J. McClean.)

A second branch that flows westward south of Socotra, is also indicated by meridional gradients of mixed-layer depth (Fig. 17a), and possibly may also receive waters from the WICC. Exactly how the Somali Current inflow connects with the NMC and possibly cross-equatorial northward interior flows (the Ekman transports on both sides of the equator are northward during this season; Levitus, 1988) is presently unknown.

In the Bay of Bengal, the EICC reverses direction twice a year. It flows northeastward from February until September with a strong peak in March–April and southwestward from October to January with strongest flow in November. The surface circulation in the interior of the Bay of Bengal is best organized from February to May, when the EICC forms the western boundary current of a basin-wide anticyclonic gyre. This gyre disappears during the summer monsoon, when the boundary current splits at the 10°N confluence. In the interior, the circulation then seems to consist of several rings. During winter, there seems to be a cyclonic gyre in the interior of the Bay which is coupled to the then southward flow of the EICC.

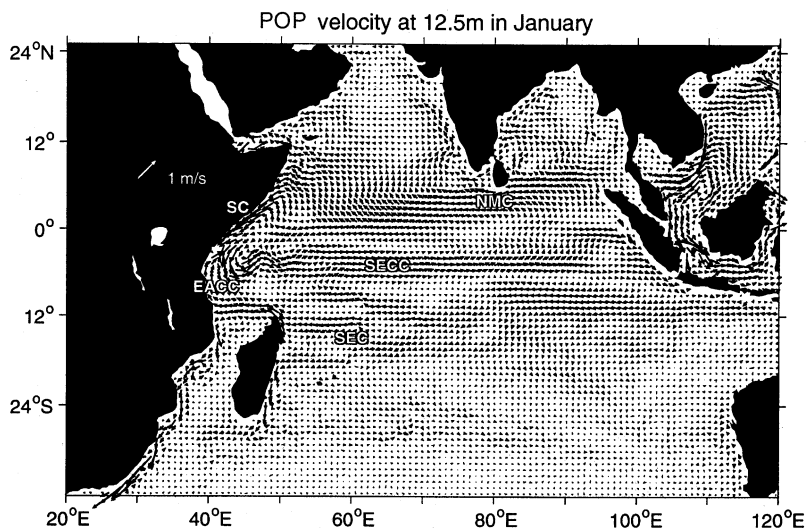


Fig. 14. Same as 13, but for January.

*Equatorial regime:* A particular phenomenon, singular to the Indian Ocean owing to the semiannual eastward winds along the equator (Fig. 1), is the occurrence of strong eastward surface jets (Wyrтки, 1973) during the transition seasons between the monsoons, i.e., April to June and October to December (not indicated in the schematic figures). Their effect is to carry warm upper-layer waters eastward, lowering sea level and decreasing mixed-layer thickness in the west but increasing them in the east (e.g., Rao et al., 1989; Fig. 17b,d; Fig. 19b,d) thereby causing an eastern temperature maximum in the 100-m map (Fig. 15d,f). Here we note the reason why the years of dipole-mode events (see Section 10) were left out of the altimetry seasonal means: including them would have added large negative anomalies in the fall for these two years and thus eliminated the typical boreal fall SSH maximum in the eastern tropical Indian Ocean. These eastward-flowing, upper-layer, current anomalies propagate poleward along the eastern boundary of the basin, and remote effects of these processes are discussed in more detail in later sections.

The lack of sustained westward equatorial winds is the reason for another Indian Ocean peculiarity, namely, that an eastward Equatorial Undercurrent (EUC) occurs only during part of the year, typically February to June. It can appear in other seasons as well, when anomalous easterlies occur.

*Indonesian Throughflow:* The flow of Pacific water into the Indian Ocean through the Indonesian passages, the Indonesian Throughflow, appears to be larger during the boreal summer than winter (e.g., Meyers, Bailey, & Worby, 1995), and estimates of throughflow transports are indicated in Figs. 9 and 8 (see Section 7). The pathways taken by Throughflow water within the Indian Ocean are still very much a matter of debate. Both, water-mass analyses and model solutions clearly indicate that the bulk of it flows toward Madagascar within the SEC, but there are disagreements among model solutions as to the paths followed by the throughflow waters toward the western boundary and its further spreading from there. The Throughflow water might pass through the Mozambique Channel and merge into the Agulhas Current and so take the ‘warm water route’ into the Atlantic. Alternatively, it could take the ‘cold water route’, flowing eastward at higher latitudes south of Madagascar to round Australia passing back into the Pacific and so eventually into the Atlantic. While water-mass properties indicate that during the time of low equatorward winds, some throughflow water may take the shortcut route via the Leeuwin Current along the west coast of Australia and thence back to the Pacific, model evidence does not really support this pathway (Section 7).

*Marginal seas:* The northern marginal seas, the Red Sea and Persian Gulf (sometimes referred to as the Arabian Gulf), inject water masses into the Indian Ocean that are identifiable over long distances by their

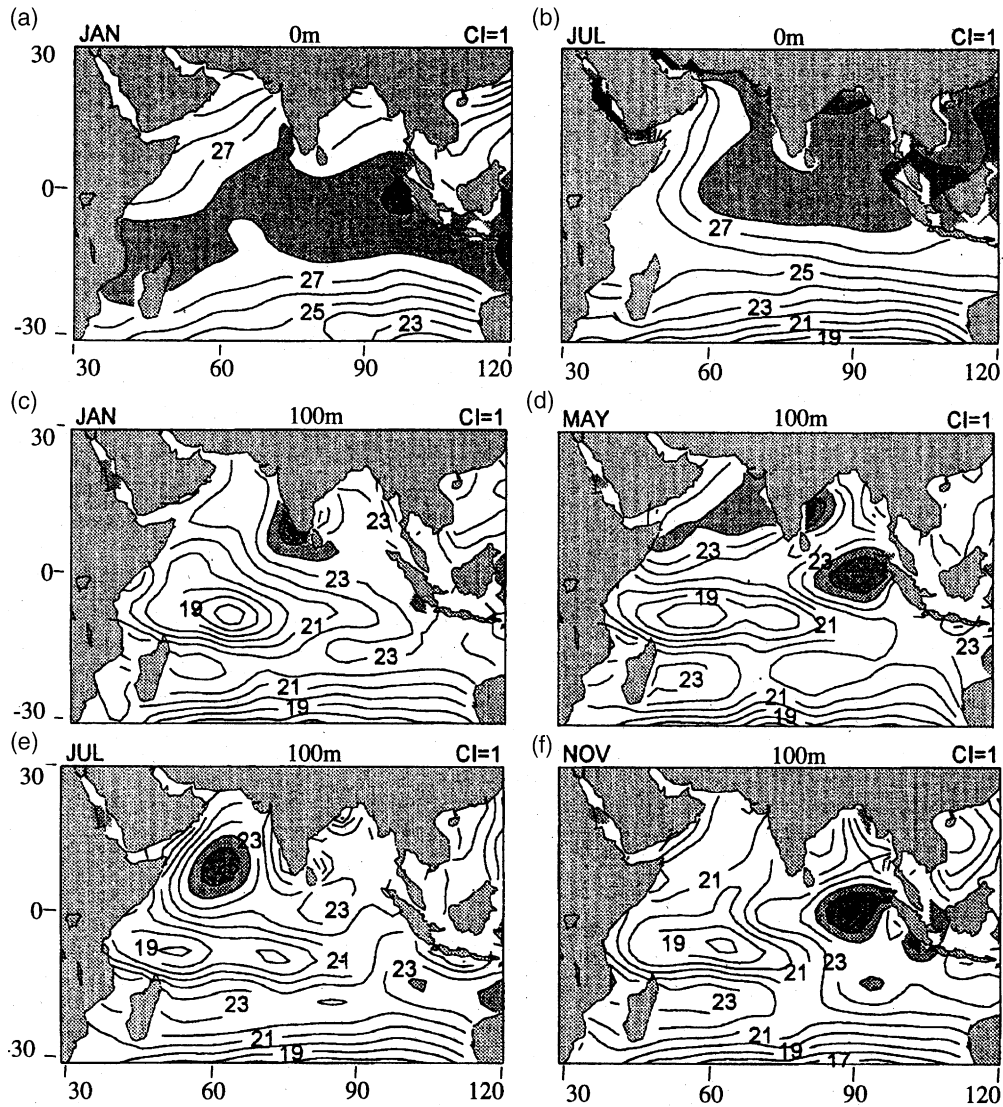


Fig. 15. Climatological temperatures at a,b) the surface during January and July; c–f) at 100 m depth during January, May, July and November; areas of relatively high temperatures are shaded. (From Rao & Sivakumar, 2000.)

high salinities at core densities (Fig. 7; Section 8). The dynamics of the two marginal seas are quite different. The Red Sea is deep and separated from the Gulf of Aden by a shallow sill, similar to the situation of the Mediterranean, whereas the Persian Gulf shoals northwards from the outflow channel. There is a seasonal cycle in the outflow of the Red Sea Water into the Indian Ocean for which a winter maximum has been documented (Murray & Johns, 1997); its further spreading as a core layer can be traced as a salinity maximum well into the Mozambique Channel. A seasonal modulation of the outflow is even traceable underneath the northern Somali Current, but is probably driven by the Arabian Sea monsoonal forcing.

*Meridional overturning cells:* The schematic monsoon circulation diagrams presented above do not show the meridional overturning circulations that occur in the Indian Ocean. Two types of cells have been

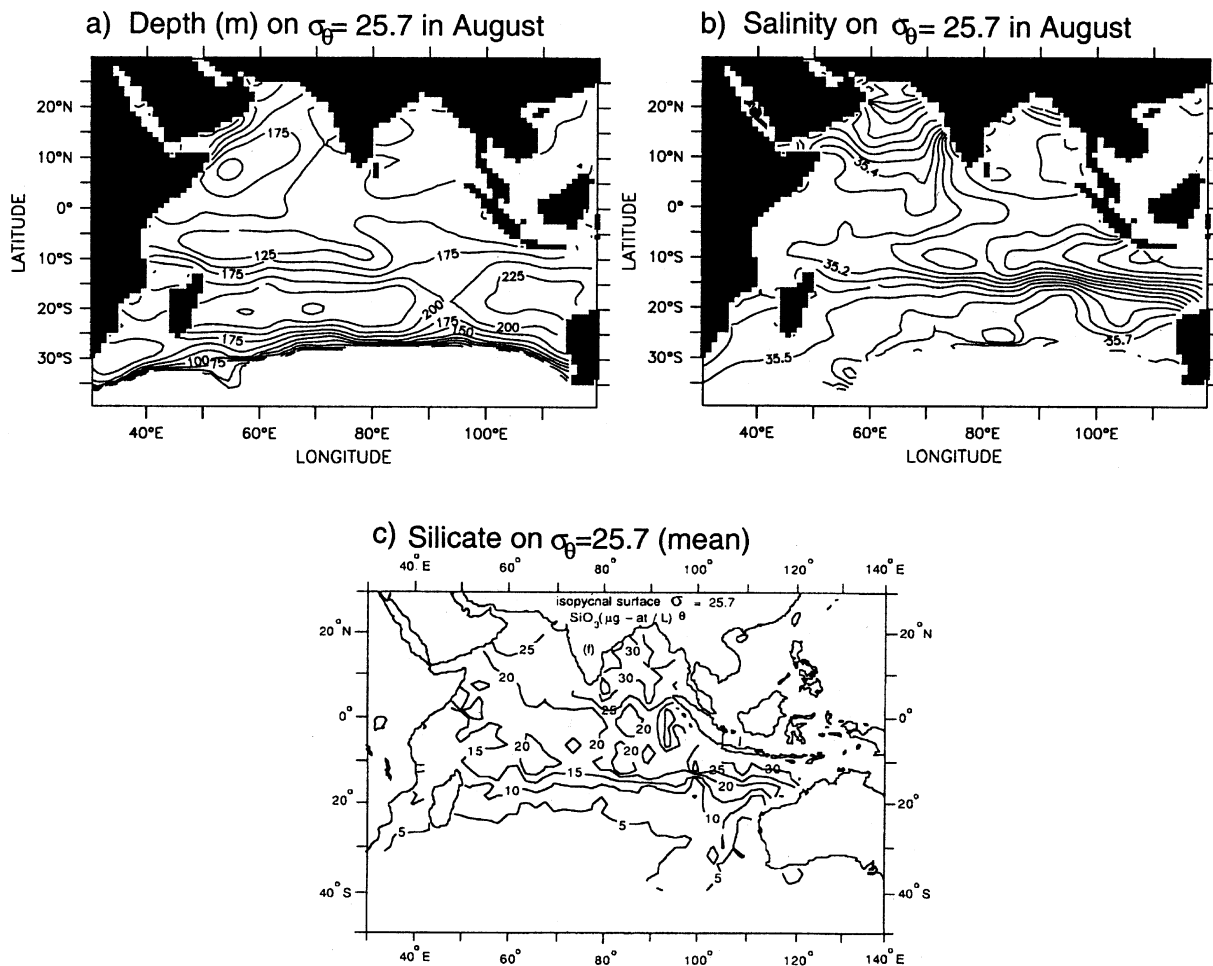


Fig. 16. a) Depth (Aug.); b) salinity (Aug.); c)  $\text{SiO}_3$  ( $\mu\text{g-at/L}$ ; annual mean) on the  $\sigma_\theta = 25.7 \text{ Kg m}^{-3}$  potential density surface.

discussed in the literature: firstly shallow overturning cells for which the pathways and the mechanisms are reasonably well understood and vary strongly with the monsoons; secondly a deep mean overturning cell for which there is compelling indirect evidence but little physical understanding.

Indirect evidence from water masses, circulation patterns and Ekman transports, as well as model results, suggest that the shallow cells carry cool thermocline water from subduction regions in the southern, subtropical Indian Ocean via the SEC, EACC, and Somali Current to the upwelling regimes off Somalia and Arabia. Southward return flow of surface water appears to cross the equator in the interior ocean by Ekman flows.

The deep inflow of Circumpolar Deep Water (Fig. 7) has two possible meridional routes for northward spreading, given the subdivision of the deep Indian Ocean by the Ninety East Ridge and Central Indian Ridge (Fig. 20): either through the Crozet and Madagascar basins in the west, or through the Australian Basin in the east. There is agreement among the results of different studies that there is a net northward inflow into the three closed basins, but the results differ widely as to the fate of this inflow. This deep cell is less close to the focus of our review, since it is mostly driven by thermohaline forcing. Nevertheless,

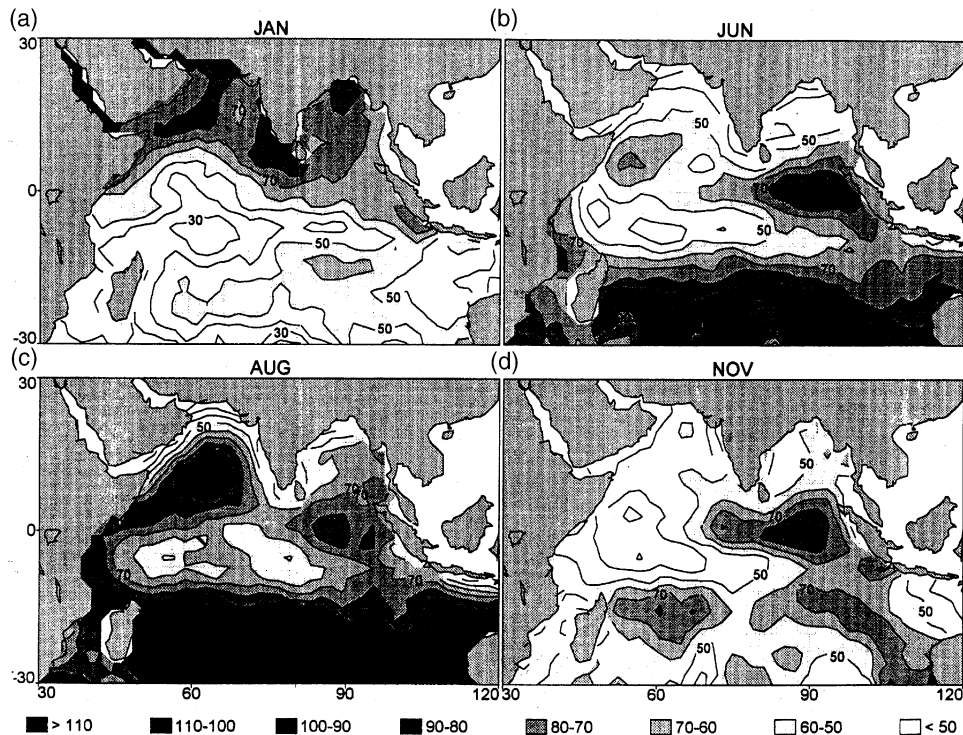


Fig. 17. Mixed-layer depths for a) January; b) June; c) August; d) November. (From Rao et al., 1989.)

the monsoon winds impose deep-reaching effects on the structure of the deep cell, sloshing water masses back and forth seasonally. For this reason, we comment on recent studies of this deep cell in Section 9.

### 3. Equatorial regime

The wind field that drives the equatorial Indian Ocean is unique in that its annual mean is weak and westerly, and its annual cycle has a strong semiannual component. Consequently, the equatorial currents are quite different in character to those in the other oceans, particularly in being relatively more variable. Here, we review work that has been carried out to understand prominent aspects of these wind-driven currents, namely, the development of surface jets and their reflection from the eastern boundary of the basin (Section 3.1), the development of the equatorial undercurrents (Section 3.2), and deep jets and vertically propagating signals (Section 3.3). Finally, we discuss the intraseasonal variability in the period range of a few weeks, commenting on remaining questions about its generation, either by mean-current instabilities or direct wind forcing (Section 3.4).

#### 3.1. Wyrski Jets

##### 3.1.1. Observations

Ship-drift climatology indicates that the surface currents in the equatorial Indian Ocean reverse direction four times a year, flowing westward during the winter, weakly westward in the central and western ocean during the summer, and strongly eastward during the spring and fall (Fig. 21a). The eastward currents

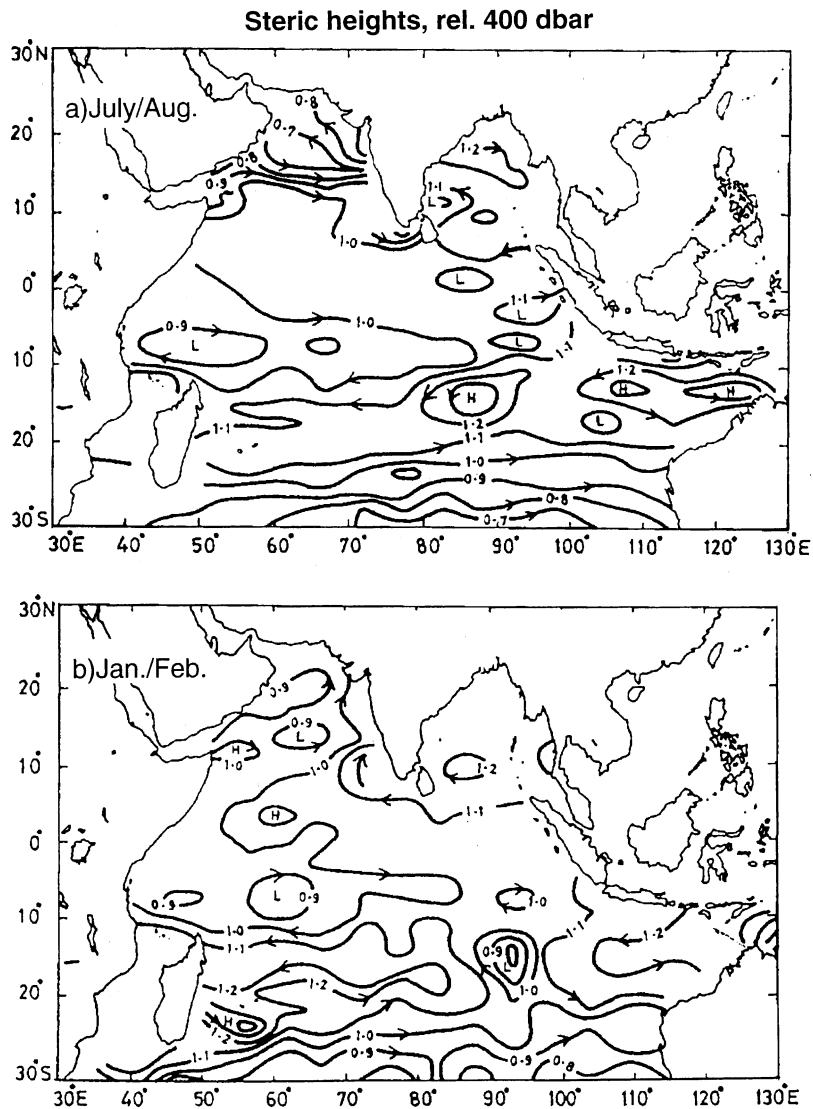


Fig. 18. Steric height distributions for a) July–August; b) January–February, relative 400 dbar, determined from a mixed hydrography and temperature (BT/XBT) climatology and using regional-mean T,S relations. (From Peter & Mizuno, 2000.)

were first identified by Wyrki (1973), and they are now commonly referred to as either Wyrki Jets (WJs) or Equatorial Jets (EJs). The two WJs have roughly the same strength of about 100 cm/s, being somewhat stronger in the fall than in the spring in the smoothed data of Fig. 21a. As shown later, the intraseasonal and interannual variability of the WJs can be large; hence, the relative strengths of the two jets in seasonal-mean displays depend on which observations are averaged into the climatology. Maximum speeds in the unsmoothed data can exceed 120 cm/s, as observed in the ADCP observations of Reppin et al. (1999) for the fall 1993 WJ (Figs. 22 and 23), but it has to be noted that 1993–94 was an anomalous year for the zonal forcing and WJs (Fig. 5).

Currently, the ship-drift observations are the only data set that is sufficiently long to estimate a reliable WJ climatology. These data were recently discussed by Han, McCreary, Anderson, and Mariano (1999).

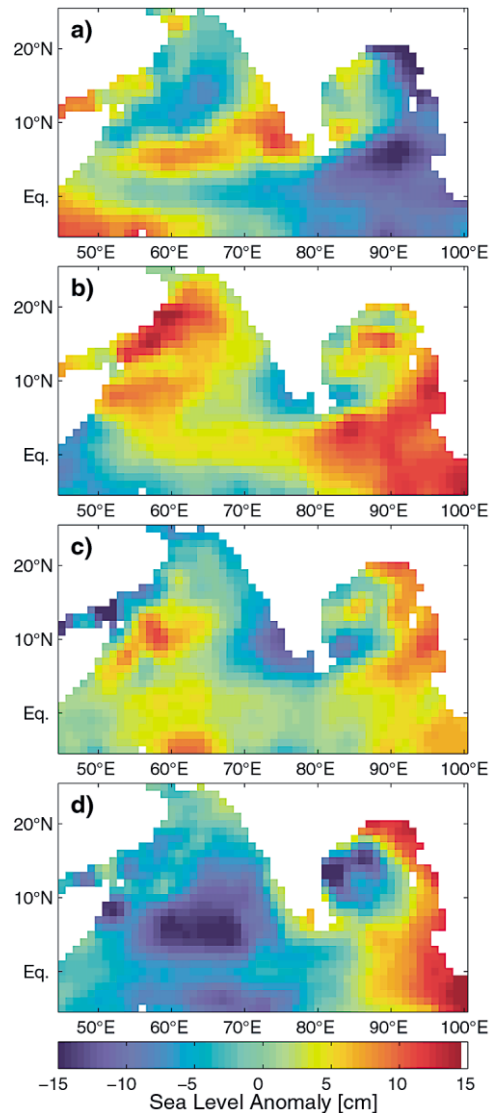


Fig. 19. Monthly-mean anomalies of sea surface height from T/P altimetry for a) February; b) June; c) August; d) November. Maps are means for 1992–99 but without the anomalous years 1994 and 1997. See Section 2.3 for details. (Courtesy P. Brandt.)

The total currents in Fig. 21 are dominated by contributions from their time-averaged mean, annual, and semiannual Fourier components (>85%). The mean flow is eastward in the interior ocean, attaining a maximum speed of about 30 cm/s at 80°E (Fig. 21b). The maximum amplitude of the annual component occurs at the western boundary in the annually reversing Somali Current, but there is also a significant relative maximum (25 cm/s) in the central ocean (Fig. 21c). The maximum amplitude of the semiannual component (Fig. 21d) occurs in the central ocean (70 cm/s), and is nearly three times as strong as the annual component there. Higher-frequency contributions do not have an organized structure, and hence appear to be noise. Their contribution to the total current, however, is not insignificant. For example, a superposition of the mean, annual and semiannual components in Fig. 21 produces a fall WJ that is about

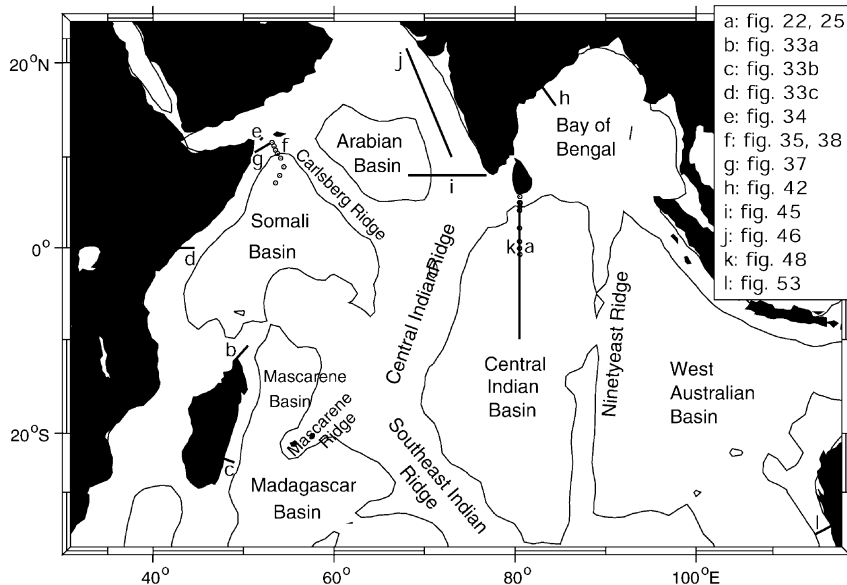


Fig. 20. Map of Indian Ocean basins and topographic ridges, showing is the smoothed 4000 m depth contour. Also shown are locations of current meter arrays and hydrographic sections with the number of the corresponding figure listed in the inset.

30 cm/s stronger than the spring one; it is the high-frequency components (primarily the 4-month variability) that eliminates this tendency.

The WJs transport surface waters eastward over a time period of two months, decreasing the mixed-layer thickness and sea level in the west but increasing them in the east; see Fig. 17b,d for layer thickness, and Fig. 15d,f for the eastern warming and western cooling at the 100 m level, and Fig. 19b for sea level oscillations. After arriving at the eastern end of the basin, part of the WJ signal is reflected as Rossby waves, and part propagates polewards as eastern-boundary waves. Along the way, the eastern-boundary waves generate slowly-propagating mid-latitude Rossby waves that radiate into the Bay of Bengal and eastern Arabian Sea (Perigaud & Delecluse, 1992; Basu, Meyers, & O'Brien, 2000; see the discussion in Sections 4 and 5). As models suggest, the northward-traveling boundary waves carry equatorial variability around the margin of the Bay of Bengal and even around Sri Lanka into the Arabian Sea, but so far this has not been confirmed by observations. Southward-traveling WJ signals that have also been observed recently affect the Indonesian boundary and throughflow regime (Sprintall, Gordon, Murtugudde, & Susanto, 2000).

Clarke and Liu (1993) investigated the seasonal sea-level cycle at the eastern end of the equatorial Indian Ocean using tide-gauge data, and they found a large difference between the annual and the semiannual components. While the semiannual components, with amplitudes of about 5 cm and maxima in May and November, were in-phase for stations between 8°N and 8°S, the annual components were out-of-phase across the equator with maximum amplitudes of about 10 cm. They concluded that this semiannual signal was largely a response to the reflection of equatorial Kelvin waves and that the annual cycle was determined by the alongshore monsoonal winds. These winds are southeasterly from April to September, raising sea level in the northern hemisphere and lowering it in the south, but during the other half of the year the wind and sea-level gradient are directed oppositely. They excite coastally trapped waves that radiate poleward from the equator, thereby establishing an alongshore pressure-gradient field that balances the wind. Morrow and Birol (1998) also reported a large annual reversal in sea-level in the open ocean offshore

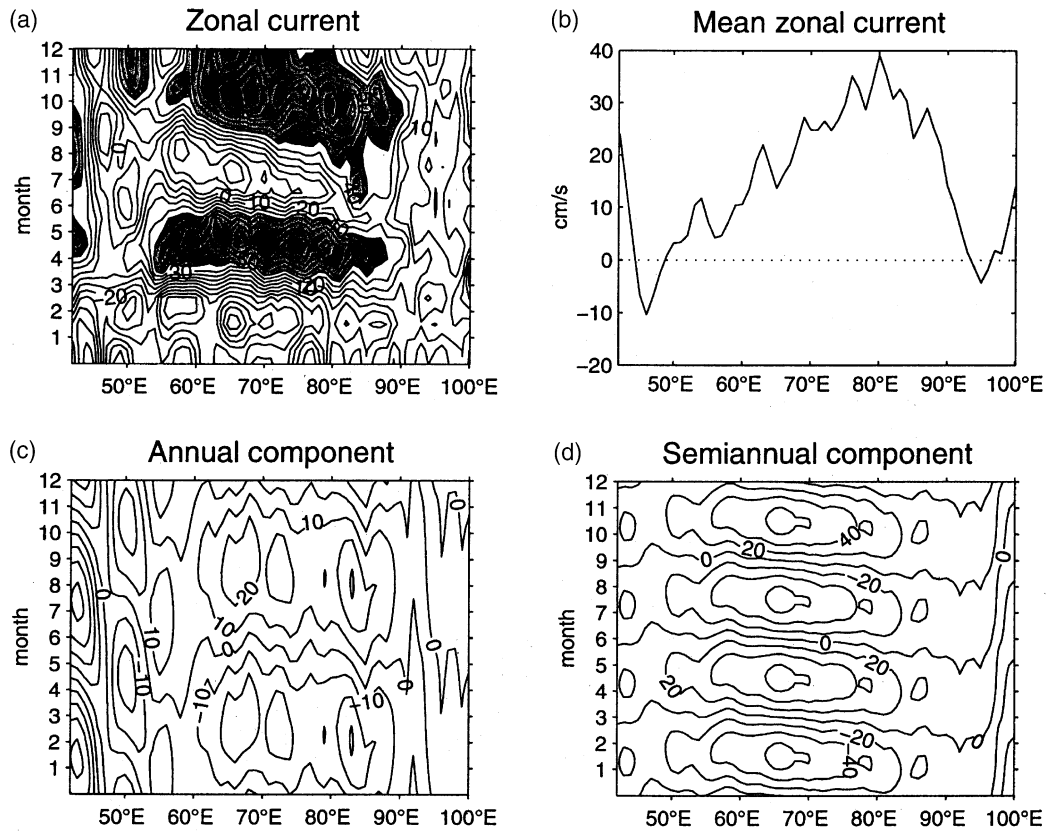


Fig. 21. Longitude-time plots of zonal currents in the 1°S–1°N latitude band, showing the a) total current; and its b) annual-mean; c) annual; and d) semiannual components. (After Han et al., 1999.)

from South Java, which indicates that processes other than forcing by the alongshore winds and coastal-wave propagation are also involved in the seasonal adjustment.

### 3.1.2. Models

A number of modelling studies have sought to identify the forcing mechanisms of the WJs, and to assess their relative importance. In his original paper, Wyrtki (1973) suggested that the eastward jets are forced directly by the equatorial westerlies between the two monsoons. Shortly after, O'Brien and Hurlburt (1974) used a 2-layer model to demonstrate that a strong eastward jet does develop as a direct response to switched-on westerlies. They also noted that Rossby waves reflected from the eastern boundary of their model basin were an important part of the equatorial response, that tended to cancel the directly forced eastward jet two months after the wind onset.

Based on a current record obtained near Gan Island (0°41'S, 73°10'E), Knox (1976) and McPhaden (1982) confirmed the importance of direct wind forcing. Knox (1976) determined further that the pressure-gradient term was a significant part of the zonal momentum balance at Gan, indicating the importance of remote forcing by propagating equatorially trapped waves. McPhaden (1982) later noted the presence of signals with vertical phase propagation there, an almost certain indicator of wave propagation (see Section 3.3).

Cane (1980) studied equatorial currents using a 1½-layer model with a constant-thickness mixed layer

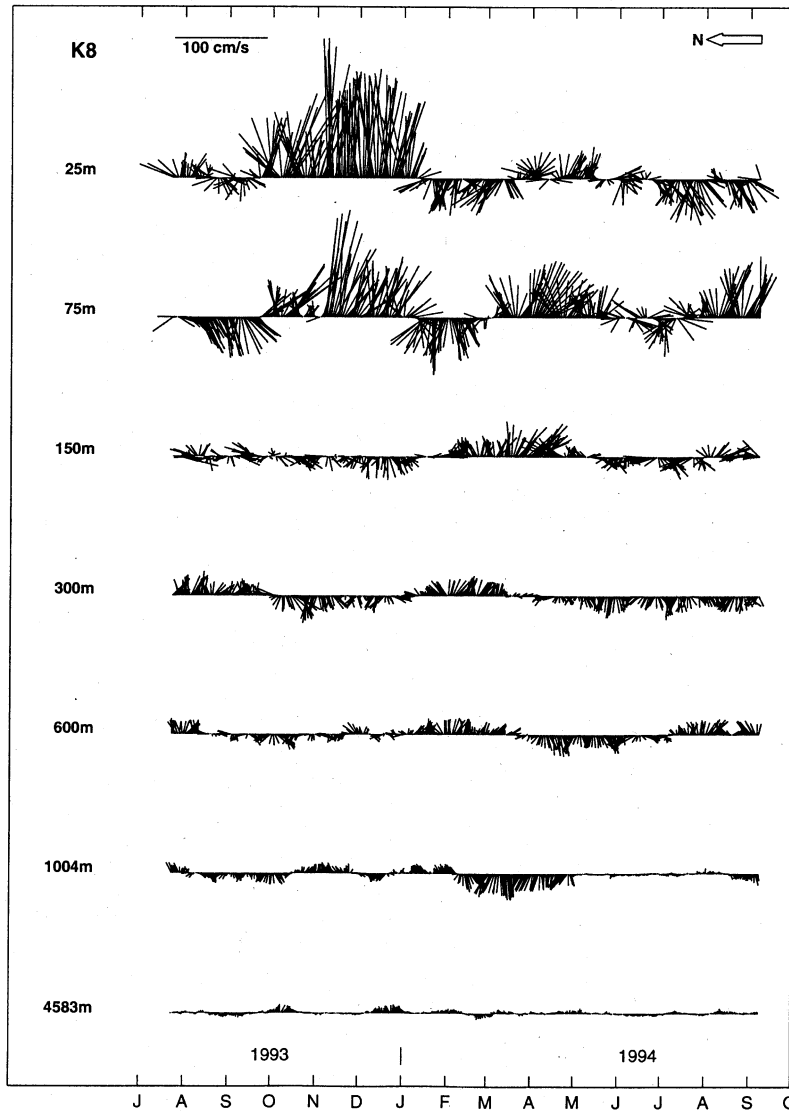


Fig. 22. Time series of 40-hour low-passed current vectors (up is eastward) for July 1993–September 1994 on the equator at 80.5°E for different depths. Instrumentation in the upper 600 m were two ADCPs and located below were 600 m rotor current meters. Note strong fall 1993 and weak spring 1994 Wyrki Jets. (After Reppin et al., 1999.)

imbedded in the active layer. Wind-driven surface jets were strengthened in his solutions, essentially by concentrating them within the thinner mixed layer. Reverdin (1987) reached the same conclusion in his study of annual variability in the Indian Ocean. He utilized a continuously stratified, linear model in which the mixed layer was parameterized as a region of constant density at the top of a prescribed background density profile. The WJs were stronger when this region was thinner.

As noted above, reflected Rossby waves weaken the directly forced interior jet when the wind is switched-on. When the wind is periodic, however, the Rossby waves can enhance the interior flow if the wind, and hence the directly forced jet, reverse direction by the time the reflected waves propagate back

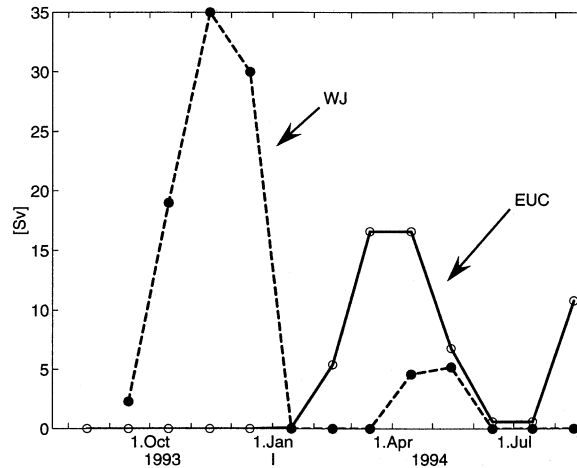


Fig. 23. Eastward transports of the Wyrтки Jet and Equatorial Undercurrent, determined from the moored array at 80.5°E. (From Reppin et al., 1999.)

into the interior ocean. Indeed, Cane and Sarachik (1981) demonstrated that a single baroclinic mode can resonate with the forcing in this way. Essentially, resonance occurs when the period of the oscillation is a multiple of the time it takes a Kelvin wave to cross the basin and a first-meridional-mode ( $l=1$ ) Rossby wave to return. (Also see Cane & Moore, 1981, who obtained an elegant closed expression for such a resonant mode). Jensen (1993) argued that resonance of this sort involving the second ( $n=2$ ) baroclinic mode accounted for the relatively large amplitude of the semiannual response in his  $3\frac{1}{2}$ -layer Indian-Ocean model.

Recently, Han et al. (1999) obtained solutions to a hierarchy of ocean models ( $2\frac{1}{2}$ -layer to  $4\frac{1}{2}$ -layer, linear and nonlinear systems) designed to isolate each process that drives the WJs, and to estimate the relative contribution of each to the total response. To illustrate their analyses, Fig. 24 shows a decomposition of the upper-layer, equatorial, zonal velocity field from their linear,  $2\frac{1}{2}$ -layer solution into directly wind-forced and reflected-wave parts for the annual and semiannual harmonics, respectively. Note that the semiannual wind-forced component is considerably stronger than its annual counterpart (Fig. 24a,c), and that the two semiannual components clearly interfere for enhanced amplitudes in the central Indian Ocean (Fig. 24c,d). The authors concluded that direct forcing by the semiannual component of the wind is the dominant forcing mechanism of the WJs, accounting for 81% of their maximum amplitude. Almost half of this amount (35%) resulted from the models having a mixed layer, which concentrates the WJs into a thinner layer as in the Cane (1980) study. Precipitation during the summer and fall was an important process in this increase, strengthening the fall WJ in the eastern ocean by thinning the mixed layer by 50 m in some locations. Reflected Rossby waves and resonance contributed the remaining 19% to WJ strength.

### 3.1.3. Enhanced semiannual response

In Han et al.'s (1999) most comprehensive (realistic) solution, as well as the ship-drift data, the semiannual response is more than twice as large as the annual one even though the wind components have similar amplitudes. They concluded that the disproportionate response has several causes. One is the different zonal structures of the semiannual and annual winds, the more complex structure of the latter generating a weaker oceanic response (Fig. 24a,c). Another is the  $n=2$  mode being near resonance at the semiannual period (similar to the constructive interference in Fig. 24c,d), as also found in the earlier linear wind-forced model calculation of Clarke and Liu (1993). Finally, mixed-layer shear strengthens the semiannual response

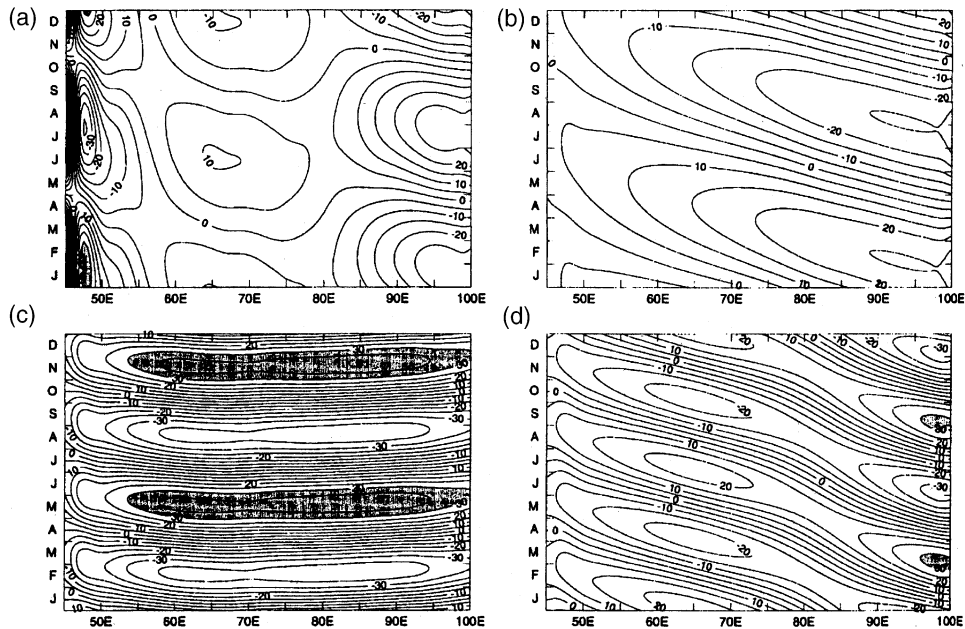


Fig. 24. Zonal velocities from the upper layer of a solution to a linear,  $2\frac{1}{2}$ -layer model, showing a) directly wind-forced, b) reflected wave components for the annual harmonic and c), d) for the semiannual harmonic. (After Han et al., 1999.)

but not the annual one, because the locally forced, shear-flow contribution interferes constructively (destructively) with the remotely forced, wave response for the semiannual (annual) component.

#### 3.1.4. Weak fall WJs

There are now a number of models forced by realistic winds that can simulate circulations throughout the Indian Ocean quite well. Typically, however, these solutions have fall WJs that are weaker than the spring ones, particularly in the eastern ocean (Anderson, Carrington, Correy, & Gordon, 1993; MKM, Jensen, 1993; Han et al., 1999). In all of these solutions, the underlying reason for this difference in strength is that the annual component of the winds drives a response that tends to strengthen the spring WJ but to weaken the fall one. Interestingly, the ship-drift data do not exhibit the same tendency, showing WJs of roughly equal strengths.

The reasons for this model/data discrepancy are not clear. One possible explanation is inaccuracies in the wind fields. As noted in Section 2.1, there are considerable differences between wind-stress climatologies (Fig. 3). Anderson and Carrington (1993) compared equatorial observations with results of their primitive-equation model, driven by different wind products. They obtained a weaker fall jet using the HR wind stresses, but a stronger fall jet when applying the UKMO winds (Fig. 26a,b). Han et al. (1999) also reported the sensitivity of their solution to different wind products. Another possible explanation for the model/data discrepancy is errors in the ship-drift climatology because of windage, or there could be an affect of the large interannual variability of the equatorial currents (see Section 10) on the mix of fall and spring observations being averaged into the climatology of Fig. 21.

#### 3.2. Undercurrents

In the other oceans, the EUC is defined to be the quasi-permanent eastward current at the top of the thermocline, driven by the eastward pressure-gradient force caused by prevailing easterlies. The surface

current above the EUC is typically westward. In the Indian Ocean, the situation is different because of the large, seasonally varying component to the forcing. An obvious indication of this difference is that equatorial upwelling, a key property of the permanent EUCs in the other oceans, is absent in the eastern Indian Ocean (or anywhere else along the equator). Another indication is their highly transient nature, which contrasts with the quasi-steady nature of the Atlantic and Pacific EUCs. In fact, the Indian Ocean EUCs are better viewed as transient equatorial-wave phenomenon, rather than features of the mean circulation. Here, then, we define EUCs more generally, as being any current cores at the upper thermocline level that lie beneath opposite-flowing surface currents, or more generally, even below weaker surface currents of the same direction. Note that with this definition EUCs can be either eastward or westward.

### 3.2.1. Observations

An eastward EUC is only observed consistently during boreal spring. An EUC was first documented by Taft (1967) at several positions along the equator between 53°E and 91°E during the months of March and April, 1963, but was not detected during the Southwest Monsoon of 1962. Swallow (1967) reported the existence of a shallow EUC in March, 1964, at 58°E and 67.5°N, but by April the surface-layer flow had reversed (the springtime Wyrtki jet) and the ‘classical’ EUC vanished. Similarly, Knox (1976) reported an EUC with westward surface flow in March, 1973, at Gan Island near 73°E, but no such EUC occurred in the spring of 1974. Sections across the equator by a small vessel were carried out at 55°E by Leetmaa and Stommel (1980), who confirmed the existence of the EUC in boreal spring during both observational years, 1975 and 1976. They also reported a meandering of the EUC, whereby its core was at times displaced by more than 100 km south of the equator.

A number of cross-equatorial ADCP sections were carried out in the 50–60°E longitude band during the WOCE cruises of April to September, 1995. In April, 1995, the ‘Meteor’ cruise M32/1 found a well developed undercurrent at 57°E with the equivalent of an Equatorial Intermediate Current in the depth range from 200–500 m. In June, the flow at the undercurrent level reversed, so that by August all currents above 200 m were directed westward on the equator (Schott, Fischer, Garternicht, & Quadfasel, 1997; Walter, 1997).

Reppin et al. (1999) reported moored ADCP observations from the region south of Sri Lanka for June, 1993 to August, 1994. One of the moorings was located on the equator with both an upward- and downward-looking ADCP, hence providing good vertical resolution from 25–700 m. The monthly-mean zonal velocities for the upper 150 m of these observations (Fig. 25) showed that there was an EUC between 50–150 m from February to May, 1994. As expected, it disappeared in June, but, contrary to earlier assumptions about the extent of the EUC season, it reappeared again in August, although at a shallower depth and with less transport (Fig. 23). Westward flow was observed at the same time during 1993.

### 3.2.2. Models

Modelling studies forced by idealized winds demonstrate that an EUC structure can develop in the time it takes equatorially trapped Kelvin and Rossby waves to propagate across the zonal extent of the basin, or of the wind itself for a wind patch confined within the interior of the basin, thereby establishing the necessary pressure gradient to drive the flow (Philander & Pacanowski, 1980; McCreary, 1985). The studies suggest further that, because of nonlinear effects, eastward EUCs are more likely to occur than westward ones. In different wind-stress climatologies, patches of easterly (and westerly) winds occur at different locations, times and intensities, and consequently different EUCs might be expected in solutions driven with different wind products.

Overall, numerical models are able to simulate the springtime appearance of the eastward EUC in the Indian Ocean, that is, to develop a current structure with surface westward flow and subsurface eastward flow at the thermocline level. For example, Anderson and Carrington (1993) found that the springtime EUC (Fig. 26d) was quite similar in solutions forced by either HR or UKMO winds (Fig. 26a), but that

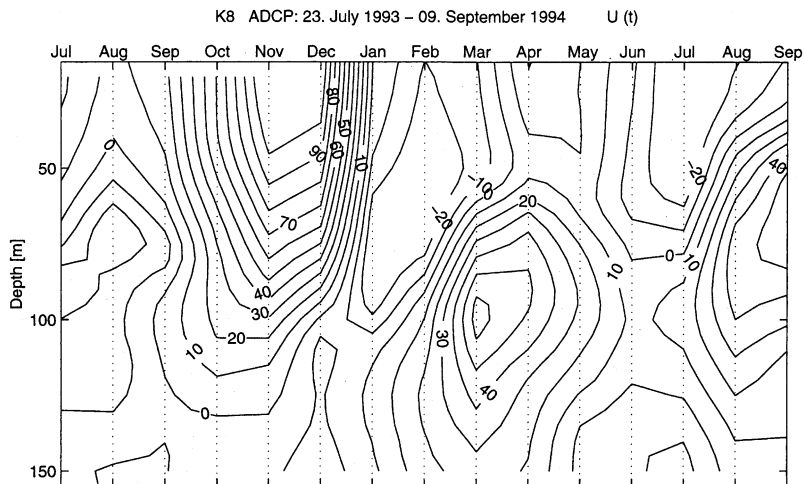


Fig. 25. Monthly-mean zonal current components in upper 150 m at 80.5°E on the equator, measured by upward-looking ADCP (also see Fig. 22) showing eastward WJs in boreal fall 1993 and spring 1994, and eastward EUCs during February–May 1994 and at a shallower depth in August 1994 (see also transports of Fig. 23).

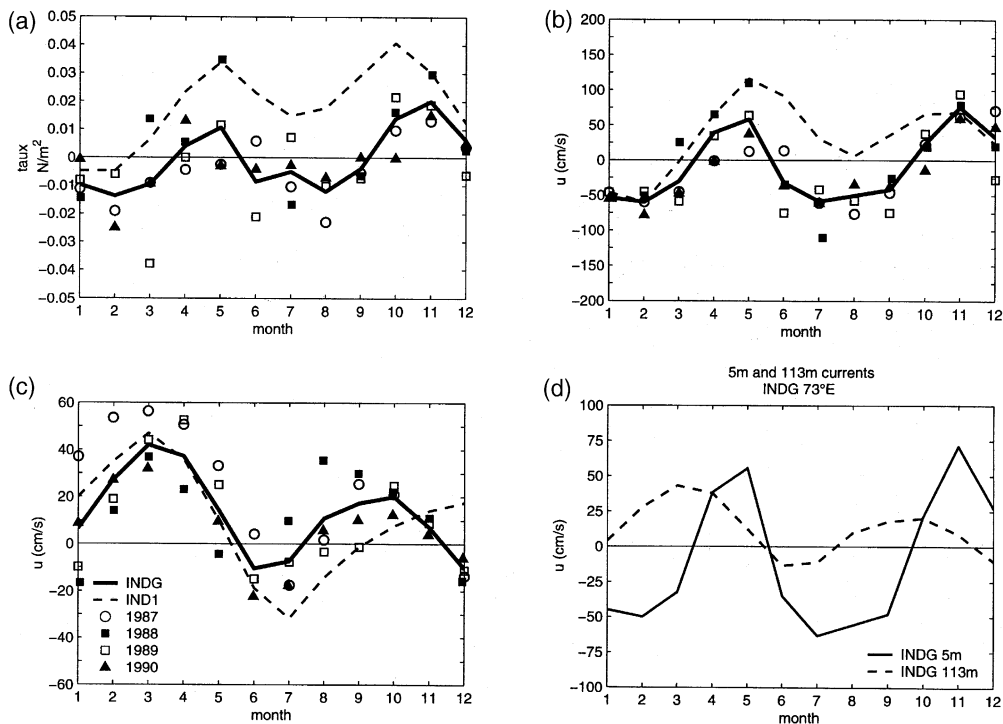


Fig. 26. a) Wind stresses on the equator at 73°E from HR (dashed) and UKMO (1987–90; heavy) climatologies; b) surface model currents for winds of a); c) currents at 113 m, the level of the EUC; and d) model currents of b) and c) plotted together for the HR forcing case, showing the EUC character for January–March and August–September. Realizations for the individual years are also shown (see lower left). (After Anderson & Carrington, 1993.)

the surface jets were rather different (Fig. 26b). The seasonal cycle in Fig. 26d also shows that currents at the EUC level are eastward throughout most of the year, but they do not have an undercurrent character when overlaid by the stronger surface WJs. A distinct undercurrent structure was achieved again from August to September, when the surface current is again westward. There were several such years in which an eastward EUC reappeared during the fall.

Several models have obtained a westward undercurrent structure that begins to form in May (Fig. 27) and persists throughout the summer monsoon (Jensen, 1991; MKM). It is most pronounced in the west, and Jensen (1991) commented that its arrival at the western end was the cause of the disappearance of the northward Somali coastal undercurrent in spring (see Section 4.3). The MKM solution developed a ‘classical’ Equatorial Undercurrent (EUC) structure during January, February, and March. Han (1999; pers. comm.) forced a  $4\frac{1}{2}$ -layer model with monthly-mean NCEP/NCAR reanalysis winds for the time period 1988–98, and found the reappearance of the EUC during fall 1994, in agreement with the Reppin et al. (1999) observations. In fact, there were several years in Han’s model analysis when the EUC reappeared in boreal fall in the central Indian Ocean. It is transient waves, however, that determine the nature of the zonal current profiles and with them the occurrence of subsurface maxima varying along the extent of the equatorial Indian Ocean in model simulations. This variation suggests that care has to be taken in drawing conclusions about the zonal extent of the EUC from observations at specific longitudes.

### 3.3. Vertically propagating waves and deep equatorial jets

#### 3.3.1. Observations

**3.3.1.1. Deep jets:** Luyten and Swallow (1976) were the first to draw attention to the fact that the deep flow along the equator is remarkably complex. They reported a set of velocity profiles taken in the western Indian Ocean during May and June of 1976. The currents were characterized by small vertical scales throughout the water column, and were trapped within a few degrees of the equator. In addition, all the profiles were similar, suggesting that the predominant time scales of the deep currents were longer than one month. In a subsequent analysis, Ponte and Luyten (1990), using coordinates stretched by the Vaisala frequency according to WKB theory, determined a spectral peak at 450–550 ‘stretched’ meters (sm). Similar signals were subsequently discovered in the other equatorial oceans, as well.

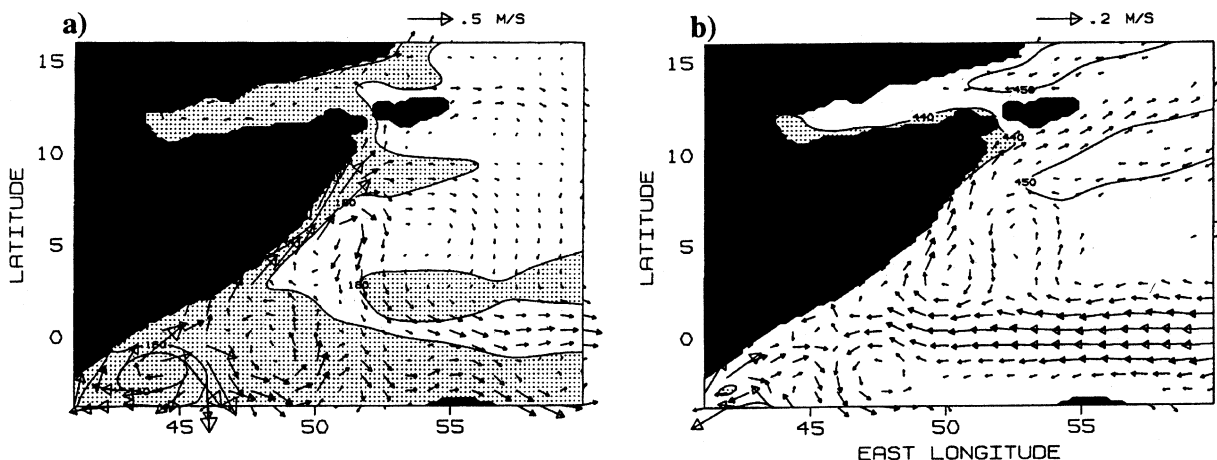


Fig. 27. Model currents for mid-May from seasonally driven 312 layer model run of Jensen (1991) for a) upper layer and b) second layer, showing a westward undercurrent in the western basin in second layer.

During the WOCE cruises of 1995, a number of sections across the equator were obtained with direct current observations by an LADCP and a Pegasus profiler, which confirmed the vertical structure of these deep equatorial jets. Dengler and Quadfasel (2002), using Pegasus profiles from a section crossing the equator at 80.5°E, south of Sri Lanka, determined a vertical scale of 650 m, suggesting that there is a vertical broadening of the jets toward the east. They showed the zonal velocity and vertical displacement field of the jets to be consistent with a high ( $n=16$ ) vertical mode, first-meridional-mode, long-wavelength, equatorial Rossby wave. They also noted certain differences between the Indian Ocean deep jets and those observed in the Pacific. In the Pacific, deep-jet reversals have not been reported, whereas in the Indian Ocean such a reversal was observed in profiles collected 2.5 years apart at 80°E and another occurred between April and August 1995 in the ‘Meteor’ sections at 57°E. Furthermore, the Indian-Ocean jets are more pronounced at depth than those in the Pacific below 2000 m (e.g., Muench, Kunze, & Firing, 1994).

*3.3.1.2. Penetration of the seasonal cycle:* From his analysis of current-meter data from Gan Island at 73°E, McPhaden (1982) concluded that the phase associated with semi-annual variations propagated upward, a certain indicator of the presence of a downward-propagating free wave. Luyten and Roemmich (1982) reported both upward and westward phase propagation along the equator in their equatorial current-meter array located from 47°E to 62°E, and concluded that a downward-propagating, first-meridional-mode, Rossby wave was present in their data. In the moored current observations reported by Reppin et al. (1999), the annual plus semiannual harmonics were found to make up a large part of the deep current variance, and again upward phase propagation was confirmed. The vertical scale of this signal is large, of the order of one cycle or less over the basin depth. This scale is very different from that of the deep jets, indicating that they are distinctly different phenomena. Vertically propagating signals of this scale have also been reported in other oceans, e.g. the annual wave in the equatorial Pacific (Lukas & Firing, 1985; Kessler & McCreary, 1993).

### *3.3.2. Models*

In an effort to explain the Luyten and Swallow (1976) observation of deep jets, Wunsch (1977) obtained solutions to a linear, continuously stratified model. He found analytical solutions for an unbounded basin, representing them as expansions in Hermite functions. The model was forced by a surface distribution of vertical velocity (presumably driven by the wind) that had the form of a westward-propagating sinusoidal wave with a period of one year. In qualitative agreement with the observations, the solutions had a rich vertical structure that was narrowly confined to the equator.

The Wunsch (1977) model, however, was very specialized in that it was limited to zonally periodic forcing, and consequently it was not possible to tell the precise location of the surface region where the deep energy was generated. McCreary (1985) reported a series of solutions forced more realistically by wind patches (i.e., the forcing was of limited zonal extent) oscillating at fixed periods. His solutions illustrated how wave energy generated by the wind at the ocean surface propagates into the deep ocean along ray paths. There was a different ray path for each wave type, namely, Kelvin waves and a suite of Rossby waves associated with each particular meridional wavenumber  $l$ . These ray paths were identifiable as distinct ‘beams’ of energy descending into the deep ocean at the angles  $\sigma/N_b$  for the Kelvin beam and  $-(2l+1)(\sigma/N_b)$  for the Rossby beams, where  $N_b$  is the value of the local Vaisala frequency. Solutions demonstrated that the deep-jet character of Wunsch’s (1977) solutions only existed because of the zonally periodic nature of his forcing.

Indeed, it is fair to say that there is still no adequate explanation for the deep jets, although other modelling studies have attempted to account for them (McCreary & Lukas, 1986; Hua, Moore, & Le Gentil, 1997). How, for example, can existing stacked jets be maintained despite the kinetic energy losses resulting from dissipation or reflection at boundaries. As Muench and Kunze (2000) showed, energy transfer between

the internal wave field and the deep jets can occur through momentum flux divergence and internal waves encountering vertical critical layers.

On the other hand, the concept of beams is likely to explain the presence of downward propagating, annual and semiannual waves. The idea has been successfully used to explain similar signals in the Pacific: Kessler and McCreary (1993) used a model based on that of McCreary (1985) to interpret the observed vertically propagating, annual signal in the Pacific as being an  $l=1$  Rossby beam generated by zonal winds in the central and eastern equatorial ocean. An analogous model/data comparison, however, has not yet been carried out for the Indian Ocean.

### 3.4. Intraseasonal oscillations

#### 3.4.1. Observations

Already in earlier observations, strong fluctuations were reported from the tropical Indian Ocean with distinct spectral peaks in frequency bands higher than the seasonal. For example, a strong energy maximum was found at a period centered about 27 days in the meridional velocity field of the current-meter records of Luyten and Roemmich (1982) from the western equatorial Indian Ocean near 60°E (Fig. 28c,d). By

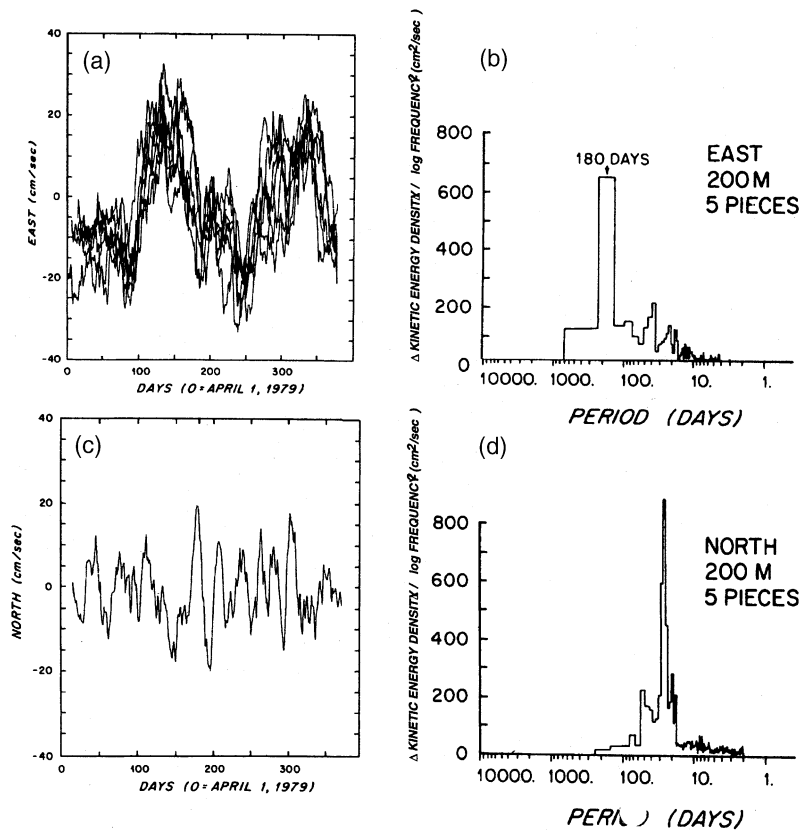


Fig. 28. Intraseasonal oscillations observed in subsurface moored current observations in the equatorial Indian Ocean at 50–62°E: a),c) time series of the zonal and meridional current components from 200 m depth and b),d) variance-conserving spectra for both components. Note that the zonal currents are dominantly semiannual, while the meridional currents show a dominant period at 27 days, indicative of intraseasonal Yanai waves. (From Luyten & Roemmich, 1982.)

contrast, the zonal currents showed a dominant semiannual component (Fig. 28a,b). In addition, there was clear upward and westward phase propagation in the meridional velocity records: The currents were more energetic at the surface than at depth, and at a depth of 200 m they intensified to the east. The lack of a corresponding peak in the zonal current on the equator suggested that antisymmetric Yanai waves caused the signal, a conclusion that was also reached in a follow-up study by Reverdin and Luyten (1986) that included drifter trajectories. The oscillations exhibited strong seasonality, beginning in August and continuing until February. These in situ results were later supported by the satellite SST analysis of Tsai, O'Brien, and Luther (1992), who found a dominant peak at 26 days in oscillations in the western basin that were antisymmetric about the equator and had an amplitude maxima at  $3^\circ$  latitude, in good agreement with Yanai-wave characteristics. Their seasonal maximum occurred from July to September.

Recently, shorter-period variability with a period of about two weeks was reported by Reppin et al. (1999) from moored ADCP measurements on the equator near  $80^\circ\text{E}$ . Fig. 29a,b shows time series of the filtered zonal and meridional current components in the near-surface layer for a period of about one year. The intraseasonal energy peak in the meridional component of this record was at 14 days (Fig. 29c) when calculated for the entire record length, and the seasonal maximum occurred from September to November. The 14-day peak also was present in the zonal component, in addition to the semiannual harmonic. At the same time, wind variability at a nearby surface buoy was also at a maximum in the 14-day band, suggesting that these signals were generated by local forcing. An equatorial-wave fit to the current observations showed that much of the variance was explained by Yanai waves, but that some Kelvin-wave energy was also involved (J. Reppin, 1999; pers. comm.). There is also energy at longer intraseasonal periods in the record that is mostly in the zonal component, with peaks near 23 days for the first 6 months and at 30–40 days for the last 6 months. This intraseasonal frequency behavior of the central Indian Ocean is obviously quite different from the earlier findings reviewed in the previous paragraph.

### 3.4.2. Models

Moore and McCreary (1990) used a linear, continuously stratified model to investigate the equatorial waves that are excited in the Indian Ocean by wind fields oscillating at intraseasonal periods (30 and 60 days). Fig. 30 shows an equatorial section from their solution forced by a zonal wind oscillating at a 30-day period. Kelvin and Yanai waves corresponding to several vertical modes superpose to carry energy downward along ray paths. One result is that there is a shadow zone near the western boundary, roughly bounded by the ray path from the bottom of the forced region at the western edge of the basin. The downward propagating energy extends all the way to the ocean bottom and reflects back. Because the waves evident in these solutions have short wavelengths, they are not directly forced by the broad-scale wind field. Rather, they are generated almost entirely at the western boundary of the model. The currents generated by the broad-scale wind impinge on the boundary and generate short-scale reflected waves there, as a result of the boundary condition of no normal flow.

The structure of this solution compares favorably with the observations of 27-day variability reported by Luyten and Roemmich (1982), suggesting that it captures the basic properties of the radiation field. In particular, the solution's shadow zone is consistent with the property that the observed variability strengthens to the east at a depth of 200 m. On the other hand, the model velocities in response to a realistic zonal wind-stress amplitude of  $0.25 \text{ dyn/cm}^2$  are much smaller than those observed. Moreover, the sharpness of the spectral peak in the velocity record is not at all reflected in the wind spectrum, which has little indication of any similar peak. These discrepancies support the idea that boundary-current instability is the more likely energy source for the oscillations.

Model simulations using  $1\frac{1}{2}$ -layer (reduced-gravity) models and driven by climatological winds were also able to reproduce the equatorial 27-day wave in the tropical western Indian Ocean (Kindle & Thompson, 1989; Woodberry, Luther, & O'Brien, 1989). The fluctuation was identified in both studies as a Yanai wave, for which Kindle and Thompson (1989) determined a dominant wavelength of 1000–1200 km in

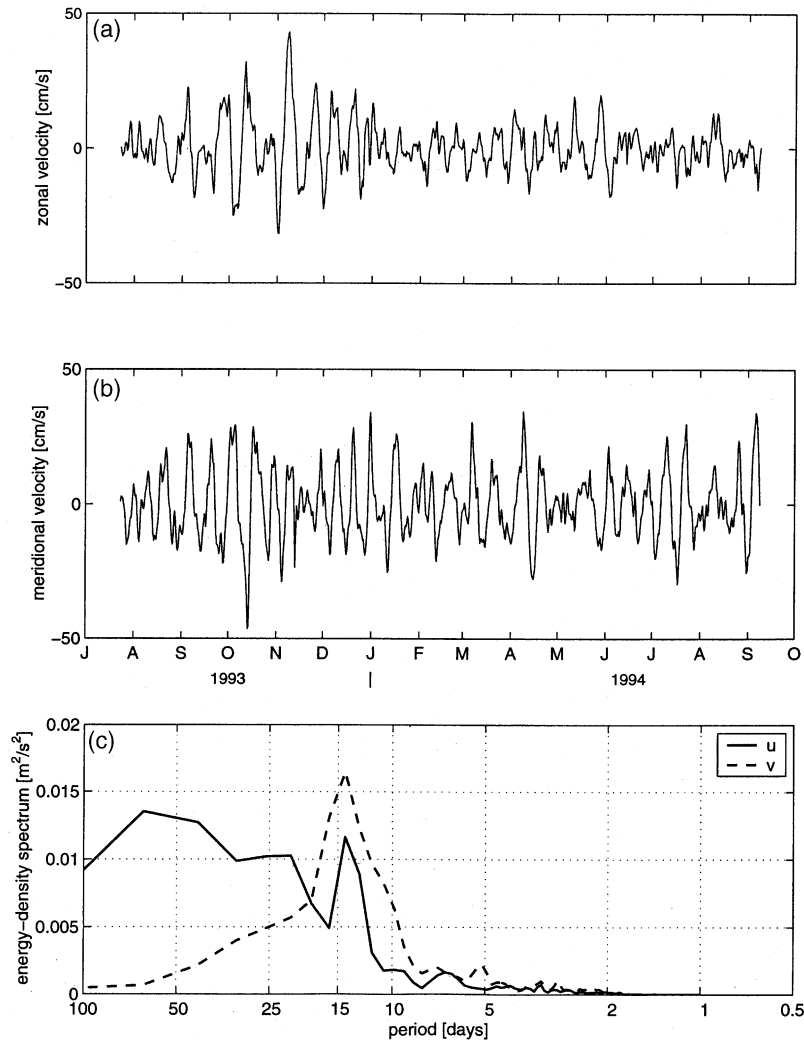


Fig. 29. Intraseasonal oscillations in the near-surface (25 m depth) moored observations 1993–94 on the equator at 80.5°E: a) zonal and meridional current time series, after filtering with 30d high-pass filter; b) spectrum of unfiltered timeseries. The dominant period is 14 days and it is present in both components.

the western basin. The strength of the oscillation weakened to the east, and its maximum amplitude occurred from summer to fall. Interestingly, the oscillations occurred despite the models being forced by monthly-mean wind stresses, so that their existence cannot be explained by direct wind forcing. In addition, since the  $1\frac{1}{2}$ -layer models used in these studies do not support baroclinic instability, barotropic instability is the only possible generation mechanism for the waves. Instability of the strong near-equatorial currents in the western ocean appears to be likely cause, but just which currents are involved (Southern Gyre, EACC, SECC, etc.) is not clear.

It is noteworthy that such instability waves are much less pronounced in more recent model simulations with high vertical resolution that are also forced by smoothed (monthly-mean) winds such as the POCM. Hence, it may be that the earlier  $1\frac{1}{2}$ -layer models, which do not allow baroclinic instability artificially enhanced barotropic instabilities. On the other hand, in a  $3\frac{1}{2}$ -layer model simulation forced by monthly-

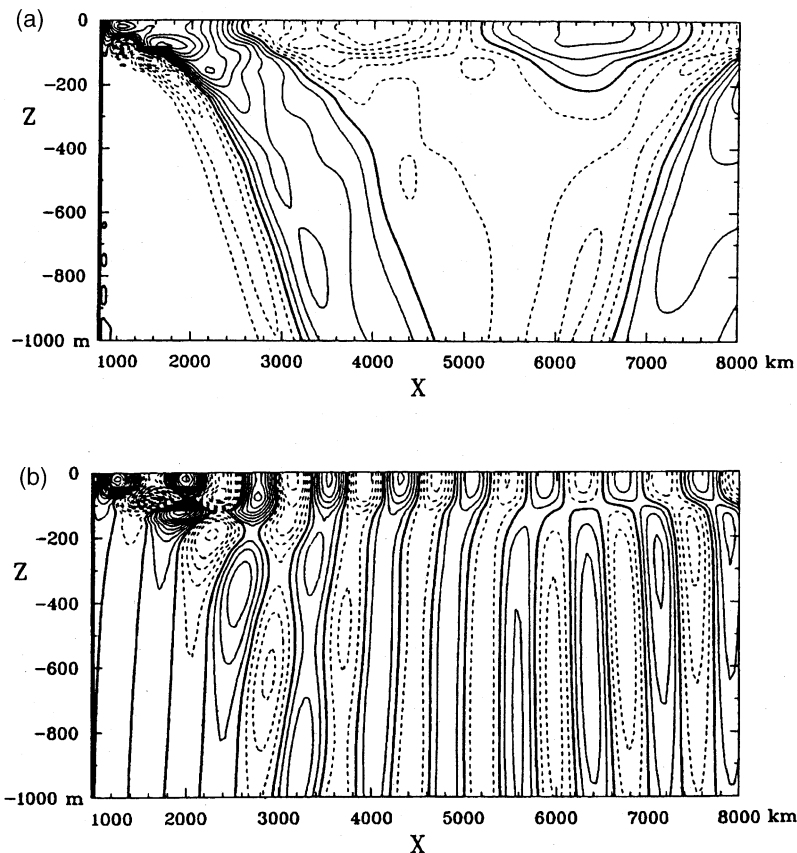


Fig. 30. a) Zonal currents along the equator from a solution for a semi-infinite basin forced by zonal winds oscillating at a period of 30 days. They are generated by Kelvin waves propagating into the deep ocean along ray paths, and there is a shadow zone in the subsurface western ocean; b) as a) but meridional currents forced by meridional wind fluctuations, and the waves are now Yanai waves. (After Moore & McCreary, 1990.)

mean climatological winds, Potemra, Luther, and O'Brien (1991) also obtained Yanai waves of about monthly period. Alternately, it may be that the vertical mixing inherent in the modern highly resolved GCMs is sufficiently strong to inhibit these instabilities.

In a recent study, Sengupta et al., (2001) forced a GCM with daily NCEP wind stresses, and obtained two interesting results concerning intraseasonal variability. First, there were fluctuations in the 12–15 day band, which were identified to be Yanai waves directly forced by the wind. This conclusion was verified in a test solution forced by winds that only contained the seasonal cycle, in which the short-period fluctuations did not exist. Second, they also found longer-period fluctuations, in the 30–50 day band, which were not directly wind-forced since they remained in the test solution. These oscillations were located in the western equatorial regime and in the central equatorial region around Sri Lanka. The authors concluded that they were generated in the central Indian Ocean by unstable currents, the instability occurring when Rossby waves propagating from the eastern ocean encountered the local, eastward mean flow. In the west, the intraseasonal fluctuations of the seasonally forced run are generated by boundary current instabilities that radiate eastward as Yanai waves, as in the earlier model studies noted above. The Yanai waves also propagate downward (as in Fig. 30), and thus were not contributing to the intraseasonal variability south of Sri Lanka.

#### 4. Somali Current and northern Arabian Sea

Historically, describing and understanding the remarkable annual cycle of the Somali Current system with its reversal of an entire current system (Fig. 31) has been one of the greatest challenges to face the Indian-Ocean oceanographic community, and much of this section is devoted to this topic. We begin with a review of the surface Somali Current during both monsoons (Sections 4.1 and 4.2), and then discuss evidence for Somali undercurrents and their dynamics (Section 4.3). Next, we consider circulations in the central Arabian Sea, commenting on their connection to the Somali Current and on the marked summertime deepening of the thermocline there (Section 4.4). Finally, we review circulations in the northern Arabian Sea (Section 4.5).

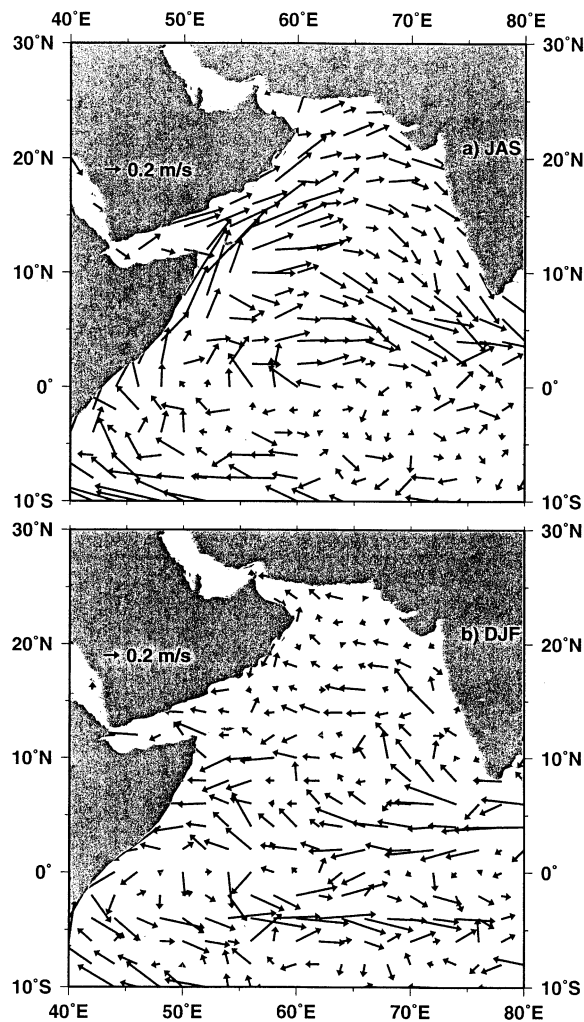


Fig. 31. Surface current vectors from drifter climatology for a) July–September; and b) December–February. (Courtesy A. Mariano.)

#### 4.1. Somali Current, summer monsoon

##### 4.1.1. Observations

The seasonal development of the Somali Current system was described by Schott et al. (1990). Their description is updated here, and illustrated schematically in Fig. 32. In subsequent chapters we comment on the physics of the individual phases.

*March–May:* Before the onset of the monsoon the southern Somali Current is an extension of the East African Coast Current (EACC) that flows northward across the equator to about 3–4°N. There, it turns offshore, and a cold wedge develops along its shoreward shoulder. Farther north, alongshore winds cause an upwelling regime to develop with a shallow northward coastal flow overlying a southward undercurrent (see Section 4.3). Its width scale is of the order of 50–100 km.

*June–July:* With the monsoon onset in June, the ‘Great Whirl’ develops from 4–10°N, and a second cold wedge appears at the latitude where it turns offshore (10–12°N). Schott and Quadfasel (1982) discussed observations from moorings in the northern Somali-Current regime. During their observational year there was a sudden onset of the monsoon, and they reported there were distinct westward-propagating signals after the onset. They interpreted them as first-mode Rossby waves, and concluded that the onset of the Great Whirl was a response to the very strong anticyclonic wind-stress curl offshore from the Somali coast by these long Rossby waves which reflected into short Rossby waves at the boundary, accumulating energy there. The importance of this forcing mechanism is supported in several of the modelling studies discussed in Section 4.1.2.

The cross-equatorial flow continues during this time, now transporting about 20 Sv in the upper 500 m (Fig. 33c). It leaves the coast south of 4°N, where part turns eastward and part flows back across the equator in a circulation pattern referred to as the ‘Southern Gyre’ (Fig. 32). The fraction of the direct cross-equatorial offshore return flow in the Southern Gyre appears to vary from year to year (Schott et al., 1990), and the mechanisms responsible for this split, as well as the fate of the eastward outflow north of the equator, need further study. Water-mass signatures of both gyres indicate that there is very little exchange between the Great Whirl and the Southern Gyre at this time. Thus, water that crosses the equator with the shoreward part of the Southern Gyre does not continue to flow up the Somali coast, but instead bends eastward with part recirculating southward across the equator (as marked in Fig. 32) and part flowing across the Arabian Sea near the equator (Figs. 10 and 13).

Meridional currents cannot cross the equator freely because the flow has to reverse the sign of its potential vorticity when changing hemispheres. As a result, subsurface cross-equatorial exchange must take place largely via the western boundary current, where frictional effects can compensate the vorticity change. On the other hand, near-surface exchange can occur in the interior ocean as a result of forcing by the wind stress curl (see Section 8.2). After crossing the equator, western boundary currents typically turn offshore to join near-equatorial eastward flows in the interior ocean, as do the North Brazil Current in the Atlantic and the New Guinea Coastal Current in the Pacific. The eastward deflections generally occur after the boundary current first overshoots the latitude band of the eastward flow and then retroflects equatorward. The Southern Gyre appears to develop from a retroflexion of this sort (see Section 4.1.2.2).

At this time, there is a net upper-layer outflow from the Somali Current system into the Gulf of Aden through the passage between Socotra and the Horn of Africa (Fig. 34a). From moored current-meter observations in the passage, the mean northward outflow throughout the summer monsoon was estimated to be about 5 Sv (Schott et al., 1997), and the upper-layer water masses have characteristics of upwelled subsurface water (Fischer, Schott, & Stramma, 1996). A cut through the Great Whirl for the mean currents of the summer monsoon (Fig. 35b), determined from a line of moored stations (K12–K19) south of Socotra, shows that the Great Whirl reaches down to almost 1000 m with speeds of 10 cm/s, and that the gyre structure remains visible even at greater depths.

*August–September:* In the late phase of the summer monsoon the Great Whirl has become an almost-

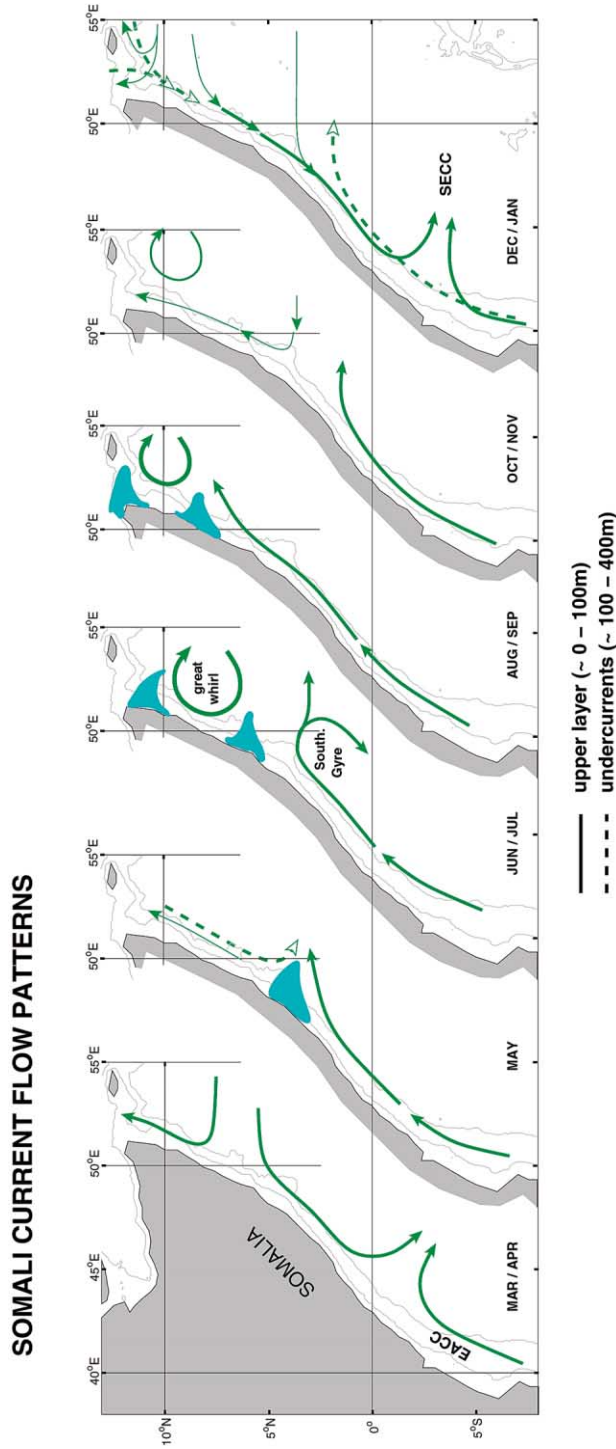


Fig. 32. Schematic diagram of the Somali Current upper-layer flow patterns over the course of the year. Also marked are undercurrents as presently known (after Schott et al., 1990, with revisions). See Figs. 8, 9 and Appendix for acronyms and text for details.

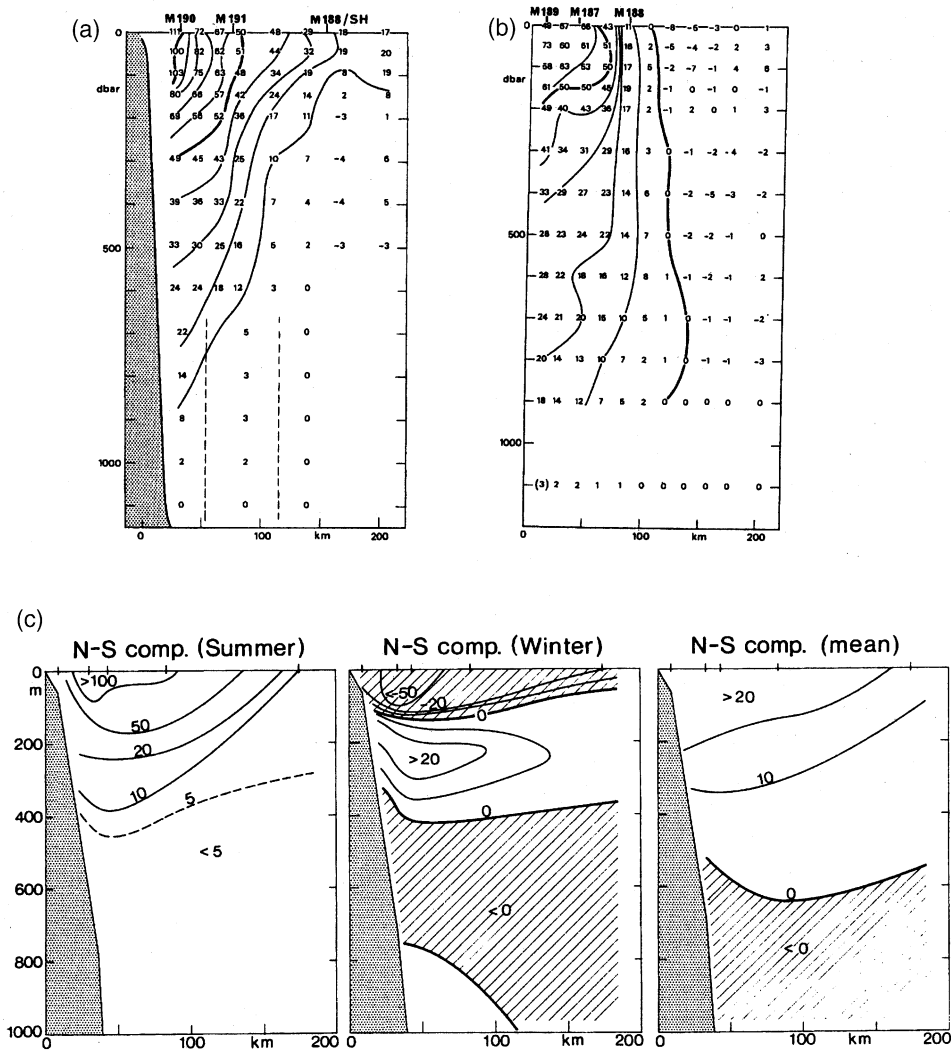


Fig. 33. Mean velocity sections across Indian Ocean western boundary currents for a) Northeast Madagascar Current at Cape Amber (westward is positive); b) Southeast Madagascar Current at 23°S (southward is positive), both from Swallow et al. (1988); and c) Somali Current on the equator (northward is positive) during the summer monsoon (left), during the winter monsoon (middle) and annual mean (right; from Schott et al., 1990); section locations see Fig. 20.

closed circulation cell (Fig. 36) with very little exchange between its offshore recirculation branch and the interior Arabian Sea, as is apparent from the differences in surface salinities between the GW and the region to the east of it (Fig. 36). In these observations, as well as in a previous ship survey during the late summer monsoon of 1993 (Fischer et al., 1996), a band of northward-flowing current was found east of the Somali Current system, extending from 4–12°N. It was carrying lower-salinity water northward past Socotra where it merged into the Socotra Gyre, thus effectively shutting off the connection between the Great Whirl and the interior Arabian Sea. This water does not originate from the outflow of the cross-equatorial flow within the Southern Gyre, and hence must be coming from the interior of the Arabian Sea. Transports in this late summer monsoon phase can exceed 70 Sv (Fischer et al., 1996; Schott et al., 1997).

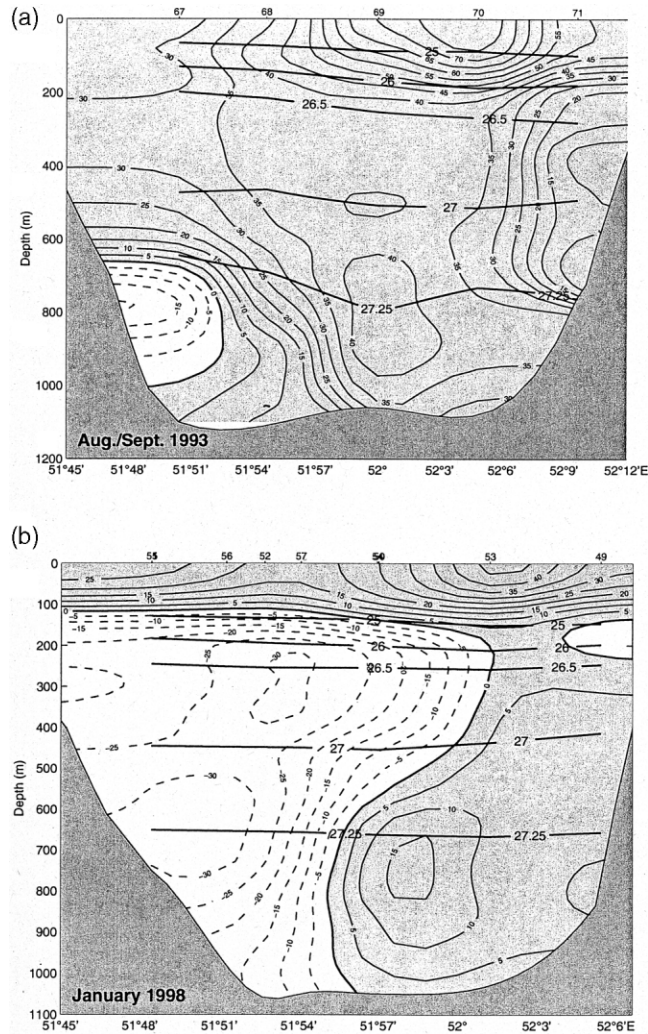


Fig. 34. Shipboard ADCP/LADCP sections across the Socotra Passage (between Socotra and the African continent), a) during the summer monsoon of 1993 (after Fischer et al., 1996) and b) during the winter monsoon of 1997/98 (from Schott & Fischer, 2000). Several isopycnals are also shown.

Strong upwelling exists where this flow turns offshore. Fig. 37 shows a section off northern Somalia during a particularly strong upwelling episode with upwelled waters colder than 17°C. Typical upwelling temperatures are in the 19–23°C range.

Some observations have suggested that the two-gyre system may at times collapse, when satellite SST images (Evans & Brown, 1981) have indicated a rapid (~1 m/s) northward propagation of the southern cold wedge. This interpretation has been supported by ship-survey measurements suggesting that low-salinity southern waters were present in the wake of the migrating southern cold wedge (Schott, 1983; Swallow et al., 1983). In some cases, the southern wedge merged with the northern one, suggesting that the Southern Gyre and Great Whirl had coalesced, as sketched in Fig. 32. It has to be noted, though, that such a breakdown was not documented in the 1995–96 WOCE observations (e.g., Schott et al., 1997). Its occurrence may be a rare event, and in that respect our August/September schematic may not represent

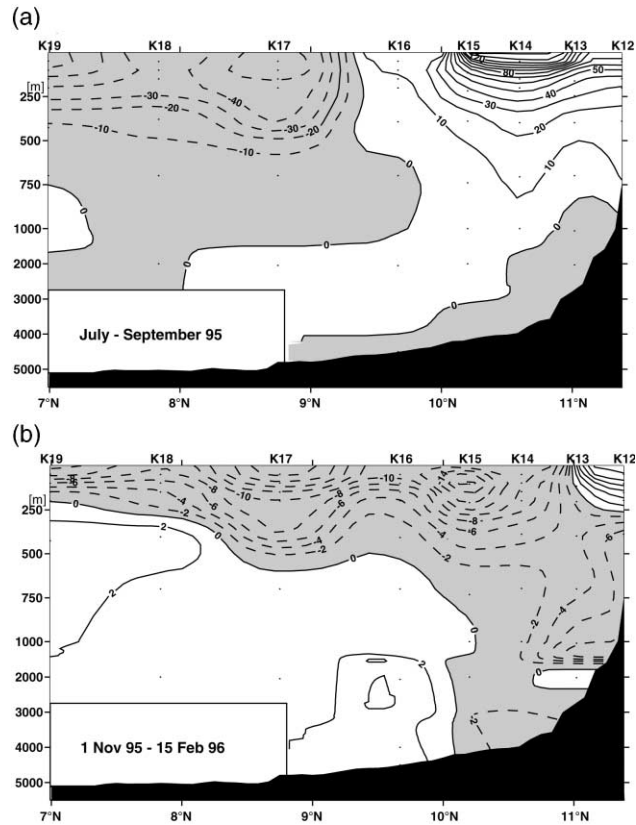


Fig. 35. Seasonal mean currents from moored array 1995/96 along a section south of Socotra across the Somali Current/Great Whirl (positive is eastward) during a) winter monsoon (from Schott & Fischer, 2000), and b) summer monsoon; section location see Fig. 20.

the typical seasonal cycle; rather, the typical case may be a continuation of the July situation throughout the summer monsoon.

*October–November:* When the Southwest Monsoon dies down, the cross-equatorial Somali Current turns offshore again at 3°N, while the Great Whirl continues to spin in its original position (Fig. 32). The Great Whirl is even discernible underneath the developing Northeast Monsoon circulation well toward the end of the year (Bruce, Fieux, & Gonella, 1981).

*Interannual variability:* Significant interannual differences in the system of cold upwelling wedges off Somalia and their movements during the course of the Southwest Monsoon had already been reported earlier (Evans & Brown, 1981; Schott, 1983). Recently, based on the WOCE moored and shipboard observations during 1993–96, new analyses as to the location and intensity of the Great Whirl have been made (Fig. 38). In 1993, the northern boundary of the Great Whirl was located about 200 km south of the banks of Socotra (Fischer et al., 1996). In 1995, it was banked right against the slope south of Socotra (Schott et al., 1997), and it was well developed as one large organized circulation cell until mid-October. In 1996, it was again located much more to the south, similar to the 1993 situation, the gyre transports were weaker than in 1995, and the Great Whirl was already becoming disorganized in August. These observations could not be explained in any obvious way by observed forcing field variability.

*Depth of monsoon response:* In the 1979 moored observations of Schott and Quadfasel (1982) mentioned above the response to a sudden monsoon onset was seen down to 2000 m, but there were no deeper

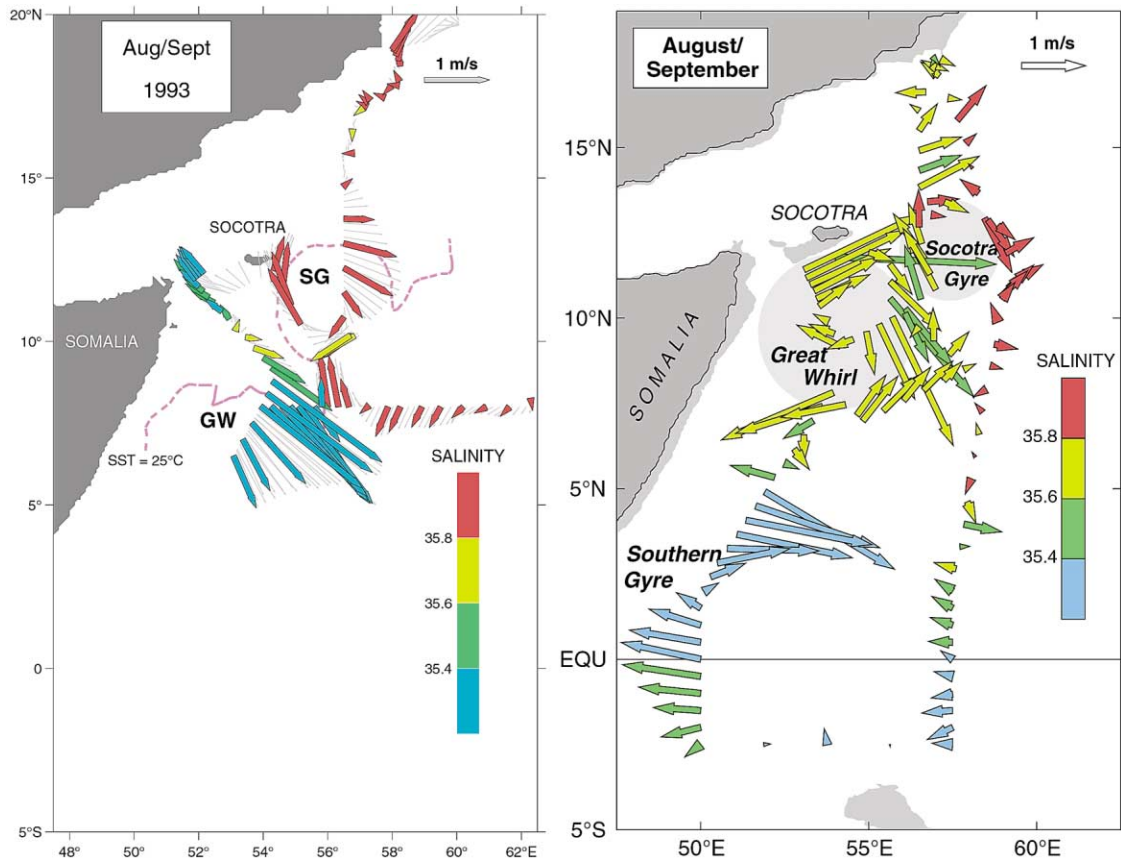


Fig. 36. Somali Current flow patterns during the late summer monsoon phases of a) 1993 (after Fischer et al., 1996) and b) 1995, (after Schott et al., 1997). Marked are the Southern Gyre, Great Whirl and Socotra Gyre. Near-surface salinities (colour-coded on the current vectors) indicate that lower-salinity waters originating from the southwestern and upwelling regions recirculate in the Great Whirl and do not leave the Somali Current zone toward the east in the 4°–12°N latitude belt. Instead, outflow from the northern Somali Current during the summer monsoon occurs through the Socotra Passage. Note also that the GW in 1995 was located much more northerly, against the banks of southern Socotra, than in 1993.

instruments in that experiment. From a moored array under the GW during 1995 and 1996 (Fig. 38), Dengler, Quadfasel, Schott, and Fischer (2002) concluded that the depth of the response of the GW to the monsoon during those years was less than 1500 m in the interior basin, whereas Beal, Molinari, Robbins, and Chereskin (2000b) reported reversing deep circulations between two ship sections sampled in June and September 1995. However, there was a deep effect of the monsoon in the mooring records expressed as intraseasonal fluctuations with a period of about 40 days, which generated a deep variance maximum. So, Dengler et al. (2002) suggested that the reversals of near-bottom circulations seen by Beal et al. (2000b) were associated with these shorter time scales. These intraseasonal fluctuations seem to be confined to the region of the GW, as found in a wavelet analysis of T/P altimetry (P. Brandt, 2002; pers. comm.). Their generation mechanism and role in GW dynamics still need to be determined.

#### 4.1.2. Models

A considerable number of modelling studies have attempted (over more than 30 years) to simulate the Somali Current response to the summer monsoon and to understand the processes that cause it. Both local

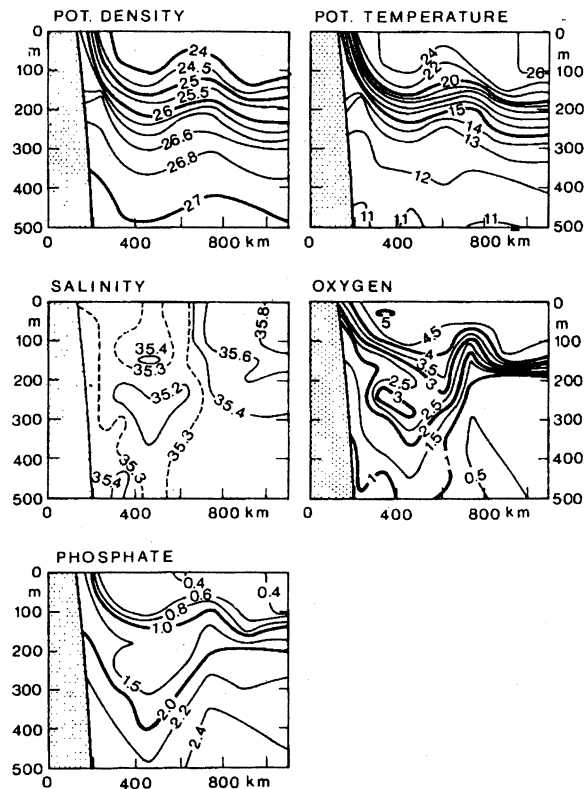


Fig. 37. Section along approx.  $12^{\circ}\text{N}$  through the northern Somali Current upwelling regime taken 29 August–1 September 1964 during a particularly strong upwelling episode, showing potential density ( $\text{kg/m}^3$ ), potential temperature, salinity, oxygen ( $\text{ml l}^{-1}$ ) and phosphate ( $\mu\text{gatl}^{-1}$ ). (After Swallow & Bruce, 1966; see Fig. 20 for section location.)

and remote forcing mechanisms have been proposed. ‘Local forcing’ is defined here to be direct driving by the alongshore component of the coastal winds, and ‘remote forcing’ is any other process. Remote forcing includes offshore wind fields that excite baroclinic Rossby waves that subsequently propagate to the African coast, and several categories of such waves have been considered: i) equatorially trapped Rossby waves; ii) Rossby waves that radiate off the Indian coast; and iii) Rossby waves generated by the wind curl offshore from Somalia. A prominent example of the latter is the region of very strong negative wind curl along the eastern side of the Findlater Jet; it is expected to drive an anticyclonic circulation, and several studies have suggested that the Great Whirl may be a directly forced response to this curl (Schott & Quadfasel, 1982; Luther, O’Brien, & Meng, 1985). Another possible remote-forcing mechanism is the inertial overshoot of the northward-flowing Somali Current across the equator.

This subsection provides a historical overview of this modelling effort and comments on unresolved issues. Collectively, the studies indicate that local forcing is the primary forcing mechanism of the summertime Somali Current, but that remote effects are also important, and in some cases significantly alter the coastal flows. (Remote effects are even more apparent during the winter monsoon and for the Somali undercurrents; see Sections 4.2 and 4.3) Another important outcome is the realization of the dynamical importance of the near  $45^{\circ}$  slant of the western boundary.

**4.1.2.1. Equatorial waves:** Lighthill’s (1969) seminal work was the first modelling study of the Somali Current. His solutions to a linear, continuously stratified model demonstrated that a northward cross-equa-

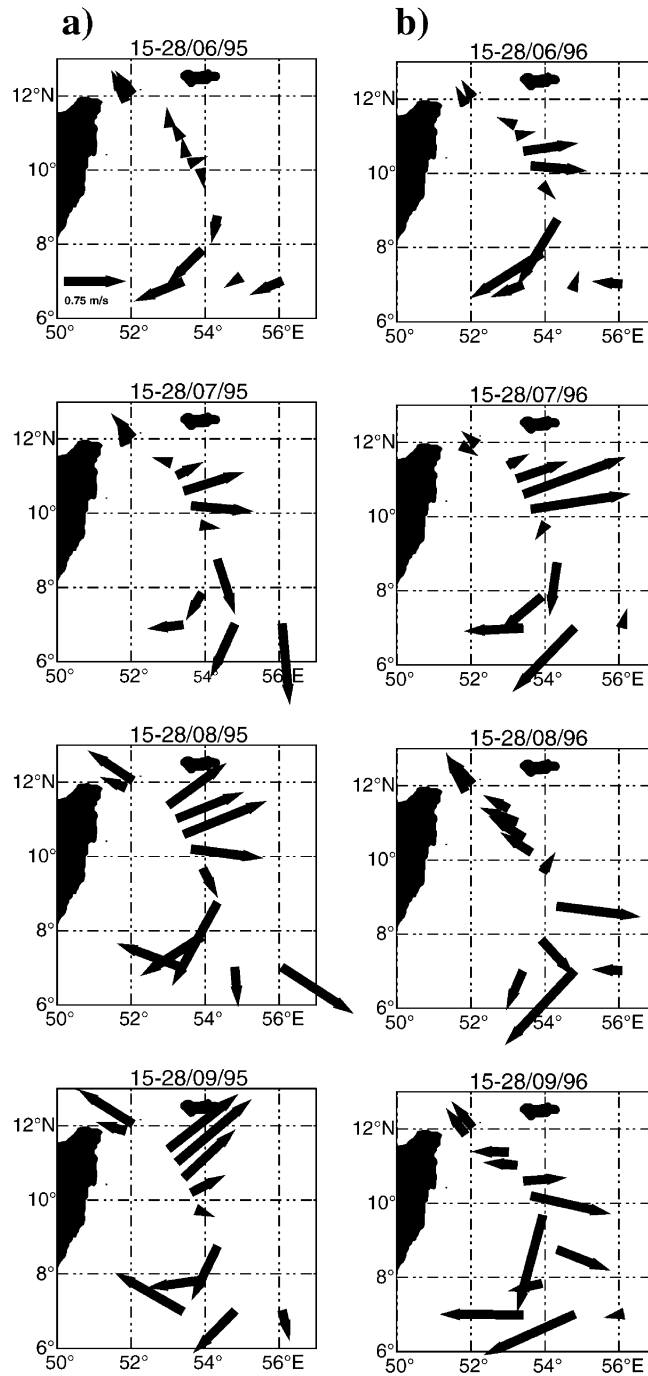


Fig. 38. Time series of near-surface current vector plots from the Great Whirl and Socotra Passage region (15 day means) for June–September, a) 1995; b) 1996. Note the differences in GW intensities of both years and that the 1996 GW collapsed much earlier. (Courtesy R. Schoenefeldt.)

torial Somali Current could be generated by westward-propagating, long-wavelength, equatorially trapped Rossby waves, excited by wind-stress curl in the open ocean. After their arrival at the western boundary, the waves reflect into short-wavelength Rossby waves that superpose to form the boundary current. The time scale for the setup of a western-boundary current by this mechanism is about one month. One motivation for Lighthill's study was the suggestion by several authors that northward cross-equatorial flow began before the alongshore winds turned northward. Leetmaa (1972, 1973), however, noted that the Somali Current turns northward even before the remote winds strengthen, suggesting that this interesting hypothesis is unlikely to be correct.

The potential influence of equatorially trapped waves on the Somali Current was explored further by Cane and Gent (1984) who derived a condition for the reflection of Rossby waves at an inclined coast. Visbeck and Schott (1992) applied this condition in their analysis of the Somali-Current annual cycle in which they fitted Rossby and Kelvin waves to the equatorial currents in the GFDL model interior and evaluated the resulting boundary current signal based on the Cane and Gent (1984) reflection law (see Section 4.3).

*4.1.2.2. Inertial overshoot:* Anderson and Moore (1979) used an  $1\frac{1}{2}$ -layer analytic model to propose another remote forcing mechanism for the cross-equatorial Somali Current, namely, inflow from the south by the EACC driven by the southern-hemisphere trades (Fig. 8). In this mechanism, southern-hemisphere winds drive a western-boundary current that inertially overshoots the equator and forms the Southern Gyre (Anderson & Moore, 1979; Knox & Anderson, 1985). The theoretical bases for their model are similar to those in Gulf-Stream model of Charney (1955), in which the structure of the boundary current is determined by invoking conservation of potential vorticity and the Bernoulli function and by matching to an interior Sverdrup regime. An interesting result was that for a realistic cross-equatorial transport of 15 Sv and a layer thickness of 100 m at the equator, the interface had to reach the surface at about  $4.5^{\circ}\text{N}$ ; thus, the Somali Current had to turn off the coast at that latitude, in agreement with the observed latitude of the Southern-Gyre turnoff (e.g., Swallow et al., 1983). The authors corroborated the conclusions of their theoretical study by obtaining solutions to a numerical version of their model, driven by an idealized representation of the southern-hemisphere trades (Anderson & Moore, 1979).

McCreary and Kundu (1988) used a  $2\frac{1}{2}$ -layer numerical model to investigate this mechanism further. They reported two solutions forced by an idealized representation of southern-hemisphere winds: one in a rectangular basin as in Anderson and Moore (1979), and the other with a boundary slanted at a  $45^{\circ}$  angle beginning at  $5^{\circ}\text{S}$ , similar to the actual Somali coastline. As in Anderson and Moore (1979), the rectangular-basin solution in McCreary and Kundu (1988) developed a cross-equatorial western-boundary current that did not separate from the coast until about  $8^{\circ}\text{N}$ . In contrast, in their slanted-boundary solution the boundary current turned offshore at and south of the equator, and failed to penetrate into the Northern Hemisphere. So, the authors concluded that the Southern-Hemisphere easterlies are unimportant for generating major features of the Somali Current circulation, especially for the Southern Gyre that turns offshore at  $4^{\circ}\text{N}$ . Conversely, the observed northward flow that appears at and south of the equator at the end of April before the onset of the monsoon (Leetmaa, 1972, 1973; Swallow et al., 1983; Schott et al., 1990) could very well be forced in this way.

*4.1.2.3. Alongshore winds and local wind curl:* An obvious possibility for a powerful Somali-Current forcing mechanism is the local alongshore wind associated with the Findlater Jet, as well as its offshore weakening that produces a region of strong negative curl. A number of studies have examined the response of the Somali Current region to forcings of this sort. The models differ in the slant of the western boundary, in whether the driving wind is spatially uniform or weakens offshore (and so has offshore curl), and in the presence or absence of Socotra.

*Rectangular basins:* The earliest models obtained solutions in rectangular basins forced by essentially

uniform southerly winds (i.e., without offshore curl). In these solutions, a swift coastal jet quickly developed in response to the coastal winds. In addition, one or more eddies formed on the coastal jet; however, in all the cases except one (Philander & Pacanowski, 1981) the eddies either never stopped propagating northward or they dissipated (Hurlburt & Thompson, 1976; Lin & Hurlburt, 1981; Philander & Delecluse, 1983; McCreary & Kundu, 1988). In the GCM solution of Philander and Pacanowski (1981), a cold wedge formed and stopped propagating northward eventually after 200 days. However, the reason for it stalling was likely because coastal Kelvin waves, generated along the eastern boundary, propagated around the basin to generate a southward flow along the northern portion of the western boundary, thereby inhibiting the northward movement of the wedge. A similar difficulty was encountered by Lin and Hurlburt (1981) when they used a closed, rather than open, northern boundary.

McCreary and Kundu (1988) reported a solution forced by a wind that weakens offshore. After 30 days the solution was quite similar to the solution forced by  $x$ -independent winds, but by day 180 it had very nearly adjusted to an eddy-free, completely steady state. In this solution, Rossby waves are excited in the region of offshore curl that propagate westward, adjusting the interior flow field toward Sverdrup balance. In this state, there is southward drift in the offshore curl region, eastward and westward flows at the northern and southern edges of the wind field region, respectively, and a connecting northward western boundary current. The extensive differences between the  $x$ -independent and  $x$ -dependent solutions demonstrate clearly how strongly remote forcing by offshore wind curl can affect solutions.

Cox (1979, 1981) obtained a similar response in an oceanic GCM forced by an alongshore wind with offshore curl. He integrated the model only for a period of 90 days, however, and during that time the solution continued to shed eddies that propagated northward. The corresponding McCreary and Kundu (1988) solution suggests that the eddies would have vanished had Cox integrated the model for a longer time. In support of this idea, the eddies in his solution were clearly weakening in the later stages of his calculation.

Perhaps the most important contribution of these idealized studies is a negative one: the lack of quasi-stationary coastal gyres points toward the models' lacking essential physics (e.g., a slanted western boundary). Another contribution is the demonstration of the sensitivity of the Somali Current to the presence or absence of offshore wind curl.

*Slanted western boundary:* Cox (1979) first noted the crucial importance of a slanted western boundary in Somali-Current dynamics. He obtained solutions in a basin with a western boundary slanted at the same angle as in the actual Somali coastline, and forced the model with an alongshore wind that weakened offshore. He noted the presence of striking gyres and cold wedges in this solution, and argued that they were an effect of the boundary slope.

McCreary and Kundu (1988) corroborated the importance of the slanted boundary in gyre generation, and commented on the sensitivity of the gyres to wind structure. Two of their test solutions were forced by alongshore winds that weakened offshore, differing in the alongshore structure and strength of the winds. In one solution, the winds were independent of the alongshore coordinate with a maximum stress of 2 dyn/cm<sup>2</sup>. This solution adjusted to a state that contained a western-boundary current that inertially overshoot the equator and had one stationary gyre centered near 6°N. It is noteworthy that the structure of this gyre did not at all resemble that of the wind-curl forcing (which was uniform alongshore), an indication that gyre dynamics are not dominated by simple Ekman pumping. In the other solution the winds were confined north of the equator and attained a maximum of 5 dyn/cm<sup>2</sup> off Somalia, similar to the structure of the Findlater Jet. In this case, a gyre quickly began to spin up in the southern half of the wind patch, a second one formed somewhat later north of it, and after 180 days there was a well-developed two-gyre system with two cold wedges quite similar to the observed pattern. Shortly thereafter, the southern gyre started to move northward; it began to interact with the northern gyre after 210 days, and by 240 days the two gyres had coalesced.

*Influence of Socotra:* Luther and O'Brien (1989) reported solutions to a layer model with and without

Socotra Island. With Socotra, the Great Whirl was blocked to the south of the island, but without Socotra it continued to migrate northwards. This result contrasts with the McCreary and Kundu (1988) solutions, in which only a slanted coastline was needed to stall the gyre's northward propagation, and it points toward the sensitivity of gyre dynamics to model parameters and physics.

Recently, Esenkov (pers. comm., 2000) further explored the influence of Socotra topography, by varying the water depth around Socotra in a high-resolution MICOM simulation. In the standard run, the water depth over Socotra is 300 m, whereas in a test calculation all depths shallower than 400 m were set to zero. This modification led to significant changes in the circulation, blocking the northward advance of the Great Whirl in the late summer monsoon and causing stronger interaction of the Great Whirl and Southern Gyre.

*4.1.2.4. Collapse of the double-gyre structure:* A mystery that is still unresolved is the collapse of the two-gyre system. The observational evidence for it is rather scant, which suggests it may happen in some years but not in others. The relaxation of the wind field at the end of the Southwest Monsoon has frequently been suggested as being the cause of the northward movement of the Southern Gyre. Schott (1983), however, pointed out that observations do not support this idea because, in two of the three years that he analyzed, the monsoon continued at maximum strength for quite some time after the migration had begun. The McCreary and Kundu (1988) solution suggested that the collapse may simply be a response to the full-strength winds, and thus does not require any subsequent forcing change to trigger it. If so, then the critical question is simply whether coalescence has enough time to occur before the Southwest Monsoon ends. It is also possible that the two-gyre system might be disturbed by Rossby waves forced by offshore wind curl or by Rossby waves originating from the southwest coast of India as a result of remote effects from the Bay of Bengal (see Section 5). Finally, although a collapse of the two-gyre system into a continuous flow along the coast was not obtained in the GW simulation studies of Wirth et al. (2002), their results suggest that such a collapse may result from internal instabilities.

*4.1.2.5. Interannual variability:* Several model runs forced by interannually varying winds have been carried out in recent years (Luther, 1999; Esenkov, pers. comm., 2000; Kindle, pers. comm., 1999). In particular, Kindle has attempted to reproduce observed interannual Great Whirl variability during the 1995–96 observational phase of WOCE. In a prognostic simulation alone, he could not obtain a solution for 1996 with a Great Whirl much further south than in 1995 even by using different wind forcing fields, in disagreement with the observations (Fig. 38). He could only simulate the difference if he assimilated T/P altimetry into his model, basically imposing the Great Whirl anticyclonic structure onto the model at the right place.

A new study on interannual variability and GW dynamics has been carried out by Wirth et al. (2002). They compared high-resolution model runs with repeated climatological seasonal forcing with results from interannually forced model runs. Their conclusion was that interannual GW variability is basically stochastic, predominantly determined by internal processes, and not by the interannual variations of the wind field. Therefore, comparisons with observations would not be meaningful for individual realizations, only for ensembles of output fields.

## 4.2. Somali Current, winter monsoon

### 4.2.1. Observations

During the Northeast Monsoon, the winds blow away from the Indian subcontinent (Fig. 1) and the surface Somali Current reverses to flow southward. After crossing the equator, it encounters the northward-flowing EACC, resulting in a confluence and eastward turnoff at 2–4°S (Düeing & Schott, 1978; Swallow et al., 1991) that supplies the South Equatorial Countercurrent (Figs. 9 and 32). At the equator, the south-

ward Somali Current is quite shallow, carrying 5 Sv in the upper 150 m, because there is a northward undercurrent at this time (see Section 4.3).

Until quite recently, few observations had been carried out in the northern Somali Current during the winter monsoon. Bruce et al. (1981) reported that the Great Whirl can actually preserve summer monsoon conditions underneath the developing winter monsoon surface circulation for some time into the winter monsoon. Quadfasel and Schott (1983) carried out an analysis of historical hydrographic data and some moored observations at 3–5°N, yielding some information on the mean vertical structure. The moored-array observations made during WOCE 1995–96, and shipboard sections of winter 1997/98 of Schott and Fischer (2000) south of Socotra and in the Socotra Passage, show that the northern Somali Current during this time was characterized by an inflow from the east, as shown by the mean winter section in Fig. 35; this caused a divergence to develop at the coast somewhere near 6–8°N, with northward surface flow north of these latitudes and equatorward flow south of them. The northward surface flow passes through the Socotra Passage (Fig. 34b), but also veers eastward along the southern banks of Socotra. It then flows northward through the region occupied by the Socotra Eddy during the summer (Fig. 8). The westward upper-layer inflow into the Somali Current system north of 7°N during the winter monsoon is also confirmed by the XBT analysis of Donguy and Meyers (1995). From a line running about southward from Socotra and the one running from Perth (Australia) to the Red Sea they obtained a westward transport of 11 Sv above 400m.

#### 4.2.2. Models

MKM commented extensively on the Somali Current during the winter monsoon in their solution, and on the mechanisms that drive it. Fig. 11 shows the upper-layer thickness  $h_1$  and current  $v_1$  fields from that solution during January. Consistent with the observations, a strong, southward coastal current develops along much of the Somali coast from 7–8°N across the equator to 2.5°S, and north of 8°N there is a weak northward countercurrent. Causes of these currents are apparent in the structure of the  $h_1$  field. Prominent features are a band of shallow  $h_1$  extending across the southern Arabian Sea, and a band of thick  $h_1$  located to its north (Fig. 11b). The low- $h_1$  band was generated along the west coast of India during the Southwest Monsoon, and subsequently propagated westward as a Rossby wave. After the onset of the Northeast Monsoon, it is also intensified by local Ekman pumping, which tends to move water from southeast to northwest of the wind axis. The region of low  $h_1$  centered near 3°N, 53°E, results primarily from this latter process. Note that the upper-layer flow circulates about this region. The band of high  $h_1$  was also generated during the Southwest Monsoon, and is deepening further via Ekman convergence.

There is a westward current across the interior of the Arabian Sea located between the bands of deep and shallow  $h_1$  where  $h_{1y} > 0$ . (It is worth noting that this current is consistent with quasi-steady Sverdrup theory, which lends support to the idea that wind curl in the interior of the Arabian Sea is an important driving mechanism of this feature.) This current reaches the Somali Coast near 8°N, and most of it turns southward to provide water for the southward-flowing Somali Current; the rest circulates around the western edge of the high- $h_1$  band to form the coastal countercurrent.

Interestingly, the countercurrent was already present in the solution by November, but in January it is weaker because of the stronger northeasterly winds. It re-strengthens in March as the winds weaken near the end of the Northeast Monsoon. Anderson, Carrington, Correy, and Gordon (1991) report a similar countercurrent in their GCM solution, commenting that it represents the last vestige of the Great Whirl that had formed 6 months earlier. Quadfasel and Schott (1983) suggested that the observed countercurrent was forced by local wind curl. Indeed, test calculations reported by MKM indicated that this process does contribute to the model countercurrent during March, but that it is less important than the remote forcing from the previous Southwest Monsoon.

Schott and Fischer (2000) compared the winter-monsoon circulation of the high-resolution POCM simulation with their observations. In that solution, the Somali Current is supplied from the east by three main

inflows: one at low latitudes that is supplied out of the NMC, one south of Socotra, and one in the 5–7°N range (Fig. 39a). A countercurrent offshore from the southward Somali Current is not apparent in the POCM simulation.

### 4.3. Somali Undercurrents

#### 4.3.1. Observations

Three Somali undercurrents have been observed at different locations and at various times during the year, as indicated in Fig. 32. In April to early June, a southward undercurrent develops just beneath the

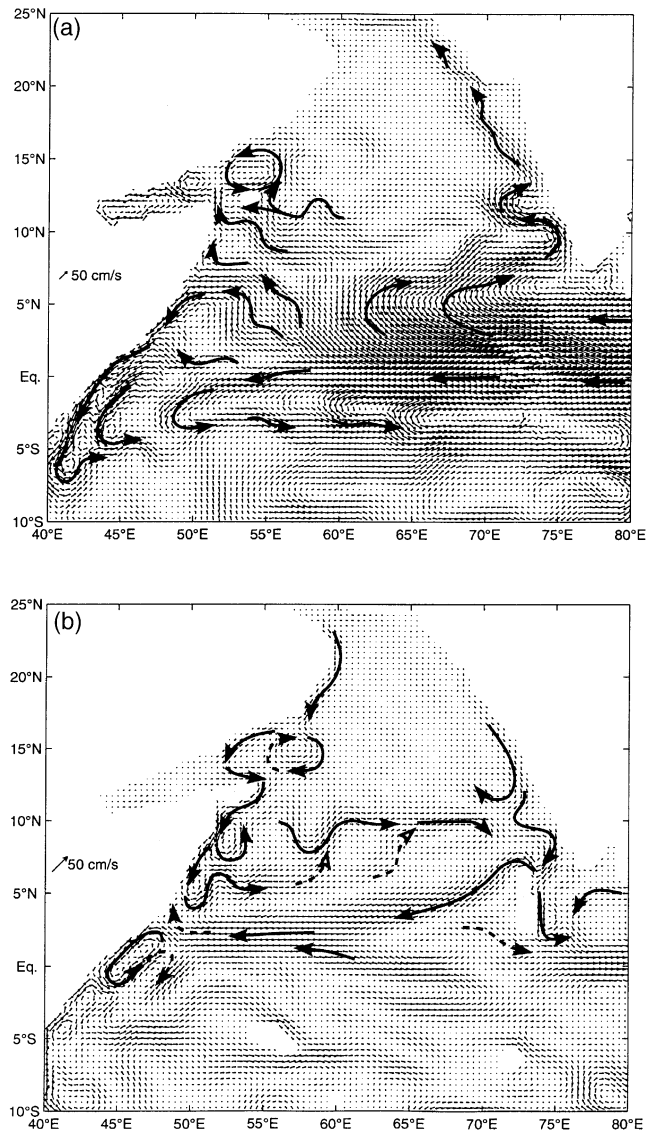


Fig. 39. Winter monsoon circulation of the Arabian Sea of the Parallel Ocean Climate Model (POCM), a) surface currents; b) currents at undercurrent level. (From Schott & Fischer, 2000.)

northward surface flow in a depth range from about 100 to 300 m. It has a maximum instantaneous speed as large as 60 cm/s (Leetmaa, Quadfasel, & Wilson, 1982), although the monthly average speed has a maximum of only about 20 cm/s (Quadfasel & Schott, 1983; Schott & Quadfasel, 1982). This undercurrent turns offshore near 4°N and is terminated by the establishment of the deep-reaching Great Whirl.

During fall and winter, a southward undercurrent was observed underneath the northward-flowing branch of the Somali Current in the 8–12°N latitude band (Quadfasel & Schott, 1983), and its existence has recently confirmed by Schott and Fischer (2000). The latter measured southward velocities of about 30 cm/s below 100 m in the passage between Socotra and the mainland in January 1998. The moored time series in the passage together with the water mass properties showed that the lower part of this undercurrent was the main supplier of Red Sea Water out of the Gulf of Aden into the Indian Ocean (Fig. 34b). A second branch of this undercurrent enters the region from the northeast around Socotra (Schott & Fischer, 2000).

Finally, during winter there is a northward, cross-equatorial undercurrent in a depth range from 150–400 m (right panel of Fig. 33c). Its transport almost balances that of the southward surface flow of the Somali Current, a drastic difference in the net cross-equatorial transport between the two monsoon seasons (Schott, 1986; Schott et al., 1990). Except for the equatorial moorings used to construct Fig. 33c, observations during this phase are sparse, and it is not known how the cross-equatorial undercurrent connects with coastal currents farther to the north or with the interior flows. It is plausible that it might represent a continuation of a quasi-permanent northward EACC underneath the reversing surface flow. This idea, however, is not supported by the moored observations reported by Düeving and Schott (1978), which show the winter confluence of the EACC and Somali Current: The flow was northward at 4°S at the undercurrent level, but was fluctuating at 2–3°S.

#### 4.3.2. Models

Using a linear, continuously stratified model, McCreary and Kundu (1985) derived a general result for wind-driven circulations along western-ocean boundaries, with important implications for the dynamics of Somali undercurrents. In a solution forced by winds without offshore curl, the surface jet was very strong and there was essentially no coastal undercurrent, in striking contrast to the eastern-boundary response (McCreary, 1981). These differences result from a fundamental dynamical difference between the two situations: At an eastern boundary low-order modes radiate offshore as packets of Rossby waves, leaving higher-order ones behind to generate an undercurrent, whereas at a western boundary this process is reversed, and a strongly sheared (highly baroclinic) flow cannot develop. Not surprisingly given this negative result, non-traditional processes have been proposed to explain the Somali Undercurrents.

*4.3.2.1. Spring undercurrent north of 5°N:* The observed springtime wind is southwesterly, reaches its maximum strength well to the north of 5°N, and is associated with a region of large, negative wind curl off the coast. In an effort to simulate the southward undercurrent at this time, McCreary and Kundu (1985) forced their model with an idealized representation of this wind. Southward flow developed in the region of wind curl, consistent with the system adjusting toward Sverdrup balance. This flow turned onshore near the southern edge of the wind region, and part of this current turned southward at the coast, thereby generating an undercurrent south of the region of strong winds.

In the MKM solution, a southward undercurrent is present in the lower layer from about 5°N to the equator during the late spring. It was, however, not generated by the mechanism proposed by McCreary and Kundu (1985). Rather, it appeared to be primarily remotely forced by Rossby waves that had radiated from the coast of India. To confirm this result, MKM obtained a test solution in which winds in the Arabian Sea were deleted throughout the year, finding that in late spring (May) the model Somali Undercurrent remained largely unchanged from the main run. In the test, this flow was clearly associated with a region of high  $h_1$  that earlier had propagated as a packet of mode-2 Rossby waves across the southern Arabian Sea from the coast of India. During January, this region is visible in the main run as a region of high  $h_1$

extending partially across the basin (Fig. 11), and by April the region reaches the western boundary. The springtime Somali undercurrent is the geostrophically balanced, lower-layer current that circulates about this band in a direction opposite to that of the upper-layer currents (a mode-2 response), joining the westward- and eastward-flowing branches north and south of this band. Thus, in the MKM solution it is remote forcing from the Bay of Bengal, which earlier generated the high along the west coast of India, that is the primary forcing mechanism of the model's springtime undercurrent.

*4.3.2.2. Fall and winter, northern undercurrent:* The MKM solution has a southward Somali undercurrent that by November extends from the tip of Somalia down to 3°N. It is fed by a westward flow across the interior of the northwestern Arabian Sea. This flow appears in October with the weakening of the Southwest Monsoon winds, and it lasts through February. Similar to the springtime undercurrent, it is evident that it is a geostrophically balanced, lower-layer current circulating about a band of high upper-layer depth  $h$ , and this close relationship between the thermocline layer velocities and layer thickness holds throughout its existence (see Fig. 11). The band of high  $h$  was generated in the central Arabian Sea during the Southwest Monsoon and it propagated westward as a Rossby wave after the weakening of the winds. Thus, this fall Somali Undercurrent is really a remnant from the previous summer. Consistent with the MKM solution, Anderson et al. (1991) noted that a Somali Undercurrent was present in their solution during November, but they did not discuss its cause. On the other hand, the observations of Quadfasel and Schott (1983) at 5°N indicate that southwestward, subsurface flow reappeared considerably earlier, in August. The cause of this model/data discrepancy is not clear, but it is possibly because of year-to-year differences in the arrival times of remotely forced waves.

Schott and Fischer (2000) analysed the POCM model and found that the northern undercurrent, including its two supply routes from the east and through the Socotra Passage, were well simulated (Fig. 39b). The northern undercurrent is also reproduced by the MICOM simulation of Esenkov and Olson (2002), who specifically analysed the annual cycle of Socotra-Passage and eastern pathways, finding that most of the undercurrent water (~75%) is supplied from the east. In their solution, they established the southward undercurrent as a supply route of high-salinity water from the north for the Somali upwelling regime in the summer. Consistent with the MKM solution, they found that its onset resulted from the arrival of a packet of Rossby waves at the northern Somali coast in October that were generated by wind curl in the interior of the Arabian Sea. These waves were associated with thermocline thickness anomalies like mode-2 waves, which caused northward surface and southward subsurface flows at the coast.

It has not yet been determined why the northern undercurrent veers offshore near 4°N. Topographic effects generated by a bump in that shelf region, which were suspected to be important by Quadfasel and Schott (1983), do not seem to play an important role, because in the MICOM solution the undercurrent was not affected much when deep topography was artificially changed. The interpretation from MKM is that the offshore bending of the undercurrent is the result of offshore geostrophic flow at the southern edge of the band of high  $h_1$ .

*4.3.2.3. Winter, cross-equatorial undercurrent:* In the MKM solution the lower-layer western-boundary flow remains northward to about 2.5°N, forming a cross-equatorial, coastal undercurrent that lasts through February (Fig. 11). This feature is consistent with the observations, but in contrast to the solution, the observed flow does not weaken until April. Unfortunately, MKM were unable to diagnose the cause of this model undercurrent. A plausible explanation is that it results from the inertial overshoot of the western-boundary current (see Section 4.1.2.2), but most of the model flow turns offshore just south of the equator. It is likely that this undercurrent does not have a single cause in the model.

In his high-resolution (0.2°×0.2°) 3½-layer model study of Somali undercurrents, Jensen (1991) also reproduced the cross-equatorial undercurrent, and found that its disappearance in spring was related to the arrival of a westward equatorial undercurrent (Fig. 27) associated with remotely forced Rossby waves that

are generated by semiannual winds in the interior equatorial ocean. Visbeck and Schott (1992) also investigated the possible role of remote forcing by equatorial Rossby waves on the subsurface flow. Their study was motivated by Schott's (1986) observation that both the local wind and the surface flow of the near-equatorial Somali Current are dominated by the annual period, but that the annual and semiannual components are of comparable strength for the subsurface flow. Fitting Rossby waves to the Geophysical Fluid Dynamics Laboratory (GFDL) model currents in the equatorial interior, Visbeck and Schott (1992) calculated the transports caused by the short Rossby waves that were generated by reflection at the western boundary. They concluded that transport fluctuations of the order of 5 Sv could be generated by Rossby-wave reflection in the depth range from 150–800 m. These were, however, antisymmetric about the equator with maxima at 2–3° latitude and therefore not verifiable with the moored array of Schott et al. (1990) that was located right on the equator.

#### 4.4. Deep mixed layer during the SW monsoon

A striking feature of the Arabian Sea surface-mixed layer development is the bowl-shaped deepening in the central Arabian Sea after the onset of the monsoon (Fig. 17c). It is accompanied by a 4°C warming compared to November at the 100-m level (Fig. 15e,f).

A number of recent studies have addressed the question of whether Ekman pumping or mixed-layer entrainment force this mixed-layer deepening. Weller et al. (1998) analyzed the mixed-layer deepening in the central Arabian Sea, using data from a buoy located at 15.5°N, 61.5°E on the climatological axis of the Findlater Jet. They found that much of the mixed-layer variability there could be explained by local mixed-layer processes alone. Lee et al. (2000) compared the mixed-layer deepening of a Kraus-Turner model ( $w_{KT}$ ) with the vertical velocities caused by Ekman pumping ( $w_{EP}$ ) for the northern Arabian Sea during the summer monsoon, using wind stresses of a new climatology compiled at Southampton Oceanography Centre (Josey, Kent, & Taylor, 1999). Fig. 40 shows the distributions they obtained for both kinds of vertical velocity for the early (June) and late (August) phases of the summer monsoon. In both months, Ekman pumping is at work on the right side of the wind axis and Ekman suction on the left. However, the local (Kraus-Turner) mixed-layer deepening on the left side dominates the Ekman suction throughout the summer monsoon. On the right side of the wind axis, local mixing and Ekman pumping both deepen the mixed layer in the early part of the summer monsoon. In the later part of the monsoon, the local wind over the interior Arabian Sea slackens while the heating continues, resulting in a shallowing of the mixed layer that works against the continuing downward effect of Ekman pumping.

Rao and Sivakumar (2000) evaluated the historical data base of the Indian Ocean to investigate the respective roles of local forcing (i.e., mixed layer entrainment) and lateral advection (i.e., Ekman pumping) for the heat budget. They confirmed the dominance of local forcing for most of the Arabian Sea. In the central Arabian Sea, a modest improvement was obtained in the heat budget when including lateral advection, in agreement with the above findings.

These issues have been discussed in a number of modelling studies. McCreary and Kundu (1989) and MKM note the importance of both Ekman pumping and mixed-layer entrainment in their solutions. McCreary and Kundu (1989) contrasted solutions with and without advection of the mixed-layer thickness field (their Figs. 3 and 4), thereby providing measures of the influences of both processes. Bauer, Hitchcock, and Olson (1991) noted the importance of Ekman pumping in their theoretical study. McCreary, Kohler, Hood, and Olson (1996a), using a 4½-layer physical-biological model, noted that the thickening of the mixed layer was largest under the Findlater Jet, and concluded that this thickening was mostly the result of mixed-layer entrainment.

McCreary et al. (2001) used the McCreary et al. (1996a) coupled biological/physical model forced by the fluxes recorded at a buoy in the central Arabian Sea (Weller et al., 1998) to investigate the influence of diurnal forcing on the mixed layer and biological activity there. Key diurnal processes were identified

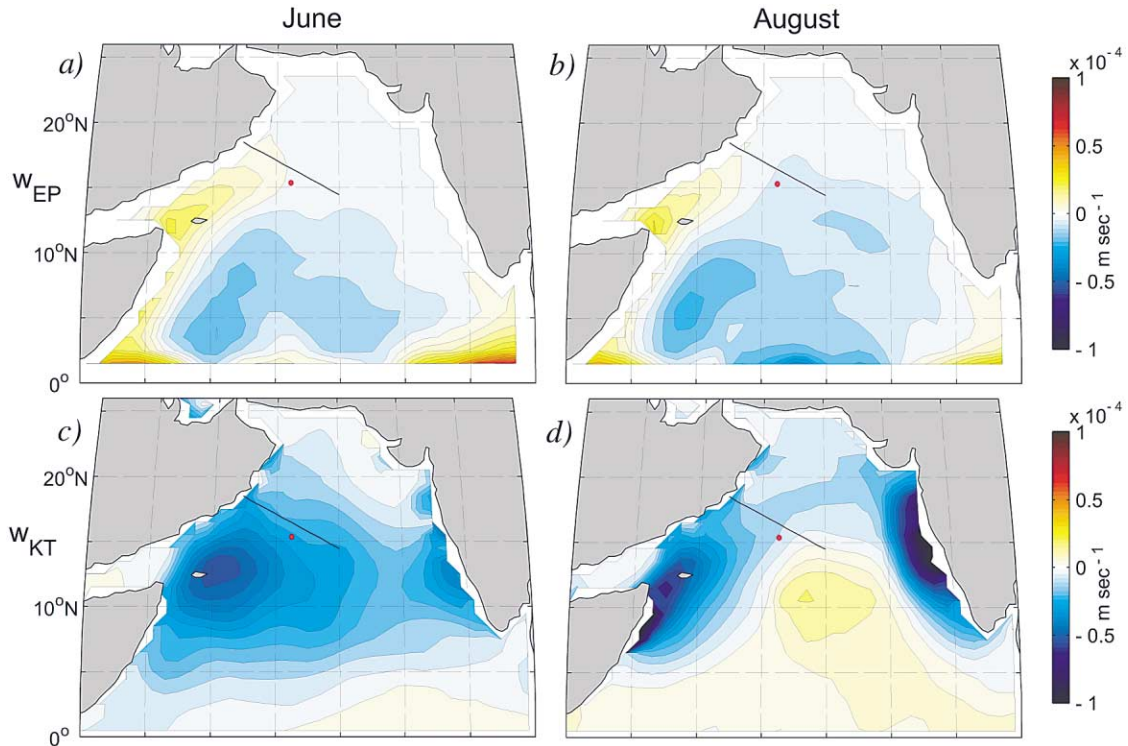


Fig. 40. Comparison of a),b) vertical velocities due to Ekman pumping ( $w_{EP}$ ) for June, August and c),d) mixed-layer deepening velocity due to Kraus-Turner entrainment ( $w_{KT}$ ) for the northern Arabian Sea. (From Lee et al., 2000.)

to be increased vertical exchange between the mixed and subsurface layers, and variability of the penetration of short-wave radiation. Among other things, these effects extended the time that the mixed layer stayed thick during the Northeast Monsoon, delayed the spring plankton bloom by 2–3 weeks, and weakened the spring and fall blooms, resulting in overall better agreement with observations. This model study again confirmed that much of the mixed layer variability at the location of the moored station of Weller et al. (1998) could be accounted for by local one-dimensional effects (i.e., entrainment rather than Ekman pumping).

Rochford, Kindle, Gallacher, and Weller (2000) used a layer model with a surface mixed layer to confirm the importance of diurnal forcing at the buoy site. They applied wind stresses and heat fluxes from different climatologies and operational weather forecast models (ECMWF, FNMOC) and found that the differences of model results with observed SST and mixed-layer depths mostly resulted from the stresses used and to a lesser degree the winds entering into the heat flux calculations. Forcing the model by FNMOC stresses and fluxes yielded the best comparison. Limitations reported by both McCreary et al. (2001) and Rochford et al. (2000) were that the observed mixed-layer thickness was distorted by the passage of mesoscale eddies over the mooring site; these eddies could not be accounted for properly in the simulations, and this limited the quality of the model/data comparisons.

An interesting aspect of the summertime mixed-layer deepening is the possibility of geostrophic circulations evolving from the induced pressure gradients. In the southern Arabian Sea, such flow should be directed against the prevailing eastward flow. So far, analyses based on observations have not been carried out to confirm the importance of this process.

## 4.5. Northern Arabian Sea

### 4.5.1. Observations

**4.5.1.1. Monsoon circulations and mesoscale features:** Broad eastward flow during the summer monsoon across the whole latitude range of the Arabian Sea and over to the Indian coast is suggested by ship-drift currents (Fig. 31a). From the observations in the Great-Whirl regime, however, significant eastward flow across the central Arabian Sea is not to be expected because of the large recirculation within the Somali-Current gyres (see Section 4.1). Instead, most of the Somali Current outflow must exit the region through the Socotra Passage, and only then flow eastward.

The anticyclonic summer monsoon circulation south of Socotra was also present in the XBT analysis of Donguy and Meyers (1995). From the two lines mentioned earlier they determined a clockwise recirculation south of Socotra carrying about 20 Sv in the upper 400m. The dynamic height estimates of Fig. 18a indicate a band of upper-layer eastward geostrophic flow (relative to 400 dbar) north of about 12°N, in agreement with the findings of the northward Somali Current outflow. On the other hand, the Donguy and Meyers (1995) line running from Perth to the Persian Gulf did not show eastward transport, in contrast to the contours of Fig. 18a, suggesting that the seasonal pattern still needs more data to be firmly established.

The ship-drift maps can be expected to be smoother and of larger horizontal scale than the geostrophically derived circulations for two reasons: They contain the Ekman drift which has the scale of the wind field, but they are also affected by ‘windage’, which adds an artificial current component in the direction of the wind.

Recently, during 1994–1996, the northern Arabian Sea has been extensively studied, as part of the Joint Global Ocean Flux Study (JGOFS). The observations consisted of repeated ship sections normal to the Omani coast, of special frontal surveys and of satellite SST and altimetry. For the summer monsoon circulation off the Arabian peninsula, it was shown that a northeastward coastal jet developed along the south coast of Oman in early May and persisted throughout the summer monsoon. This jet has been called Ras Al Hadd Jet by Böhm, Morrison, Manghnani, Kim, and Flagg (1999). It flows past Ras al Hadd at the southeast corner of Oman (Fig. 8) and meanders into the interior, transporting cooler coastal upwelling waters into the warmer environment of the Gulf of Oman, and therefore is easily identifiable in satellite SST observations. The jet is associated with an anticyclonic gyre just south of its offshore turning point and a cyclonic one to its north (Flagg & Kim, 1998; Böhm et al., 1999). Its maximum velocities reach 1 m/s, its transport is largest in September, generally varying between 2–8 Sv. Further west, in 1993–95, Shi, Morrison, Böhm, and Manghnani (1999) determined a time series of the alongshore flow from a combination of T/P altimetry, JGOFS hydrography and Ekman transports and found the maximum eastward flow occurred earlier in the monsoon, and decreased in strength from about 10 Sv in 1993 to about 2 Sv in 1995, in correspondence to a decrease in monsoonal wind forcing between these three years. The cause of this alongshore northeastward flow is an onshore pressure gradient established by the upwelling, which reduces sea level near the coast by about 30 cm, as seen in the altimetry signal (Shi et al., 1999).

Other circulation cells exist elsewhere along the Omani coast, their locations apparently linked to protruding capes of the Arabian peninsula. Between these cells, upwelled waters can be transported offshore in filaments or squirts, which extend as far as 400 km offshore and can be detected in satellite SST and color imagery. In these filaments, which have widths of up to 100 km, offshore currents in excess of 50 cm/s have been observed (Brink et al., 1998), and their transports have been estimated at 1–2 Sv. A strong anticyclone of this sort was identified southeast of Ras ash Sharbatat (located near 18°N) by Flagg and Kim (1998); it persisted throughout the Southwest Monsoon and into November. A similar feature was present in earlier ADCP observations reported by Elliot and Savidge (1990).

Overall, JGOFS investigators concluded that four persistent filaments are present off the Arabian peninsula during the Southwest monsoon. Their total offshore transport is estimated to amount to 4–8 Sv, which

is larger than would be expected for the offshore Ekman transport for a typical monsoon strength. A plausible interpretation is, then, that the offshore jets are deflections of the alongshore flow that carry surface, as well as upwelled, water offshore (K. Brink, pers. comm. 2000). This may also be part of the recirculating gyres, in which the offshore flow of the filaments is partially balanced by onshore currents to either side.

Farther offshore, the interior of the northern Arabian Sea is filled with mesoscale eddies. These have been noted in repeat ADCP surveys along lines normal to the Arabian coast by Flagg and Kim (1998), and confirmed subsequently by Kim, Flagg, and Howden (2001) who evaluated the 1993–96 T/P altimetry in comparison to the ship-track analysis. Kim et al. (2001) determined the eddy scale to be several hundred kilometers near the Arabian coast, decreasing to 100–200 km in the interior ocean, and they found the maximum eddy energy to occur about 300 km offshore. They also found substantial eddy kinetic energy in the 50–120 day band in the northern Arabian Sea, but little intraseasonal variability south of about 15°N.

During the winter monsoon, the ship drifts indicate weak westerly flows in the northern Arabian Sea (Fig. 31b), and the steric height fields show disorganized weak patterns in the northern Arabian Sea (Fig. 18a). From January to June, the western-boundary current of the Gulf of Oman north of Ras al Hadd is comparatively weak (Flagg & Kim, 1998). Warm water now flows southward past Ras al Hadd into the open Arabian Sea, so that the coastal jet is fed from the north, rather than the west as during the summer monsoon (Fig. 9). Along the rim of the northern Arabian Sea, the mean flow during the winter monsoon is westward with downwelling along the coast and an offshore-directed pressure gradient (Shi et al., 2000).

*4.5.1.2. Upwelling and subduction:* There has been a long-running discussion about the respective roles of coastal vs. open-ocean upwelling off Oman during the Southwest Monsoon. In a first attempt to estimate the upwelling off Arabia, Smith and Bottero (1977) evaluated geostrophic transports from ship sections normal to the coast between 52–60°E for the summer monsoon of 1963 and Ekman transports from ship winds. They estimated upwelling velocities close to the shelf in excess of  $3 \times 10^{-3}$  cm/s and an upwelling transport of about 2 Sv into the upper 50 m, which was compensated by onshore geostrophic flow in the 50–350 m depth range. Shi et al. (2000) analyzed the upwelling off Oman for the summers of 1993–95 between Ras al Hadd and about 55°E (an alongshore extent of about 600 km), and found that the coldest water occurred closest to the topography within two bays in the western part of their study domain. The steady decrease of surface temperatures offshore indicated that upwelled waters originated near the coast rather than from open-ocean upwelling. From a box budget calculation they estimated a summer-monsoon mean upwelling of 2.2, 1.4, and 0.6 Sv, for the years of 1993–95, explaining the decrease with reduced winds during this time period.

During the winter monsoon, the cold and dry Northeast Monsoon winds, combined with Ekman pumping, cause subduction of high-salinity surface waters in the interior northern Arabian Sea (Morrison, 1997; Schott & Fischer, 2000). This generates the widespread Arabian Sea Water salinity maximum just underneath the mixed layer (Fig. 7).

#### 4.5.2. Models

Coastal currents develop along the Omani coast in all of the ‘realistic’ Arabian-Sea models noted above, but none of them focus much attention on the area. Some of the highly resolved solutions develop eddy fields in the interior of the northern Arabian Sea, but comparisons with the recent analyses of the mesoscale energy field noted above have yet to be carried out. So far, none of the models develops coastal squirts and filaments, probably because either their horizontal resolution is insufficient or (in the case of layer models) they did not allow for the upwelling of cool subsurface waters into the surface layer.

Another issue, already discussed for the interior Arabian Sea in Section 4.4, has been the relative importance of alongshore winds versus positive wind stress curl *west* of the axis of the Findlater Jet in forcing upwelling in the northern Arabian Sea. This is an important biological issue, as it has been commonly

accepted that such open-ocean upwelling provides the nutrients for the region's strong summertime blooms (Smith & Bottero, 1977; Brock, McClain, Luther, & Hay, 1991). As shown by Lee et al. (2000) the local mixed-layer entrainment overwhelms the Ekman suction resulting from the wind stress curl and also for most of the northern open-ocean upwelling regime (Fig. 40). In the MKM solution, most of the open-ocean upwelling occurs at the mouth of the Gulf of Aden where the amplitude of the wind curl is largest, whereas off the Omani coast, most of the upwelling occurs at the coast, and is driven by the coastal alongshore winds (McCreary et al., 1996a).

The model simulations of Rochford et al. (2000) suggested that the importance of horizontal advection is higher in explaining the heat budget at the site of the northern Arabian Sea mooring of Weller et al. (1998) during the winter monsoon than during the summer. How well a simulation of winter mixed-layer depths agreed with observations depended on how well the wind forcing used in that simulation generated the required advection.

## 5. Bay of Bengal, monsoon currents, central and eastern Arabian Sea

Like the western Arabian Sea, the western Bay of Bengal is subjected to strong seasonal reversals of wind-stress forcing. As a result, the processes that influence the EICC are similar to those that affect the Somali Current system. However, the local winds have weaker effects because remote forcing is relatively more important for the EICC than they are for the Somali Current. Indeed, remotely forced coastally-trapped waves and Rossby waves crossing the interior of the Bay are major contributors to EICC variability. Moreover, the influence of these waves extends around Sri Lanka to affect the west coast of India as well as the eastern and central Arabian Sea, and so these regions are included in the discussion in this section. A second complicating factor in the Bay is the large fresh-water flux from both rainfall and river discharges, which among other things prevents the accurate determination of geostrophic currents through the application of a mean T/S-relation to the available XBT temperature data base.

### 5.1. Observations

#### 5.1.1. Bay of Bengal and EICC

The seasonal cycle of the EICC and Bay of Bengal circulation has been investigated from analyses of ship-drift currents and shipboard surveys by Shetye et al. (1991a,b, 1993, 1996), and more recently by Vinayachandran and Yamagata (1998), Basu et al. (2000) and Eigenheer and Quadfasel (2000) using T/P altimetry. As for the Arabian Sea, circulation patterns in the interior of the Bay of Bengal contain many mesoscale features, but there do not appear to be any seasonally reoccurring coastal gyres analogous to the Southern Gyre and Great Whirl.

With the onset of the summer monsoon, the northward surface currents in the EICC off India do not strengthen, as might be expected. Rather, northward flow weakens or reverses in its northern part and a southward current appears off eastern Sri Lanka (Fig. 41). Shetye et al. (1991b) report that after the onset of the Southwest Monsoon of 1987, there were many indications of active upwelling along the east coast, with near-surface isotherms and isopycnals tilting upward from depths of about 80 m within 40 km of the coast, and deeper ones sloping downward suggestive of a southward undercurrent (Fig. 42). There is no indication of fresh water close to shore at this time (Fig. 42b). However, farther offshore Shetye et al. (1991b) found a southward-drifting plume of low-salinity waters, originating from the Brahmaputra and Ganges river outflows (Fig. 43a).

Using ship-drift currents and surface geostrophic flows derived from T/P (Fig. 44a,b), Eigenheer and Quadfasel (2000) showed that at the height of the summer monsoon there is a western-boundary confluence near 10°N, with the EICC flowing northwards to the north of 10°N and southwards to the south (Fig. 8).

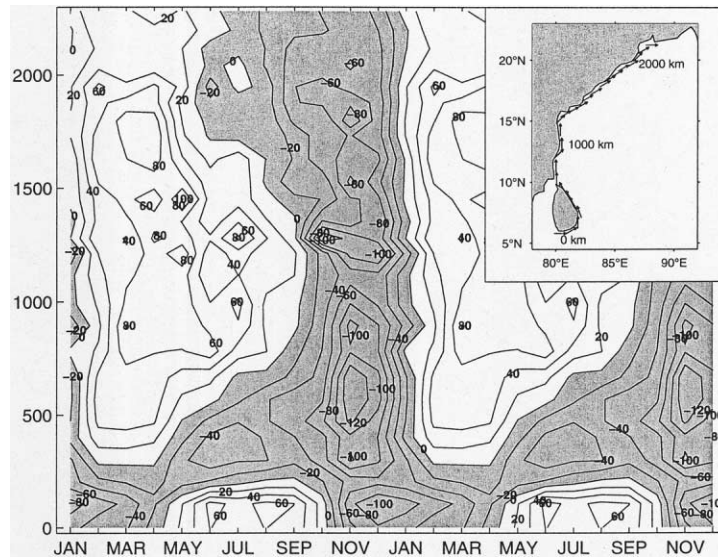


Fig. 41. Seasonal cycle of alongshore surface currents (from ship drifts) off East India and Sri Lanka as function of alongshore distance (see inset), starting at the southern tip of Sri Lanka. Current direction in each segment indicated in inset, positive is northward. (From Eigenheer & Quadfasel, 2000.)

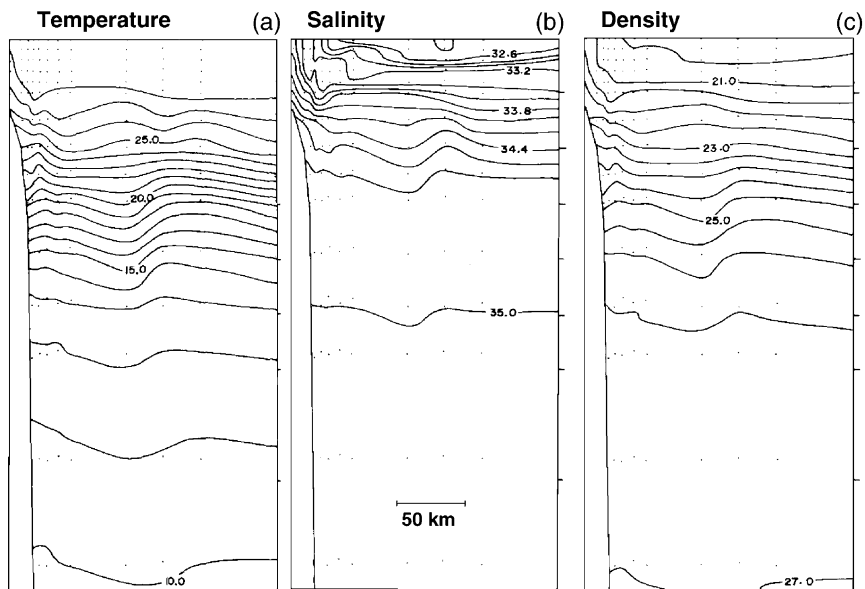


Fig. 42. Section across the EICC near 16°N during the Southwest Monsoon of a) potential temperature; b) salinity and c) potential density, indicating that coastal upwelling comes from shallow depths; section location see Fig. 20. (From Shetye et al., 1991b; section location see Fig. 20.)

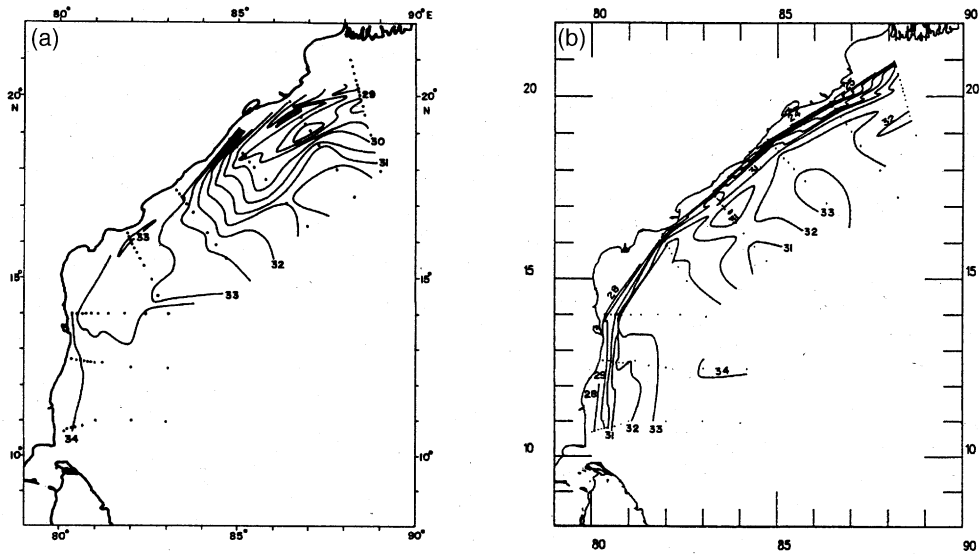


Fig. 43. Surface salinity in the western Bay of Bengal a) during the summer monsoon, showing offshore southward propagation of low-salinity waters (from Shetye et al., 1991b) and b) during the winter monsoon, showing narrow low-salinity plume along coast. (From Shetye et al., 1996.)

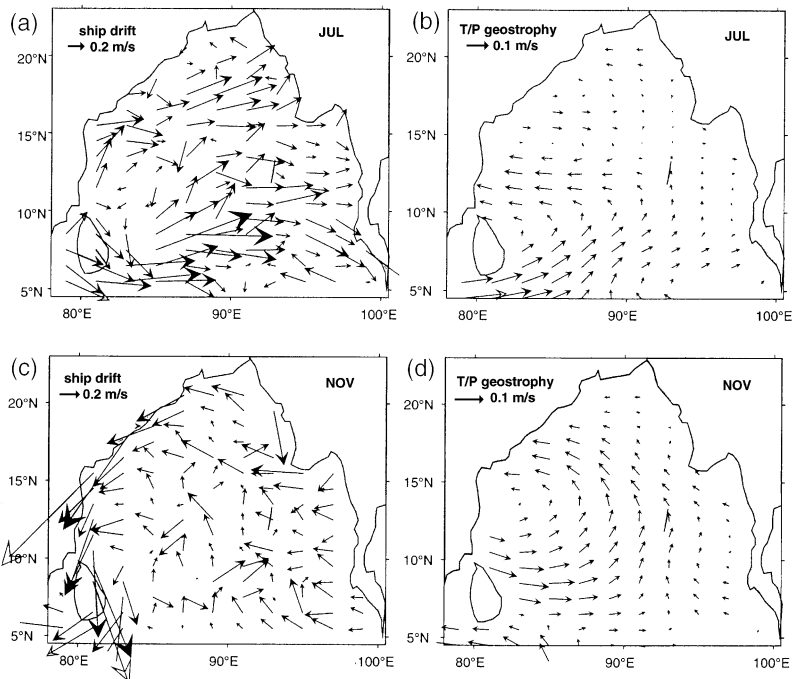


Fig. 44. Surface currents in the Bay of Bengal, for the a) summer monsoon (July) from ship drifts and b) geostrophic current anomalies from T/P altimetry; c) and d), as a), b) but for November (from Eigenheer & Quadfasel, 2000).

According to Vinayachandran, Masamoto, Mikawa, and Yamagata (1999a) this confluence is supplied mostly by the SMC across 6°N that circulates cyclonically about a dome of low SSH (Figs. 8 and 19), termed the Sri Lanka Dome by Vinayachandran and Yamagata (1998).

In late September, the EICC begins to flow southwards, and by November ship-drift currents show southward flow everywhere along the east coasts of India and Sri Lanka (Fig. 41). At this time, T/P altimetry suggests there is a slow cyclonic circulation around the Bay of Bengal (Fig. 44c,d), which breaks up into several cells as the monsoon season develops (Eigenheer & Quadfasel, 2000). In an analysis of sections observed during December 1991 between the northern end of the Bay and 10°N, Shetye et al. (1996) found the geostrophic transport relative to 1000 dbar increased southward from 2 Sv to about 8 Sv. Close to the entire east coast, they found a shallow low-salinity plume with a width of about 50 km (Fig. 43b).

During January, at the height of the winter monsoon before the winds begin to relax, the southward EICC decreases in strength and even reverses direction north of 15°N (Fig. 41), changes that must result from remote forcing. From March to May, the poleward-flowing EICC strengthens (Fig. 41) and extends southward to 10°N, even though the local winds are very weak. Shetye et al. (1993) estimated a transport of about 10 Sv for the northward EICC at this time, and concluded that it was the western-boundary current associated with a wind-driven, anticyclonic gyre in the interior of the Bay.

### 5.1.2. WICC

Striking developments along the west coast of India during the late spring are the shallowing of the thermocline, and an equatorward surface current and a weak (5–10 cm/s) poleward coastal undercurrent. Ship-drift observations show that southward flow appears along the west coast in March, reaches peak strength in July (Fig. 31a), and vanishes by October (Cutler & Swallow, 1984; Shetye & Shenoi, 1988). Isotherms tilt upward toward the coast from April until September, indicative of a poleward undercurrent (Antony, 1990). These features were confirmed by Shetye et al. (1990), who calculated the dynamic topography relative to 1000 db at various locations along the coast, finding that during the Southwest Monsoon there was an equatorward coastal current and a poleward undercurrent with its core at 150 m or below. A salinity section parallel to the shelf edge observed by Shetye et al. (1990) showed that the shallow spreading of high-salinity waters was southward and spreading of low-salinity waters at 100–200 m was northwards (Fig. 45).

Stramma et al. (1996) described the undercurrent along an 8°N section from shipboard ADCP measurements compared with geostrophy (Fig. 46). At the time of their survey in August, 1993, the winds were weak and northerly off the shelf edge, and the surface current was flowing northward counter to the prevailing winds at a speed of 40 cm/s. Offshore, the undercurrent core was detected at 100 m depth, and its total transport from the surface to 300 m was 4.7 Sv. Water-mass properties indicated that water at the shelf edge was a mixture of low-salinity water advected out of the Bay of Bengal around Sri Lanka and higher-salinity Arabian-Sea water.

The upwelling-favorable (equatorward) component of the winds along the Indian west coast strengthens in April, reaches a peak strength of 0.5 dyn/cm<sup>2</sup> in August and then weakens again in October (Shetye & Shenoi, 1988). For this reason Shetye et al. (1990) suggested that the coastal currents are forced locally by these winds. As noted below, however, numerical models suggest that they are predominantly forced remotely from the Bay of Bengal.

The WICC flows northward during the winter monsoon (Figs. 9 and 31b). In their analyses of several ship sections normal to the Indian coast taken from December 1987 to January 1988, Shetye et al. (1991c) found that the surface current decreased in width from about 400 km off South India near 10°N to just 100 km in the north at 22°N, where the geostrophic transport amounted to 7 Sv. A southward undercurrent was found underneath the northward surface flow. The ship-drift currents indicate that at this time the

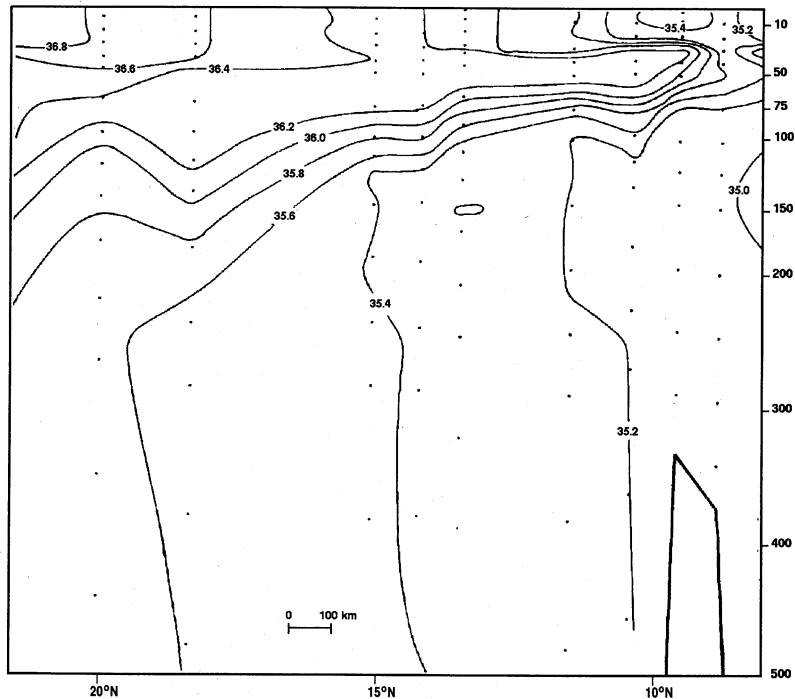


Fig. 45. Salinity distribution off western India during the summer monsoon along a section running parallel to the shelf edge; section location see Fig. 20. (From Shetye et al., 1990).

northward WICC was at its strongest for the year, and yet the coastal winds were very light or absent. This property lends strong support for the importance of remote forcing.

### 5.1.3. Laccadive High and Low

In January, an anticyclonic gyre, the Laccadive High (LH), develops off the southwest coast of India just north of the Laccadives and at the southern end of the WICC, where it is visible as a strong SSH anomaly maximum during the late winter monsoon (Figs. 19a and 9). It is accompanied by a temperature increase at the 100-m level (Fig. 15c). It was first described by Bruce et al. (1994) in an analysis of Geosat altimetry, hydrographic observations and model results. They found swirl velocities of about 30 cm/s, and estimated the total transport around the LH to be about 15 Sv. They concluded that its decay during the fall was related to Rossby-wave radiation into the southern Arabian Sea. This westward propagation is also visible in the phase plots along 7°N of Perigaud and Delecluse (1992) and was discussed in comparison with ship section observations by Brandt et al. (2002). With regard to the large-scale circulation in the eastern Arabian Sea, the existence of the LH means that the connection from the NMC to the WICC has to take a large westward detour around the LH, as observed in the winter monsoon steric height field (Fig. 18b). During the summer monsoon, the LH is replaced by a region of low sea level, the Laccadive Low (LL; Fig. 8) which is apparent in the detours that the steric heights take around that region (Fig. 18a) and in altimetry (Fig. 19c).

### 5.1.4. Eastern and central Arabian Sea

Ship-drift currents (Fig. 31a) for the summer monsoon indicate that there is a band of eastward flow to the north of the equator. These eastward currents are weaker in the 5–10°N latitude range and then increase

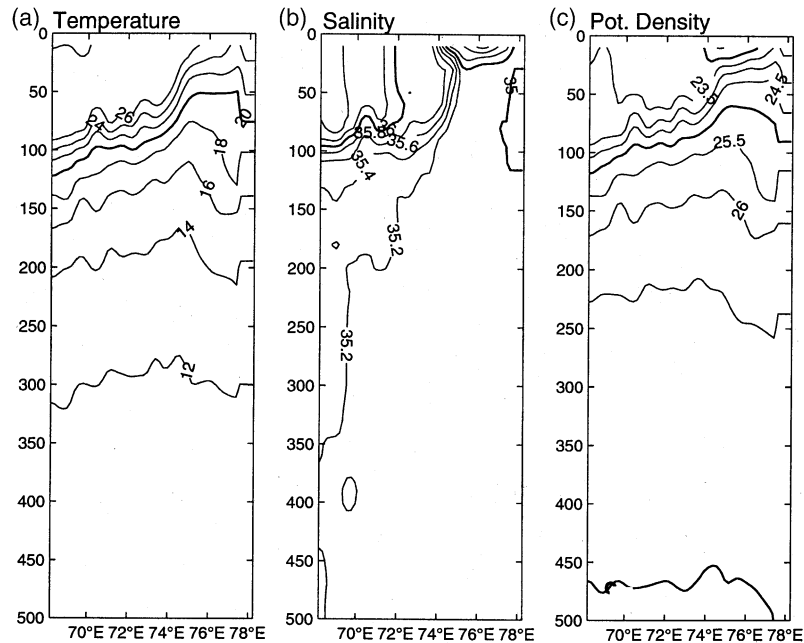


Fig. 46. Section off the west Indian coast along  $8^{\circ}\text{N}$  during the summer monsoon showing a) potential temperature; b) salinity and c) potential density; the spreading of isopycnals at shelf edge indicates northward undercurrent. (After Stramma et al., 1996.)

again toward the northern Arabian Sea (see Section 4.5). The seasonal-mean sea-level anomaly map (Fig. 19c) shows an extended high east of the northern Somali current, and low topography extending eastward off Arabia, indicating eastward geostrophic flow in the northern Arabian Sea that should then circulate around the LL to join the SMC. The low-latitude branch is indicated by the ridge of high sea level that extends zonally north of the equator in Fig. 19c. As described in Section 4.1, while there is low-latitude outflow from the Somali Current regime (out of the Southern Gyre) throughout summer monsoon supplying the zonal flow north of the equator, there is very little outflow into the central Arabian Sea in the  $5\text{--}10^{\circ}\text{N}$  latitude range (Figs. 32 and 36). The low-latitude flow extends all the way across the Arabian Sea to connect with the SMC (see Section 5.2.7).

During the winter, there is low-latitude westward flow toward the Somali Current south of India and northwestward flow along the west coast of India that does not merge into an organized westward pattern in the north (Figs. 11, 31, 39). There is, however, also some inflow in the  $5\text{--}10^{\circ}\text{N}$  band toward the Somali Current, consistent with the moored measurements in the region (Fig. 35b). The dominant feature of the southeastern Arabian Sea during the fully developed, winter monsoon is the circulation associated with the LH, as seen in the altimetry signal (Fig. 19a). This circulation cell takes up part of the westward-flowing NMC south of Sri Lanka (Fig. 9), and another part continues westward across the Arabian Sea.

The relation between the LH/LL and the interior Arabian Sea was studied by Brandt et al. (2002) and Stramma, Brandt, Schott, Quadfasel, and Fischer (2002) who analysed WOCE ship sections along  $8^{\circ}\text{N}$  from the summer and winter monsoons in conjunction with T/P altimetry. They fitted first- and second-mode annual Rossby waves to the seasonal differences along part of the section in the central Arabian Sea, and concluded that much of the seasonal differences in stratification and meridional circulation there could be explained by the propagation of Rossby waves from the west Indian coast.

5.1.5. Monsoon currents

The region between Sri Lanka and the equator is a bottleneck for the zonal currents in the northern Indian Ocean, providing the major pathway for the exchange of water between the Arabian Sea and Bay of Bengal. As known from ship drift observations (Cutler & Swallow, 1984), this current reverses with the monsoons. It flows eastward as the SMC from June to September (Fig. 31a) and westward as the NMC from November to February (Fig. 31b). This is also apparent from the reversing sea level slope in Fig. 19a,c. Thus, while the variability is mostly semiannual in the equatorial band, it is mostly annual for the monsoon currents.

5.1.5.1. Southwest Monsoon Current: Schott, Reppin, Fischer, and Quadfasel (1994) found that the SMC decayed so quickly with depth that its transport had to be determined either by extrapolating ADCP and current-meter observations to the surface or by using seasonal-mean ship-drift currents as surface values (Fig. 47a). Based on shear extrapolation, the eastward SMC transport between 4–6°N was estimated to be 8.4 Sv, with 70% in the top 100 m. The current and transport time series also exhibited strong intraseasonal

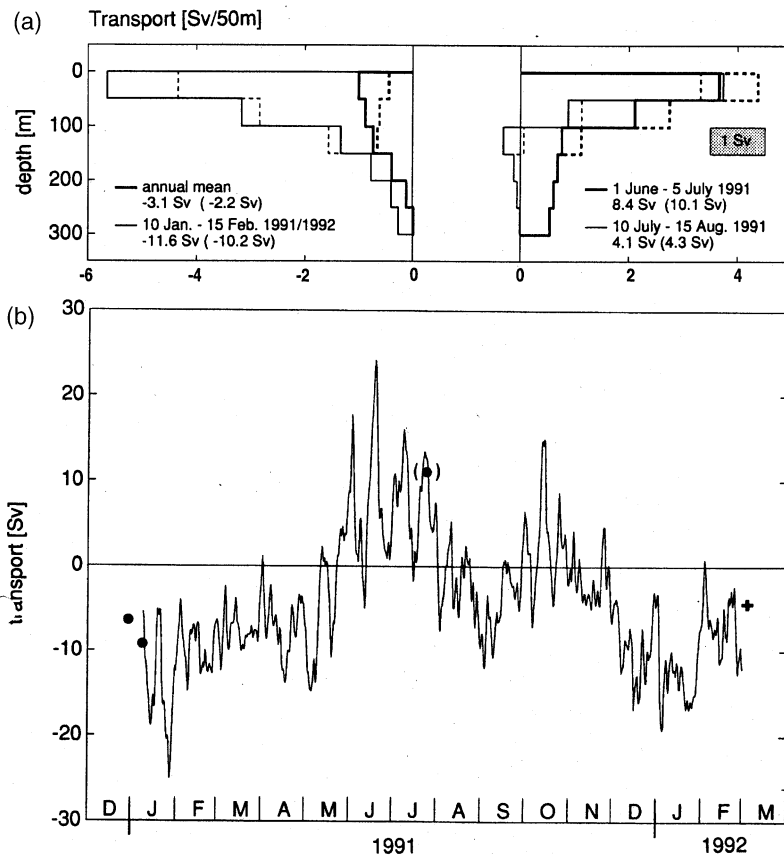


Fig. 47. Monsoon Current transport south of India-Sri Lanka. a) Decomposition into depth bins using two different extrapolation schemes from the top instrument level toward the surface: extrapolation of moored current-meter shear from uppermost levels (solid) or using shipdrifts as surface values (dashed). The heavy curve on left side shows annual mean. b) Transport time series, based on shear extrapolation; dots mark shipboard ADCP sections for comparison. (From Schott et al., 1994.)

variability (Fig. 47b). In the shipboard measurements of August 1993 (Fig. 48a), the eastward core of the SMC is shown to be near 4°N, and separated from the eastward equatorial flow by a zone of weak currents. There is a westward undercurrent underneath the SMC core, which is also seen in the mooring data.

An intriguing feature in Fig. 48a is the presence of a narrow westward current just south of Sri Lanka from 5.5 to 6°N. The low salinity water near the Sri Lankan coast (Fig. 48b) clearly indicates that it originates in the Bay of Bengal. It is likely that this current results from coastally trapped waves traveling around Sri Lanka that have been generated by winds within the Bay. Consistent with this idea, stations taken near the Sri Lankan east coast exhibited a band of southward flow (D. Quadfasel, pers. comm., 1999), which was an extension of the seasonal southward flow along the western boundary of the southern Bay of Bengal (Fig. 41).

Thus, the source of water for the SMC ultimately must be in the western Arabian Sea, and as discussed earlier, two inflowing branches are supplied by the near-equatorial outflow of the Southern Gyre and by the northern outflow of the Somali Current, respectively. The latter connection appears in the steric height contours of Fig. 18b. The relative transport contributions from the northern Somali Current and the Southern Gyre outflow are still unknown.

After passing Sri Lanka, much of the SMC turns northward into the Bay of Bengal, flowing around the cyclonic Sri Lanka Dome (Figs. 8, 18b and 19c). From XBT and T/P analyses, Vinayachandran et al. (1999a) estimated that northward transport of the SMC across 6°N is about 10 Sv. Whether a second SMC

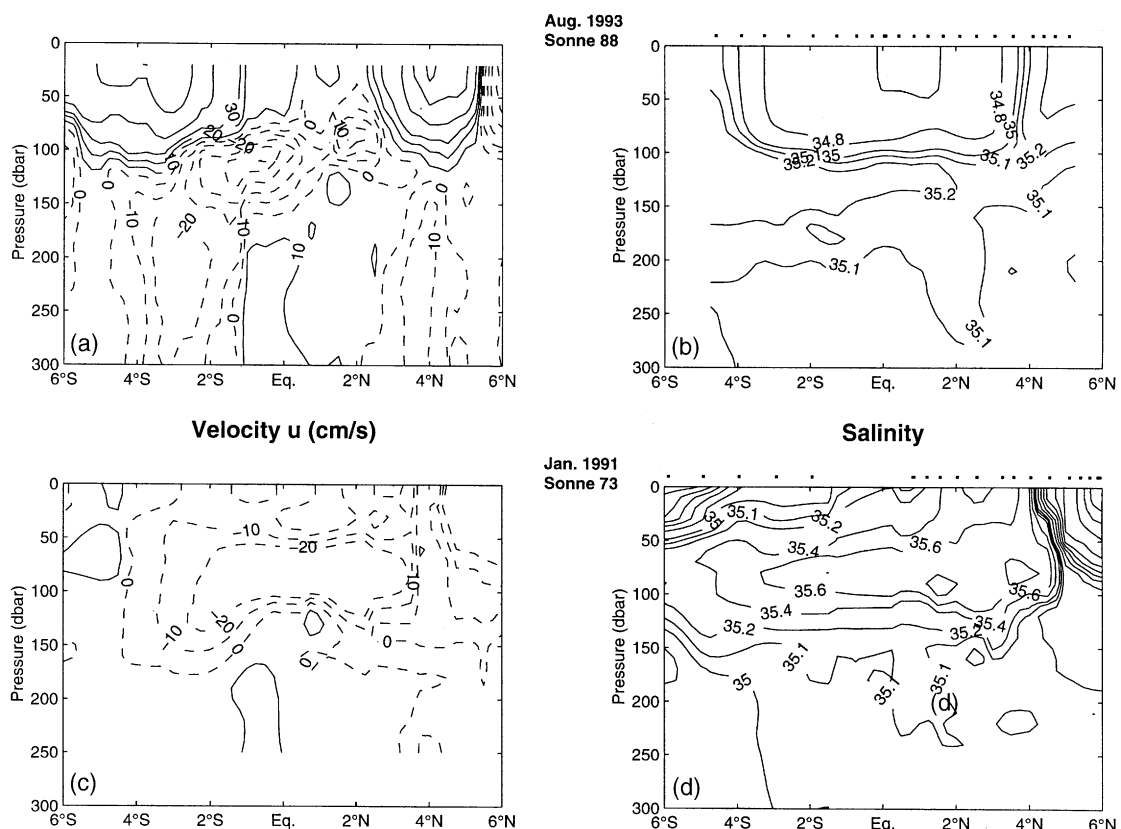


Fig. 48. Sections of a) zonal currents and b) salinity observed along 80.5°E south of Sri Lanka during the summer monsoon, August 1993, and c,d) during the winter monsoon, January 1991; section location see Fig. 20.

branch continues to flow eastwards and eventually bends southward to cross the equator is unclear. Such a flow, however, cannot be large because the  $6^{\circ}\text{N}$  transport is about the same as that carried by the SMC eastward past Sri Lanka.

**5.1.5.2. Northeast Monsoon Current:** The NMC flows westward south of India (Fig. 9), and during 1991 its transport was observed to be 11 Sv (Schott et al., 1994). This transport is larger than the estimated SMC transport, and results in a net annual-mean transport of 2.5 Sv to the west for 1991 (Fig. 47a). The westward NMC flow persists through March, as seen in the observations of Hacker, Firing, Hummon, Gordon, and Kindl (1998); Fig. 49a, called NEC there), and into April (Fig. 47a). The NMC partly carries fresher water from the Bay of Bengal, the properties of which are detectable in the WICC further to the north (Fig. 46; Stramma et al., 1996).

During the ship observations of January, 1991, the NMC did not extend deeper than about 120 m and was marked by very reduced salinities ( $<33$ ) at the northern end of the section originating in the Bay of Bengal (Fig. 48c,d). It was separated from the equatorial regime by a band of weak easterly flow in the  $3\text{--}4^{\circ}\text{N}$  latitude band. The large seasonal differences in the salinities of the equatorial zone evident in Fig. 48b,d are remarkable. Although climatological salinities are somewhat higher during winter in the central equatorial Indian Ocean than during boreal summer (Levitus & Boyer, 1994a), the cause of the large positive anomaly of January, 1991, needs further investigation.

The larger-scale circulation at the end of the 1994–95 winter monsoon was surveyed by Hacker et al. (1998). From their upper-layer ADCP vector distributions (Fig. 49), they concluded that from early March, 1995, the NMC was supplied by recirculating water brought eastward north of the equator.

## 5.2. Models

### 5.2.1. EICC

An important driving mechanism of the EICC annual cycle is certainly the winds within the Bay, which also reverse with the monsoons (see Fig. 1). However, the peak months of the monsoons (January and July) do not coincide with the times of maximum current speed (March and November), so the relationship between the winds and the currents is not obvious. Indeed, four different driving mechanisms have been

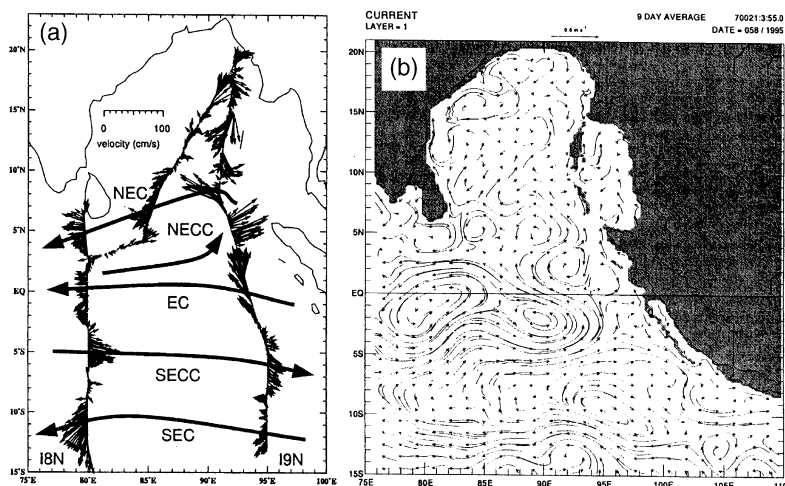


Fig. 49. Comparison of near-surface currents in the eastern tropical Indian Ocean between a shipboard ADCP survey from early March and a model result. See text for details. (From Hacker et al., 1998.)

proposed to account for various aspects of EICC variability: interior Ekman pumping, ‘local’ alongshore winds adjacent to the Indian and Sri Lankan coasts, ‘remote’ alongshore winds adjacent to the northern and eastern boundaries of the basin, and remotely forced signals that propagate into the Bay from the equator. Each of these processes has been investigated in recent model studies, but the observational base whereby model results can be compared is still sparse, as reviewed above.

Yu, O’Brien, and Yang (1991) and Potemra et al. (1991) proposed that remote forcing from the equator could have an important effect within the Bay. In this mechanism, equatorial Kelvin waves reflect off the eastern boundary of the Indian Ocean, partly as a packet of coastal Kelvin waves that propagate around the perimeter of the Bay, and partly as a packet of Rossby waves that radiate westward back into its interior. MKM commented on the relative importance of this process in their solution, suggesting that it was influential primarily during the Southwest Monsoon when it tends to drive southwestward flow in the EICC against the prevailing winds. Equatorial forcing is important at seasonal time scales because the Kelvin waves propagate so quickly. For example, mode-1 Kelvin waves in the MKM model have a speed of 347 cm/s, and so take only about 18 days to propagate around the perimeter of the Bay (~5500 km); for mode-2 waves, which dominate in the MKM solution, the corresponding wave speed and propagation time are 125 cm/s and 50 days.

Shetye et al. (1993) proposed that Ekman pumping in the interior of the Bay is the primary forcing mechanism of the northeastward EICC from February to May. They noted that during these months the wind-stress curl is negative over most of the Bay and that, based on ship-drift evidence, there is a large anticyclonic gyre in the northern Bay, a finding which is in agreement with the anticyclonic gyre observed in T/P altimetry by Eigenheer and Quadfasel (2000). Shetye et al. (1993) therefore hypothesized that the EICC is a northeastward, western boundary current that compensates for southward Sverdrup transport in the interior ocean.

MKM suggested that forcing by both local and remote alongshore winds also influences the EICC. Local alongshore winds drive an EICC in the direction of the wind. Remote alongshore winds affect the EICC by exciting not only coastal Kelvin waves that propagate anticlockwise around the perimeter of the Bay, but also Rossby waves that radiate westwards from the eastern boundary. MKM argued that the collapse of the local alongshore winds at the end of the Southwest Monsoon causes the southwestward EICC in the fall and winter (see Section 5.2.4 for a discussion of this process), and that remote alongshore winds are responsible for the onset of the northeastward EICC in February.

Shankar, McCreary, Han, and Shetye (1996) studied the effects of forcing over the interior of the Bay with an analytical model, and found that interior Ekman pumping produced barotropic and baroclinic Rossby waves that, by reflection at the western boundary, cause a northward (southward) coastal current if the interior wind stress curl is anticyclonic (cyclonic). An important result was that the Ekman-pumping contribution to the seasonal EICC cycle amounted to about 30% of the observed EICC surface current seasonal amplitude estimated from ship-drift currents. The superposition of forcing by local alongshore winds and offshore Ekman pumping yielded a model EICC surface flow that was in good agreement with the ship drifts from June to December, but the onset of northward flow in spring occurred later than in the observations. Furthermore, the model transport was only about half the reported summer monsoon value of about 10 Sv (Shetye et al., 1993).

McCreary, Han, Shankar, and Shetye (1996b) extended the Shankar et al. (1996) study using a linear numerical model to investigate the relative contributions of four processes that force the EICC, namely, alongshore winds, Ekman pumping, equatorial effects and Rossby waves from the eastern end of the basin. Fig. 50 plots the EICC total transport at two locations, at 16°N and 8°N, together with the contributions from each forcing. The contributions were isolated in a suite of test solutions that selectively removed effects generated by the other three forcings, and were found to change significantly along the coast and at different times of the year. At 8°N, the effects of local alongshore winds are nearly offset by the large Ekman-pumping contribution during the summer monsoon, while equatorial effects are important in the

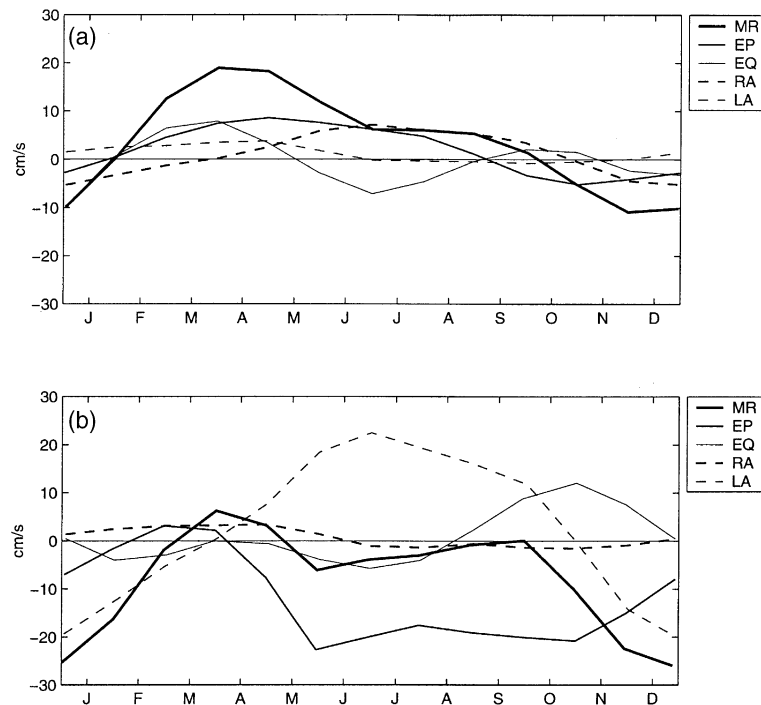


Fig. 50. Contributions to total model surface currents of the EICC (MR, heavy) by different forcing mechanisms at a) 16°N and b) 8°N: local alongshore wind forcing (LA, thin dashed), interior Ekman pumping (EP, intermediate solid), remote alongshore wind forcing along the eastern coast (RA, heavy dashed) and waves originating at the eastern equatorial end (EQ, thin solid). (After McCreary et al., 1996b.)

fall. At 12°N, the equatorial contribution does not show the fall maximum and Ekman pumping is only important in the winter monsoon. Remote forcing by Rossby waves from the eastern boundary is a weak process throughout the year and makes only a relatively small contribution to the northward EICC from January to May.

### 5.2.2. EICC undercurrent

McCreary et al. (1996b) found an EICC undercurrent in their solution but only during the Southwest Monsoon. From May to July, the solution had a southwestward flow along the Indian east coast extending from the surface to depths greater than 1000 m, which was driven primarily by equatorial forcing (Fig. 50). From July to September, the southwestward flow weakened, became overlain by a northeastward surface current, and was only present as a shallow subsurface counterflow. As for the Somali undercurrents, this EICC undercurrent was not directly forced by the local alongshore winds, but rather was primarily remotely driven by equatorial forcing and interior Ekman pumping. While there are no direct current measurements of this coastal undercurrent, there are indications of it in hydrographic sections (Fig. 42).

### 5.2.3. Sri Lanka Dome

McCreary, Han, Shankar, and Shetye (1996b) and Vinayachandran and Yamagata (1998) both discussed the dynamics of the Sri Lanka dome in their respective solutions. They both noted the presence of strong cyclonic wind-stress curl over the southwestern region of the Bay during the summer monsoon (Fig. 2b), and concluded that Ekman pumping associated with this curl was the dominant process that forced the Sri

Lanka dome. In support of this idea, the region of positive Ekman pumping shifted northward as the season progressed, and the dome (*i.e.*, a region of low sea level and cyclonic circulation) appeared to follow along with it (see Figs. 2 and 5d of McCreary et al., 1996b, and Fig. 4 of Vinayachandran & Yamagata, 1998). In January, it became a well-defined anticyclonic circulation cell centered near 10°N just off the Indian coast which Vinayachandran and Yamagata (1998) referred to as the ‘Bay of Bengal’ dome. This seasonal progression also occurred in the MKM solution (Figs. 10 and 11). Note also that the Sri Lanka dome in the MKM solution was part of an extended belt of thin surface-layer thickness linking it to the LL west of India and to the WICC (Fig. 10; see Section 5.2.4).

#### 5.2.4. WICC

As noted above, the annual variability of the currents along, and offshore from, the west coast of India is significant, but the local winds are weak and not likely in themselves to be able to account for the observed circulation changes. A similar property holds in the MKM solution, and they concluded that the model WICC was almost entirely remotely driven by winds in the Bay of Bengal during both monsoons.

At the onset of the Southwest Monsoon, the upper layer of the MKM solution thinned along the west coast, and a southward WICC with a northward undercurrent developed there. This thinning was contiguous with thinning along the east coast of India and across the southern Bay of Bengal (Fig. 10). This property suggests that remote forcing by winds in the Bay of Bengal and south of India causes the west-coast thinning via the northward propagation of coastal Kelvin waves. MKM carried out two test calculations to confirm this idea. In a test without Bay-of-Bengal winds, the upper layer did not thin anywhere along the Indian coasts, and there were no west coast currents at all. Conversely, in a test without Arabian-Sea winds, the main-run and test solutions were hardly changed near the west coast of India. The only notable difference between them was that the coastal region of cool SST extended only to 12°N along the coast in the test run whereas in the main run it extended to 17°N, implying that forcing by the local winds was enhancing the model upwelling.

In November, the MKM solution developed a northward surface current and a southward undercurrent along the west coast of India as far north as 20°N (Fig. 11). In addition, a southward surface current existed everywhere along the east coast of India, intensifying to the south. Both currents resulted from the collapse of the Southwest Monsoon winds in the Bay of Bengal as follows. During the summer, a southwestward pressure gradient developed along the east coast of India to balance the alongshore winds there, and as a result the interface beneath the upper layer tilted upwards markedly toward the south. When the upwelling-favorable alongshore winds vanished in the Bay at the end of the monsoon, water flowed down the pressure gradient until the tilt was eliminated, thickening the upper layer by 50 m or more near the tip of India and causing the southward EICC. This thickening propagated around Sri Lanka and poleward along the west coast as a packet of coastal Kelvin waves, generating the geostrophically balanced northward WICC there.

In both monsoon seasons, then, the west coast of India is tightly linked to forcing in the Bay of Bengal via coastally trapped waves traveling around the Indian subcontinent. It should be pointed out though, that direct observational evidence for such waves is still lacking.

#### 5.2.5. Laccadive High and Low

Models indicate that, even though the LH is located in the southeastern Arabian Sea (Fig. 8), it derives its existence from remote forcing outside the Bay of Bengal by a continuation of the processes discussed in the preceding subsection. Specifically, it results from the offshore propagation of the deep-thermocline region along the west Indian coast as a packet of Rossby waves. The Rossby waves propagate offshore much faster nearer the equator (since their speed is inversely proportional to the Coriolis parameter), thereby creating the distinctive structure of the LH (Fig. 11). MKM argued that the LL was generated similarly by the radiation of a remotely generated shallow-thermocline region from the west coast (Fig. 10). Bruce et al. (1994) also presented evidence, based on upper-layer thickness, currents and tracers injected into a

$2\frac{1}{2}$ -layer model, for a strong Bay of Bengal influence on the LH. Shankar and Shetye (1997) showed the existence of the LL and LH in a linear model, underlining the fact that linear wave dynamics are the important generation mechanism. The LH is also a prominent feature in the POCM solution (Fig. 39a), with part of its low-latitude westward flow circulating anticyclonically around it to supply the northward WICC (Schott & Fischer, 2000).

#### 5.2.6. *Eastern and central Arabian Sea*

During summer, the low-latitude outflow from the Southern Gyre in the MKM solution is trapped along the equator in the western ocean but then is split in the central basin into a northern branch (the SMC) and a branch south of the equator after it encounters a Rossby wave generated in the east by WJ reflection (Fig. 10). In the central Arabian Sea, MKM upper-layer currents are weakly anticyclonic, turning around the LL off the southwest Indian coast. In the POCM simulation, the outflow from the Arabian Sea is via the WICC around the LL and from low latitudes in the west, similar to the MKM solution; however, in contrast to MKM, it has no focused eastward branch near the equator (Fig. 13). During winter, the NMC in the MKM and POCM solutions flows anticyclonically around the LH (Figs. 11 and 14). In contrast, in the POCM solution it flows farther westward far into the Arabian Sea, with some of its flow turning northward toward India around an elongated LH and some continuing toward Somalia (Fig. 14).

A prominent process that drives these flows is remote forcing by Rossby waves originating in, or propagating across, the central Arabian Sea as has recently been confirmed from observations (Brandt et al., 2002). Details of these propagating signals have already been discussed earlier in the sections on the winter monsoon and Somali undercurrents (see Sections 4.2 and 4.3). The causes of the differences in flow patterns between the MKM and POCM solutions are not clear, but a likely candidate is differences in the representation of Ekman flows (see next subsection).

#### 5.2.7. *Southwest Monsoon Current*

MKM and Vinayachandran et al. (1999a) both discuss the physics of the SMC. Two driving mechanisms contribute to the SMC in their solutions, both of which begin in April and May. One is local forcing by the wind stress curl, a process that is strongest in the southwestern Bay of Bengal (Fig. 2b) where it generates the Sri Lanka dome. This forcing causes the upper layer of the model to thin north of the wind axis, to deepen south of it, and hence to produce an eastward geostrophic current. The other process is the reflection of an equatorial Kelvin wave associated with the spring WJ as a packet of downwelling-favorable Rossby waves. This process affects currents more in the central and eastern Bay, and accounts for the initial northward bending of the SMC into the Bay. The wave in the MKM solution is evident in Fig. 10 as the region of thick  $h_f$  in the eastern, tropical ocean.

Consistent with the observations, models indicate that the source of water for the SMC is a drift across the Arabian Sea. In the MKM solution (Fig. 10), however, this drift turns much more to the south than it does in the ship-drift observations. Indeed, some of it first flows to the equator before returning northward to join the SMC. A similar flow field is present in the GCM solution of Anderson et al. (1991; see their Fig. 14). A possible cause for this model/data disparity is the lack of sufficient vertical shear in the MKM layer model, which may underestimate the importance of wind-drift flows confined to the mixed layer. In support of this idea, Hastenrath and Greischar (1991) computed geostrophic currents relative to 400 db from historical data and Ekman currents from surface wind data for the tropical Indian Ocean. They concluded that the flow across the southern Arabian Sea is primarily an eastward Ekman drift. Another possible cause is windage.

Several models obtain westward undercurrents beneath the SMC, in agreement with the observations (Fig. 48). Potemra et al. (1991), using a  $3\frac{1}{2}$ -layer model, obtained an annual harmonic of 6 Sv transport amplitude for the zonal Monsoon Current south of Sri Lanka in their top layer and a strong semiannual harmonic in their undercurrent layer. The result was a westward undercurrent during June to August and

a weak eastward undercurrent during October to November. The mechanism found to be responsible was an equatorial Rossby wave. This mechanism was confirmed by the MKM solution, in which this undercurrent is clearly caused by the Rossby-wave packet reflected from the eastern boundary. This packet is composed mostly of mode-2 baroclinic waves, and the undercurrent is the reversed lower-layer flow associated with this wave.

#### 5.2.8. *Northeast Monsoon Current*

Three processes contribute to the NMC in the MKM solution. In the southern Bay of Bengal, it is forced by local Ekman pumping, which thins the upper layer south of the wind axis and thickens it north of the axis, thereby generating a westward geostrophic flow. In the southwestern Arabian Sea, it is driven by the westward radiation of downwelling Rossby waves from the west coast of India (the westward extension of the LH), which generates an eastward geostrophic flow along its southern edge. The third process is remote forcing via an upwelling-favorable, mode-2, equatorial Kelvin wave and its reflection from the eastern boundary as a packet of upwelling-favorable Rossby waves, which is generated by strengthened easterly winds in the western and central oceans.

For the POCM current field (Fig. 39a), the prominent role of the LH in taking up the part of the NMC that does not continue westward at low latitudes has already been alluded to above. A model circulation field for the eastern part of the NMC of Hacker et al. (1998; Fig. 49b) shows that there may also be significant cross-equatorial exchange in the eastern basin, supplying water from the Southern Hemisphere out of the SECC to be carried back westward by the NMC. The MKM solution also shows this northward flow across the equator in the eastern basin (Fig. 11).

## 6. Southern hemisphere

Although the effects of monsoon forcing are most apparent in the Northern Hemisphere, there is also significant seasonal variability in the southern subtropical and midlatitude Indian Ocean, related in part to the monsoons. Here, we discuss the prominent southern-hemisphere currents and their seasonal variability. We begin with a brief section on the low-latitude circulation along the eastern Indonesian boundary and the NW Australian shelf (Section 6.1). Next, we review the Leeuwin Current off the west Australian coast, which is the only eastern-boundary current in the world ocean that flows poleward against the prevailing winds (Section 6.2). Finally, we discuss interior circulations and western boundary currents (Section 6.3).

### 6.1. *Low-latitude eastern-boundary circulation*

#### 6.1.1. *Near-equatorial boundary circulation*

Based on the hydrography, sea-level data, and ship-drift currents available at the time, Wyrtki (1961) developed composite seasonal circulation patterns for the seas within and neighboring the maritime continent. For the South Java Current, he estimated a maximum eastward transport of 4 Sv during the late winter monsoon and weak westward flow during the summer monsoon (Figs. 8 and 9). Based on ship-drift data, Quadfasel and Cresswell (1992) showed that the South Sumatra Current had a southward flow year-round farther to the northwest. They confirmed the patterns of weak seasonal surface currents, which they had derived in an earlier analysis of ship-drift currents along the Indonesian island arc. They also found that alongshore speeds of individual drifters could reach a maximum of 1 m/s, compared to monthly-mean ship-drift maxima of only 0.2–0.3 m/s. Near the equator, the climatological ship-drift flow is also mostly southeastward throughout the year, except at times when equatorial Kelvin waves associated with the WJs reflect from the eastern boundary (Section 3), when it splits to flow into both hemispheres.

Recently, Shenoi et al. (1999), analyzing seasonal currents from a large number of drifter tracks, also

found that the boundary flows at and south of the equator at the eastern end were dominantly southward. In particular, their analysis showed that the spring and fall WJs predominantly feed the southward, rather than the northward, eastern-boundary flows. The mixed-layer depth climatology (Fig. 17b,d) also supports the idea that effects of the WJs extend beyond the southern end of Sumatra. Furthermore, the sea-level gradient along the eastern boundary and its annual cycle reported by Clarke and Liu (1993; see Section 3.1.1), which is presumably driven by the local alongshore winds, is also consistent with such eastern-boundary flows. Thus, near the eastern boundary there appears to be a mean southwestward cross-equatorial flow, with strong annual and semiannual signals superimposed. Transport time series of the South Java Current near Sunda Strait were derived by Meyers (1996) from his XBT trackline analysis and showed considerable interannual variability with transports occasionally up to 10 Sv, but the narrowness of the current means it may not have been adequately resolved by the XBT spacing.

Numerical models are able realistically to simulate basic properties of the annual cycle of these currents, but miss a number of features. In the MKM solution, for example, the South Java Current flows strongly eastward during the winter monsoon, but is weakly eastward during the summer monsoon (Figs. 11 and 10). Off the Sumatra coast, although the annual-mean flow is southeastward, the flow reverses from January through March (Fig. 11). In solutions typically the cross-equatorial eastern-boundary current is weak, and does not appear in either monsoon season in the solutions of Wacongne and Pacanowski (1996) and MKM.

Little modelling work has focussed on understanding the dynamics of these coastal currents. As discussed in Section 3, Clarke and Liu (1993) concluded that the reflection of equatorial Kelvin waves was involved in determining their semiannual cycle, whereas the coastal adjustment to the monsoon winds was important for the annual cycle, but these ideas have not been verified in numerical solutions. Other unresolved issues are the influences of the Indonesian Throughflow from the Lombok and Timor Straits on the coastal currents, and the dynamical connection of the low-latitude eastern-boundary currents to the currents along the Australian coast.

#### *6.1.2. Northwest Australian shelf and Arafura Sea*

The XBT tracklines established during the WOCE period, running parallel to the Australian shelf edge from Perth up to Sumatra and from Port Hedland to Timor allow the estimation of geostrophic transports, not only with respect to the Indonesian throughflow (Meyers et al., 1995; Meyers, 1996) but also into the Northwest Australian shelf regions (Fig. 51a). Godfrey and Mansbridge (2000) evaluated seasonal cycles of Ekman transports across a line running parallel to the shelf edge (from point Q to N in Fig. 51a) and geostrophic transports between XBT time series from boxes around those points, using a mean T/S relation and a reference level of 400 m. They found strong monsoonal cycles in the Ekman transports, but small annual mean transport onto the shelf region and into the Arafura Sea (Fig. 51b). The onshore Ekman transport onto the shelf regions rises to a maximum from May to July and falls to a minimum from December to February, suggesting that coastal upwelling occurs during the austral summer. In contrast, in the Arafura Sea the Ekman transport is almost out-of-phase with the shelf Ekman transport, indicating that the strongest upwelling in the Arafura Sea occurs from June to August. Interestingly, the onshore geostrophic transport onto the shelf in the top 200 m has a seasonal cycle that nearly cancels that of the shelf Ekman transport (Fig. 51c), yielding an almost constant combined onshore transport over the year of about 2.5 Sv.

Godfrey and Mansbridge (2000) also estimated the heat budget of the shelf region, and concluded that there is substantial offshore heat export from the shelf regions in summer by the Ekman transports. For the northern shelf and Arafura Sea, they concluded that there is wintertime upwelling of about 1 Sv, supplied by an onshore deep inflow (from below 200 m) onto the shelf and balanced by a westward Ekman surface transport. This overturning circulation requires a warming of the deep inflow by about 8°C, and Godfrey and Mansbridge (2000) emphasized the role of bottom tidal mixing in accomplishing this water-mass transformation.

## NW Australian Shelf-Arafura Sea

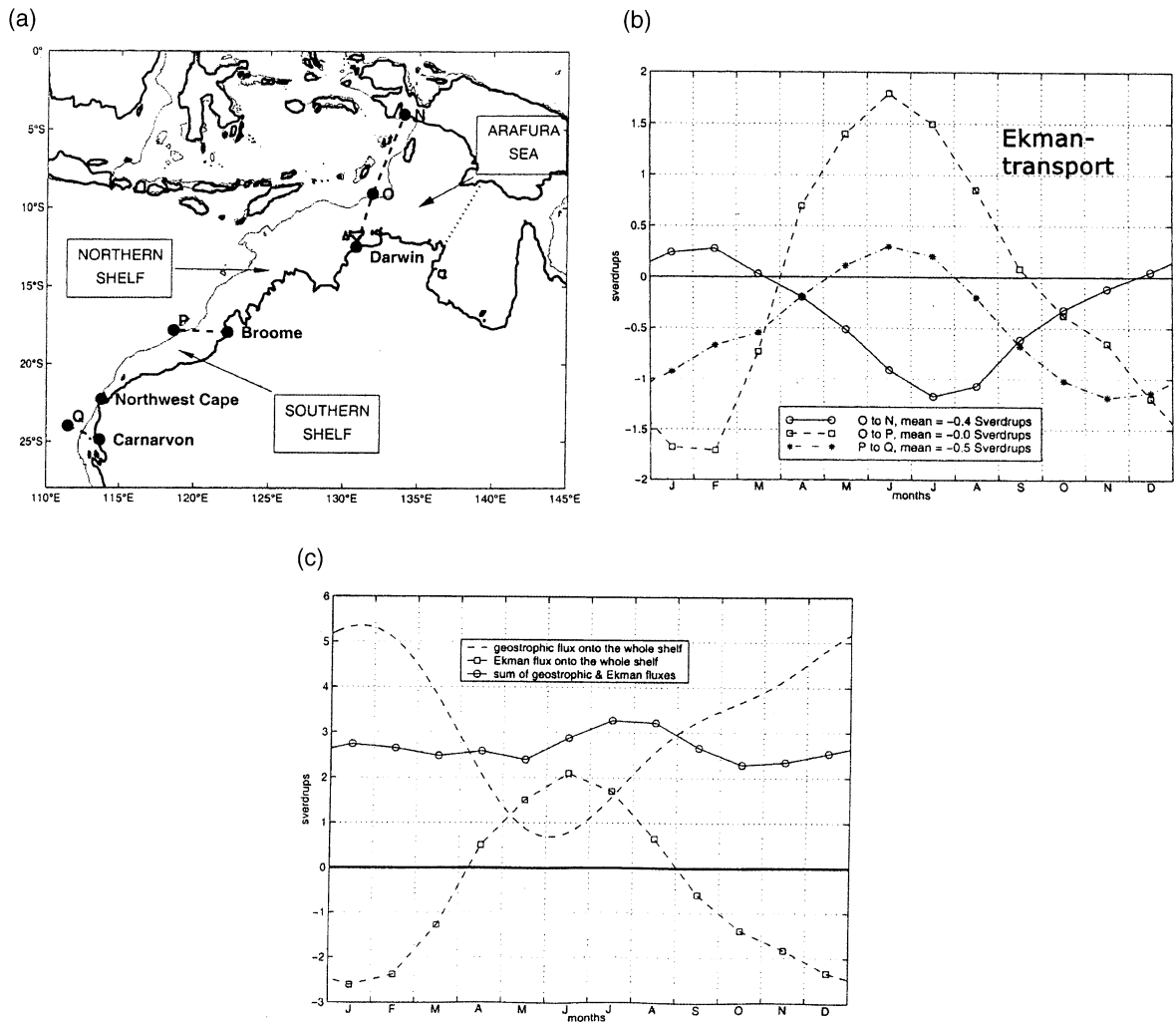


Fig. 51. a) Northwest Australian shelf region and Arafura Sea with points N to Q. b) Seasonal cycles of Ekman transports into the Arafura Sea (across segment NO), and onto the shelf (across segments OP and PQ, respectively). c) Seasonal cycle of geostrophic transport above 200 m and Ekman transport onto the shelf across segment OQ, as well as their sum. (From Godfrey & Mansbridge, 2000.)

### 6.2. Leeuwin Current

#### 6.2.1. Observations

The Leeuwin Current flows southward along the West Australian coast (Fig. 52). Off southwest Australia, it is about 50 km wide, extends to depths of about 250 m, and has a mean speed of about 30 cm/s with a seasonal maximum of 60 cm/s (Smith et al., 1991). It follows the coast around Cape Leeuwin at the southwest corner of Australia to beyond 120°E (Cresswell & Petersen, 1993). An equatorward undercurrent, the Leeuwin Undercurrent, is found offshore from the shelf break (Fig. 52).

Moored-array observations yielded an annual-mean transport of about 4 Sv past the southwestern tip of

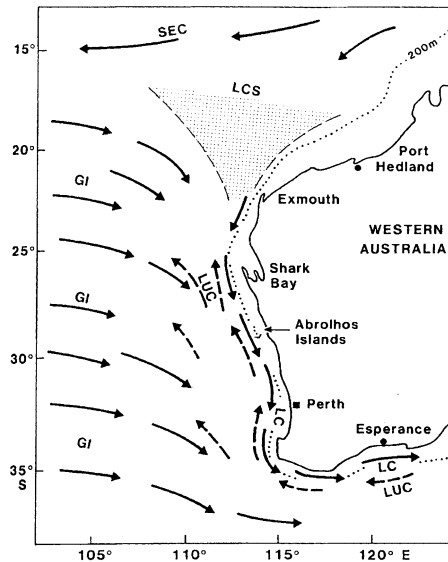


Fig. 52. Schematic diagram showing the Leeuwin Current (LC) off western Australia, the geostrophic inflow from the west (GI), the Leeuwin Undercurrent offshore (LUC) and the presumed Leeuwin Current source area (LCS). (From Pearce, 1991.)

Australia and a seasonal cycle with a maximum in May (Smith et al., 1991). The mean flow near 30°S, as well as two 72-day averages for periods of high and low transport, are shown in Fig. 53a. Stratification and geostrophic flows at times of maximum and minimum flows are shown in Fig. 53b. Water-mass properties suggest that the southern Leeuwin Current is at least partially supplied by tropical waters during June/July when the current is strongest, and by subtropical waters from the west during the winter when it is at its weakest. Farther to the north along the shelf edge near 17–19°S, Holloway (1995) described the Leeuwin Current from shipboard ADCP and moored current observations as being about 250 km wide, extending deeper to 450 m with top speeds of about 20 cm/s. He determined transports of about 4 Sv, and suggested that some degree of continuity exists from this latitude to locations further south along the coast.

The winds off western Australia cannot be the driving mechanism of the Leeuwin Current. Throughout the year they have a northward component (Fig. 54) that is strongest in November to February and weakest in June (Fig. 54), and so are always directed against the flow of the Leeuwin Current. Indeed, they appear to act to retard it, as the current is strongest (weakest) when the winds are weakest (strongest).

Another possible forcing mechanism is the mean southward pressure gradient that exists between the warm and fresh Indonesian Throughflow waters and the cooler, saltier waters off southwest Australia, which is evident in T/S curves from both regions (curves ITF and LC in Fig. 7). In an analysis of historical hydrographic data, Godfrey and Ridgeway (1985) determined the annual mean and seasonal variability of this pressure gradient, and showed that there was a southward alongshore gradient throughout the year that reached a maximum amplitude in May/June (Fig. 54). Smith et al. (1991) estimated the zonal pressure gradient from individual ship surveys and surface Ekman effects over the year of the experiment, and found the meridional (alongshore) pressure gradient to dominate by far, in agreement with the climatological data of Fig. 54. Recent evaluations of T/P altimetry and XBT trackline data (Morrow & Birol, 1998) show a strong semiannual component as well, which causes a secondary maximum during November (see below). They also reported large-amplitude interannual variability of the alongshore pressure field.

The poleward drop in dynamic height actually occurs over much of the southern Indian Ocean, and it is considerably larger than the corresponding drops in the Atlantic and Pacific Oceans. Godfrey (1996) provided a possible explanation for why this is so. In contrast to the Atlantic and Pacific, there is warm

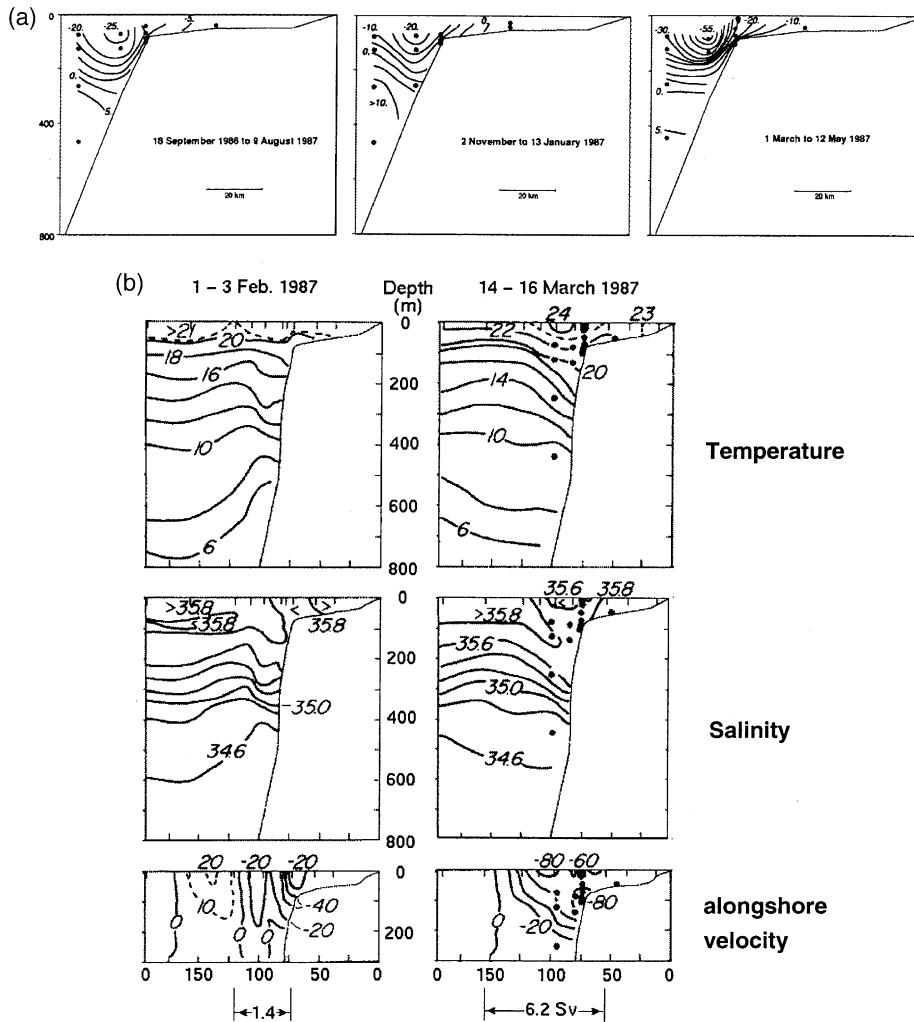


Fig. 53. Observations in the Leeuwin Current near 29°S. a) Alongshore currents from moored current meters for about one year, September 1986–August 1987 (left), the period of minimum currents (2 November 1986–13 January 1987, middle) and the period of maximum currents (1 March–12 May 1987, right). b) Potential temperature, salinity, geostrophic current (rel.300db) for low-current period (1–3 February 1987, left) and high-current period (14–16 March, right). See Fig. 20 for section location. (From Smith et al., 1991.)

surface water in the tropical Indian Ocean because of the Indonesian Throughflow. The prevailing easterlies in the southern Indian Ocean drive these warm waters southward via Ekman drift, resulting in a heat loss to the atmosphere and thicker mixed layers during winter. Thus, the wintertime cooling extends deeper than it does in the other oceans, leading to the larger drop in dynamic height and to a stronger eastward geostrophic flow.

The meridional pressure gradient may also be sustained by vertical mixing as a result of the large tides on the northwest Australian shelf. New work on tidal dissipation from T/P altimetry shows the importance of the northwest Australian shelf in contributing to the global tidal dissipation budget (Egbert & Ray, 2000). Its contribution is three times larger than results from tidal dissipation in the Indonesian Seas, which has also received considerable attention (see Section 7).

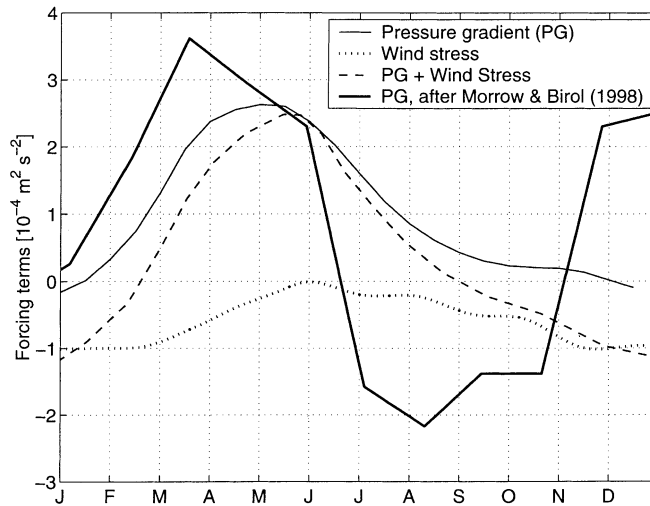


Fig. 54. Annual cycle of forcing terms off western Australia, showing meridional pressure gradient from climatological hydrographic data (PG, thin solid) and wind stress (dotted), as well as their sum (dashed; after Godfrey & Ridgeway, 1985) and new evaluations of pressure gradient from T/P altimetry (heavy solid) by Morrow and Birol (1998). Note the strong semiannual component in the latter curve.

### 6.2.2. Models

A number of modeling studies have investigated the roles of various processes in Leeuwin-Current dynamics. These processes include the Indonesian Throughflow, the local alongshore winds, and the meridional pressure-gradient field off the west coast of Australia.

Godfrey and Ridgeway (1985) first suggested that the Leeuwin Current might be driven by the Indonesian Throughflow, through the high dynamic-height field caused by low-density Pacific water entering the Indian Ocean. Kundu and McCreary (1986) investigated this idea, using a linear, continuously stratified model with an eastern boundary that included a gap across which the throughflow transport was prescribed. For model solutions without vertical mixing, the simulated throughflow continued to flow westward across the interior of the Indian Ocean, whereas with mixing it partially turned southward to form a poleward coastal current. The authors, however, concluded that for realistic model parameters this mechanism could not account for the observed strength of the Leeuwin Current, and that the bulk of the throughflow should therefore flow westward as observed.

Hirst and Godfrey (1993) used a GCM to pursue the idea that the Indonesian Throughflow causes the Leeuwin Current. They noted that the Leeuwin Current in their solution was a Rossby-wave-like feature trapped near the coast by mixed-layer processes. This result was confirmed by MKM, who noted a similar process occurring in their solution with a prescribed Throughflow. This mixed-layer mechanism plays a similar dynamical role to the vertical mixing in the Kundu and McCreary (1986) model: Both processes damp Rossby waves before they can propagate very far offshore, thereby trapping the current to the coast. The Leeuwin Current in both solutions, however, was weak in comparison to the observations.

McCreary, Shetye, and Kundu (1986) showed that a strong Leeuwin Current could be driven by offshore thermohaline forcing. They forced a linear, continuously stratified model by a prescribed density field in which density in the upper 200 m increased southward as is observed. The resulting solution developed a near-surface, southward pressure gradient in the interior ocean, which caused an eastward geostrophic flow. This inflow caused downwelling at the coast, and generated a poleward surface current and an equatorward undercurrent. McCreary et al. (1986) were also able to simulate the observed annual cycle by including a seasonally varying meridional wind stress like that in Fig. 54. They concluded that the annual-mean Leeu-

win Current was driven by the offshore density gradient, and that the alongshore winds, which always act to weaken the Leeuwin Current, account for its annual cycle.

Several modelling studies of the Indonesian Throughflow using basin or global GCMs have commented on the Leeuwin Current in their solutions (Godfrey & Weaver, 1991; Schiller, Godfrey, McIntosh, Meyers, & Wijffels, 1998; Schneider, 1998). Although these models include all of the forcing mechanisms noted above, none of them produce a Leeuwin Current with realistic strength. The reasons for this deficiency are unclear. It may simply result from the model's lacking sufficient vertical and horizontal resolution. It may also reflect problems with the model's vertical mixing parametrizations, which could weaken the poleward drop in dynamic height in the southern Indian Ocean or represent the processes that trap Rossby waves to the coast inadequately. Finally, as mentioned above, there is new evidence for strong tidal mixing in the north, which has not been accounted for properly in any of the models.

### 6.3. Subtropical circulation and western-boundary currents

#### 6.3.1. Observations

**6.3.1.1. South Equatorial Current:** Ship-drift currents (e.g., Cutler & Swallow, 1984) and drifter tracks (Shenoi et al., 1999) show the SEC as a band of westward flow between 10°S and 20°S extending across the basin. During the southern winter, the SEC appears to be more organized at the western end of the basin than it is in summer. As already mentioned, the Ekman divergence at the northern edge of the SEC leads to a doming (Fig. 16a). At times, this divergence appears to be strong enough to upwell subsurface waters into the mixed layer (Fig. 15; also see Section 9.2.1).

Estimates of the SEC transport have typically been determined by geostrophy, using hydrographic data with an assumed reference level at intermediate depths. Based on Levitus (1982) climatology, Schott et al. (1988) estimated the SEC transport above 1000 db to be 39 Sv across 54°E. Stramma and Lutjeharms (1997) constructed a transport diagram for the southern Indian Ocean from individual hydrographic sections that did not extend to the northern end of Madagascar, and therefore they obtained a westward SEC flow of only 25 Sv, with no branch passing north of Madagascar.

**6.3.1.2. South Equatorial Countercurrent:** At the western boundary during the winter monsoon, the northward EACC and the southward Somali Current cause a confluence at 2–3°S (Düeing & Schott, 1978) that merges into an eastward-flowing countercurrent, the SECC (Fig. 9). The SECC has been well defined in the western ocean by hydrographic sections and ship-drift currents (e.g., Swallow et al., 1991). In the basin's interior it is still present as a continuous eastward band from 3–6°S in surface-drifter current maps (Fig. 31b). Farther east, the ship survey of Hacker et al. (1998) also showed what might be identified as a band of SECC at 80°E and 95°E (Fig. 49). In the monthly drifter current maps of Shenoi et al. (1999), the SECC is best developed in February when it forms a continuous band across the Indian Ocean, causing high sea level in the east at this time (Morrow & Birol, 1998).

**6.3.1.3. Northeast and Southwest Madagascar Currents:** The SEC bifurcates at the coast of Madagascar near 17°S, generating the Northeast Madagascar Current (NEMC) and Southeast Madagascar Current (SEMC) to the north and south, respectively. Off north Madagascar, the NEMC rushes past Cape Amber with near-surface speeds of 70 cm/s that decay monotonically down to a depth of 1000 m (Fig. 33a). An evaluation of the NEMC transport and its variability was carried out by Swallow et al. (1988). From a number of geostrophic sections referenced by year-long moored current observations they estimated the annual-mean transport of the NEMC at Cape Amber to be  $29.6 \pm 8$  Sv.

A second survey with moored stations and ship sections was carried out across the SEMC at 23°S, where the southward transport was determined by the same method to be  $20.6 \pm 6$  Sv (Swallow et al., 1988).

South of Madagascar, the SEMC feeds into a retroreflection system (Fig. 9) in which part of it continues toward the Agulhas system, much of it via eddy shedding, and part returns eastward north of the subantarctic front, eventually to recirculate within the southern subtropical gyre (e.g., Stramma & Lutjeharms, 1997; Schmitz, 1996). The large standard deviations of both transport numbers are due to intraseasonal variability in the 40–60 day period band (Section 6.3.1.6).

The NEMC and SEMC were found to have a weak seasonal cycle, one that could not be significantly distinguished from the strong intraseasonal variability in the year-long current-meter records (Schott et al., 1988). From the slight seasonal cycle in the ship-drift currents north of Cape Amber, Swallow et al. (1988) estimated a seasonal transport variation of approximately  $\pm 2$  Sv for the NEMC transport at 10–12°N, with maximum (minimum) westward flow during August/September (January/February). At 23°S, a seasonal cycle could not be detected at all. The large standard deviations on the transport numbers of the NEMC and SEMC are caused by undulations in the 40–60 day period band which we will discuss below.

**6.3.1.4. Mozambique Channel flow:** Individual surveys over the past decades showed a complex structure of the flow pattern in the Mozambique Channel with the presence of energetic, partially bottom-trapped, eddies, and consequently firm throughflow estimates could not be derived. Unfortunately, this passage has not been covered by moored stations with adequate cross-channel resolution until only very recently (W. de Ruijter, 2000; pers. comm.), and so all existing throughflow estimates are based on indirect methods.

From water mass distributions, Gordon (1986) had hypothesized that the water stemming from the Indonesian Throughflow should pass around northern Madagascar and then through the Mozambique Channel toward the Agulhas. Swallow et al. (1991) compared NEMC transports in various isopycnal ranges with those obtained in the EACC at 4–5°S and at the equator (Fig. 8). They concluded that nearly all of the near-surface NEMC water (above  $\sigma_\theta=24.5$ ) continues to flow to the equator, but in the upper thermocline about 7 Sv of water is lost between the NEMC and the EACC in the density range from 24.5–26.8  $\sigma_\theta$ , because it was not found recirculating eastward into the SECC (Fig. 55). The missing transport was presumed to turn southward to join the Mozambique Channel throughflow (Fig. 8). This estimate was in agreement with an earlier inverse box model result of Fu (1986) who obtained 6 Sv of southward flow through the channel. In a recent estimate of the Mozambique Channel flow from a global hydrographic inverse model, Ganachaud, Wunsch, Marotzke, and Toole (2000; see Section 9 for more details) obtained a much larger southward throughflow of  $15\pm 5$  Sv (Fig. 56). Based on recent shipboard section and altimetric studies of the Mozambique Channel, de Ruijter (2000; pers. comm.) argued against a significant mean throughflow. Instead, they suggest the transport to be a result of the continuous passage of a train of 4–5 large (300–km scale) eddies per year, which results in a net transfer of about 15 Sv (as sketched into Fig. 8). These eddies continue southwards to join the Agulhas Current, and eventually cause the shedding of retroreflection eddies at the tip of Africa.

**6.3.1.5. Subtropical Rossby waves:** Perigaud and Delecluse (1992) first noted the presence of westward-propagating signals in the tropical-subtropical South Indian Ocean in Geosat altimetry, which they interpreted to be annual Rossby waves. The waves had a large amplitude, attaining a maximum of more than 10 cm at 10–15°S and 90–100°E. Perigaud and Delecluse (1992) concluded that the source of this signal was located east of 100°E, but the mechanism for its generation was not obvious since the wind-stress curl is weak in the region where the signal has its maximum amplitude (Fig. 2). Morrow and Birol (1998) confirmed the earlier analysis, using the newer and more precise T/P altimetry.

From an analysis of the variability in the depth of the 20°C isotherm in a time series of XBT track-lines, Masumoto and Meyers (1998) reported annual Rossby waves in the eastern Indian Ocean between the tropics and 20°S, with westward phase propagation across the interior basin. They obtained an amplitude maximum in the same region south of the equator that Perigaud and Delecluse (1992) had found earlier. By comparing these observations with an OGCM solution, they further concluded that waves propagating

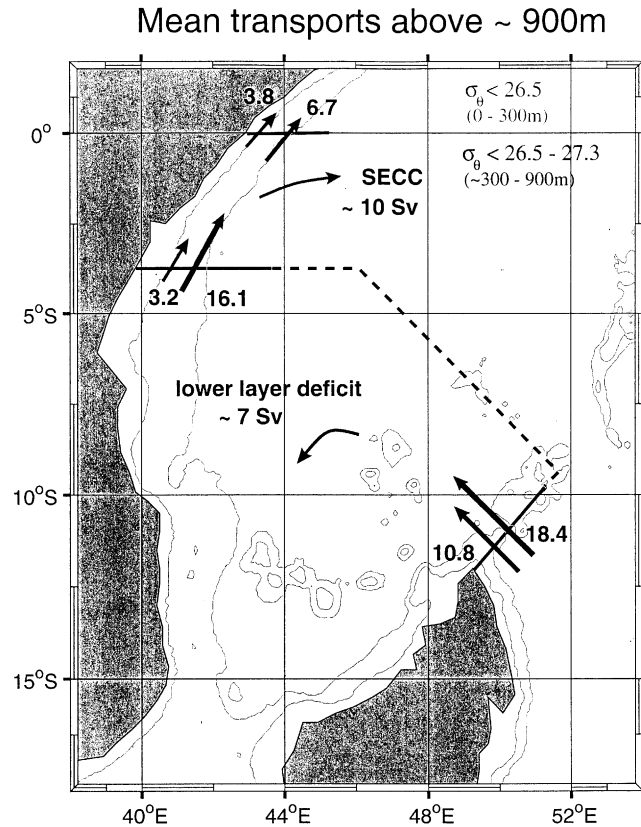


Fig. 55. Schematic of the mean transports in the near surface and thermocline layers past northern Madagascar and in the Somali Current at the equator, derived by Swallow et al. (1991) from moored and shipboard observations. There is a loss of 7 Sv out of the thermocline layer, presumably entering the Mozambique Channel.

from the eastern boundary are strongly modified by Ekman pumping along their propagation path, *i.e.* that these signals were not free waves but partially forced.

Morrow and Birol (1998) also reported semiannual Rossby waves at 20–35°S with wavelengths of 300–600 km. They appeared to be free waves emanating from the eastern boundary, but their generation mechanism was not clear.

As previously noted in other subtropical and midlatitude oceans (Chelton & Schlax, 1996), the phase speed of the observed Rossby waves is generally larger than expected from linear theory, for which the speed of long-wavelength Rossby waves is  $c_r = \beta R^2$ , where  $R$  is the Rossby radius of deformation. For the semiannual waves, the discrepancy between  $c_r$  (estimated to be 3 cm/s using climatological values of  $R$ ) and the observed propagation speed is particularly large, nearly a factor of 2 (Morrow & Birol, 1998). Killworth, Chelton, and de Szoeke (1997) proposed that nonlinearities associated with the vertical shear of a background zonal circulation might account for the enhanced speed. Masumoto and Meyers (1998) noted that interference between free Rossby waves and a locally forced interior response might also be the case.

**6.3.1.6. Intraseasonal variability in the western subtropical ocean:** At the western end of the subtropical regime, pronounced variability at intraseasonal time scales has been observed. Schott et al. (1988) reported strong fluctuations of 40–50 days period in the year-long moored current records east of Madagascar, and

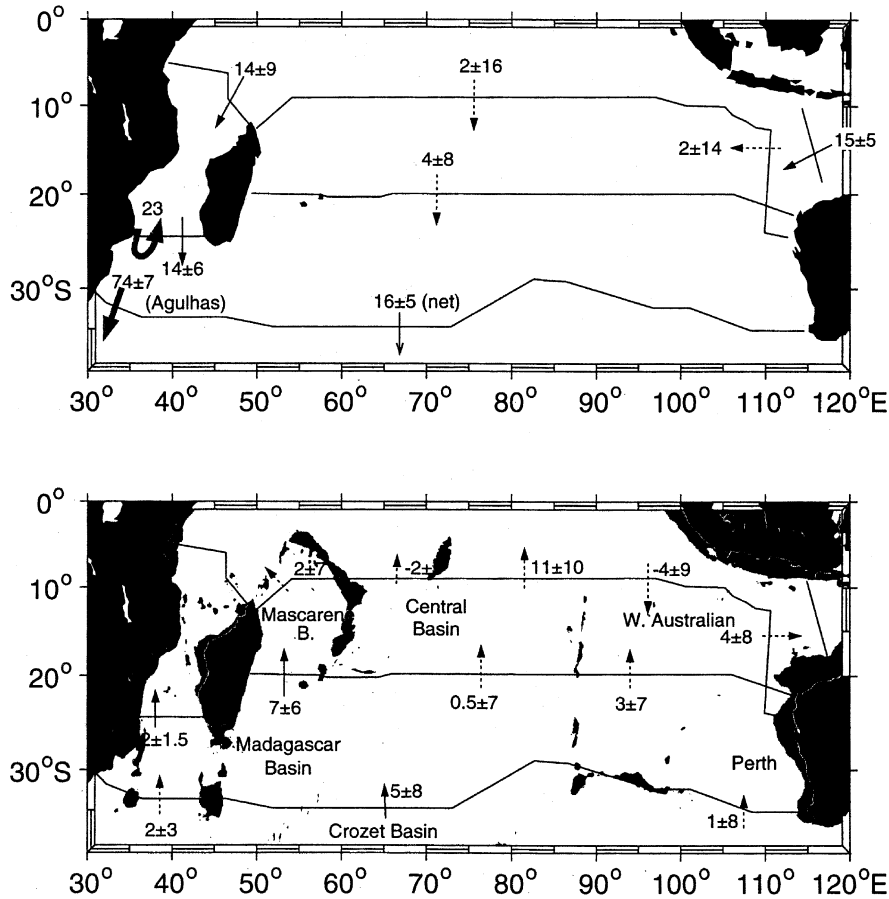


Fig. 56. Integrated mass transports from the box inverse model of Ganachaud et al. (2000), showing a) total section transport and b) deep transports below neutral density 27.96 (approx. 2000 dbar) in individual basins (topography see Fig. 20); dotted arrows indicate transports with large uncertainties.

they were more pronounced off northern Madagascar than at 23°S. Quadfasel and Swallow (1986) analyzed shipboard ADCP observations from a region north of Madagascar and found them to be consistent with Rossby waves in this period band.

Recently, Warren, Whitworth, and LaCasce (2002) analyzed a 20-month record of deep currents from a mooring array that extended 200 km offshore from the east coast of Madagascar at 20°S. They found fluctuations of about two months period and 10 cm/s amplitude which were propagating westward at about 7 cm/s across the zonal extent of the array. They concluded that they were barotropic Rossby waves, given the signal's near-constant vertical phase and that the shortest possible period of a first-mode baroclinic Rossby wave is longer than 100 days for the region's stratification. As a plausible generation mechanism, the authors identified resonant forcing by the wind stress curl over the width of the Mascarene Basin. Support for this idea came from variability of T/P altimetry, which showed a sharp spectral peak at the 60 day period over the Mascarene Basin but not east of the Mascarene Ridge. In addition, the intraseasonal variability of the T/P altimetry was higher at 15°S than at 20°S, consistent with the earlier current-meter observations of Schott et al. (1988). Warren et al. (2002) further suggested that the shorter period of 45

days of the intraseasonal peak at 12°S could be explained by these longer-period Rossby waves being advected westward by the mean SEC.

At the western boundary, incoming intraseasonal Rossby waves can trigger eddies that then migrate through the Mozambique Channel (de Ruijter, 2001; pers. comm.) or southward with the East Madagascar Current and subsequently connect with the Agulhas Current. However, the physical mechanism relating annual or 40–60 day period Rossby waves with the generation of the 4–5 eddies counted per year has not been established yet.

### 6.3.2. Models

**6.3.2.1. Mean circulation branches:** Most of the observed circulations mentioned in the preceding subsection have been simulated in models. Indeed, the basic properties of the SEC, SECC, and western boundary currents east of Madagascar, as well as the northward continuation via the EACC toward the Somali Current, were already realistically simulated in early  $1\frac{1}{2}$ -layer models (e.g., Woodberry et al., 1989). Subsequent GCM solutions all show these major current branches as well (e.g., Wacongne & Pacanowski, 1996; Garternicht & Schott, 1997; Lee & Marotzke, 1998; the POP currents in Figs. 14 and 13).

Haines, Fine, Luther, and Ji (1999) studied Lagrangian pathways of the flows emerging out of the SEC using a multi-layer model in which an Indonesian Throughflow of 11 Sv was prescribed as an eastern boundary condition. Fig. 57 shows the fate of particles inserted in the eastern part of the basin. Within 6 years, 95% of the particles reached the western boundary and after the end of the 50-year integration, 66% passed southward through the Mozambique Channel, and 21% to the east of Madagascar. After 18 years, 11% of them made it to the Arabian Sea where they can participate in the upwelling there.

**6.3.2.2. Seasonal response to wind stress forcing:** A striking aspect of the observed circulation is the small seasonal signal at the western subtropical boundary (Swallow et al., 1988; Schott et al., 1988). This small amplitude contrasts markedly with the North Atlantic case: Both regions face a similar forcing situation (i.e., forcing by subtropical wind stress curl; see Fig. 2), but the western-boundary current in the subtropical North Atlantic has a very large seasonal cycle. The annual amplitude there is estimated to be 15 Sv, based on seasonal averages of multi-year time series obtained with moored current meter stations along 26.5°N off the northern Bahamas (Lee, Johns, Zantopp, & Fillenbaum, 1996). Such a large amplitude was predicted earlier in a quasi-steady Sverdrup calculation (e.g., Böning, Doescher, & Budich, 1991a), and from a high-resolution GCM (Böning, Doescher, & Budich, 1991b). In the subtropical southern Indian Ocean, a quasi-steady Sverdrup response would require an annual variation of boundary current inflow (Fig. 12) of the same magnitude as in the subtropical North Atlantic, with the SEC carrying 20 Sv westward between 11° and 23°S in December/February versus about 50 Sv from June to September (e.g., Schott et al., 1988). In agreement with the observations, however, the seasonal transport variation of the SEC north

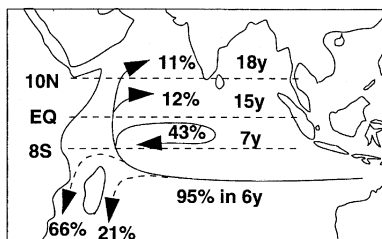


Fig. 57. Schematic representation of upper-layer trajectories of Lagrangian particles released in the eastern SEC in an Indian Ocean multilayer model with a mean throughflow of 11 Sv. Times indicate when certain percentages of total released particles have reached the marked areas. See text for details. (After Haines et al., 1999.)

of Madagascar only had an amplitude of 1 Sv in the  $1\frac{1}{2}$ -layer model of Woodberry et al. (1989), and the seasonal SEC amplitude of the GFDL model was also small, in agreement with the observations.

The reason for this difference between the subtropical seasonal cycles in the two ocean basins is not clear. A plausible explanation is that the Indian Ocean meridional ridges, in particular the Seychelles Plateau just a few degrees east of Madagascar, are playing a role. These topographic features may block the westward propagation of Rossby waves generated farther to the east. Consistent with this idea, the quasi-steady Sverdrup transport variability generated by forcing between the Seychelles Plateau and Madagascar amounts to just the small observed magnitude. The above-mentioned observations from the subtropical North Atlantic also support this interpretation. In that case, the best agreement between the quasi-steady Sverdrup transport variability and observed boundary-current variability was obtained when only the wind-stress curl west of the mid-Atlantic Ridge was integrated (Lee et al., 1996).

**6.3.2.3. Mozambique Channel throughflow:** The role of the Mozambique Channel differs considerably between model simulations. One reason for these differences is that the models are both global and regional. In the latter case, the southern exit is typically part of, or close to, the models' southern boundary, and so is influenced by the southern boundary conditions (often a numerical buffer zone where the models are relaxed to climatology). In the former case, the magnitude of the Indonesian Throughflow is the determining factor for the Mozambique Channel throughflow (see Section 7). For a mean Indonesian Throughflow of 11 Sv, the Haines et al. (1999) solution to a regional model has a large fraction of the SEC mean flow going through the channel (Fig. 57). The surface currents of the POP solution generally show southward near-surface flow in the channel (Figs. 14 and 13). In POP time series for 1985–96 (Maltrud, Semtner, & Malone, 1998; see their Fig. 9), the channel flow exhibits large throughflow variations, ranging from 30 Sv southward to 10 Sv northward with a mean of about 5 Sv southward. The southward flow has a maximum from July to September and a minimum from March to May.

**6.3.2.4. Intraseasonal variability:** In the earlier  $1\frac{1}{2}$ -layer model studies (Kindle & Thompson, 1989; Woodberry et al., 1987; also see Section 3.4.2), intraseasonal 40–60 day oscillations were a prominent feature north of Madagascar. Their amplitude was large, and there was no corresponding peak in the spectrum of the wind that forced the models, suggesting that its cause was an oceanic instability. Given that a  $1\frac{1}{2}$ -layer model does not allow for baroclinic instability, the authors concluded that barotropic instability associated with shear between the SEC and SECC was the generation mechanism. As pointed out in Section 6.3.1.6, however, the new observations reported by Warren et al. (2002) suggest that the variability may actually result from remotely forced Rossby waves.

## 7. Indonesian Throughflow

The Indonesian Throughflow has long been a focus of considerable research interest from local, regional and global perspectives. Locally, there are large changes in water-mass structure within the Indonesian Seas, because of surface freshwater input, bottom friction, and mixing by the vigorous tidal currents over sills. Regionally, it is important to understand how the throughflow and its variability relate to neighboring current systems in the western Pacific and near Australia, particular regarding the Leeuwin Current (Section 6.2). Globally, it is considered one of the choke points of the global circulation system, and its variability is believed to affect climate on interannual and longer time scales.

## 7.1. Annual-mean circulation

### 7.1.1. Observations

The annual-mean Indonesian Throughflow is directed from the Pacific to the Indian Ocean, as is clearly indicated by water-mass characteristics. The dominant route through the Indonesian Seas is from the North Pacific via the Mindanao Current, then through the Makassar Straits into the Banda Sea, and finally past Timor into the eastern Indian Ocean (Fig. 58; Gordon & Fine, 1996; Meyers et al., 1995). Some throughflow, estimated at  $\sim 2$  Sv by Murray and Arief (1988), exits through the Lombok Straits and it is likely that further leakage occurs through other passages between Lombok and Timor (Fig. 58). Little water of Southern-Hemisphere origin participates in the throughflow, and that portion seems to be mostly subthermocline water that passes through the Halmahera and Maluku Seas (Wyrki, 1961; Hautala, Reid, & Bray, 1996).

Within the Indian Ocean, the main fraction of the throughflow waters pass westward with the SEC, causing a zonal salinity minimum and silica core all across the Indian Ocean (Fig. 16). An unresolved question is just which route the water takes to exit the basin in the southwest Indian Ocean: Does it exit by turning southward along the Mozambique eastern coast, or through the Mozambique Channel along the African coast, or both? Swallow et al. (1991) estimated that 7 Sv of thermocline water in the isopycnal range from  $24.5$  to  $26.8 \sigma_\theta$  was lost along the way from North Madagascar to the equatorial Somali Current, and they conjectured that this flow might have entered the Mozambique Channel from the north (Section 6).

A variety of estimates exist for the strength of the throughflow. Earlier estimates, summarized by Gordon (1986), were based on either large-scale budget studies or regional indirect observations, and ranged from just a few Sv to about 20 Sv. Fieux et al. (1994) and Fieux, Molcard, and Ilahude (1996) carried out the

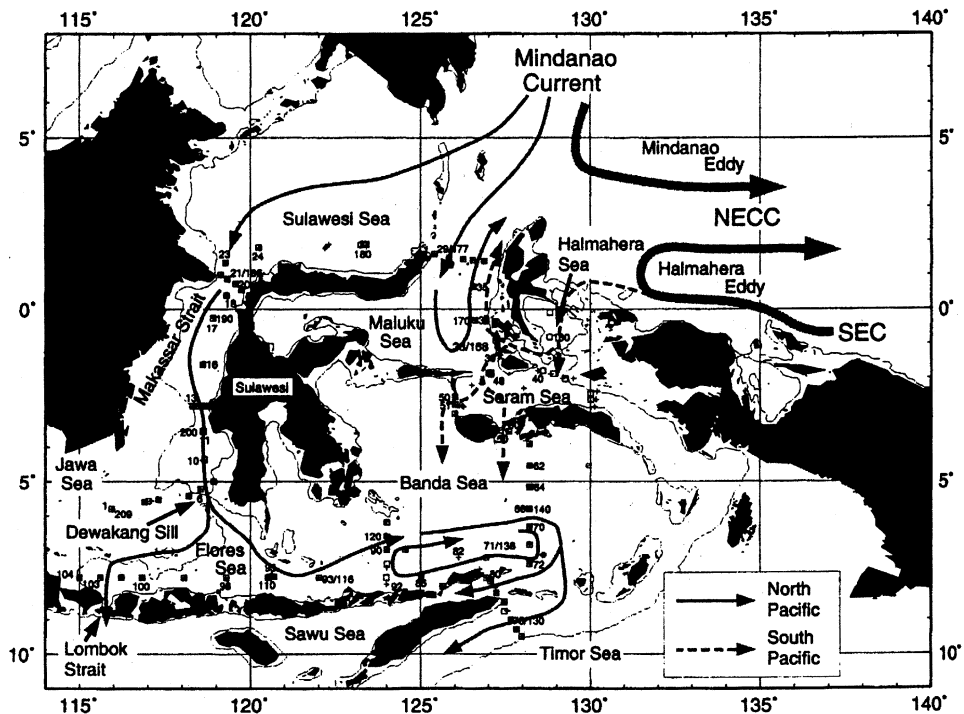


Fig. 58. Island geography and schematic pathways of western Pacific boundary currents and of Indonesian Throughflow. (From Gordon & Fine, 1996.)

first modern shipboard section observations across the exit region between Australia and Bali, and reported a throughflow transport of  $18.6 \pm 7$  Sv from a ship section taken in August, 1989, but a *negative* (towards the Pacific) transport of  $2.6 \pm 7$  Sv from a similar section in March, 1992. Meyers, Bailey, & Worby (1995), using XBT section data from repeat sections with a mean T/S relation, determined 5 Sv for the transport in the upper 400 m, calculated using 400 m as a reference level. When extended to greater depths using climatological hydrography, their estimate increased to about 11 Sv.

From the annual means of moored current-meter observations in the narrow Makassar Strait, Gordon and Susanto (1999) estimated a mean transport of about 5–15 Sv, depending on the method of extrapolating their subsurface data both to the surface and laterally to the margins. Little information is available on the deep structure from direct measurements. The moored observations of Molcard, Fioux, and Ilahude (1996) in the Timor Passage show significant currents and transport contributions at depths below 500 m, which makes estimates based on hydrographic sections under the assumption of vanishing deep shears and barotropic contributions questionable.

Several recent global inverse studies yield estimates in the range of 7–10 Sv for the most acceptable throughflow transports (e.g., Macdonald, 1998, Sloyan & Rintoul, 2001; see Section 9), whereas the global box model inverse calculation of Ganachaud and Wunsch (2000) gave a higher value of  $15 \pm 5$  Sv. The reasons behind these differences between solutions partially using the same hydrographic sections are still being explored.

### 7.1.2. Models

Several models of varying complexity have been applied to study the throughflow transports, Indonesian passage pathways, regional and global connections, and to derive the important driving mechanisms. The influence of the Indonesian Throughflow on the Leeuwin Current was discussed in Section 6.2.2, where it was noted that the connection is weak in existing model simulations.

**7.1.2.1. Transports:** Several models have yielded transport values that are rather low. These include the POCM of the Naval Postgraduate School (Semtner & Chervin, 1992; Gartnericht & Schott, 1997; Potemra et al., 1997), the multi-layer model of the Naval Research Laboratory (Metzger & Hurlburt, 1996), and the Los Alamos Parallel Ocean Program (POP) model (Maltrud et al., 1998), all of which yield a mean transport of about 7 Sv. Other models, however, give estimates that are about double this value. The earlier global model of Hirst and Godfrey (1993) which was of fairly low resolution ( $1.6^\circ \times 2.8^\circ$ ) and was driven with the HR winds estimated a mean throughflow of 17 Sv (see below). In a solution to the Japan Marine Science and Technology Center (JAMSTEC) OGCM, which has a horizontal resolution of  $0.25^\circ \times 0.25^\circ$  and 55 vertical levels, the estimated transport was 15.6 Sv. The solution to the robust-diagnostic model of Miyama, Awaji, Akimoto, and Imasato (1995) had a total mean transport of 19 Sv, with a primary surface core and secondary deep one (5 Sv), the latter flow consistent with the observations of deep throughflow reported by Molcard et al. (1996). Moreover, this deep core consisted of subthermocline water (AAIW) that flowed into the Indian Ocean via the Banda Sea, in agreement with the observational analyses of Wyrski (1961) and Hautala et al. (1996). Finally, Lebedev and Yaremchuk (2000) studied the output of a global OGCM with a resolution of  $0.16^\circ \times 0.16^\circ$  in the Indonesian Seas; they diagnosed the annual-mean transport to vary from 10.4 to 13.7 Sv depending on the wind stress field that was forcing the model. The reasons for these differences are not clear, but are likely to involve a number of factors (model resolution, vertical mixing parametrization, wind forcing, etc.).

**7.1.2.2. Indonesian passage pathways:** Gordon and McClean (1999) analyzed the throughflow paths and water-mass properties within in the Indonesian Seas in a solution to the POP model with  $0.28^\circ \times 0.28^\circ$  resolution that was driven by ECMWF wind stress fields for the period 1985–95. They noted several obvious discrepancies with the observations. One was that the Makassar throughflow, rather than turning

eastwards through the Flores and Banda Seas and then entering the Indian Ocean through the Timor Sea, mostly exited through the Lombok Straits, a property also shared by the solution of the JAMSTEC model (T. Miyama, 2000; pers. comm.). Another discrepancy was that the model allowed significant exchange between the Coral Sea and the Indonesian Seas, thereby allowing unrealistically larger amounts of South Pacific water to flow directly into the Indian Ocean.

In the Lebedev and Yaremchuk (2000) solution, an important source of Pacific water for the Indonesian Seas is through the South China Sea. This water enters the region in two locations, as a boundary current along the eastern coast of Borneo (beginning near 5°N, 119°E in Fig. 58) and to the south of Borneo via the Jawa Sea. The importance of the South-China-Sea pathway has been noted in earlier modelling studies (Masumoto & Yamagata, 1996; Miyama et al., 1995; Metzger & Hurlburt, 1996).

Model-to-model differences for the same forcing and seaward boundary conditions depend largely on the selected topography, model resolution, and parametrizations. Furthermore, as pointed out by Wajswicz (1999), the particular pathways taken by the throughflow depend on the choice of forcing fields through their influence on the throughflow strength; typically, the throughflow will select the westernmost passage, and then successively fill up the more eastern passages as the transport increases.

*7.1.2.3. Indian-Ocean pathways:* Several model studies have addressed the pathways taken by throughflow water in the Indian Ocean. Godfrey and Weaver (1991) obtained solutions to a GCM in a simplified basin, in which a western-Pacific sector was included to provide a reservoir of fixed T/S properties and the Indian Ocean was connected to a reservoir south of Australia. They found that almost all the throughflow flowed across the basin to the western boundary before returning to the Pacific south of Australia. Nonlinear effects were important in the circulation through convective overturning and by advection, both of which strongly affected the solution's heat budget. In addition, as pointed out by Godfrey (1996) and mentioned in the Section 6.2, local air sea interaction may play a role in connecting the throughflow with the Leeuwin Current. Hirst and Godfrey (1993) followed this up with a systematic study of throughflow effects using a more realistic global GCM in which they totally blocked the passages, only allowed baroclinic exchanges or changed the throughflow thermohaline properties to those of the eastern Indian Ocean. Results from the run with free throughflow (with a mean transport of 17 Sv, see above) minus that with blocked passages show that the upper part of the throughflow crosses the Indian Ocean at the latitude of the Indonesian passages, passes southward through the Mozambique Channel toward the tip of southern Africa and then joins the Agulhas retroflection to flow back eastward. A secondary branch feeds into a return flow from the East Madagascar coast to the Leeuwin Current, where it reduces the wind-driven upwelling off western Australia. The result for the heat budget was that small effects on the northern and tropical Indian Ocean resulted but large heat losses in the southern Indian Ocean. Making the throughflow purely baroclinic or changing its properties still dominantly affected the SW Indian Ocean in that study.

Coupled model studies have investigated the throughflow effect, as well. Schneider (1998) compared two solutions to the coupled global ECHO model of MPI, Hamburg, in which the Indonesian passages were either open or closed. The comparison showed that the passage controls the location of the western Pacific warm pool, that the Indian Ocean would be cooler and have reduced sea level if the passage were closed, and that the model throughflow waters take a southwesterly slanted path across the Indian Ocean towards Madagascar, where they return eastward toward southern Australia within the ACC, rather than following the 'warm water route' towards the Agulhas Current (Gordon, 1986). The study of Wajswicz and Schneider (2001), who analyzed the COLA coupled model with the Indonesian passages open or closed, also showed a rather different streamfunction pattern (Fig. 59b) from the ocean-only model of Hirst and Godfrey (1993; their Fig. 12a) with a near-zonal streamfunction anomaly. Blocking of the Indonesian throughflow resulted in a stream function in which the throughflow had a zonally inclined path towards the southern tip of Madagascar, while between the equator and 25°S anticyclonic and cyclonic gyres were generated. These two gyres are generated by air-sea flux feed back loops that affects the wind pattern and

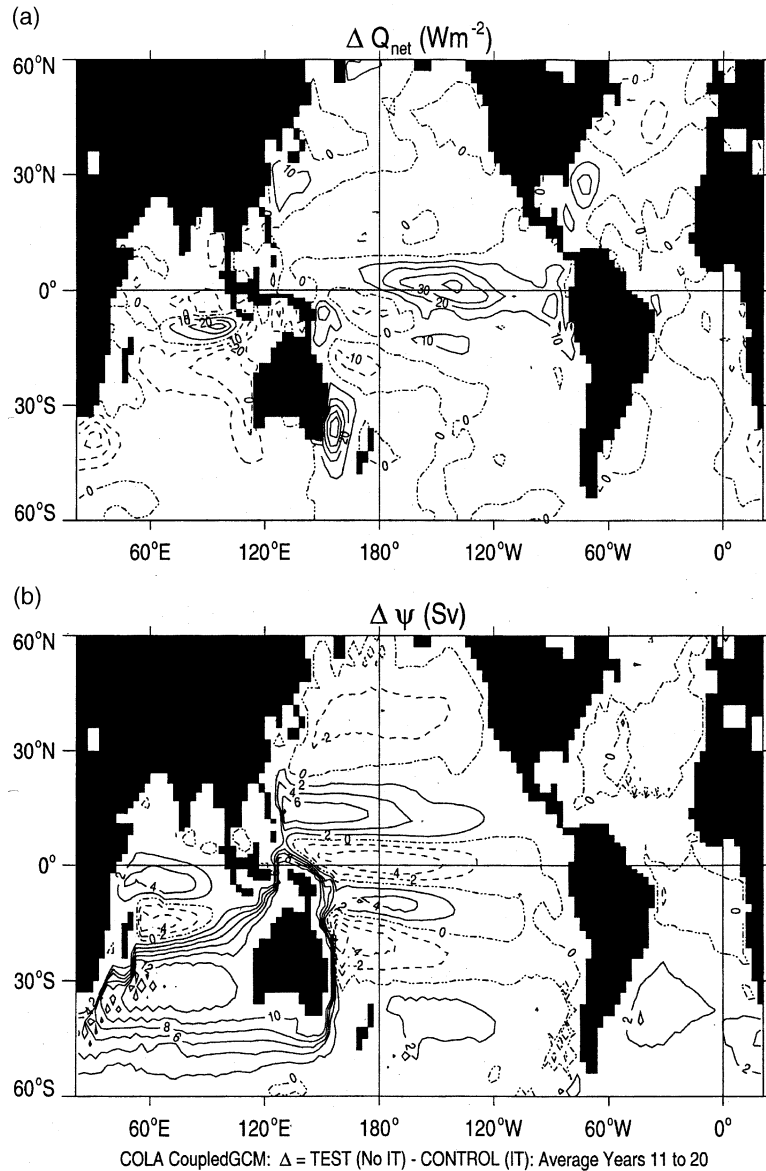


Fig. 59. Difference in 10-year averages of a) net surface heat flux and b) barotropic stream function between the run with Indonesian passages closed and the control run in the coupled COLA model simulation of Wajsowicz and Schneider (2001). Contour intervals are  $10 \text{ Wm}^{-2}$  and  $2 \text{ Sv}$ , respectively.

thus account for the difference from Throughflow effects in ocean-only models. Further, throughflow blockage resulted in cooler SSTs in the eastern tropical Indian Ocean and increased Southeast Trades with an associated latent heat loss (Fig. 59a), creating a pattern similar to an ‘Indian Dipole Mode’ event (see Section 10). Overall, heat flux effects of the throughflow in the coupled models are about double the size as in the ocean-only study, amplified by feedback mechanisms. As in Hirst and Godfrey (1993), the effect of the throughflow on the heat budget and circulation of the northern Indian Ocean is small (Fig. 59).

**7.1.2.4. Pacific-Ocean pathways:** Lu, McCreary, and Klinger (1998) used a  $3\frac{1}{2}$ -layer model to investigate the circulations generated by the Indonesian Throughflow within the Pacific Ocean. In their model, the throughflow was specified by a prescribed outflow of 10 Sv in the model's upper two layers from 1–6°N (the model's Indonesian passages), and a compensating inflow across the model's southern boundary at 35°S. No water flows directly from the southern boundary to the outflow port. Instead, it first upwells into layer 1, mostly in the eastern, equatorial ocean but also in the subpolar region of the North Pacific. Some of the layer-1 water that upwells along the equator circulates in the northern tropics, joins the model Philippine Current, and flows out of the outflow port. The rest subducts into layer 2 in the North Pacific, circulates about the subtropical gyre, and exits in layer 2. Thus, consistent with the observed circulation, all the water that exits the basin comes from the Northern Hemisphere. McCreary and Lu (2001) extended the Lu et al. (1998) study by including an additional layer to represent North Pacific Intermediate Water (NPIW; layer 3) and AAIW (layer 4) separately. They concluded that the throughflow circulation is the reason why not much NPIW recirculates in the northern tropics and why AAIW flows into the far North Pacific.

In the Pacific the result of blocking the throughflow in the coupled model analyzed by Wajsowicz and Schneider (2001) was an ENSO like heat flux anomaly centered on the equator, flanked by colder off-equatorial anomalies. A similar result was obtained in the GCM study (see above) by Hirst and Godfrey (1993).

## 7.2. Seasonal cycle

Results from observational and modelling studies vary concerning the seasonal cycle, but generally suggest that the maximum throughflow occurs in June/July and the minimum in February. Observational results of the seasonal cycle are still scarce and mostly indirect. Wyrski (1987) evaluated the pressure head between the western Pacific and eastern Indian Ocean, using the sea level difference between Davao (Philippines) and Darwin (Australia), and found a maximum in late boreal summer. Based on their analysis of upper-layer geostrophic transports, determined from XBT track-lines across the throughflow regime, Meyers (1996) concluded that there was a maximum inflow transport (relative to 400 db) across the section from Java to Northwest Australia in August/September, with a minimum throughflow in spring and a large semiannual component superimposed. These results are in agreement with the results from the two sections across the throughflow reported by Fieux et al. (1994, 1996), which yielded  $18.6 \pm 7$  Sv in August and  $-2.6 \pm 7$  Sv in March.

Seasonal cycles of throughflow transports have been reported from a number of model simulations. The POCM model analyses of Garternicht and Schott (1997) and Potemra et al. (1997) showed a throughflow that varied seasonally ranging from 4 Sv in December/January to 11 Sv in September (Fig. 60), with significant interannual variability superimposed. Potemra et al. (1997) also commented on the potential influence of Ekman transports to this variability. The winds over the passages during the boreal summer are directed towards the northwest, but they are weakly southeasterly in boreal winter. They estimated the contribution of Ekman transport to the throughflow to be about 4 Sv toward the Indian Ocean at the height of the summer monsoon and slightly eastward in winter, yielding a contribution to the annual-mean throughflow of 1.7 Sv. In the throughflow time series for 1985–96 of the POP model, driven by 3-day winds and analyzed by Maltrud et al. (1998), visual inspection shows that the transport rose to a maximum in June–July and fell to a minimum in February–March. This model also shows significant shorter-period variability superimposed.

Miyama et al. (1995) used particle tracking to trace water-mass movements in the Indonesian Seas throughout the year. In the surface layer, North-Pacific water from the Mindanao Current is supplied to the Makassar Straits during boreal spring to summer, whereas during the other seasons, it flows back to the Pacific Ocean to join the NECC. In the thermocline layer, a pronounced inflow from the Mindanao

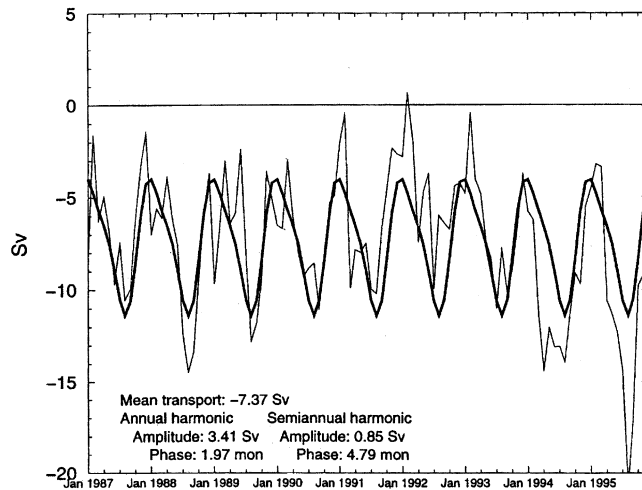


Fig. 60. Timeseries 1987–95 of POCM throughflow from the Pacific to the Indian Ocean and its mean seasonal cycle (heavy curve). Also marked are the annual and semiannual harmonic amplitudes and phases. (From Potemra et al., 1997.)

Current occurs from the boreal winter to spring, when the subsurface link between the currents and the EUC tends to weaken. Lebedev and Yaremchuk (2000) comment on the seasonal changes in circulation patterns within the Indonesian Seas. They note that during the winter most of the throughflow exits the region through the Lombok Straits (as in the Gordon & McClean, 1999, solution mentioned above), whereas during the summer most exited via the Timor Sea, consistent with the observations. They also report that inflow from the South China Sea via the Java Sea occurs only during the winter when the winds are favorable.

### 7.3. Interannual variability

Wyrtki (1987) first tried to estimate the Pacific to Indian Ocean pressure head using the sea level stations mentioned above and concluded that it did not contain an ENSO signal. However, as pointed out subsequently by Meyers (1996), Darwin is in fact representative of the Pacific during an ENSO cycle, and therefore this sea level difference is not indicative of the pressure head.

Time series of the Indonesian Throughflow in the Indian Ocean have been obtained for more than a decade along XBT tracklines running from Australia to the Indonesian passages. Meyers (1996), combined the observations of SST, thermocline depth and dynamic height along the track using the empirical orthogonal function (EOF) statistical technique. The first EOF was well correlated with ENSO and it showed the same relationship between these parameters during an ENSO episode as in the western Pacific. The transports, calculated with a mean TS relationship and relative to 400 m, showed maxima (1) toward the Indian Ocean during La Niña phases and minima during El Niño, the peak to peak amplitude of the ENSO signal being about 5 Sv. This is in agreement with the theory of Clarke and Liu (1994) who concluded that during La Niña phases westward wind anomalies over the equatorial Pacific would increase sea level at the western end of the Pacific and thus drive a larger throughflow. The second EOF had shorter time scales than ENSO, was related to the seasonal cycle and was coupled to the zonal winds over the Indian Ocean. Its amplitude was particularly large toward the end of the time series used by Meyers (1996), i.e. in 1994. This mode had similarities with the ‘dipole mode’ discussed in Section 10.2 below suggesting that this mode is unique to the Indian Ocean.

New current and temperature measurements in the Makassar Straits during 1996–98 have provided

additional insight on throughflow variability, as the time span included effects generated by the large 1997/98 ENSO event (Gordon & Susanto, 1999). In these investigations, it was found that during the El Niño phase of December 1997 to February 1998, the transport through the straits was 5 Sv, but during the La Niña period from December 1996 to February 1997, it was 12 Sv. Furthermore, a high correlation was found between throughflow transport and thermocline temperature, with the thermocline shallowing during El Niño and deepening during La Niña. As a consequence, significant ENSO effects on the regional heat budget are to be expected.

Recently, sea-level variability in the throughflow regime and wider influence areas has become available from T/P altimetry. The altimetry/model comparison of Potemra et al. (1997) was aimed at finding indices to estimate the transport variability. They found no clear relation between the seasonal throughflow cycle and the larger-scale Pacific-to-Indian Ocean sea-level difference. Interannual throughflow variability seemed mostly to be controlled by changes in Pacific sea level. Ageostrophic processes were also found to be important, so that pure sea-level differences or hydrographic section transports across passages would not be expected to be well correlated with throughflow transports.

Interannual variability in the POCM model (Fig. 60) involves large anomalies of throughflow transport. Larger than average transports were obtained for 1988, 1994 and 1995 whereas there was anomalously low throughflow transport in 1991–92. We note here, for reference in Section 10, the event that occurred in 1994, in which peak model transports of 14 Sv appeared 4 months before the average seasonal maximum. In the Maltrud et al. (1998) simulation with the POP model the throughflow in 1995 was also large, but the 1994 maximum was less pronounced than in Potemra et al. (1997) and the 1988 and 1989 anomalies were relatively larger. Since a number of other global models are operated at the present time, it can be expected that results on the causes of such model-to-model transport differences (e.g., their dependence on the different types of forcing, resolution and passage topography) will be forthcoming.

Recently, Wajsowicz and Schopf (2001) explored the role of throughflow variability on the Indian Ocean and Arabian Sea heat budget, using an ocean model coupled to a prescribed atmosphere. Changing the throughflow by less than 4 Sv yielded air-sea heat-flux differences greater than 20 W/m<sup>2</sup> east of Madagascar and over the Somali Current. These changes were found to be caused partially by the changed meridional transport and partially by the changed heat input provided by the throughflow. Additionally, the throughflow decreased the heat export out of the Arabian Sea into the Southern Hemisphere which in turn increased Arabian Sea SST in that model study.

As indicated by above examples the scope and complexity of the model studies on the physics and climatic impact of the Indonesian Throughflow are expanding rapidly. In addition, new programs for observations are planned. We therefore anticipate that rapid progress in this field will be made in the near future.

## 8. Red Sea and Persian Gulf

These two marginal seas are sources of salty RSW and PGW thermocline layers in the Indian Ocean, with cores that can be traced into the interior of the Arabian Sea; RSW can even be traced across the equator. Both outflows pass over shallow sills and have small transports. Here, we briefly review the known facts and hypotheses about the generation of RSW and PGW and their exchanges with the Arabian Sea.

### 8.1. Red Sea

#### 8.1.1. Circulation and exchange through Bab el Mandeb

Evaporation exceeds precipitation over the Red Sea by about 2m/year (Morcos, 1970). This leads to thermohaline overturning (Phillips, 1966) and to very high salinity waters ( $S \geq 40$ ) filling the deep basin. The mechanism of deep-water formation is still not well understood, but shelf convection, caused by flow

of relatively cool, salty, bottom water out of the Gulf of Suez during winter, is considered to be one important source (Woelk & Quadfasel, 1996). As Cember (1988) argued on the basis of tracer (carbon-14 and tritium-helium) distributions, the northern convection should generate two water masses: not only a deep water that fills the basin from the bottom but also an intermediate water that propagates southward over the deep water and underneath the near-surface pycnocline. In between these two southward-flowing water masses he conjectures there must be a northward return flow. Cember (1988) estimated a formation rate of 0.12 Sv for the intermediate water.

The Red Sea is separated from the Gulf of Aden by a narrow sill at Bab el Mandeb, which is only 160 m deep. There are vigorous exchanges across this sill that vary seasonally in both structure and intensity. During the winter monsoon, the flow over the sill is two-layered, with high-salinity Red Sea Water (RSW) leaving the basin at the bottom, and fresher water from the Gulf of Aden entering near the surface. At this time the prevailing winds are southeasterly and favor this thermohaline exchange. Fig. 61 presents horizontal maps and a cross-section of currents taken through the Bab el Mandeb passage by ADCP obser-

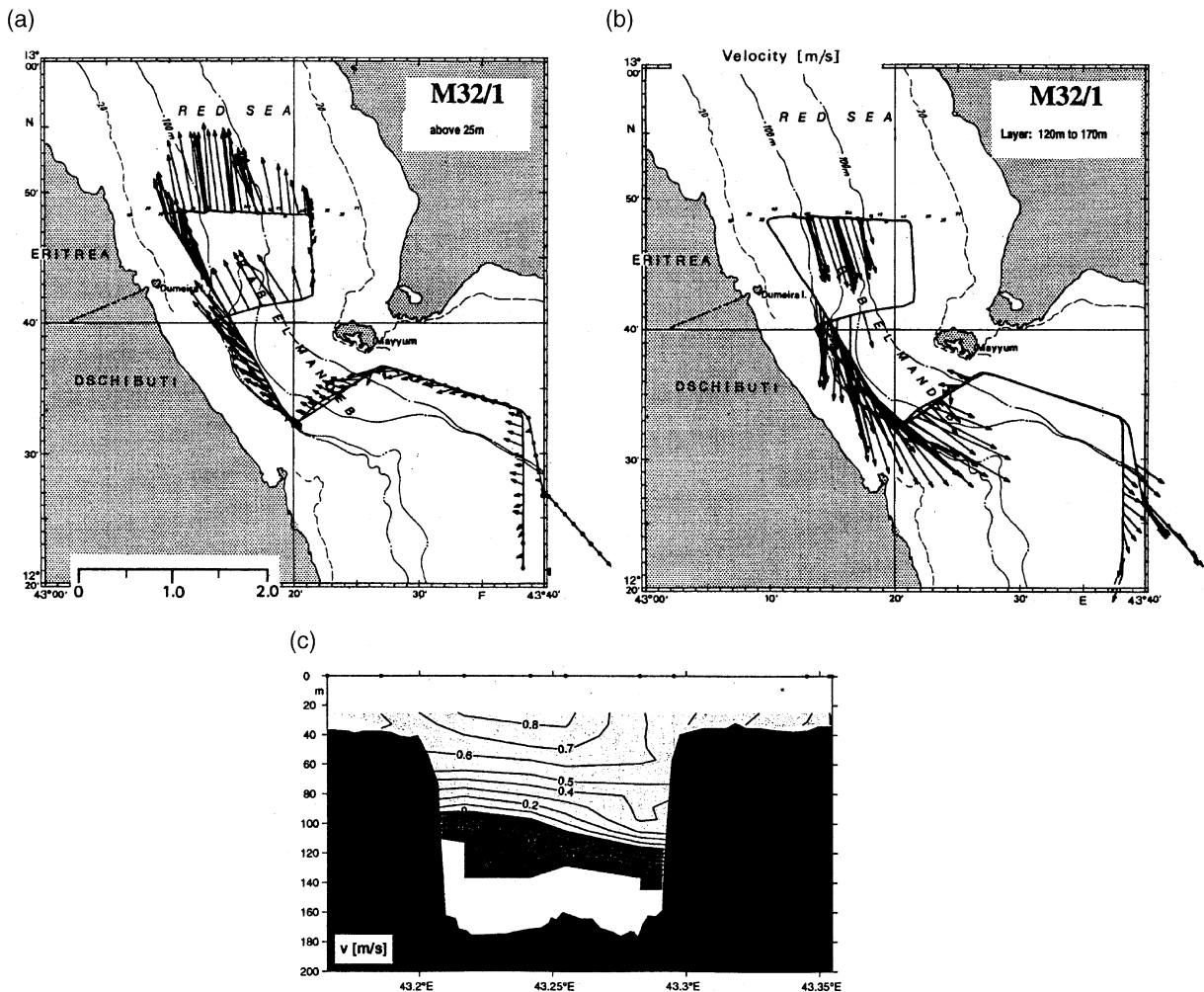


Fig. 61. Exchange through the Straits of Bab el Mandeb, measured by shipboard ADCP on 'Meteor' cruise M32/1: a) upper layer flow vectors, b) near-bottom flow vectors, and c) currents (positive northward) across the northern section.

vations during ‘Meteor’ cruise M32/1 in April, 1995. Fig. 61a shows the broad upper-layer inflow with maximum northward speed in the innermost section of 90 cm/s. The flow of the near-bottom outflow plume (Fig. 61b,) exceeded 100 cm/s, and the outflow transport, estimated by extrapolating the ADCP currents toward the bottom was estimated at about 0.3 Sv.

During the summer monsoon, the structure becomes three-layered (e.g., Maillard & Soliman, 1986). There is still a bottom outflow of salty RSW, but the inflow of fresher ( $S < 36.5$ ) and colder Gulf-of-Aden Intermediate Water now occurs at mid-depths and is overlain by a thin layer of higher-salinity ( $S > 37$ ) outflow at the surface. This structure probably is a response to the summertime northwesterly winds, but there may also be a contribution from the alongshore pressure-gradient field caused by upwelling off the southwest Arabian coast (Patzert, 1974). Smeed (1997) traced the development of this intermediate inflow layer of Gulf of Aden Intermediate Water into the Red Sea using the historical XBT temperature data file. He found the intrusion propagates at a speed of 6 cm/s and covers a distance of about 800 km in the Red Sea between early June and early October. Following the onset of the winter monsoon in September, downwelling in the Gulf of Aden cuts off the supply of cold water to the intermediate layer.

Already in the earlier studies, the outflow transport was found to be seasonally variable with the maximum outflow in winter and near-zero values in summer (Siedler, 1968; Maillard & Soliman, 1986). Murray and Johns (1997) reported recent observations from moored current meters that were deployed just north of Bab el Mandeb to measure the Red Sea outflow. They confirmed that the outflow shows a strong seasonal cycle (Fig. 62) rising to a maximum of 0.7 Sv in February and a minimum  $< 0.1$  Sv during the summer monsoon. Murray and Johns (1997) obtained an annual-mean outflow value of 0.39 Sv, and derived a net heat flux into the Red Sea corresponding to a heat loss of 10 W/m<sup>2</sup> over the entire surface of the Red Sea. Superimposed on the seasonal cycle, they found further large variability with periods from days to weeks (Fig. 62).

The changing outflow situation with the two-layer and three-layer flow regime during the winter and summer monsoons, respectively, has been investigated for its hydraulic control recently by Pratt, Johns, Murray, and Katsumata (1999). Using the Murray and Johns (1997) moored current data they found that for both situations the flow was subcritical, except possibly in instances of strong superimposed tides. Eshel, Cane, and Blumenthal (1994) used a linear inverse model to study the meridional-mean circulation

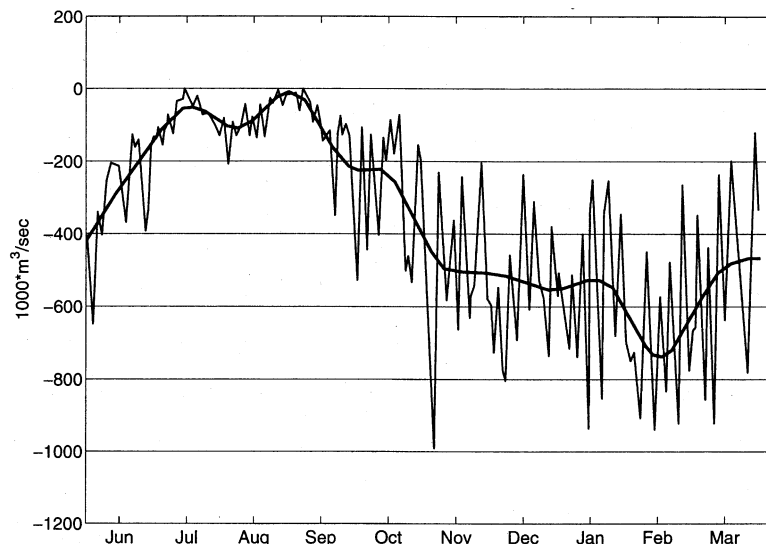


Fig. 62. Transport time series of Red Sea outflow. (After Murray & Johns, 1997.)

in the Red Sea, requiring the system to balance heat, mass, salt, and tritium. They concluded that the flow is dominantly driven by thermohaline forcing, with the direction of the surface flow being directed opposite to the prevailing wind during winter. The authors also concluded that there are two different ventilation processes in the northern Red Sea, both of which are driven by winter cooling. These generated two different water masses, deep and the upper-thermocline waters, which merged at Bab el Mandeb to supply the outflow into the Gulf of Aden.

Within the Red Sea the monsoon circulation, in particular the dynamics of intermediate water formation during the winter, was subsequently investigated in a numerical GCM study of Eshel and Naik (1997). The model had 12 km horizontal resolution, with 14 vertical levels and a constant depth of 1500 m. Surface forcing was by observed fluxes using an advective planetary boundary layer model. They obtained formation of an intermediate water mode similar to the one earlier deduced from observations by Cember (1988), with a circulation pattern driven by the northward density gradient that results from northern surface cooling. This density gradient causes cross-channel geostrophic flow, with a divergence and upwelling on the western side and a convergence and downwelling on the eastern side. The divergence on the western side is supplied by two western boundary currents, from the north and south, respectively. The water in the northern boundary current is the denser and so subducts under the southward flow, thus generating the intermediate water. They obtained a formation rate of 0.11 Sv, very close to the value of Cember (1988).

The intraseasonal variability of the exchange (Fig. 62) observed by Murray and Johns (1997) can to a large degree be explained by a simple channel model driven by atmospheric-pressure and wind-stress variations over the interior of the Red Sea (W. Johns, 1999; pers. comm.).

### 8.1.2. *Spreading in the Indian Ocean*

After passing the narrows of Bab el Mandeb, the outflow appears to flow through two separate gateways. There is a northern route along a narrow channel that can be seen in the eastern corner of the survey of Fig. 61, and a southern route that follows the topography along the African continent (Siedler, 1968). Further into the Gulf of Aden, the outflow plume of RSW descends to a core depth of about 700 m with a density of  $\sigma_\theta=27.2$  (Fig. 7), and propagates along the southern boundary of the Gulf of Aden as shown by Bower, Hunt, and Price (2000; their plate 4). Bower et al. (2000) applied the outflow plume model of Price and Barhinger (1994) to the RSW outflow and found that the combination of low outflow transport and low latitude resulted in Ekman numbers of  $O(1)$ , making the outflow a frictional density current modified by rotation, rather than a geostrophic density current modified by friction. They estimated a dilution factor of about 2.5 between the source water at the sill and the final RSW product after it has reached its equilibrium density level.

Beyond the Horn of Africa, the main pathway of RSW into the Arabian Sea is through the passage between Socotra and the African continent, where Schott and Fischer (2000) found maximum southerly flows during the winter monsoon of 1995/96. This RSW transport cycle confirms the earlier findings of Schott et al. (1990; their Fig. 7), who reported that the seasonal salinity maximum at the core density of RSW ( $\sigma_\theta = 27.2$ ) occurs from February to April off Somalia (8–12°N). Most likely the throughflow cycle in the Socotra Passage is dependent on the monsoon winds but one can also imagine that baroclinic boundary waves may communicate variable transport signals from the narrows of Bab el Mandeb to the Socotra Passage.

In a recent study of RSW distributions using WOCE data, Beal et al. (2000a; their plate 3) also found maximum monsoonal RSW variability in the Gulf of Aden and northern Somali Current, but no significant seasonality could be detected in the Arabian Sea. The mean spreading of RSW outside the Arabian Sea appears to occur along the western boundary through the Mozambique Channel. No eastward extension of the maximum into the Bay of Bengal has been found (Beal et al., 2000a).

## 8.2. Persian Gulf

The Strait of Hormuz separates the Persian Gulf (sometimes called the Arabian Gulf) from the Gulf of Oman. In contrast to the Red Sea, the Persian Gulf is shallow, being only about 60–80 m deep in the interior of the basin. It deepens to about 100 m in the narrow exit passage through the Straits of Hormuz, which is therefore not an outflow sill. There is an exchange of water across the Straits, with fresher water moving into the Persian Gulf at the surface and salty bottom water exiting with salinities  $>40$ . Based on a salt budget, Koske (1972) estimated the annual-mean exchange rate through the straits to be 0.1 Sv.

No seasonal cycle in PGW outflow has so far been identified, and indeed all indications from previous studies suggest that if it exists it is weak. Johns and Olson (1999), however, report an annual cycle in recent observations restricted to the Omani side of the Straits. Although the near-surface currents in their records were dominated by large-amplitude variations at short periods, they found a mean upper-layer outflow during the fall and winter and weak inflow during spring. However, since their observations were limited to the western side of the Gulf, it cannot be concluded that this result holds for the upper layer inflow across the full width of the Gulf. Consistent with the earlier estimates, currents in the near-bottom outflow core stayed quite constant throughout the year, with an annual-mean deep outflow of 0.28 Sv.

Surveys of the Persian Gulf outflow south of the Straits of Hormuz during WOCE did not reveal a strong identifiable outflow plume at the western side of the Gulf of Oman, but rather suggested a field of mesoscale eddies. Further downstream at the exit of the Gulf of Oman, PGW propagates southeastward along the western boundary, its core salinity is 37.50–38.5, and its core density  $\sigma_\theta = 26.6$  (Fig. 7). Bower et al. (2000) determined a dilution factor of about 4 for the Persian-Gulf outflow between the source water and the PGW after it has reached equilibrium in the open ocean. They suggested that this higher value than for the Red Sea (only about 2.5) resulted from the smaller Persian-Gulf outflow transport and larger initial density difference.

As outlined in Section 4.5, outflow from the Gulf of Oman during the summer monsoon will encounter the Ras al Hadd Jet, which flows eastward past the southeastern tip of Oman and meanders into the interior (Fig. 8) carrying PGW with it. During winter, PGW flows southwestward in a western-boundary current along the Omani coast (Fig. 9). PGW is present throughout the northern Arabian Sea, identifiable by its core salinity maximum (Fig. 7), but it loses its identity farther to the south.

Chao, Kao, and Al-Hajri (1992) used a GCM to explore effects of thermohaline and wind-stress forcing for the Persian Gulf and Straits of Hormuz. In the northern Gulf, they found that wind stress alone would cause an anticyclonic circulation system, but that thermohaline forcing by river discharge dominates, causing a cyclonic circulation instead. Evaporation results in high salinity within the Gulf and reduces the net heat gain, thus causing a pressure gradient for the upper-layer flow that is directed into the Persian Gulf. In the model this thermohaline-driven flow is opposed and weakened by northwesterly winds in winter but favored by the shallower thermocline and weaker winds in summer. In a section from the solution near the Straits of Hormuz (Fig. 63d), the summer inflow is seen on the eastern side, but on the western side there is outflow. In winter, the model inflow is to the center and there is again westward outflow (Fig. 63b), in agreement with the observations reported above.

## 9. Meridional overturning cells

Two types of meridional overturning cells in the Indian Ocean have been discussed. One involves flow of deep water into the basin from the south with compensating outflow at intermediate depths. The other involves shallower circulations that carry thermocline water from subduction areas in the Southern Hemisphere to upwelling regions north of the equator. In this section, we review the observational and modeling studies that investigate these circulations and their variability (Sections 9.1 and 9.2), and then discuss their

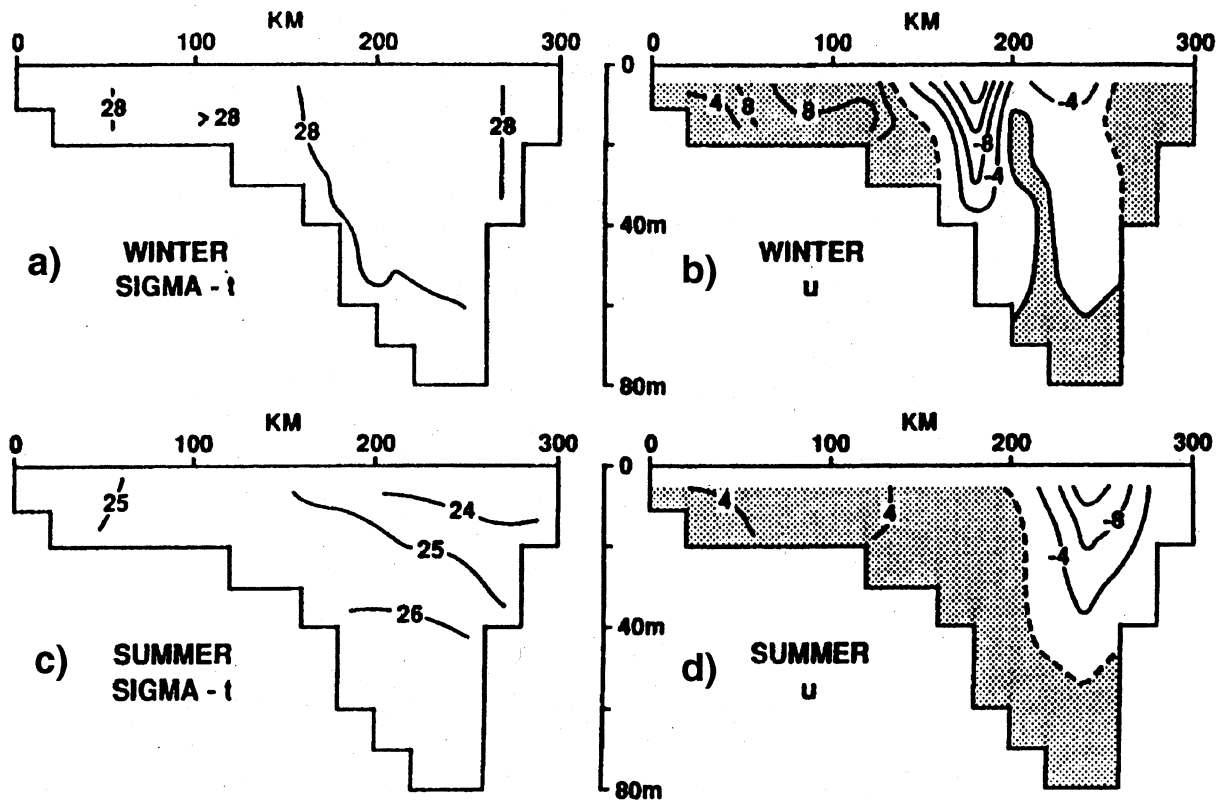


Fig. 63. Section through the Persian Gulf west of the Straits of Hormuz from the model of Chao et al. (1992), showing a) density, b) eastward currents (outflow is shaded) for the winter monsoon, and c),d) for the summer monsoon.

influence on heat transport (Section 9.3). We discuss both the mean circulation of the cells and their annual variability, since it is not possible to understand the latter without first discussing the former.

## 9.1. Deep circulations

### 9.1.1. Observations

The mean, deep, meridional overturning circulation of the Indian Ocean and its associated heat transport are still a matter of much scientific debate, with conflicting results depending on the particular observations and methods of analysis used. As has been long known (e.g., Warren, 1980; Mantyla & Reid, 1995), Antarctic Bottom Water and Circumpolar Deep Water (CDW) enter the Indian Ocean in the west off Madagascar and East Africa, and in the east along the Ninety East Ridge (Fig. 20). In a first analysis of the deep meridional basin-wide circulation, Warren (1981) estimated a mean, deep inflow of 16 Sv across a hydrographic section at 18°S. This transport, when distributed as uniform deep upwelling across the area north of that latitude, results in an upwelling velocity of some  $4 \times 10^{-7}$  m/s, about 3 times larger than estimated for the Pacific and Atlantic Oceans.

In an analysis of a modern hydrographic section with eddy-resolving station spacing near 32°S, Toole and Warren (1993) used subjectively determined reference levels for determining geostrophic transports. They concluded that there was a very strong, deep, meridional overturning cell, consisting of an inflow of  $27 \pm 10$  Sv below about 1800 m, and a corresponding outflow above that depth that was augmented by an

Indonesian Throughflow of 6.6 Sv (Fig. 64). Subsequently, Robbins and Toole (1998) found that this solution would transport too much silica into the northern basin, and arrived at a reduced deep inflow of  $12 \pm 3$  Sv from that same section, which was accomplished through a decrease in the net northward inflow in the eastern basin (Fig. 64). However, both solutions were based on a large volume transfer from CDW into shallower levels, above neutral density 28.1, corresponding to a depth of about 2800 m.

Recent re-evaluations of the deep overturning transports, using box inverse model calculations with partially different sections and constraints, have been carried out by Macdonald (1998), Ganachaud and Wunsch (2000), Ganachaud et al. (2000), and Sloyan and Rintoul (2001). While they all obtained deep inflow into the southern Indian Ocean, their results on the magnitude of the overturning and upwelling differed drastically. We now contrast two of them.

Ganachaud et al. (2000) estimated deep inflow based on the 32°S section noted above, on WOCE sections along 20°S and 8°S, the Mozambique Channel, and the Indonesian Throughflow regime, and on sections in both hemispheres of the other oceans. They obtained a much reduced deep inflow of  $11 \pm 4$  Sv across all three zonal sections (Fig. 56). By contrast, Sloyan and Rintoul (2001), using the aforementioned 32°S section and a 18°S section observed earlier in the Indian Ocean as well as other, sections in the southern regions of the other two oceans, obtained a much larger deep inflow of  $23 \pm 4$  Sv (Fig. 64). Despite this large inflow, they were able to balance the silica budget because their southward return flow occurred at deeper depths than in the Toole and Warren (1993) calculation, as can be seen from a comparison between the transport functions shown in Fig. 64 in neutral density classes. The Ganachaud et al. (2000) solution, on the other hand, has a transport-function profile similar to that of Robbins and Toole (1998), with a

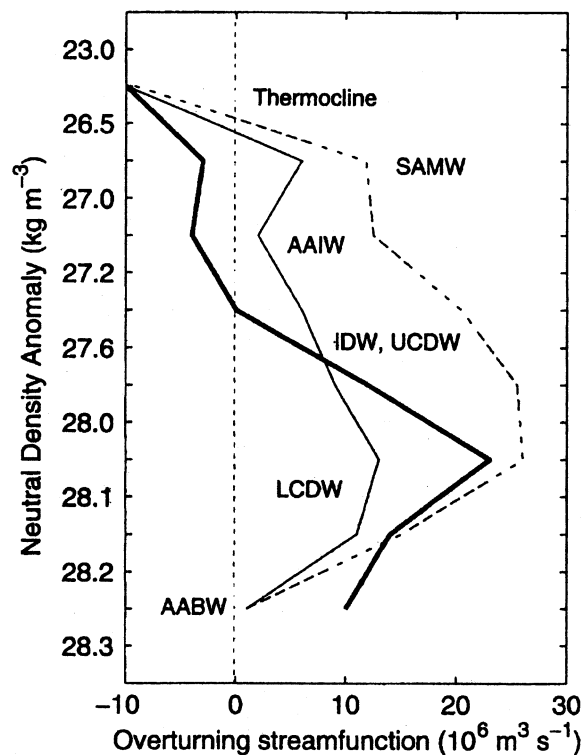


Fig. 64. Overturning transport function for 32°S section, based on analysis of Toole and Warren (1993, dashed), on the revised calculation of Robbins and Toole (1998, thin solid) and the Sloyan-Rintoul inverse box model, heavy solid. (From Sloyan & Rintoul, 2001.)

maximum near 28.05 neutral density, that is, with upwelling to fairly shallow layers. The large discrepancies between these two inverse study results lead to correspondingly large differences in the estimated deep upwelling velocities and are yet to be satisfactorily explained. One possible cause might be the use of different sections in each study, but perhaps more importantly the models differ in their treatment of diapycnal fluxes (A. Ganachaud and S. Rintoul, pers. comm., 2001).

Not much is known from observations about seasonal differences in the basin-wide transports. Stramma et al. (2002) and Brandt et al. (2002) analyzed the 8°N section across the Arabian Sea for both seasons and concluded that there was a deep northward flow below 2500 dbar during both seasons of about 5 Sv with an opposite shallow overturning cell in the upper 500 m (see Section 9.2).

### 9.1.2. Deep upwelling and mixing

A theoretical basis for deep overturning is provided by the classical work of Stommel and Arons (1960). In their study, the deep circulation is thought of as a uniform deep layer, out of which a horizontally uniform upwelling velocity continually draws water into the upper part of the water column, and then returns it to the deep ocean in localized sinking areas (e.g., North Atlantic, Weddell Sea). Geostrophy and vorticity conservation in the deep layer require that the meridional component is directed poleward everywhere and that there are boundary currents (not part of the model) that close the deep circulation system to ensure mass continuity.

So far there is no glaring conflict between the meridional directions of observed boundary currents in the ocean basins and this concept (Warren, 1980). Even so, questions persist as to how this deep upwelling actually takes place and what the relevant physics are. A mean deep upwelling of about  $4 \times 10^{-7}$  m/s requires an amount of vertical diffusion of about  $4 \times 10^{-4}$  m<sup>2</sup>/s based on an assumed vertical advective-diffusive balance and the typical stratification of the deep Indian Ocean yielding a value of  $\rho_z/\rho_{zz} \sim 1000$  m (M. Dengler, 2000; pers. comm.).

How does this upwelling rate compare to estimates from observations? It is now accepted that the diapycnal eddy diffusivity in the abyssal ocean away from rough topography is of the order of  $1 \times 10^{-5}$  m<sup>2</sup>/s (Munk & Wunsch, 1998), far less than what is required for the above balance. For the equatorial regime, estimates of deep mixing within the equatorial ‘stacked jets’ have yielded similar values of  $2\text{--}3 \times 10^{-5}$  m<sup>2</sup>/s (Dengler & Quadfasel, 2002). In the northern Somali Basin and western Arabian Basin, however, new estimates of abyssal eddy diffusivities have yielded higher values of  $1\text{--}3 \times 10^{-4}$  m<sup>2</sup>/s (Dengler, 2000; pers. comm.), as a consequence of intraseasonal current fluctuations interacting with the Carlsberg Ridge and thus sustaining an elevated abyssal internal wave field. Although such high mixing coefficients occur in localized ‘hot spots’, the basin-averaged mixing levels still remains significantly below what is required to maintain the upwelling balance ( $4 \times 10^{-4}$  m<sup>2</sup>/s). On the other hand, new calculations of tidal dissipation from T/P altimetry by Egbert and Ray (2000) indicate that the area around the Mascarene Ridge and south of Madagascar accounts for more than 10% of the estimated total tidal dissipation for the global abyssal ocean, so upward revisions of the basin-averaged mixing rates may be forthcoming.

### 9.1.3. Models

Annual-mean meridional streamfunction plots for the prognostic model solutions of Wacongne and Pacanowski (1996), of the POCM (as analyzed by Garternicht & Schott, 1997), and the adjoint model of Lee and Marotzke (1998) are shown in Fig. 65a, d and g, respectively. There are considerable differences between the three solutions, which are partly attributable to differences in model formulation. For example, the POCM evaluated by Garternicht and Schott (1997) is global, whereas the other two are regional and hence require prescribed southern and Indonesian Throughflow boundary conditions. At the southern boundary, both basin models employ a sponge layer to relax the stratification to the climatologies of Levitus (1982) and of Levitus and Boyer (1994a,b), respectively. The Wacongne and Pacanowski (1996) model was closed in the throughflow region, and Lee and Marotzke (1998) also relaxed their stratification to

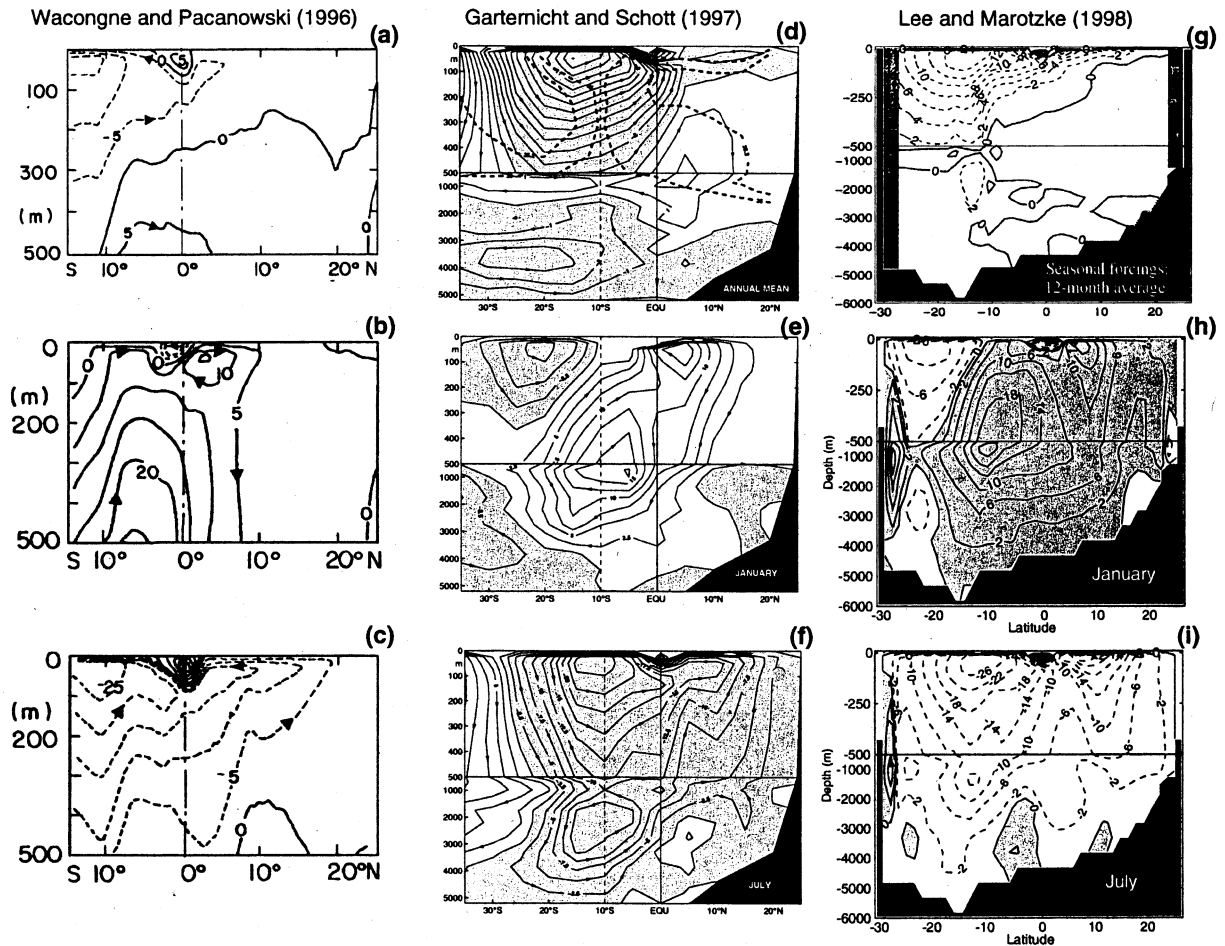


Fig. 65. Meridional transport streamfunctions ( $S_v$ ) for a)–c) the GFDL model (after Wacongne & Pacanowski, 1996; only upper 500 m are shown), d)–f) the POCM model (Gartemicht and Schott, 1997; dashed contours in d) indicate zonal-mean salinities), and g)–i) Lee and Marotzke (1998). Streamfunctions are shown for the annual mean (top panels), for the winter monsoon (middle panels) and for the summer monsoon (bottom panels) flow fields.

climatology there. The models also differ in their horizontal and vertical resolutions, their mixing parameterizations, and in the windstress products used to force them. The streamfunctions shown from Lee and Marotzke (1998) are for the case where the model assimilates monthly temperature and salinity climatology from Levitus and Boyer (1994a,b).

In the mean meridional circulation, the Wacongne and Pacanowski (1996) solution (for which only the upper 500 m are shown in Fig. 65a) has inflow from the south in the 50–800 m depth range across 15°S, which mostly returns the southward Ekman transport northward. The Lee and Marotzke (1998) model also does not show a deep cell (Fig. 65g). There is some deep inflow, about 3 Sv below 4000 m, and outflow between 800 m and 4000 m in the global POCM (Figs. 65d and 64). Overall, none of these three simulations represents the deep overturning in the South Indian Ocean as was deduced from the analysis of the 32°S section. For the two regional (Indian-Ocean) models, this may of course be related to their use of similar climatological data sets at the southern buffer zones. In support of this possibility, Lee and Marotzke (1998) found distorting effects of the Throughflow buffer zone on the mean overturning.

The streamfunctions in all three solutions show large reversals of the deep circulation between the monsoon seasons (Fig. 65). The largest seasonal changes occurred near 10°N and 10°S, where the seasonal wind stress differences were also largest (Fig. 1). Lee and Marotzke (1998) carried out an analysis of the processes involved in the seasonal changes by decomposing the streamfunctions into barotropic (external mode), vertical shear (resulting from baroclinic geostrophic motion and topographic, frictional effects), and Ekman components, where the Ekman transport was determined from the zonal-mean wind stress. This decomposition is shown in Fig. 66 for the July transport streamfunction anomaly, that is, the difference between the July transport streamfunction (Fig. 65i) and the annual-mean one (Fig. 65g). The equatorial strip is blanked out because of geostrophy and Ekman degeneration. Lee and Marotzke (1998) concluded that the largest contribution to the seasonal variability (and correspondingly, also to the seasonal heat transport cycle discussed below) was caused by the Ekman component and its compensation by barotropic

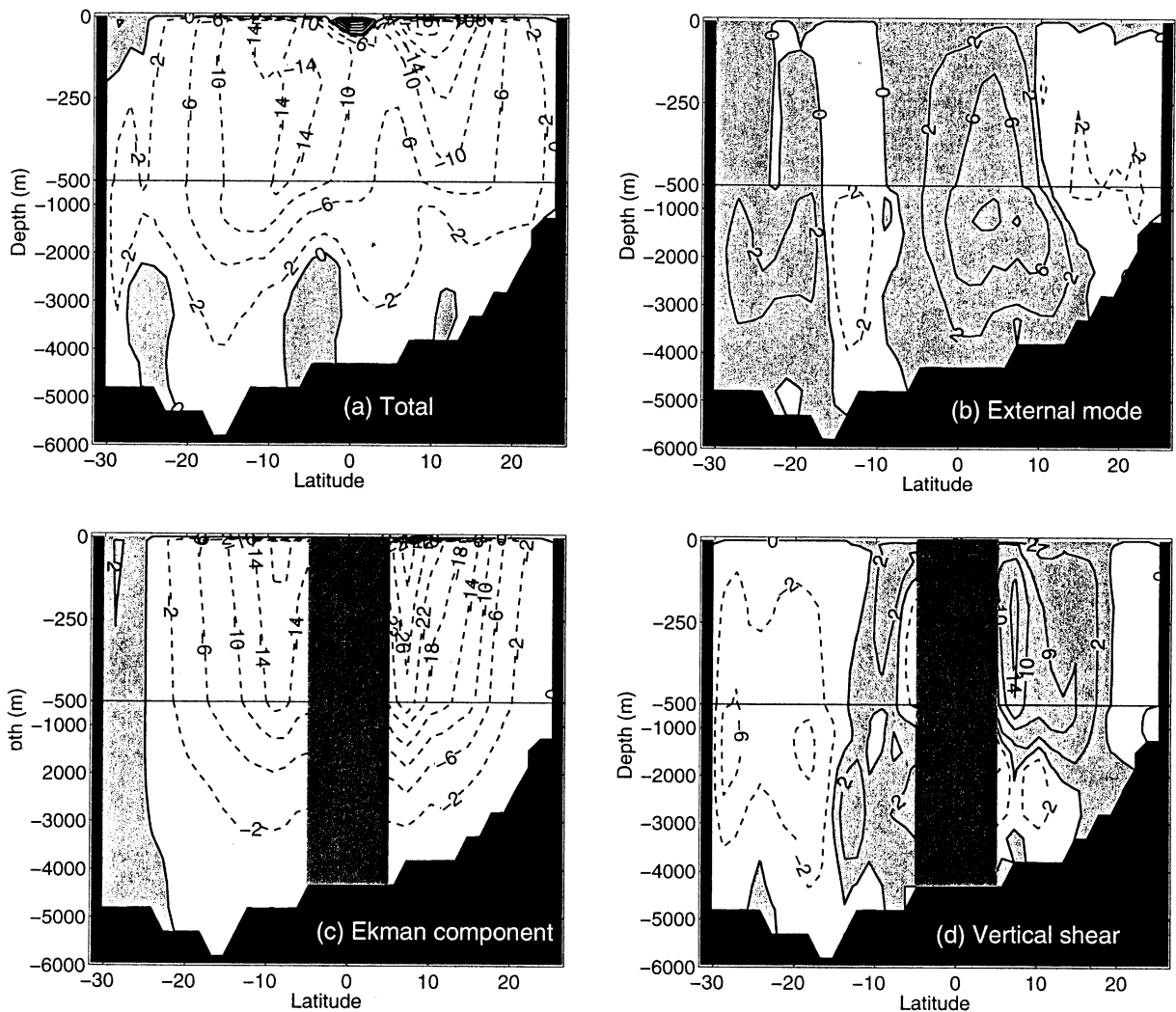


Fig. 66. Decomposition of a) the meridional transport streamfunction anomaly for the summer monsoon, into b) the barotropic (external) mode, c) the Ekman contribution, and d) the vertical shear mode. See text for details. (From Lee & Marotzke, 1998.)

motion (Fig. 66c), yielding an apparent overturning  $>20$  Sv. Interestingly, the barotropic component itself has vertical structure, giving the impression of an overturning motion. This structure is present in the zonally averaged streamfunction because of zonally varying bottom topography in regions where a strong boundary current over shallower topography (in this case the Somali Current) moves in one direction and the deep, weak offshore flow moves in another. Therefore this barotropic ‘overturning’ mode has its maximum ( $\sim 8$  Sv) just north of the equator where the model Somali Current is strongest (Fig. 66b). For the vertical-shear (baroclinic) component the largest contributions are not from the interior but come from vertical shear in the western-boundary currents of both hemispheres (Fig. 66d). In addition, the shallow baroclinic cell in the Arabian Sea could partially be the effect of the annual Rossby wave causing this type of overturning (see Section 9.2).

The seasonal streamfunctions in Fig. 66 give the impression that there is large variability in the strength and structure of the deep overturning circulations. Physically, however, the variability mostly represents an adiabatic sloshing back-and-forth of water masses, and not diabatic, across-isopycnal flow. Thus, it is indicative mostly of changes in heat storage, rather than of cell strength.

## 9.2. Shallow cells

### 9.2.1. Observations

Shallow overturning cells exist in the tropical-subtropical Atlantic and Pacific Oceans. They consist of subduction in the subtropics, upwelling in the tropics and the circulations that connect the two regions. In contrast to the Atlantic and Pacific Oceans, significant upwelling does not occur along the equator in the Indian Ocean, but predominantly occurs in the Northern Hemisphere off Somalia, Oman and India; the subduction regions are largely confined to the Southern Hemisphere. Thus, this Indian Ocean cell necessarily involves currents that cross the equator, and for this reason we refer to it as the ‘Cross-Equatorial Cell’. (Another possible Indian Ocean shallow overturning cell is discussed at the end of Section 9.2.2).

The surface branch of the Cross-Equatorial Cell is largely Ekman transport. As indicated by the wind stress distribution (Fig. 1), the meridional Ekman transports on both sides of the equator are southward during the summer monsoon and northward during the winter monsoon, and hence one expects a seasonally reversing meridional cell. So far, however, there is little quantitative evidence from observations for the shallow cell, and so here we have to rely heavily on model results (Section 9.2.2). We first discuss the upwelling and subduction branches of the cell, and then report on reversing shallow overturning within the Arabian Sea.

*9.2.1.1. Arabian Sea upwelling:* Off Somalia, upwelling is typically concentrated in the cold wedges associated with the two-gyre system (Fig. 32). As Fig. 37 shows for the northern wedge, the upwelled water can come from depths of 200–300 m, with temperatures colder than  $15^{\circ}\text{C}$  and densities in excess of  $26.5\text{ kg/m}^3$ . These densities correspond to surface densities in the southern subtropics near  $40^{\circ}\text{S}$  (curve LC in Fig. 7). However, there is large interannual variability in upwelling intensity and surface temperatures observed in 1993 and 1995 in the northern cold wedge off Somalia were in the  $25\text{--}27^{\circ}\text{C}$  range, that is, the upwelled water originated from the upper 100 m. The relatively low salinities of the water upwelled off Somalia identified it as being of Southern-Hemisphere origin (Fischer et al., 1996). This property is supported by salinity and silica distributions on the  $25.7\text{ kg/m}^3$  isopycnal surface (Fig. 16) and by a comparison of a T/S curve from the northern Somali upwelling wedge taken in August 1993 (marked SC in Fig. 7) with the climatological T/S curve from the EACC just south of the equator (marked EACC in Fig. 7). There is only a slight offset in salinity between the two curves, presumably caused by mixing with higher-salinity waters along the way northward. The Omani upwelling regime is presumably supplied from the south by the net northward throughflow through the Socotra Passage (Fig. 8), but there is also local subduction in winter (see below). The amount of upwelling off India is estimated to be small in comparison with the intensive regimes off the northwestern coasts.

*9.2.1.2. Is there open-ocean upwelling at 5–10°S?* There are indications that upwelling may sometimes exist in a band from 5–10°S in the Central and Western Indian Ocean, a result of Ekman divergence at the northern edge of the SECC. Climatological mixed-layer depths show a zonally extended minimum there during both monsoons (Figs. 17 and 16), and the thermocline domes so that at 100 m temperatures are at a minimum (Fig. 15c–f). Further support for this upwelling is provided by satellite imagery of ocean color, which sometimes indicates that phytoplankton blooms occur along the band (Murtugudde et al., 1999). On the other hand, climatological SST does not show a zonal minimum in this region, since it is a gradient region with SSTs increasing northwards (Fig. 15a,b). As discussed in Section 10, SST anomalies of this region are significantly correlated with East African rainfall and they are also correlated with the doming, suggesting the importance of the upwelling.

*9.2.1.3. Subduction in the southern hemisphere and pathways:* Southern-hemisphere waters that are subducted in the southeastern subtropical Indian Ocean (Zhang & Talley, 1998; Karstensen & Quadfasel, 2001) move westward in the SEC and then northward in the EACC. A flow of about 30 Sv passes the northern tip of Madagascar above about 1000 m (Swallow et al., 1988; Figs. 8 and 33a), but only about 10 Sv crosses the equator with the Somali Current in the annual mean (Fig. 33c), the rest either turning southwards into the Mozambique Channel (Figs. 55 and 56) or flowing eastward just south of the equator as part of the SECC (Section 6.3). While the annual-mean northward cross-equatorial flow of the Somali current is 10 Sv, the summer monsoon mean (at the time when the upwelling actually occurs) is 22 Sv (Fig. 33c). This does not imply, however, that there is an upwelling of this strength in the Northern Hemisphere; rather much of this transport is related to the seasonal ‘sloshing’ discussed in the previous section, which just changes the heat storage in both hemispheres seasonally.

One should mention that some subduction also takes place in the Arabian Sea. Most of the water subducted is Arabian-Sea surface water, which has been cooled and augmented in salinity by cold, dry, winter-monsoon winds. From the JGOFS surveys, Morrison (1997) found high-salinity surface waters with  $\sigma_\theta > 24.8$  in the northern Arabian Sea during the winter monsoon, and Schott and Fischer (2000) also reported in winter observations salinity-maximum waters entering the thermocline from the region north of Socotra. The curl field during the winter monsoon is anticyclonic over the northern Arabian Sea, supporting insertion of mixed-layer waters into the thermocline by Ekman pumping. Small quantities are also introduced into the middle and upper thermocline by the Red Sea and Persian Gulf outflows, respectively (see Section 8).

*9.2.1.4. Shallow overturning in the Arabian Sea:* In the tropical and subtropical interior Indian Ocean the Ekman transport is southward during the summer monsoon, as noted in several previous sections. In the Arabian Sea surface layer, southward Ekman transports during the summer monsoon reach nearly 20 Sv (Chereskin et al., 1997). This process appears to be the primary mechanism for removing surface water from the northern Indian Ocean and returning it to the southern subtropics, thus closing the Cross-Equatorial Cell.

In their comparative analysis of the 8°N section across the Arabian Sea for August 1993 and January 1998, Stramma et al. (2002) found that the Ekman transport was balanced by shallow geostrophic flow in the upper 400m. The geostrophic transport for August 1993 was 14 Sv northward in the upper 300 m compared to 9 Sv southward for the winter section. As mentioned in Section 5.1.4, the physical mechanism for this shallow overturning in the central Arabian Sea is the superimposition of mode-1 and -2 annual Rossby waves (Brandt et al., 2002). This yielded 10 Sv northward in the upper 300 m at the central part of the section in August 1993, and 8 Sv southward in January 1998.

## 9.2.2. Models

A number of modelling studies have produced shallow overturning circulations that are consistent with the observations discussed above. They also point toward the existence of features that are yet to be detected (e.g., equatorial rolls and an Indian Ocean ‘Subtropical Cell’).

*9.2.2.1. The Subtropical Cell:* MKM extensively discussed the shallow overturning circulations in their solution. It contained a Cross-equatorial Cell with a strength of 5 Sv closed by upwelling in the northern ocean, but also a second cell, the Subtropical Cell (called Tropical Cell by MKM), with a strength of 6.5 Sv closed by a band of upwelling located across much of the interior Indian Ocean from 5–10°S. The annual-mean streamfunction plots in Fig. 65 also indicate upwelling out of the northward thermocline flow into the southward Ekman transport in this latitude band. Note in the upper middle panel, for example, that some dashed streamlines rise to the surface in the Northern Hemisphere as part of the Cross-Equatorial Cell, while others intersect the surface from 5–10°S as the upward branch of the Subtropical Cell. Upwelling within the Subtropical Cell may be overemphasized in numerical models, since, as noted above, observational evidence for it is not conclusive at this time.

*9.2.2.2. Three-dimensional pathways:* The three-dimensional circulation patterns followed by water parcels in the Cross-Equatorial and Subtropical Cells are much more complex than suggested in the 2-dimensional streamfunction maps. For example, in the MKM solution lower-layer water circulates around the subtropical gyre in the Southern Hemisphere, and some joins the EACC. It then either crosses the equator within the EACC to feed the upwelling off Somalia and Oman or turns offshore just south of the equator to join the SECC. Most of the SECC water then bends southward to provide water for the open-ocean upwelling in the 5–10°S band and to participate in the Subtropical Cell; the rest reverses to flow westward along the equator, and subsequently moves into the Northern Hemisphere. In the surface layer, upwelled water flows eastward and southward across the interior Arabian Sea, eventually crossing the equator within the interior of the ocean (similar to Fig. 10). Haines et al. (1999) and Miyama (2000, pers. comm.) diagnosed similar flow patterns for both annual-mean and seasonally varying circulations by tracking Lagrangian tracers and drifters in their solutions. In the latter study, the circulations were confirmed to appear in several types of ocean models, varying in complexity from the MKM 2½-layer system to the JAMSTEC GCM.

*9.2.2.3. Cross-equatorial surface flow:* The seasonal streamfunction maps of Lee and Marotzke (1998) suggest that a major contributor to the seasonal surface circulation in the tropics is Ekman transport, which is directed southwards on either side of the equator in summer and northward in winter, and amounts to >20 Sv in each season (Fig. 66). A difficulty with this interpretation, though, is that Ekman flow breaks down near the equator, so that the flows that actually carry water across the equator are not specified.

Godfrey et al. (2001) and Miyama, McCreary, Jensen, Loschrigg, Godfrey, and Ishida, Structure and Dynamics of the Indian Ocean Cross-Equatorial Cell (Manuscript in preparation) provide a theoretical explanation that resolves this dilemma. They note that during both monsoons the zonal component of the winds nearly vanishes at the equator but is roughly proportional to  $y$  on either side. For this wind field, the Ekman pumping velocity ( $1/\rho_0$ ) curl ( $\tau/f$ ) is zero. As a result, isopycnals are not shifted vertically, and hence no geostrophic currents can be generated, only Ekman flows. Moreover, the concept of Ekman flow is valid all the way to the equator because both  $\tau^x$  and  $f$  vanish as  $y$  goes to zero so that  $\tau^x/f$  remains well defined. Thus, even the cross-equatorial currents that connect the off-equatorial Ekman flows can also be interpreted as being Ekman drift.

An equivalent interpretation is that the cross-equatorial flow is a quasi-steady Sverdrup flow driven by wind curl. A Sverdrup flow is composed of both Ekman and geostrophic components. Since this special zonal wind (i.e., proportional field to  $y$ ) drives no geostrophic currents, the cross-equatorial flow again is equal to the Ekman drift. Mathematically, the equivalence is apparent from the relation  $v = \text{curl}(\tau^x/\beta) = -\tau^x/f$ , where  $\beta = f_y$ . Consistent with this idea, the quasi-steady Sverdrup flow has southward, cross-equatorial transports in excess of 20 Sv at the height of the summer monsoon, and weaker, northward, cross-equatorial transports in winter (Fig. 12).

*9.2.2.4. Equatorial rolls:* Note in Fig. 65 that there are very shallow overturning cells centered on the equator in all the solutions, which reverse their sense of rotation from summer to winter. These ‘equatorial rolls’ are not an artifact of zonal averaging but occur across much of the interior ocean. They were first noted by Wacongne and Pacanowski (1996). In their solution, the roll is strongest during the summer (Fig. 65c). As a consequence, at this time the antisymmetric zonal wind drives net southward flow across the equator in the upper 100 m, but near the equator it typically occurs beneath a northward surface current associated with the equatorial roll. An oppositely directed and weaker circulation exists during the winter (Fig. 65b), with a southward surface current on the equator and a northward subsurface flow that connects the northward Ekman flow in each hemisphere.

Wacongne and Pacanowski (1996) concluded that the rolls were a response to cross-equatorial winds that are present during the monsoons (Fig. 1), as suggested earlier by Philander and Pacanowski (1980); see McCreary, 1985, for further discussion). Similar equatorial rolls developed in Philander and Pacanowski’s (1980) solutions forced by uniform meridional winds, consisting of cross-equatorial surface flow in the direction of the wind, upwelling on the upwind side, and downwelling on the downwind side. A meridional pressure gradient developed that tended to balance the surface wind, and it drove the subsurface counterflow. Miyama et al., (2001; manuscript in preparation) confirmed that meridional winds are the driving force for the Indian-Ocean rolls, by analyzing solutions to both linear and nonlinear models forced by realistic winds with and without a meridional component.

Whether the rolls cause diapycnal fluxes depends on the mixed-layer physics of the respective model. This does not occur in the models described above because their rolls are contained within the mixed-layer and so have no effect on the heat budget. Schiller et al. (1998) commented on the diapycnal fluxes of the cells in their GCM study. They found that when the mixed-layer depth was less than the vertical scale of the equatorial roll, as was the case in their simulation during May, there was a band of heat uptake by the upwelled water south of the equator.

### 9.3. Heat transports

#### 9.3.1. Mean meridional transport

From the observational and model discussion above it is apparent that Indian-Ocean heat transport must occur predominantly via the Cross-Equatorial Cell. If a deep cell exists as consistently analyzed by section and inverse analyses (see Section 9.1) it must return the deep inflow at somewhat shallower depths; however, the temperature of the outflow does not differ substantially from the inflow temperature, so the deep cell contributes little to the heat transport.

The meridionally integrated mean heat transports from the air-sea flux evaluations of Hsiung (1985) and Hastenrath and Greischar (1993) are shown in Fig. 67. These curves correspond to the heat that has to be transported meridionally by ocean processes under the assumption that there is no change in heat storage. They vary significantly from each other as biases in bulk parameterizations add up along the way southward, so that Hsiung (1985) found the annual-mean heat export across the equator to be about 0.8 pW, while Hastenrath and Greischar (1993) obtained only about half that value. These heat transports can be checked against oceanographic determinations of meridional heat flux from section inversions; however, equivalence only applies until the latitude of the Pacific-to-Indian Ocean throughflow is reached, and further to the south assumptions about the throughflow have to be made to close the heat budget (e.g., Toole & Warren, 1993), or alternatively combined Indian and Pacific sections of the southern ocean have to be analyzed (e.g., Macdonald, 1993; Ganachaud et al., 2000).

The mean heat transports of the solutions analyzed by Wacongne and Pacanowski (1996), Garternicht and Schott, (1997) and Lee and Marotzke (1998) can be compared in Fig. 67. The annual-mean heat transports in the first two models are considerably weaker than those estimated from the air-sea flux studies, with only 0.2 pW being exported southward across the equator, whereas Lee and Marotzke’s (1998) result

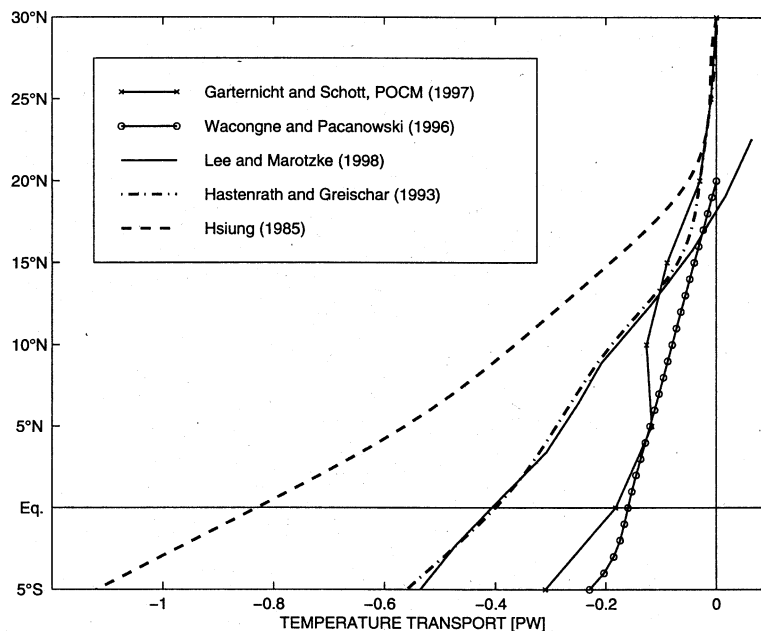


Fig. 67. Mean Indian Ocean meridional heat transports north of the Throughflow latitude from the atmospheric flux determinations of Hsiung (1985) and Hastenrath and Greischar (1993), and from model heat transports of Wacongne and Pacanowski (1996), Gartnericht and Schott (1997) and Lee and Marotzke (1998).

from the hydrographic inverse model solution agrees quite well with the Hastenrath and Greischar (1993) curve. An interesting result of the Lee and Marotzke (1998) study was that the annual-mean heat flux was changed little if the model was forced by annual-mean winds and fluxes rather than by seasonally varying ones, implying that rectification of seasonal meridional variability is not an important factor.

As mentioned in Section 7, Wajsowicz and Schneider (2001) discussed the influence of the Indonesian Throughflow on the mean heat budget of their numerical solution. They noted that it mostly affects the region west and south of the throughflow (Fig. 59) but it also affects the equatorial regime by reducing the Arabian Sea heat export.

### 9.3.2. Seasonal variability

Seasonal meridional heat transports for the Indian Ocean north of 5°S are shown in Fig. 68 from the studies of Gartnericht and Schott (1997) for the POCM solution and of Hsiung, Newell, and Houghtby (1989) and Hastenrath and Greischar (1993) using observed data. The latter were calculated by combining the air-sea fluxes with heat storage changes based on the hydrographic climatologies. Although there were differences in data sets used in these studies, there is basic agreement in the result that the ocean exports heat in excess of 1 pW southward across the equator during the summer monsoon and carries a lesser amount northward during the winter monsoon. There is good agreement between the model and the meteorologically derived seasonal cycles. The two other models show similar results for the seasonal heat transport variability.

The Lee and Marotzke (1998) decomposition of the model meridional transport stream function for July, corresponding to the transport decomposition of Fig. 66, is shown in Fig. 69. It suggests that most of the seasonal heat transport variability results from Ekman transport, with some contribution north of the equator from the shear and external components resulting from the Somali Current (see previous section). As also pointed out earlier, this seasonal heat transport anomaly is dominantly a ‘sloshing’ motion that increases

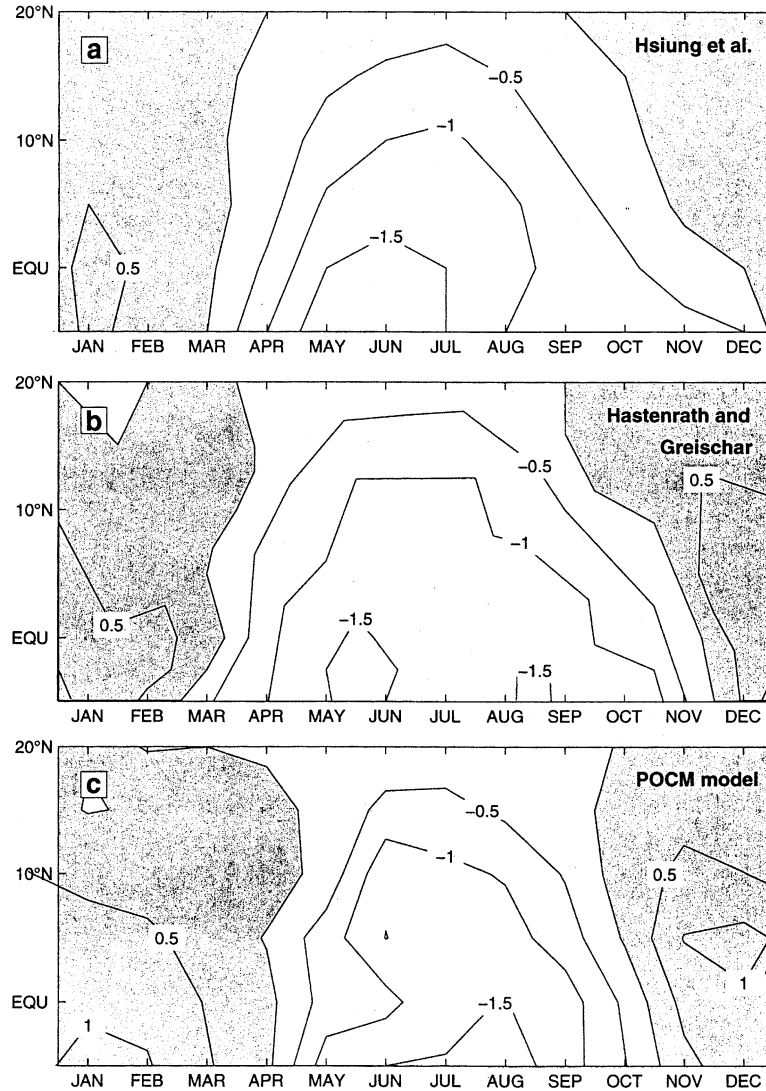


Fig. 68. Seasonal cycle of meridional heat transport ( $10^{14}$ W), from air-sea flux calculations of a) Hsiung et al. (1989), b) Hastenrath and Greischar (1993) and c) from the POCM model analysis. (From Gartnrecht & Schott, 1997.)

heat storage in the northern part of the basin during the winter monsoon but decreases it during the summer monsoon. Results from the Gartnrecht and Schott (1997) analysis of the POCM solution for 1987–89 also support the importance of Ekman flow. There is a tight correlation between monthly values of meridional model heat fluxes and zonal-mean wind-stress variability north of the Indonesian throughflow latitude where the basin is closed (Fig. 70), with the regression slope reversing sign between the hemispheres according to the sign of the Ekman transport. South of the Throughflow latitude, the correlation is reduced because of the uncorrelated component of heat input generated by the variability of the Throughflow. The importance of the Ekman component to seasonal heat transport variability had also been shown earlier for the tropical Atlantic by Böning and Herrmann (1994).

Besides the strong Ekman transport, baroclinic flows in the interior may regionally contribute to the

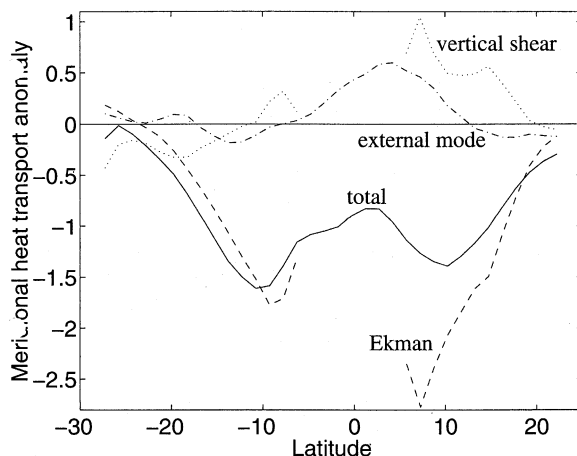


Fig. 69. Decomposition of the total model heat transport anomaly for July into components due to the barotropic mode, vertical-shear and Ekman transport. See Fig. 66 and text for details. (From Lee & Marotzke, 1998.)

seasonal heat transport cycle. In the section analysis by Stramma et al. (2002), the heat transport across 8°N in the Arabian Sea was estimated to be 0.60 pW southward in August 1993 and 0.24 pW northward in January 1998. In this case, the Ekman transport was compensated by geostrophic flow in the upper 300 m (not by a barotropic current as was suggested to be dominant above), much of it accomplished by a baroclinic annual Rossby wave (see Section 9.3). This would account for about half of the 8°N values obtained from air-sea flux integration (Fig. 68), the other half then to be contributed by the Bay of Bengal.

## 10. Climate modes

Significant links between oceanic and atmospheric variables in the Indian Ocean have been known for some time. For example, Nicholls (1989) noted a correlation between Australian rainfall and an SST anomaly pattern of one sign in the Indonesian region and the opposite sign in the southeastern Indian Ocean. Yasunari (1989) and Meehl (1997) described the tropical biennial oscillation (TBO), in which anomalies of air-sea variables in the eastern Indian and western Pacific Oceans tend to have opposite signs in consecutive years.

There are also significant correlations between Indian-Ocean air-sea parameters and Asian rainfall (e.g., Nicholls, 1995) and ENSO (e.g., Barnett, 1983). Hastenrath, Nicklis, and Greischar (1993) investigated the seasonal cycles and interannual variability of rainfall over East Africa and India, equatorial SST and Wyrski Jet intensity and noted that anomalies were both, related to ENSO and locked to the seasonal cycle. Indeed, the ENSO correlations are large enough (Murtugudde et al., 2000) to indicate that a portion of Indian-Ocean climate variability is externally forced by ENSO; on the other hand, they are also small enough to suggest that other climate processes are also involved. An intriguing hypothesis is that the ocean and atmosphere interact in the Indian Ocean to form one or more coupled modes of climate variability, and the search for such modes is now an area of active research. Identifying these modes has been difficult, however, because the region is so strongly affected by external forcing, both interannually by ENSO and seasonally by the monsoon itself.

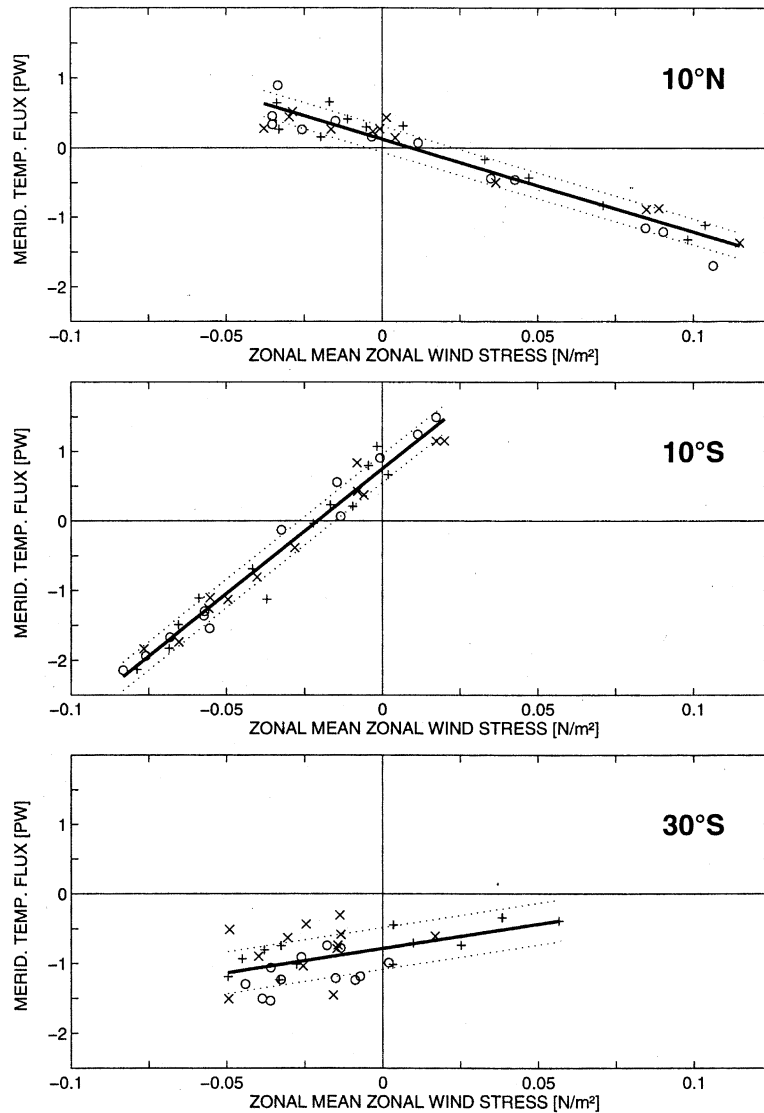


Fig. 70. Meridional heatfluxes of individual-month means in the POCM model plotted against monthly zonal-mean wind stresses, indicating that model heat fluxes at seasonal and even interannual time scales are dominantly determined by Ekman transports. (From Garternicht & Schott, 1997.)

### 10.1. Indian Ocean Equatorial mode

Recently, a mode of climate variability, rather like the Pacific’s ENSO mode, has been isolated (Webster et al., 1999; Saji et al., 1999; Murtugudde et al., 2000). It consists of intensified equatorial easterlies, large changes in equatorial ocean circulation (see below), anomalously low SST in the eastern, tropical Indian Ocean caused by intensified equatorial and Sumatran upwelling, anomalously high SST in the western, tropical Indian Ocean, greater than normal rainfall in equatorial West Africa, and Indonesian droughts. Saji et al. (1999) named this variability pattern a ‘dipole mode’ because of the observed zonal SST and sea level differences across the equatorial regime, but the true nature of this mode is still under debate.

There has already been some discussion of this mode in earlier literature based on a large event that occurred in 1961/62 (e.g., Reverdin et al., 1986; Kapala, Born, & Flohn, 1994), but historically it did not attract much scientific attention because the amplitudes of typical events are weak. Murtugudde and Busalacchi (1999) pointed out the potential dipole nature based on sea level anomalies in the western and eastern equatorial basin and accompanying zonal SST gradients for the time period 1980–95 (their Fig. 23). Indeed, there have only been three major events during the past 40 years, during 1961/62, 1993/94, and 1997/98. The two recent events are very obvious in the time series of zonal wind anomalies shown for the past decade (Fig. 5). The latter two events coincided with Pacific ENSO events, a weak El Niño in 1993/94 (i.e. the Southern Oscillation Index was negative) and a very strong El Niño in 1997/98, whereas the earliest one did not.

### 10.2. *The 1993–94 anomaly*

The 1993–94 event began with anomalous winds blowing toward the east along the equator during the fall of 1993 and showed strong westward equatorial anomalies in the second half of 1994 (Fig. 5). Fortunately, there were current-meter moorings deployed at and north of the equator to the south of Sri Lanka, and these captured the equatorial anomalies that took place during the development of the event (Reppin et al., 1999; see Section 3.1.1). The WJ during fall, 1993, was much stronger than usual with an estimated transport of 35 Sv, whereas during spring, 1994, the subsequent WJ was anomalously weak with a maximum transport of only 5 Sv (Fig. 23). Reppin et al. (1999) also reported that the EUC reappeared in August and September, 1994, whereas typically it only exists from February to June (see Section 3.2). These circulation anomalies were reproduced in the POCM-4 model of Semtner/Tokmakian that was analyzed by Reppin et al. (1999) and in a GCM/MOM study of equatorial interannual variability by Vinayachandran et al. (1999b). They clearly result from anomalous equatorial winds, so that both the reappearance of the EUC and the weak spring WJ could be attributed to anomalous easterlies.

The anomalous easterly winds also lead to sea level being anomalously low throughout the entire eastern Indian Ocean in June, 1994, just after the weak spring WJ (Potemra et al., 1997; Vinayachandran et al., 1999b). This was accompanied by low SST and the thermocline shoaling by more than 50m at the eastern equatorial end (Meyers, 1996). As a consequence, the pressure head from the Pacific to the Indian Ocean was anomalously high at this time. Consistent with this result, Potemra et al. (1997) reported that in their numerical solution forced by actual winds the Indonesian Throughflow was about 5 Sv higher than the model's mean seasonal cycle from early to mid-1994 (Fig. 60).

### 10.3. *The 1997–98 anomaly*

The 1997/98 event was even stronger than the 1993/94 one with westward equatorial wind anomalies beginning in mid-1997, followed by eastern equatorial and boundary cooling from October to December, 1997. Webster et al. (1999) documented the development of anomalies of SST, equatorial winds, and SSH from T/P altimetry during the event. They found an important aspect of the oceanic response to be the development of a large SSH ridge south of the equator during the fall of 1997, which they attributed to anomalous Ekman convergence along the northern edge of the weakened trades. Fig. 71d–e shows the development and westward migration of this striking anomaly from October, 1997, to March, 1998 in the T/P sea-level anomalies. This Ekman convergence of 1997/98 was much more pronounced than during the corresponding phase of 1994 (Fig. 71a–c).

As for the 1993/94 event, models forced by actual winds of the 1997/98 period show large changes in equatorial currents, both leading up to the event in late 1996 and after it ended in late 1998 (J. Kindle, 1999, pers. comm.; Murtugudde et al., 2000). Murtugudde et al. (2000) discussed the oceanic thermodynamic processes associated with the 1997/98 anomaly, forcing their model with observed radiation and

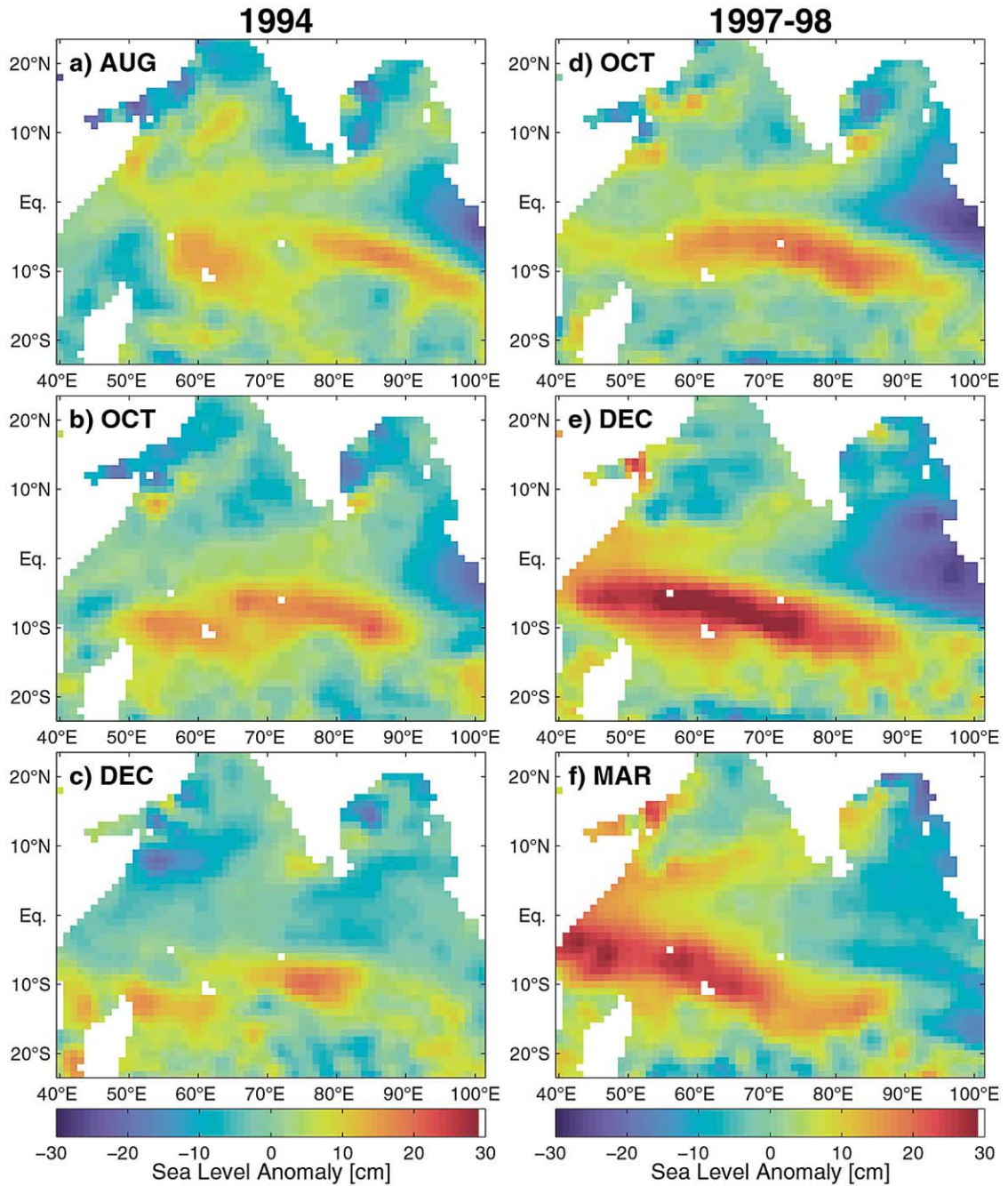


Fig. 71. Sealevel anomalies during the events of 1993/94 and 1997/98 from T/P altimetry for a) August 1994, b) October 1994, c) December 1994 and e) October 1997, December 1997, March 1998, showing low sealevel at the eastern equatorial end and the large zonal ridge due to Ekman convergence south of the equator. (Courtesy P. Brandt.)

cloudiness fields. They concluded that the anomalous cooling in the eastern Indian Ocean was driven both locally and remotely, by strengthened, upwelling-favorable winds off Sumatra and strengthened equatorial easterlies, respectively. The equatorial easterlies excited upwelling-favorable, equatorial Kelvin waves that reflected from the eastern boundary as a packet of coastal Kelvin and Rossby waves; these waves in turn raised the thermocline throughout the eastern, tropical ocean, thereby enhancing the local entrainment of cool subsurface water there. Conversely, the anomalous warming in the western ocean resulting from the propagation of downwelling-favorable Rossby waves into the western ocean, deepened the thermocline and hence reduced entrainment cooling. A prominent packet was centered at about 8°S, and generated both coastal and equatorial Kelvin waves upon reflection from the western boundary (Murtugudde, 1999; pers. comm.), consistent with the interpretation developed by Webster et al. (1999) and discussed below.

#### 10.4. *Sequential development of the equatorial mode*

All of the studies mentioned in Section 10.1 hypothesized that the equatorial or ‘dipole’ mode could be generated by internal ocean-atmosphere coupling within the Indian Ocean by some variation of the following scenario. Suppose cool SST anomalies appear in the eastern, tropical Indian Ocean, and that they initiate an eastward or northward shift of Indonesian convection. This shift weakens the Indian-Ocean Walker cell, allows organized convection to develop in the western ocean, establishes equatorial easterlies, and sets off the oceanic events discussed above. This sequence of events leads to intensified eastern cooling, and provides a positive-feedback loop similar to the one proposed by Bjerknes (1969) to explain El Niño.

A scenario of the coupled event in terms of internal ocean dynamics has been given by Webster et al. (1999) as follows (Fig. 72). Following the anomalous SST gradient along the equator of summer 1997, strong convection developed over East Africa in the fall of 1997 (Fig. 72b). This anomaly drove westward wind anomalies along the equator, and in conjunction with the weakening of the trades (Fig. 72b) a large Ekman-convergence anomaly developed south of the equator (Fig. 72c). Rossby waves were excited by this convergence and propagated westward. They deepened the thermocline at the western end, continued the warming in the interior ocean, thus sustaining the anomalous westward winds. This sequence of events, however, was not as clear for the 1993/94 event: Although anomalous Ekman convergence existed south of the equator from July to December, 1994, the arrival of a Rossby-wave signal at the western boundary was not at all obvious (Fig. 71a–c).

‘Dipole’ events end abruptly in the following spring, apparently overwhelmed by the strong monsoonal forcing during the summer. It is noteworthy that they do not reappear in the following year, possibly associated with the weakening of El Niño (at least for the 1993/4 and 1997/8 cases), which allows the Pacific convection regime to move back toward Indonesia (Fig. 72d). It may also be associated with the TBO (Yasunari, 1989; Meehl, 1997).

The debate is still continuing as to whether this Indian-Ocean mode is internally generated or externally forced. One has to note that both the events in the Indian Ocean coincided with Pacific El Niños; it is not clear whether the 1961 event, for which observations were much sparser, really was similar to these recent ones. On the other hand, the EOF analysis of Meyers (1996, see Section 7.3) yielded a different pattern of SST, thermocline depth and dynamic height in the eastern Indian Ocean for the 1994 anomaly (EOF2) than for ENSO related variability (EOF1) supports the recent coupled model study of Iizuka, Matsuura, and Yamagata (2000) that concluded that the mode is unique to the Indian Ocean.

#### 10.5. *A subtropical mode?*

A number of studies (e.g., Reason & Mulenga, 1999) have shown a significant correlation between SST anomalies in the southwestern subtropical South Indian Ocean and rainfall over southeastern Africa. Behera and Yamagata (2001) describe a subtropical dipole pattern that is phase-locked to the austral summer. It

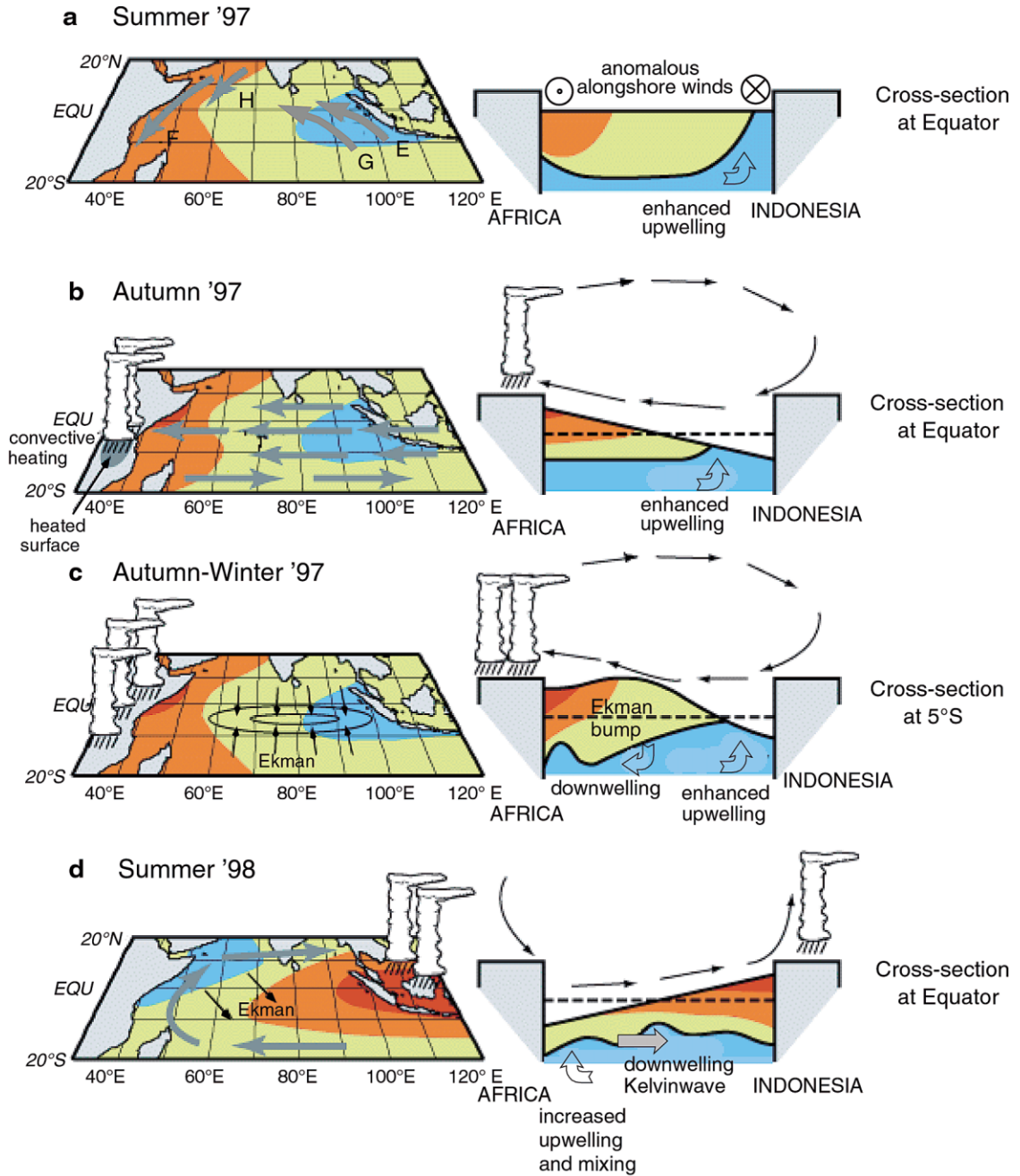


Fig. 72. The development of the Indian Ocean Mode according to Webster et al. (1999, their Fig. 4). See text for details.

usually develops in December/January, peaks in February, and dies down by May/June. This positive dipole phase is characterized by cold SSTs off Australia and warm SSTs southeast of Madagascar. Time series of the first EOF suggest that this mode may be independent of both ENSO and the equatorial mode discussed above. The authors also speculate that this subtropical anomaly might be related to the Antarctic Circumpolar Wave. However, more statistical evidence for the existence of this mode is needed, and from the perspective of this review, the ocean's role in its dynamics needs to be explored.

## 11. Summary and conclusions

In this review, we have summarized observations and model interpretations of the monsoon-related circulations in the Indian Ocean, and its adjacent regions such as the northern marginal seas, the Indonesian throughflow and the southern subtropical ocean. We have tried as much as possible to bring observational and modelling results together, since a close interaction of both approaches has been essential for the advances that have already been achieved. Indeed, although considerable progress has been made over the past decades, a number of challenging questions remain. We conclude our review with a summary of these outstanding issues, and comment on possible future developments. One of the major remaining problem areas concerns the mean thermohaline circulation. Since our focus has been on monsoon circulations, we have not discussed the thermohaline circulation in detail, and it is still addressed only in passing in this summary.

*Dynamics of Somali Current and Great Whirl:* The dynamics that determine the development of the circulation off northern Somalia in the late summer monsoon are still poorly understood. For example, the large differences between the development of the Great Whirl between 1995 and 1996; in 1996 the gyre was much more southerly and weaker, and this could not be reproduced in a model simulation driven by Arabian Sea winds. Also, why the two-gyre system collapses in some years, with the southern cold-water wedge propagating northward, has not been satisfactorily reproduced in model studies nor been substantiated in recent observational programs. The issues to be resolved are the respective importance of stochastic processes internal to the Great Whirl (e.g., Wirth et al., 2002) versus quasi-deterministic remote effects by Rossby waves generated either by the variability of the wind stress curl within the Arabian Sea or by waves travelling around Sri Lanka that then propagate across the Arabian Sea from the Indian coast (e.g., Brandt et al., 2002).

*Role of remote forcing effects in the Bay of Bengal and Arabian Sea:* So far, the interpretation of the seasonal cycle in the EICC and Bay of Bengal rests mostly on model results. These results indicate significant contributions to the EICC by two types of waves: non-equatorial low-latitude Rossby waves crossing the Bay of Bengal from the eastern boundary and coastal-trapped waves travelling around the perimeter of the Bay of Bengal. While we have good evidence for the role of the non-equatorial Rossby waves emanating from eastern coasts based on T/P altimetry (e.g., Basu et al., 2000; Brandt et al., 2002), coastally trapped waves have not yet been clearly observed. Indirectly, the mere existence of the LH proves that coastally trapped waves radiate around the southern tip of the subcontinent and up the west coast, since, as shown by MKM, Arabian Sea forcing cannot explain the LH at all. The T/P coverage at 10-day intervals may be inadequate to follow trapped waves around the Bay of Bengal, and so such analyses could be significantly improved if more sea-level data from Indian east-coast stations were to be made available.

*Equatorial undercurrents:* While earlier evidence suggested the seasonal occurrence of an eastward EUC from February to June, new observations and (re)analysis of model results show that a reoccurrence in August/September is also possible, for reasons yet unknown. It was shown that seasonal cycles of zonal equatorial wind stress differ between the climatologies used, so that model-to model differences of EUCs depend to some extent on the winds used. Furthermore, in the western basin *westward* flow at the EUC level during May to August is both observed and obtained in model simulations. The arrival of this EUC

signal at the western boundary has been associated with the disappearance of the spring Somali Undercurrent (Jensen, 1991). The interannual variability of zonal wind stress at the equator was found to be of the same magnitude as the seasonal cycle, and consequently models forced with interannually varying wind stress show large interannual differences at the EUC level. Overall, the seasonal currents at the EUC level and their anomalies have to be understood as a superposition of equatorial waves forced at various times and longitudes, rendering the interpretation of local time series difficult.

*Intraseasonal tropical variability:* Past modeling studies (Kindle & Thompson, 1989; Woodberry et al., 1989) obtained significant intraseasonal variability in the equatorial band at similar periods, about 26–28 days, as earlier observed (Luyten & Roemmich, 1982). In both, observations and models, these fluctuations could be interpreted as Yanai waves. Since the waves were obtained in these model simulations using monthly-mean wind forcing, their generation in the interior of the tropical Indian Ocean was explained by instability mechanisms of the zonal monsoon circulation. Several findings now suggest a reassessment of the intraseasonal equatorial variability. First, in some recent high-resolution model runs (e.g., the POCM model), the Yanai waves are not as prominent as in the above  $1\frac{1}{2}$ -layer model studies, indicative of model-to-model differences in instability mechanisms; and second, WOCE observations with moored stations along the equator at 80°E showed the potential importance of local intraseasonal wind forcing. In these observations, shorter period oscillations (at 14 rather than 27 days; Fig. 29) were found, and these were correlated with the local wind fluctuations which showed an energy peak at that period. Recent studies (Sengupta, Senan, & Goswami, 2001) using models forced by daily winds confirm that direct wind forcing of intraseasonal variability is indeed important in the tropical Indian Ocean. Therefore, more observational evidence on this type of variability is needed. An interesting question in that regard is whether these energetic oceanic fluctuations play an active role in the dynamics of monsoon breaks through feedbacks to the atmosphere.

*Depth of monsoonal response:* There are very few observations from the deep Indian Ocean long enough to evaluate the deep monsoon response, and they are primarily from the equatorial zone and from the northern Somali Current. We discussed the deep equatorial response in Section 3.3, distinguishing signals of larger vertical scale from the smaller scale ‘stacked jets’ (Ponte & Luyten, 1990); the former are generated at the surface by seasonal equatorial winds and then radiate into the deep ocean, whereas the latter appear to have longer periods or are quasi-stationary. In the northern Somali Basin, away from the boundary, the direct monsoon response of the Great Whirl was limited to depths shallower than 1500 m in the 1995–96 WOCE moored observations (Dengler et al., 2002). On the other hand, recent interpretations from two ship sections observed across the northern Somali Basin in 1995 (Beal et al., 2000b) suggested large-scale deep reversals (although they were not synchronous with the monsoon reversals). Evidence from moored observations in the northern Somali Basin, however, suggests that the deep variability is dominated by intraseasonal variability with about a 40-day period.

*Dynamics of Indonesian Throughflow:* Understanding the throughflow from the Pacific to the Indian Ocean through the Indonesian passages is still a major challenge for the observational community. Even after the end of WOCE, the mean transport is still not known from direct observations, and differs significantly among recent WOCE section evaluations (Section 9.1.1). Uncertainties also continue as to its seasonal cycle and interannual variability. While earlier work had hinted at a relation with the pressure head from the Pacific to the Indian Ocean, evaluations of model and altimetry results (e.g., Potemra et al., 1997) indicated several additional influential factors, thus preventing definition of a simple throughflow index based solely on sea level. Throughflow transports in the observations of Gordon and Susanto (1999) were higher for a La Niña period (1996/97) than for the El Niño period of 1997/98, but one has to note the presence of a large Indian Ocean event during the latter time period that may be unrelated to ENSO (Section 10).

*Seasonal variability of the Cross-equatorial Cell:* In Section 9.2, we discussed the likely mean pathways of the Cross-equatorial Cell, which involves subduction in the southern subtropical Indian Ocean, northward

flow in the EACC and Somali Current, upwelling off Somalia and Arabia, and near-surface southward Ekman flow in the ocean interior. There are a number of unresolved issues associated with this cell. First, we need to determine the seasonal variability of these pathways, which is large since there is no northern upwelling during winter and the interior Ekman transport is then directed northward. Second, what are the diapycnal transfers associated with this cell, and where do they take place? Third, where do interior southward cross-equatorial transports take place during the summer monsoon, which have to return about 20 Sv flowing northward with the Somali Current, and what mechanisms are involved? In this regard, how important are eastern-boundary currents? Fourth, the southward interior Ekman transport during summer is complicated at the equator by northward cross-equatorial winds forcing a shallow equatorial roll with northward flow in the upper 20 m and southward flow underneath (and the reverse situation being true for the winter monsoon). Are there diapycnal transfers involved in this mechanism? If the equatorial roll is confined within the surface-mixed layer, there are no diapycnal transfers and hence heat fluxes, but that is still to be determined. Finally, what are the heat transports associated with the seasonal and interannual variability of the cross equatorial cell?

*Climate modes:* Large interannual variability in the wind forcing, both equatorial and off-equatorial circulations, and water-mass structure have been observed in recent years. An important question concerning the interpretation of observed interannual variability is whether air-sea interaction in the Indian Ocean is a slave to ENSO or whether it has its own characteristics. Two events of particularly large variability have been observed recently, in 1993/94 and 1997/98, during which sea level and surface temperatures in the eastern tropical ocean were anomalously low, as is typical in the Atlantic and Pacific Oceans. While both recent strong events coincided with Pacific El Niños (albeit of different strengths) earlier examples were apparently not synchronous with El Niños (Saji et al., 1999; Murtugudde et al., 2000). It is also not clear whether this variability pattern really is a zonal equatorial dipole. In particular, the role of the ocean in these large anomalies needs further investigation regarding advective time scales that might serve as prediction indices. Coupled model studies are required to attain this objective.

*Improved forcing fields:* At several places in our review we have noted the critical need for accurate windstress and air-sea flux fields. These include: generation of equatorial jets and undercurrents (Section 2.2 and 3.1); investigation of local versus remote forcing effects in the Somali Current (Section 4.1), Bay of Bengal and Arabian Sea (Section 5); role of advection versus Ekman pumping and entrainment in the upper-layer heat budget (Section 4.4); role of intraseasonal local forcing versus internal instabilities and remote forcing (Sections 3.4 and 6.3); Indonesian throughflow variability (Section 7.3); and overturning circulation and heat transport (Section 9). Observational studies with moored flux buoys, similar to that of Weller et al. (1998) in the Arabian Sea, are needed in a number of key areas for better calibration and verification of operational products.

*Deep mean upwelling and physics of deep mixing:* One of the great remaining mysteries of oceanography is the conversion of cold deep waters into shallower warmer waters. Where and how do such conversions occur? For the Atlantic Ocean, one may argue that the North Atlantic Deep Water rises on its way to the Antarctic Circumpolar Current, and thus a substantial part of the conversion takes place along upward-slanting isopycnals without invoking any mysterious deep mixing mechanisms. For the Indian Ocean, however, this simple explanation cannot apply. A net deep inflow into the Indian Ocean is suggested by the results of the hydrographic transport analyses (Section 9.1), and by water-mass distributions that indicate deep northward inflow by boundary currents along Madagascar and the Ninety-East Ridge (e.g., Mantyla & Reid, 1995). Yet, while agreeing on a fairly large amount of near-bottom inflow, recent section and box inverse studies (Robbins & Toole, 1998; Ganachaud & Wunsch, 2000; Sloyan & Rintoul, 2001) yield rather conflicting results on the fate of the return flow and water-mass transformations involved. In any event, estimates of deep mixing (e.g., Dengler & Quadfasel, 2002) do not support the large amount of water-mass conversion inherent to all of these results.

These, and other challenges and open questions raised in preceding sections, call for a continued scientific

focus on the Indian Ocean. After the major observational effort of the WOCE period, a lull has occurred in observational activities. WOCE was a brief survey of all oceans during a particular time period. What is now needed is a sustained observational network of routine measurements, similar to the Tropical Atmosphere–Ocean (TAO) array of moored stations in the Pacific, that will capture the development of anomalies better. Equatorial observations should not only focus on the near-surface layers but also provide deep time series to make advances on the deep monsoonal response and resulting variability of zonal deep jets and cross-equatorial exchanges. In the southern hemisphere, a phenomenon of possible climatic relevance is the region of isopycnal doming at 5–15°S (Fig. 15), where SST has been shown to be significantly correlated with East African rainfall. This region has been proposed as one urgently needing sustained observations. In addition, longer-term observations on choke-point flows such as the Indonesian Throughflow and the Mozambique Channel are required. It is further hoped that, as part of the deployment of profiling floats within the context of the global Array of Real-time Geostrophic Oceanography (ARGO), enough resources will be made available to provide coverage of the larger-scale water mass and circulation anomalies of the Indian Ocean.

### Acknowledgements

We thank Arthur Mariano for providing ship-drift vector maps for the western Indian Ocean (Fig. 31), John Kindle for equatorial wind comparison time series (Fig. 3) and Peter Brandt for T/P altimetry plots (Figs. 19 and 71). Particular thanks go to Meike Hamann and Rena Schoenefeldt of IfM Kiel for their invaluable assistance in helping to put this complex paper together, and to Marcus Dengler for a critical reading and helpful comments. Cooperation on this paper began in October, 1999, while FS was a visitor at the International Pacific Research Center (IPRC) at the University of Hawaii. He also acknowledges support from the German CLIVAR program through Contract 03F0246A. Julian McCreary acknowledges support from the Frontier Research System for Global Change through its sponsorship of the IPRC. We thank Stuart Godfrey and another anonymous reviewer for constructive criticisms and suggestions that helped to improve the manuscript.

### Appendix A. List of acronyms

AAIW	Antarctic Intermediate Water
AAMW	Australian Mediterranean Water
ADCP	Acoustic Doppler Current Profiler
ARGO	Array for Real-Time Geostrophic Oceanography
ASW	Arabian Sea Water
BB	Bay of Bengal
CDW	Circumpolar Deep Water
COADS	Comprehensive Ocean Atmosphere Data Set
COLA	Coupled Ocean Land Atmosphere
EACC	East African Coast Current
ECHO	Coupled global Model of MPI
ECMWF	European Center for Medium-range Weather Forecast
EICC	East Indian Coastal Current
ENSO	El Nio Southern Oscillation
EUC	Equatorial Undercurrent

FGGE	First GARP Global Experiment
FNMOC	Fleet Numerical Meteorology and Oceanography Center
FSU	Florida State University
GARP	Global Atmosphere Research Program
GCM	General Circulation Model
GFDL	Geophysical Fluid Dynamics Laboratory
GW	Great Whirl
HR	Hellermann and Rosenstein
ICW	Indian Central Water
IDW	Indian Deep Water
IEW	Indian Equatorial Water
IIOE	International Indian Ocean Expedition
INDEX	Indian Ocean Experiment
IPRC	International Pacific Research Center
ITF	Indonesian Throughflow
JAMSTEC	Japan Marine Science and Technology Center
JC	South Java Current
JGOFS	Joint Global Ocean Flux Study
LADCP	ADCP lowered with CTD rosette
LC	Leeuwin Current
LH	Laccadive High
LL	Laccadive Low
MICOM	Miami Isopycnal Coordinate Ocean Model
MKM	McCreary, Kundu and Molinari
MOM	Modular Ocean Model
MPI	Max-Planck-Institut fuer Meteorologie, Hamburg
NCAR	National Center for Atmospheric Research (USA)
NCEP	US National Centers for Environmental Prediction
NECC	North Equatorial Counter Current
NEMC	Northeast Madagascar Current
NMC	Northeast Monsoon Current
NPIW	North Pacific Intermediate Water
OGCM	Ocean General Circulation Model
PGW	Persian Gulf Water
POCM	Parallel Ocean Climate Model
POP	Parallel Ocean Program
RSW	Red Sea Water
SC	Somali Current
SE	Socotra Eddy
SEC	South Equatorial Current
SECC	South Equatorial Counter Current
SEMC	Southeast Madagascar Current
SG	Southern Gyre
SMC	Southwest Monsoon Current
SOI	Southern Oscillation Index
SSH	Sea Surface Height
SST	Sea Surface Temperature
TAO	Tropical Atmosphere-Ocean

T/P	TOPEX/Poseidon
T/S	Temperature/Salinity
UKMO	UK Meteorological Office
WICC	West Indian Coastal Current
WJ	Wyrтки Jet
WOCE	World Ocean Circulation Experiment
XBT	Expendable Bathythermograph

## References

- Anderson, D. L. T., Carrington, D. J., Correy, R., & Gordon, C. (1991). Modeling the variability of the Somali Current. *Journal of Marine Research*, 49, 659–696.
- Anderson, D. L. T., & Carrington, D. J. (1993). Modeling interannual variability in the Indian Ocean using momentum fluxes from the operational weather analyses of the United Kingdom Meteorological Office and European Centre for Medium Range Weather Forecasts. *Journal of Geophysical Research*, 98, 12483–12499.
- Anderson, D. L. T., Carrington, D. J., Correy, R., & Gordon, C. (1993). The temporal evolution of equatorial currents in the Indian Ocean. Meteorological Office Climate Research Tech. Note 23, Bracknell, Berkshire, United Kingdom, 51 pp. [Available from U. K. Meteorological Office, Bracknell, Berkshire RG12 252, United Kingdom.]
- Anderson, D. L. T., & Moore, D. W. (1979). Cross-equatorial inertial jets with special relevance to very remote forcing of the Somali Current. *Deep-Sea Research*, 26, 1–22.
- Antony, M. K. (1990). Northward undercurrent along west coast of India during upwelling — Some inferences. *Indian Journal of Marine Science*, 19, 95–101.
- Barnett, T. P. (1983). Interaction of the monsoon and Pacific trade wind system at interannual time scales. Part I: The equatorial zone. *Monthly Weather Review*, 111, 756–773.
- Basu, S., Meyers, S. D., & O'Brien, J. J. (2000). Annual and interannual sea level variations in the Indian Ocean from TOPEX/Poseidon observations and ocean model simulations. *Journal of Geophysical Research*, 105, 975–994.
- Bauer, S., Hitchcock, G. L., & Olson, D. B. (1991). Influence of monsoonally-forced Ekman dynamics upon surface layer depth and plankton biomass distribution in the Arabian Sea. *Deep-Sea Research*, 38, 531–553.
- Beal, L. M., Field, A., & Gordon, A. L. (2000a). Spreading of Red Sea overflow waters in the Indian Ocean. *Journal of Geophysical Research*, 105, 8549–8564.
- Beal, L. M., Molinari, R. L., Robbins, P. E., & Chereskin, R. K. (2000b). Reversing bottom circulation in the Somali Basin. *Geophysical Research Letters*, 27, 2565–2568.
- Behara, S. K., & Yamagata, T. (2001). Subtropical SST dipole events in the southern Indian Ocean. *Geophysical Research Letters*, 28, 327–330.
- Bjerknes, J. (1969). Atmospheric teleconnections from the equatorial Pacific. *Monthly Weather Review*, 97, 163–172.
- Böhm, E., Morrison, J. M., Manghni, V., Kim, H.-S., & Flagg, C. N. (1999). The Ras al Hadd Jet: remotely sensed and acoustic Doppler current profiler observations in 1994–1995. *Deep-Sea Research II*, 46, 1531–1549.
- Böning, C. W., Doescher, R., & Isemer, H. J. (1991a). Monthly mean wind stress and Sverdrup transports in the North Atlantic: a comparison of the Hellerman-Rosenstein and Isemer-Hasse climatologies. *Journal of Physical Oceanography*, 21, 221–229.
- Böning, C. W., Doescher, R., & Budich, R. G. (1991b). Seasonal transport variation in the western subtropical North Atlantic: experiments with an eddy-resolving model. *Journal of Physical Oceanography*, 21, 1271–1289.
- Böning, C. W., & Herrmann, P. (1994). Annual cycle of poleward heat transport in the ocean: results from high resolution modeling of the North and Equatorial Atlantic. *Journal of Physical Oceanography*, 24, 91–107.
- Bower, A. S., Hunt, H. D., & Price, J. F. (2000). Character and dynamics of the Red Sea and Persian Gulf outflow. *Journal of Geophysical Research*, 105, 6387–6414.
- Brandt, P., Stramma, L., Schott, F., Fischer, J., Dengler, M., & Quadfasel, D. (2002). Annual Rossby waves in the Arabian Sea from TOPEX/POSEIDON altimeter and in-situ data. *Deep-Sea Research II*, (in press).
- Brink, K., Arnone, R., Coble, P., Flagg, C., Jones, B., Kindle, J., Lee, C., Phinney, D., Wood, M., Yentsch, C., & Young, D. (1998). Monsoons boost biological productivity in Arabian Sea. *EOS*, 27 (13), 168–169.
- Brock, J. C., McClain, C. R., Luther, M. E., & Hay, W. W. (1991). The phytoplankton bloom in the northwestern Arabian Sea during the southwest monsoon of 1979. *Journal of Geophysical Research*, 96, 733–750.
- Bruce, J. G., Fieux, M., & Gonella, J. (1981). A note on the continuance of the Somali eddy after the cessation of the Southwest monsoon. *Oceanologica Acta*, 4, 7–9.
- Bruce, J. G., Johnson, D. R., & Kindle, J. C. (1994). Evidence for eddy formation in the eastern Arabian Sea during the northeast monsoon. *Journal of Geophysical Research*, 99, 7651–7664.

- Cane, M. (1980). On the dynamics of equatorial currents, with application to the Indian Ocean. *Deep-Sea Research*, 27A, 525–544.
- Cane, M., & Gent, P. (1984). Reflections of low-frequency equatorial waves at arbitrary western boundaries. *Journal of Marine Research*, 42, 487–502.
- Cane, M. A., & Moore, D. W. (1981). A note on low-frequency equatorial basin modes. *Journal of Physical Oceanography*, 11, 1578–1584.
- Cane, M., & Sarachik, E. (1981). The response of a linear baroclinic ocean to periodic forcing. *Journal of Marine Research*, 39, 651–693.
- Cember, R. P. (1988). On the sources, formation, and circulation of Red Sea deep water. *Journal of Geophysical Research*, 93, 8175–8191.
- Chao, S.-Y., Kao, T. W., & Al-Hajri, K. R. (1992). A numerical investigation of circulation in the Arabian Gulf. *Journal of Geophysical Research*, 97, 11219–11236.
- Charney, J. (1955). The Gulf Stream as an inertial boundary layer. *Proceedings of the National Academy of Science, USA*, 41, 731–740.
- Chelton, D. B., & Schlax, M. G. (1996). Global observations of oceanic Rossby waves. *Science*, 272, 234–238.
- Chereskin, T. K., Wilson, W. D., Bryden, H. L., Ffield, A., & Morrison, J. (1997). Observations of the Ekman balance at 8°30'N in the Arabian Sea during the 1995 southwest monsoon. *Geophysical Research Letters*, 24, 2541–2544.
- Clarke, R. A., & Liu, X. (1993). Observations and dynamics of semiannual and annual sea levels near the eastern equatorial Indian Ocean boundary. *Journal of Physical Oceanography*, 23, 386–399.
- Clarke, A. J., & Liu, X. (1994). Interannual Sea Level in the Northern and Eastern Indian Ocean. *J. Phys. Oceanogr.*, 24, 1224–1235.
- Cox, M. D. (1979). A numerical study of Somali Current eddies. *Journal of Physical Oceanography*, 9, 311–326.
- Cox, M. D. (1981). A numerical study of surface cooling processes during summer in the Arabian Sea. In M. J. Lighthill, & R. P. Pearce (Eds.), *Monsoon dynamics*. Cambridge University Press.
- Cresswell, G. R., & Petersen, J. L. (1993). The Leeuwin Current south of western Australia. *Australian Journal of Marine Freshwater Research*, 44, 285–303.
- Cutler, A. N., & Swallow, J. C. (1984). Surface currents of the Indian Ocean. (To 25°S, 100°E). I. O. S. Technical Rept. 187.
- Dengler, M. A. S., & Quadfasel, D. R. (2002). Equatorial Deep Jets and abyssal mixing in the Indian Ocean. *Journal of Physical Oceanography*, (in press).
- Dengler, M., Quadfasel, D., Schott, F., & Fischer, J. (2002). Abyssal circulation in the Somali Basin. *Deep-sea Res. II*, (in press).
- Donguy, J. R., & Meyers, G. (1995). Observations of geostrophic transport variability in the western tropical Indian Ocean. *Deep-Sea Research*, 42, 1007–1028.
- Dueing, W., & Schott, F. (1978). Measurements in the source region of the Somali Current during the monsoon reversal. *Journal of Physical Oceanography*, 8, 278–289.
- Egbert, G. D., & Ray, R. D. (2000). Significant dissipation of tidal energy in the deep ocean inferred from satellite altimeter data. *Nature, London*, 405, 775–778.
- Eigenheer, A., & Quadfasel, D. (2000). Seasonal variability of the Bay of Bengal circulation inferred from TOPEX/POSEIDON altimetry. *Journal of Geophysical Research*, 105, 3243–3252.
- Elliot, A. J., & Savidge, G. (1990). Some features of the upwelling off Oman. *Journal of Marine Research*, 48, 319–333.
- Esenkov, O. E., & Olson, D. B. (2002). A numerical study of the Somali Coastal Undercurrent. *Deep-sea Res. II*, (in press).
- Eshel, G., Cane, M. A., & Blumenthal, M. B. (1994). Modes of subsurface, intermediate, and deep water renewal in the Red Sea. *Journal of Geophysical Research*, 99, 15941–15952.
- Eshel, G., & Naik, N. H. (1997). Climatological coastal jet collision, intermediate water formation, and the general circulation of the Red Sea. *Journal of Physical Oceanography*, 27, 1233–1257.
- Evans, R. H., & Brown, O. B. (1981). Propagation of thermal fronts in the Somali Current system. *Deep-Sea Research*, 28A, 521–527.
- Ffield, A., & Gordon, A. L. (1992). Vertical mixing in the Indonesian thermocline. *Journal of Physical Oceanography*, 22, 184–195.
- Fieux, M., & Stommel, H. (1977). Onset of the Southwest Monsoon over the Arabian Sea from marine reports of surface winds: structure and variability. *Monthly Weather Review*, 105, 231–236.
- Fieux, M., Andrié, C., Delecluse, P., Ilahude, A. G., Kartavtseff, A., Mantsi, F., Molcard, R., & Swallow, J. C. (1994). Measurements within the Pacific-Indian Oceans Throughflow region. *Deep-sea Research I*, 41, 1091–1130.
- Fieux, M., Molcard, R., & Ilahude, A. G. (1996). Geostrophic transport of the Pacific-Indian Oceans Throughflow. *Journal of Geophysical Research*, 101, 12421–12432.
- Findlater, J. (1971). Mean monthly airflow at low levels over the western Indian Ocean. *Geophysical Memoirs*, 115, 55.
- Fine, R. A. (1993). Circulation of Antarctic Intermediate Water in the South Indian Ocean. *Deep-Sea Research I*, 40, 2021–2042.
- Fischer, J., Schott, F., & Stramma, L. (1996). Currents and Transports of the Great Whirl-Socotra Gyre System during the Summer Monsoon August 1993. *Journal of Geophysical Research*, 101, 3573–3587.
- Flagg, C. A., & Kim, H.-S. (1998). Upper ocean currents in the northern Arabian Sea from shipboard ADCP measurements collected during the 1994–1996 U.S. JGOFS and ONR Programs. *Deep-Sea Research II*, 45, 1917–1959.
- Fu, L. (1986). Mass, heat and freshwater fluxes in the South Indian Ocean. *Journal of Physical Oceanography*, 16, 1683–1693.

- Ganachaud, A., & Wunsch, C. (2000). Improved estimates of global ocean circulation, heat transport and mixing from hydrographic data. *Nature, London*, 408, 453–457.
- Ganachaud, A., Wunsch, C., Marotzke, J., & Toole, J. (2000). Meridional overturning and large-scale circulation of the Indian Ocean. *Journal of Geophysical Research*, 105, 26117–26134.
- Garternicht, U., & Schott, F. (1997). Heat fluxes of the Indian Ocean from a global eddy-resolving model. *Journal of Geophysical Research*, 102, 21147–21159.
- Godfrey, J. S. (1996). The effect of the Indonesian Throughflow on ocean circulation and heat exchange with the atmosphere: a review. *Journal of Geophysical Research*, 101, 12217–12237.
- Godfrey, J. S., Johnson, G. C., McPhaden, M. J., Reverdin, G., & Wijffels, S. (2001). The tropical ocean circulation. In J. Church, J. Gould, & G. Siedler (Eds.), *Ocean circulation and climate*, 77 (pp. 215–246). Academic Press.
- Godfrey, J. S., & Mansbridge, J. V. (2000). Ekman transports, tidal mixing, and the control of temperature structure in Australia's northwest waters. *Journal of Geophysical Research*, 105, 24021–24044.
- Godfrey, J. S., & Ridgeway, K. R. (1985). The large scale environment of the poleward flowing Leeuwin Current, western Australia: longshore steric height gradients, wind stresses and geostrophic flow. *Journal of Physical Oceanography*, 15, 481–495.
- Godfrey, J. S., & Weaver, A. J. (1991). Is the Leeuwin Current driven by Pacific heating and winds? *Progress in Oceanography*, 27, 225–272.
- Gordon, A. (1986). Interocean exchange of thermocline water. *Journal of Geophysical Research*, 91, 5037–5046.
- Gordon, A. L., & Fine, R. A. (1996). Pathways of water between the Pacific and Indian oceans in the Indonesian seas. *Nature, London*, 379, 146–149.
- Gordon, G. L., & McClean, J. L. (1999). Thermohaline stratification of the Indonesian Seas: model and observations. *Journal of Physical Oceanography*, 29, 198–216.
- Gordon, A. L., & Susanto, R. D. (1999). Makassar Strait transport: initial estimate based on Arlindo results. *MTS Journal*, 32, 34–45.
- Hacker, P., Firing, E., Hummon, J., Gordon, A., & Kindl, J. C. (1998). Bay of Bengal currents along the northeast monsoon. *Geophysical Research Letters*, 25, 2769–2772.
- Haines, M. A., Fine, R. A., Luther, M. E., & Ji, Z. (1999). Particle trajectories in an Indian Ocean model and sensitivity to seasonal forcing. *Journal of Physical Oceanography*, 29, 584–598.
- Halpern, D., Freilich, M. H., & Weller, R. A. (1998). Arabian sea surface winds and ocean transports determined from ERS-1 scatterometer. *J. Geophys. Res.*, 103 (C4), 7799–7805.
- Han, W., McCreary, J. P. Jr., Anderson, D. L. T., & Mariano, A. J. (1999). On the dynamics of the eastward surface jets in the equatorial Indian Ocean. *Journal of Physical Oceanography*, 29, 2191–2209.
- Hastenrath, S., & Greischar, L. (1991). The monsoonal current regimes of the tropical Indian Ocean: observed surface flow fields and their geostrophic and wind-driven components. *Journal of Geophysical Research*, 96, 12619–12633.
- Hastenrath, S., & Greischar, L. (1993). The monsoonal heat budget of the hydrosphere-atmosphere system in the Indian Ocean sector. *Journal of Geophysical Research*, 98, 6869–6881.
- Hastenrath, S., Nicklis, A., & Greischar, L. (1993). Atmospheric-hydrospheric mechanisms of climate anomalies in the western equatorial Indian Ocean. *Journal of Geophysical Research*, 98, 20219–20235.
- Hautala, S. L., Reid, J. L., & Bray, N. (1996). The distribution and mixing of Pacific water masses in the Indonesian Seas. *Journal of Geophysical Research*, 101, 12375–12389.
- Hellerman, S., & Rosenstein, M. (1983). Normal monthly wind stress over the world ocean with error estimates. *Journal of Physical Oceanography*, 13, 1093–1105.
- Hirst, A. C., & Godfrey, J. S. (1993). The role of Indonesian Throughflow in a global ocean GCM. *Journal of Physical Oceanography*, 23, 1057–1086.
- Holloway, P. E. (1995). Leeuwin Current observations on the Australian North West Shelf, May–June 1993. *Deep-Sea Research I*, 42, 285–305.
- Hsiung, J. (1985). Estimates of global oceanic meridional heat transport. *Journal of Physical Oceanography*, 15, 1405–1413.
- Hsiung, J., Newell, R. E., & Houghtby, T. (1989). The annual cycle of oceanic heat storage and oceanic meridional heat transport. *Quarterly Journal of the Royal Meteorological Society*, 115, 1–28.
- Hua, B. L., Moore, D. W., & Le Gentil, S. (1997). Inertial nonlinear equilibration of equatorial flows. *Journal of Fluid Mechanics*, 331, 345–371.
- Hurlburt, H. E., & Thompson, J. D. (1976). A numerical model of the Somali Current. *Journal of Physical Oceanography*, 6, 646–664.
- Iizuka, S., Matsuura, T., & Yamagata, T. (2000). The Indian Ocean SST dipole simulated in a coupled general circulation model. *Geophysical Research Letters*, 27, 3369–3372.
- Jensen, T. G. (1991). Modeling the seasonal undercurrents in the Somali Current system. *Journal of Geophysical Research*, 96, 22151–22167.
- Jensen, T. G. (1993). Equatorial variability and resonance in a wind-driven Indian Ocean Model. *Journal of Geophysical Research*, 98, 22533–22552.
- Johns, W. E., & Olson, D. B. (1999). Observations of seasonal exchange through the Strait of Hormuz. *Oceanography*, 11, 58.

- Josey, S. A., Kent, E. C., & Taylor, P. K. (1999). New insights into the ocean heat budget closure problem from analysis of the SOC air-sea flux climatology. *Journal of Climate*, *12*, 2856–2880.
- Kapala, A., Born, K., & Flohn, H. (1994). Monsoon anomaly or an El Niño event at the equatorial Indian Ocean? Catastrophic rains 1961/62 in East Africa and their teleconnections. In *Proceedings of the International Conference on monsoon variability and prediction* (pp. 119–126). Trieste, Italy: WMO.
- Karstensen, J., & Quadfasel, D. (2002). Water subducted into the Indian Ocean subtropical gyre. *Deep-sea Res. II*, (in press).
- Kessler, W. S., & McCreary, J. P. (1993). The annual wind-driven Rossby wave in the subthermocline equatorial Pacific. *Journal of Physical Oceanography*, *23*, 1192–1207.
- Killworth, P. D., Chelton, D. B., & De Soeke, R. A. (1997). The speed of observed and theoretical long extratropical planetary waves. *Journal of Physical Oceanography*, *27*, 1946–1966.
- Kim, H.-S., Flagg, N., & Howden, S. D. (2001). Northern Arabian Sea variability from TOPEX/Poseidon altimetry data: an extension of the US JGOFS/ONR shipboard ADCP study. *Deep-Sea Research II*, *48*, 1069–1096.
- Kindle, J. C., & Thompson, J. D. (1989). The 26- and 50-day oscillations in the western Indian Ocean: model results. *Journal of Geophysical Research*, *94*, 4721–4736.
- Knox, R. (1976). On a long series of measurements of Indian Ocean equatorial currents near Addu Atoll. *Deep-Sea Research*, *23*, 211–221.
- Knox, R. A., & Anderson, D. L. T. (1985). Recent advances in the study of the low-latitude ocean circulation. *Progress in Oceanography*, *14*, 259–317.
- Koske, P. (1972). Hydrographische Verhältnisse im Persischen Golf aufgrund von Beobachtungen von FS Meteor im Frühjahr 1965. *Meteor Forschungsergebnisse*, *A11*, 58–73.
- Kundu, P. K., & McCreary, J. P. (1986). On the dynamics of the throughflow from the Pacific to the Indian Ocean. *Journal of Physical Oceanography*, *16*, 2191–2198.
- Lebedev, K., & Yaremchuk, M. (2000). A diagnostic study of the Indonesian Throughflow. *Journal of Geophysical Research*, *105*, 11243–11258.
- Lee, C. M., Jones, B. H., Brink, K. H., & Fischer, A. S. (2000). The upper ocean response to monsoonal forcing in the Arabian Sea: seasonal and spatial variability. *Deep-Sea Research II*, *47*, 1177–1226.
- Lee, T. N., Johns, W. E., Zantopp, R. J., & Fillenbaum, E. R. (1996). Moored observations of western boundary current variability and thermohaline circulation at 26.5°N in the subtropical North Atlantic. *Journal of Physical Oceanography*, *26*, 962–983.
- Lee, T., & Marotzke, J. (1998). Seasonal cycles of meridional overturning and heat transport of the Indian Ocean. *Journal of Physical Oceanography*, *28*, 923–943.
- Leetmaa, A. (1972). The response of the Somali Current to the southwest monsoon of 1970. *Deep-Sea Research*, *19*, 397–400.
- Leetmaa, A. (1973). The response of the Somali Current at 2°S to the southwest monsoon of 1971. *Deep-Sea Research*, *20*, 319–325.
- Leetmaa, A., Quadfasel, D. R., & Wilson, D. (1982). Development of the flow field during the onset of the Somali current, 1979. *Journal of Physical Oceanography*, *12*, 1325–1342.
- Leetmaa, A., & Stommel, H. (1980). Equatorial current observations in the western Indian Ocean during 1975 and 1976. *Journal of Physical Oceanography*, *10*, 258–269.
- Legler, D. M., Navon, I. M., & O'Brien, J. J. (1989). Objective analysis of pseudostress over the Indian Ocean using a direct minimization approach. *Monthly Weather Review*, *117*, 709–720.
- Levitus, S. (1982). Climatological atlas of the world ocean. NOAA Profess. Paper No 13, US. Dept. of Commerce, Rockville, MD, 173 pp.
- Levitus, S. (1988). Ekman volume fluxes for the world ocean and individual ocean basins. *Journal of Physical Oceanography*, *18*, 271–279.
- Levitus, S., & Boyer, T. (1994a). World Ocean Atlas 1994, Vol 3: Salinity. NOAA Atlas NESDIS 3, U. S. Government Printing Office, Washington D.C., 93 pp.
- Levitus, S., & Boyer, T. (1994b). World Ocean Atlas 1994, Vol 4: Temperature. NOAA Atlas NESDIS 4, U. S. Government Printing Office, Wash., D.C., 117 pp.
- Lighthill, M. J. (1969). Dynamic response of the Indian Ocean to the onset of the southwest monsoon. *Philosophical Transactions of the Royal Meteorological Society, A*, *A265*, 45–92.
- Lin, L. B., & Hurlburt, H. E. (1981). Maximum simplification of nonlinear Somali Current dynamics. In M. J. Lighthill, & R. P. Pearce (Eds.), *Monsoon dynamics*. Cambridge: Cambridge University Press.
- Lu, P., McCreary, J. P. Jr., & Klingler, B. R. (1998). Meridional circulation cells and the source waters of the Pacific equatorial undercurrent. *Journal of Physical Oceanography*, *28*, 62–84.
- Lukas, R., & Firing, E. (1985). The annual Rossby Wave in the central equatorial Pacific Ocean. *Journal of Physical Oceanography*, *15*, 55–67.
- Luther, M. E. (1999). Interannual variability in the Somali Current 1954–1976. *Nonlinear Analysis. Theory, Methods and Applications. An International Multidisciplinary Journal*, *35*, 59–83.

- Luther, M. E., & O'Brien, J. J. (1985). A model of the seasonal circulation in the Arabian Sea forced by observed winds. *Progress in Oceanography*, *14*, 353–385.
- Luther, M. E., & O'Brien, J. J. (1989). Modelling the variability of the Somali Current. In J. C. J. Nihoul, & B. M. Jamart (Eds.), *Mesoscale/synoptic coherent structures in geophysical turbulence* (pp. 373–386). Amsterdam, Netherlands: Elsevier.
- Luther, M. E., O'Brien, J. J., & Meng, A. H. (1985). Morphology of the Somali Current system during the Southwest Monsoon. In J. C. J. Nihoul (Ed.), *Coupled ocean-atmosphere models* (pp. 405–437). Amsterdam: Elsevier.
- Luyten, J. R., & Roemmich, D. H. (1982). Equatorial currents at semiannual period in the Indian Ocean. *Journal of Physical Oceanography*, *12*, 406–413.
- Luyten, J. R., & Swallow, J. C. (1976). Equatorial undercurrents. *Deep-Sea Research*, *23*, 999–1001.
- Madden, R. A., & Julian, P. R. (1972). Description of global-scale circulation cells in the tropics with a 40–50 day period. *Journal of Atmospheric Science*, *29*, 1109–1123.
- Macdonald, A. M. (1993). Property fluxes at 30°S and their implications for the Pacific–Indian Throughflow and the global heat budget. *Journal of Geophysical Research*, *98*, 6851–6868.
- Macdonald, A. M. (1998). The global ocean circulation: a hydrographic estimate and regional analysis. *Progress in Ocean*, *41*, 281–382.
- Maillard, C., & Soliman, G. (1986). Hydrography of the Red Sea and exchanges with the Indian Ocean in summer. *Oceanologica Acta*, *9*, 249–269.
- Maltrud, M. E., Semtner, A. J., & Malone, R. C. (1998). Global eddy-resolving ocean simulation driven by 1985–1995 atmospheric winds. *Journal of Geophysical Research*, *103*, 30825–30853.
- Mantyla, A. W., & Reid, J. L. (1995). On the origins of deep and bottom waters of the Indian Ocean. *Journal of Geophysical Research*, *100*, 2417–2439.
- Masumoto, Y., & Meyers, G. (1998). Forced Rossby waves in the southern tropical Indian Ocean. *Journal of Geophysical Research*, *103*, 27589–27602.
- Masumoto, Y., & Yamagata, T. (1996). Seasonal variations of the Indonesian Throughflow in a general ocean circulation model. *Journal of Geophysical Research*, *101*, 12287–12294.
- McCreary, J. P. (1981). A linear stratified ocean model of the coastal undercurrent. *Philosophical Transactions of the Royal Society of London*, *298*, 603–635.
- McCreary, J. P. Jr. (1985). Modeling equatorial ocean circulation. *Annual Review of Fluid Mechanics*, *17*, 359–409.
- McCreary, J. P., & Kundu, P. K. (1985). Western boundary circulation driven by an alongshore wind: with application to the Somali Current system. *Journal of Marine Research*, *43*, 493–516.
- McCreary, J. P., & Kundu, P. K. (1988). A numerical investigation of the Somali Current during the Southwest Monsoon. *Journal of Marine Research*, *46*, 25–58.
- McCreary, J. P., & Kundu, P. K. (1989). A numerical investigation of sea surface temperature variability in the Arabian Sea. *Journal of Geophysical Research*, *94*, 16097–16114.
- McCreary, J. P. Jr., & Lu, P. (2001). Influence of the Indonesian Throughflow on the circulation of intermediate water in the Pacific Ocean. *Journal of Physical Oceanography*, *31*, 932–942.
- McCreary, J. P. Jr., & Lukas, R. (1986). The response of the equatorial ocean to a moving wind field. *Journal of Geophysical Research*, *91*, 11691–11705.
- McCreary, J. P., Shetye, S. R., & Kundu, P. K. (1986). Thermohaline forcing of eastern boundary currents: with application to the circulation off the west coast of Australia. *Journal of Marine Research*, *44*, 71–92.
- McCreary, J. P. Jr., Kundu, P. K., & Molinari, R. L. (1993). A numerical investigation of dynamics, thermodynamics and mixed-layer processes in the Indian Ocean. *Progress in Oceanography*, *31*, 181–244.
- McCreary, J. P., Kohler, K. E., Hood, R. R., & Olson, D. (1996a). A four-component model of biological activity in the Arabian Sea. *Progress in Oceanography*, *37*, 193–240.
- McCreary, J. P., Han, W., Shankar, D., & Shetye, S. R. (1996b). Dynamics of the East India Coastal Current. 2. Numerical solutions. *Journal of Geophysical Research*, *101*, 13993–14010.
- McCreary, J. P., Kohler, K. E., Hood, R. R., Smith, S., Kindle, J., Fischer, A. S., & Weller, R. A. (2001). Influences of diurnal and intraseasonal forcing on mixed-layer and biological variability in the central Arabian Sea. *Journal of Geophysical Research*, *106*, 7139–7155.
- McPhaden, M. (1982). Variability in the central Indian Ocean. Part I: Ocean dynamics. *Journal of Marine Research*, *40*, 157–176.
- Meehl, G. A. (1997). The South Asian monsoon and the tropospheric biennial oscillation. *Journal of Climate*, *10*, 1921–1943.
- Metzger, E. J., & Hurlburt, H. E. (1996). Coupled dynamics of the South China Sea, the Sulu Sea, and the Pacific Ocean. *Journal of Geophysical Research*, *101*, 12331–12352.
- Meyers, G. (1996). Variation of Indonesian Throughflow and El Niño–Southern Oscillation. *Journal of Geophysical Research*, *101*, 12255–12263.
- Meyers, G., Bailey, R. J., & Worby, A. P. (1995). Geostrophic transport of Indonesian Throughflow. *Deep-Sea Research*, *42*, 1163–1174.

- Miyama, T., Awaji, T., Akimoto, K., & Imasato, N. (1995). Study of seasonal transport variations in Indonesian seas. *Journal of Geophysical Research*, *100*, 20517–20541.
- Molcard, R., Fieux, M., & Ilahude, A. G. (1996). The Indo-Pacific Throughflow in the Timor Passage. *Journal of Geophysical Research*, *101*, 12411–12420.
- Molinari, R. L., Olson, D., & Reverdin, G. (1990). Surface current distributions in the tropical Indian Ocean derived from compilations of surface buoy trajectories. *Journal of Geophysical Research*, *95*, 7217–7238.
- Moore, D. W., & McCreary, J. (1990). Excitation of intermediate-frequency equatorial waves at a western ocean boundary: with application to observation from the Indian Ocean. *Journal of Geophysical Research*, *95*, 5219–5231.
- Morcous, S. A. (1970). Physical and chemical oceanography of the Red Sea. *Oceanography and Marine Biology*, *8*, 73–202.
- Morrison, J. M. (1997). Intermonsoonal changes in the T-S properties of the near-surface waters of the northern Arabian Sea. *Journal of Geophysical Research Letters*, *24*, 2553–2556.
- Morrow, R., & Birol, F. (1998). Variability in the southeast Indian Ocean from altimetry: Forcing mechanism for the Leeuwin Current. *Journal of Geophysical Research*, *103*, 18529–18544.
- Muench, J. E., Kunze, E., & Firing, E. (1994). The potential vorticity structure of equatorial deep jets. *Journal of Physical Oceanography*, *24*, 418–428.
- Muench, J. E., & Kunze, E. (2000). Internal wave interactions with equatorial deep jets. Part II: Acceleration of the jets. *Journal of Physical Oceanography*, *30*, 2099–2110.
- Munk, W., & Wunsch, C. (1998). Abyssal recipes II: energetics of tidal and wind mixing. *Deep-Sea Research I*, *45*, 1977–2010.
- Murray, S. P., & Arief, D. (1988). Throughflow into the Indian Ocean through the Lombok Strait, January 1985–January 1986. *Nature, London*, *333*, 444–447.
- Murray, S. P., & Johns, W. (1997). Direct observations of seasonal exchange through the Bab el Mandab Strait. *Geophysical Research Letters*, *24*, 2557–2560.
- Murtugudde, R., & Busalacchi, A. J. (1999). Interannual variability of the dynamics and thermodynamics of the Indian Ocean. *Journal of Climate*, *12*, 2300–2326.
- Murtugudde, R., McCreary, J. P., & Busalacchi, A. J. (2000). Oceanic processes associated with anomalous events in the Indian Ocean with relevance to 1997–1998. *Journal of Geophysical Research*, *105*, 3295–3306.
- Murtugudde, R., Signorini, S., Christian, J., Busalacchi, A., McClain, C., & Picaut, J. (1999). Ocean color variability of the tropical Indo-Pacific basin observed by SeaWiFS during 1997–98. *Journal of Geophysical Research*, *104*, 18351–18366.
- Nicholls, N. (1989). Sea surface temperature and Australian winter rainfall. *Journal of Climate*, *2*, 965–973.
- Nicholls, N. (1995). All-India summer Monsoon rainfall and sea surface temperature around northern Australia and Indonesia. *Journal of Climate*, *8*, 1463–1467.
- O'Brien, J. J., & Hurlburt, H. E. (1974). An equatorial jet in the Indian Ocean theory. *Science*, *184*, 1075–1077.
- Patzert, M. C. (1974). Wind-induced reversal in Red Sea circulation. *Deep-Sea Research*, *21*, 109–122.
- Pearce, A. F. (1991). Eastern boundary currents of the southern hemisphere. *Journal of the Royal Society of Western Australia*, *74*, 35–45.
- Perigaud, C., & Delecluse, P. (1992). Annual sea level variations in the southern tropical Indian Ocean from geosat and shallow-water simulations. *Journal of Geophysical Research*, *97*, 20169–20178.
- Peter, B. N., & Mizuno, K. (2000). Annual cycle of steric height in the Indian Ocean estimated from the thermal field. *Deep-Sea Research I*, *47*, 1351–1368.
- Philander, S. G. H., & Pacanowski, R. C. (1980). The generation of equatorial currents. *Journal of Geophysical Research*, *85*, 1123–1136.
- Philander, G., & Pacanowski, R. C. (1981). The oceanic response to cross-equatorial winds (with application to coastal upwelling in low latitudes). *Tellus*, *33*, 201–210.
- Philander, G., & Delecluse, P. (1983). Coastal currents in low latitudes (with application to the Somali and El Niño Currents). *Deep-Sea Research*, *30*, 887–902.
- Phillips, O. M. (1966). On turbulent convection currents and the circulation of the Red Sea. *Deep-Sea Research*, *13*, 1149–1160.
- Ponte, R. M., & Luyten, J. (1990). Deep velocity measurements in the western equatorial Indian Ocean. *Journal of Physical Oceanography*, *20*, 44–52.
- Potemra, J. T., Luther, M. E., & O'Brien, J. J. (1991). The seasonal circulation of the upper ocean in the Bay of Bengal. *Journal of Geophysical Research*, *96*, 12667–12683.
- Potemra, J. T., Lukas, R., & Mitchum, G. T. (1997). Large-scale estimation of transport from the Pacific to the Indian Ocean. *Journal of Geophysical Research*, *102*, 27795–27812.
- Pratt, L. J., Johns, W., Murray, S. P., & Katsumata, K. (1999). Hydraulic interpretation of direct velocity measurements in the Bab al Mandab. *Journal of Physical Oceanography*, *29*, 2769–2784.
- Price, J. F., & Neil Barhinger, M. O. (1994). Outflows and Deep Water production by marginal seas. *Progress in Oceanography*, *33*, 161–200.

- Quadfasel, D., & Cresswell, G. R. (1992). A note on the seasonal variability of the south Java Current. *Journal of Geophysical Research*, *97*, 3685–3688.
- Quadfasel, D., & Schott, F. (1982). Water mass distribution at intermediate layers off the Somali coast during the onset of the southwest monsoon, 1979. *Journal of Physical Oceanography*, *12*, 1358–1372.
- Quadfasel, D., & Schott, F. (1983). Southward subsurface flow below the Somali Current. *Journal of Geophysical Research*, *88*, 5973–5979.
- Quadfasel, D. R., & Swallow, J. C. (1986). Evidence for 50-day period planetary waves in the South Equatorial Current of the Indian Ocean. *Deep-Sea Research*, *33*, 1307–1312.
- Rao, R. R., Molinari, R. L., & Festa, J. F. (1989). Evolution of the climatological near-surface thermal structure of the tropical Indian Ocean: 1. Description of mean monthly mixed layer depth, and sea surface temperature, surface current, and surface meteorological fields. *Journal of Geophysical Research*, *94*, 10801–10815.
- Rao, R. R., & Sivakumar, R. (2000). Seasonal variability of near-surface thermal structure and heat budget of the mixed layer of the tropical Indian Ocean from a new global ocean temperature climatology. *Journal of Geophysical Research*, *105*, 985–1015.
- Reason, C. J. C., & Mulenga, H. M. (1999). Relationships between South African rainfall and SST anomalies in the SW Indian Ocean. *International Journal of Climatology*, *19*, 1651–1673.
- Reppin, J., Schott, F. A., Fischer, J., & Quadfasel, D. (1999). Equatorial currents and transports in the upper central Indian Ocean: annual cycle and interannual variability. *Journal of Geophysical Research*, *104*, 15495–15514.
- Reverdin, G. (1987). The upper equatorial Indian Ocean: the climatological seasonal cycle. *Journal of Physical Oceanography*, *17*, 903–927.
- Reverdin, G., & Luyten, J. (1986). Near-surface meanders in the equatorial Indian Ocean. *Journal of Physical Oceanography*, *16*, 1088–1100.
- Reverdin, G., Cadet, D., & Gutzler, D. (1986). Interannual displacements of convection and surface circulation over the equatorial Indian Ocean. *Quarterly Journal of the Royal Meteorological Society*, *112*, 43–67.
- Robbins, P. E., & Toole, J. M. (1998). The dissolved silica budget as a constraint on the meridional overturning circulation of the Indian Ocean. *Deep-Sea Research*, *44*, 879–906.
- Rochford, P. A., Kindle, J. C., Gallacher, P. C., & Weller, R. A. (2000). Sensitivity of the Arabian Sea mixed layer to 1994–1995 operational wind products. *Journal of Geophysical Research*, *105*, 14141–14162.
- Saji, N. H., Goswami, B. N., Vinayachandran, P. N., & Yamagata, T. (1999). A dipole in the tropical Indian Ocean. *Nature, London*, *401*, 360–363.
- Schiller, A., Godfrey, J. S., McIntosh, P. C., Meyers, G., & Wijffels, S. E. (1998). Seasonal near-surface dynamics and thermodynamics of the Indian Ocean and Indonesian Throughflow in a global ocean general circulation model. *Journal of Physical Oceanography*, *28*, 2288–2312.
- Schmitz, W. J. (1996). On the World Ocean Circulation: Volume I. Technical Report, WHOI-96-03. 140 pp.
- Schneider, N. (1998). The Indonesian Throughflow and the global climate system. *Journal of Climate*, *11*, 676–689.
- Schott, F. (1983). Monsoon response of the Somali Current and associated upwelling. *Progress in Oceanography*, *12*, 357–381.
- Schott, F. (1986). Seasonal variation of cross-equatorial flow in the Somali Current. *Journal of Geophysical Research*, *91*, 10581–10584.
- Schott, F., Fieux, M., Kindle, J., Swallow, J., & Zantopp, R. (1988). The boundary currents east and north of Madagascar. Part II: Direct measurements and model comparisons. *Journal of Geophysical Research*, *93*, 4963–4974.
- Schott, F., & Fischer, J. (2000). Winter monsoon circulation of the northern Arabian Sea and Somali Current. *Journal of Geophysical Research*, *105*, 6359–6376.
- Schott, F., Fischer, J., Garternicht, U., & Quadfasel, D. (1997). Summer monsoon response of the Northern Somali Current, 1995. *Geophysical Research Letters*, *24*, 2565–2568.
- Schott, F., & Quadfasel, D. (1982). Variability of the Somali Current and associated upwelling. *Progress in Oceanography*, *12*, 357–381.
- Schott, F., Reppin, J., Fischer, J., & Quadfasel, D. (1994). Currents and transports of the Monsoon Current south of Sri Lanka. *Journal of Geophysical Research*, *99*, 25127–25141.
- Schott, F., Swallow, J. C., & Fieux, M. (1990). The Somali Current at the equator: annual cycle of currents and transports in the upper 1000 m and connection to neighboring latitudes. *Deep-Sea Research*, *37*, 1825–1848.
- Semner, A., & Chervin, R. M. (1992). Ocean general circulation from a global eddy-resolving model. *Journal of Geophysical Research*, *97*, 5493–5550.
- Sengupta, D., Senan, R., & Goswami, B. N. (2001). Origin of intraseasonal variability of circulation in the tropical central Indian Ocean. *Geophysical Research Letters*, *28*, 1267–1270.
- Shankar, D., McCreary, J. P., Han, W., & Shetye, S. R. (1996). Dynamics of the East India Coastal Current. 1. Analytic solutions forced by interior Ekman pumping and local alongshore winds. *Journal of Geophysical Research*, *101*, 13975–13991.
- Shankar, D., & Shetye, S. R. (1997). On the dynamics of the Lakshadweep high and low in the southeastern Arabian Sea. *Journal of Geophysical Research*, *102*, 12551–12562.

- Shenoi, S. S. C., Saji, P. K., & Almeida, A. M. (1999). Near-surface circulation and kinetic energy in the tropical Indian Ocean derived from Lagrangian drifters. *Journal of Marine Research*, 57, 885–907.
- Shetye, S. R., & Shenoi, S. S. C. (1988). The seasonal cycle of surface circulation in the coastal North Indian Ocean. *Proceedings of the Indian Academy of Science (Earth & Planetary Science)*, 97, 53–62.
- Shetye, S. R., Gouveia, A. D., Shenoi, S. S. C., Sundar, D., Michael, G. S., Almeida, A. M., & Santanam, K. (1990). Hydrography and circulation off the west coast of India during the Southwest Monsoon 1987. *Journal of Marine Research*, 48, 359–378.
- Shetye, S. R., Gouveia, A. D., Shenoi, S. S. C., Sundar, D., Michael, G. S., & Nampoothiri, G. (1991a). The western boundary current of the seasonal subtropical gyre in the Bay of Bengal. *Journal of Geophysical Research*, 98, 945–954.
- Shetye, S. R., Shenoi, S. S. C., Gouveia, A. D., Michael, G. S., Sundar, D., & Nampoothiri, G. (1991b). Wind-driven coastal upwelling along the western boundary of the Bay of Bengal during the southwest monsoon. *Continental Shelf Research*, 11, 1397–1408.
- Shetye, S. R., Gouveia, A. D., Shenoi, S. S. C., Michael, G. S., Sundar, D., Almeida, A. M., & Santanam, K. (1991c). The coastal current off western India during the northeast monsoon. *Deep-Sea Research*, 38, 1517–1529.
- Shetye, S. R., Gouveia, A. D., Shenoi, S. S. C., Sundar, D., Michael, G. S., & Nampoothiri, G. (1993). The western boundary current of the seasonal subtropical gyre in the Bay of Bengal. *Journal of Geophysical Research*, 98, 945–954.
- Shetye, S. R., Gouveia, A. D., Shenoi, S. S. C., Vinayachandran, P. N., Sundar, D., Michael, G. S., & Nampoothiri, G. (1996). Hydrography and circulation in the western Bay of Bengal during the northeast monsoon. *Journal of Geophysical Research*, 101, 14011–14025.
- Shi, W., Morrison, J. M., Böhm, E., & Manghnani, V. (1999). Remotely sensed features in the US JGOFS Arabian Sea Process Study. *Deep-Sea Research II*, 46, 1551–1575.
- Shi, W., Morrison, J. M., Böhm, E., & Manghnani, V. (2000). The Oman upwelling zone during 1993, 1994 and 1995. *Deep-Sea Research II*, 47, 1227–1247.
- Siedler, G. (1968). Schichtungs- und Bewegungsverhältnisse am Suedausgang des Roten Mee. *Research Meteor-Forschungsergebnisse, Reihe A. Heft, 4*, 1–76.
- Sloyan, B. M., & Rintoul, S. R. (2001). The southern ocean limb of the global deep overturning circulation. *Journal of Physical Oceanography*, 31, 143–173.
- Slutz, R. J., Lubker, S. J., Hiscox, J. D., Woodruff, S. D., Jenne, R. L., Joseph, D. H., Steurer, P. M., & Elms, J. D. (1985). Comprehensive Ocean-Atmosphere Data Set (COADS), Release 1. NOAA Environmental Research Laboratories, Boulder, CO, USA, 268 pp.
- Smeed, D. (1997). Seasonal variation of the flow in the strait of Bab al Mandab. *Oceanologica Acta*, 20, 773–781.
- Smith, R. L., & Bottero, J. S. (1977). On upwelling in the Arabian Sea. In M. Angel (Ed.), *A voyage of discovery* (pp. 291–304). New York: Pergamon Press.
- Smith, R. L., Huyer, A., Godfrey, J. S., & Church, J. A. (1991). The Leeuwin Current off western Australia, 1986–1987. *Journal of Physical Oceanography*, 21, 322–345.
- Sprintall, J., Gordon, A., Murtugudde, R., & Susanto, D. (2000). A semi-annual Indian Ocean forced Kelvin wave observed in the Indonesian Seas in May 1997. *Journal of Geophysical Research*, 105, 17217–17230.
- Stommel, H., & Arons, A. B. (1960). On the abyssal circulation of the world ocean. II. An idealized model of the circulation pattern and amplitude in oceanic basins. *Deep-Sea Research*, 6, 217–233.
- Stramma, L., Fischer, J., & Schott, F. (1996). The flow field off southwest India at 8°N during the southwest monsoon of August 1993. *Journal of Marine Research*, 54, 55–72.
- Stramma, L., & Lutjeharms, J. R. E. (1997). The flow field of the subtropical gyre of the South Indian Ocean. *Journal of Geophysical Research*, 102, 5513–5530.
- Stramma, L., Brandt, P., Schott, F., Quadfasel, D., & Fischer, J. (2002). Winter and summer monsoon water mass and heat transport changes in the Arabian Sea near 8°N. *Deep-Sea Research II*, (in press).
- Swallow, J. (1967). The equatorial undercurrent in the western Indian Ocean in 1964. *Studies in Tropical Oceanography*, 5, 15–36.
- Swallow, J. C., & Bruce, J. C. (1966). Current measurements off the Somali coast during the southwest monsoon of 1964. *Deep-sea Research*, 13, 861–888.
- Swallow, J. C., Molinari, R. L., Bruce, J. G., Brown, O. B., & Evans, R. H. (1983). Development of near-surface flow pattern and water mass distribution in the Somali Basin in response to the southwest monsoon of 1979. *Journal of Physical Oceanography*, 13, 1398–1415.
- Swallow, J. C., Fieux, M., & Schott, F. (1988). The boundary currents east and north of Madagascar, Part I: Geostrophic currents and transports. *Journal of Geophysical Research*, 93, 4951–4962.
- Swallow, J. C., Schott, F., & Fieux, M. (1991). Structure and transport of the East African Coastal Current. *Journal of Geophysical Research*, 96, 22254–22267.
- Taft, B. A. (1967). Equatorial undercurrent of the Indian Ocean, 1963. *Studies in Tropical Oceanography*, 40, 3–14.
- Toole, J. M., & Warren, B. (1993). A hydrographic section across the subtropical South Indian Ocean. *Deep-Sea Research I*, 40, 1973–2019.
- Tsai, P. T. H., O'Brien, J. J., & Luther, M. E. (1992). The 26 day oscillation observed in the satellite sea surface temperature measurements in the equatorial western Indian ocean. *Journal of Geophysical Research*, 97, 9605–9618.

- Tomczak, M., & Godfrey, S. (1994). *Regional oceanography: an introduction*. Pergamon Press.
- Vinayachandran, P. N., & Yamagata, T. (1998). Monsoon response of the sea around Sri Lanka: generation of thermal domes and anticyclonic vortices. *Journal of Physical Oceanography*, 28, 1946–1960.
- Vinayachandran, P. N., Masamoto, Y., Mikawa, T., & Yamagata, T. (1999a). Intrusion of the Southwest Monsoon Current into the Bay of Bengal. *Journal of Geophysical Research*, 104, 11077–11085.
- Vinayachandran, P. N., Saji, N. H., & Yamagata, T. (1999b). Response of the equatorial Indian Ocean to an unusual wind event during 1994. *Geophysical Research Letters*, 26, 1613–1616.
- Visbeck, M., & Schott, F. (1992). Analysis of seasonal current variation in the western equatorial Indian Ocean: direct measurements and GFDL model comparison. *Journal of Physical Oceanography*, 22, 1112–1128.
- Wacongne, S., & Pacanowski, R. (1996). Seasonal heat transport in a primitive equations model of the tropical Indian Ocean. *Journal of Physical Oceanography*, 26, 2666–2699.
- Wajsowicz, R. C. (1999). Models of the Southeast Asian Seas. *Journal of Physical Oceanography*, 29, 986–1018.
- Wajsowicz, R. C., & Schopf, P. S. S. (2001). Oceanic influences on the seasonal cycle in evaporation over the Indian Ocean. *Journal of Climate*, 14, 1199–1226.
- Wajsowicz, R. C., & Schneider, E. K. (2001). The Indonesian Throughflow's effect on global climate determined from the COLA Coupled Climate System. *Journal of Climate*, 14, 3029–3042.
- Walter, M. (1997). Die Zirkulation des westlichen tropischen Indischen Ozeans im Sommer 1995. Dipl. Thesis. University of Kiel.
- Warren, B. A. (1980). Deep-water circulation of the world ocean. In B. Warren, & C. Wunsch (Eds.), *Evolution of physical oceanography* (pp. 6–41).
- Warren, B. A. (1981). Transindian hydrographic section at lat.18°S: property distributions and circulation in the South Indian Ocean. *Deep-Sea Research*, 28, 759–788.
- Warren, B. A., Whitworth, T. III, & LaCasce, J. H. (2002). Forced resonant undulation in the deep Mascarene Basin. *Deep-Sea Research II*, (in press).
- Webster, P. J., Moore, A. M., Loschnigg, J. P., & Leben, R. R. (1999). Coupled ocean-atmosphere dynamics in the Indian Ocean during 1997–98. *Nature, London*, 401, 356–359.
- Weller, R. A., Baumgartner, M. A., Josey, S. A., Fischer, A. S., & Kindle, J. C. (1998). Atmospheric forcing in the Arabian Sea during 1994–1995: observations and comparisons with climatology and models. *Deep-Sea Research*, 45, 1961–1999.
- Woelk, S., & Quadfasel, D. (1996). Renewal of deep water in the Red Sea during 1982–1987. *Journal of Geophysical Research*, 101, 18155–18165.
- Woodberry, K. E., Luther, M. E., & O'Brien, J. J. (1989). The wind-driven seasonal circulation in the southern tropical Indian Ocean. *Journal of Geophysical Research*, 94, 17985–18002.
- Wunsch, C. (1977). Response of an equatorial ocean to a periodic Monsoon. *Journal of Physical Oceanography*, 7, 497–511.
- Wyrтки, K. (1961). NAGA Report Volume 2: Scientific Results of Marine investigations of the South China Sea and the Gulf of Thailand 1959–1961. Technical Report, Scripps Institute of Oceanography, 195 pp.
- Wyrтки, K. (1971). Oceanographic Atlas of the International Indian Ocean Expedition. National Science Foundation, Washington D.C., 531 pp.
- Wyrтки, K. (1973). An equatorial jet in the Indian Ocean. *Science*, 181, 262–264.
- Wyrтки, K. (1987). Indonesian Throughflow and the associated pressure gradient. *Journal of Geophysical Research*, 92, 12941–12946.
- Yasunari, T. (1989). A possible link of the QBOs between the stratosphere, troposphere and sea surface temperature in the Tropics. *Journal of the Meteorological Society of Japan*, 67, 483–493.
- You, Y., & Tomczak, M. (1993). Thermocline circulation and ventilation in the Indian Ocean derived from water mass analysis. *Deep-Sea Research I*, 40, 13–56.
- Yu, L., O'Brien, J. J., & Yang, J. (1991). On the remote forcing of the circulation in the Bay of Bengal. *Journal of Geophysical Research*, 96, 20440–20454.
- Zhang, H.-M., & Talley, L. D. (1998). Heat and buoyancy budgets and mixing rates in the upper thermocline of the Indian and Global Oceans. *Journal of Physical Oceanography*, 28, 1961–1978.